Professor Dr. Yuri P. Raizer
The Institute for Problems in Mechanics, Russian Academy of Sciences,
Vernadsky Street 101, 117526 Moscow, Russia

Editor:
Dr. John E. Allen
Department of Engineering Science, University of Oxford, Parks Road,
Oxford OX1 3PJ, United Kingdom

Translator:
Dr. Vitaly I. Kisin
24 Varga Street, Apt. 9, 117133 Moscow, Russia

This edition is based on the original second Russian edition: *Fizika gazovogo razryada*

1st Edition 1991
Corrected 2nd Printing 1997

ISBN 3-540-19462-2 Springer-Verlag Berlin Heidelberg New York

Library of Congress Cataloging-in-Publication Data.

Raĭzer, Ĭu. P. (Ĭurieĭ Petrovich) [Fizika gazovogo razriâda. English] Gas discharge physics / Yuri P. Raizer. p. cm. "Corr. printing 1997" – t.p. verso. Includes bibliographical references and index. ISBN 3-540-19462-2 (hardcover: alk. paper) 1. Electric discharges through gases. I. Title. QC711.R22713 1997 537.5'3–dc21 96-53988

Printed in Germany

Typesetting: Springer TEX inhouse system
Cover design: *design & production* GmbH, Heidelberg

SPIN 10565824 54/3144 – 5 4 3 2 1 0 – Printed on acid-free paper

Preface

Gas discharges are of interest to physicists and engineers in a number of fields. Several decades ago excellent textbooks were written by von Engel and Steenbeck, Loeb, Brown, Kaptsov and several other authors. These books faithfully served many generations of students, and specialists still refer to them. Nevertheless, their usefulness does suffer from the time elapsed since publication: It is not that the material they present has become obsolete and irrelevant – this has happened to a very minor extent, if at all. Rather, the subject has greatly advanced both in scope and in depth, and its emphases have somewhat shifted. Of course, new books have been written, mostly monographs devoted to narrow branches of gas discharge physics. But these books are typically intended for the specialist and not so much for the novice in the field.

The need for a new textbook that is understandable to a beginner in gas discharge physics, and that conveys the right *amount* of information (even more important: information of the right *kind*) making it also useful to the specialist is apparent. With this in mind, our intention has been to produce a book that serves both as a textbook and a handbook.

From an immense amount of material we have selected, as best we could, the parts that are required for an understanding of the physics and those points that are most frequently needed in research. As a convenient and comprehensive volume, the book contains a maximum of useful data: experimental results, results of calculations, and reference data; formulas required for estimates have been reduced to a form suitable for computations.

This work was published in Russian in 1987 as a substantially larger volume. The English edition has been abridged at the expense of ancillary material concerning collisions, elementary processes, plasma radiation, plasma diagnostics, and other topics, though the chapters dealing with the central themes of discharge physics are retained in full, and even expanded by the addition of new data.

We have decided not to cover actual circuits, techniques, or methods (we will cover the ideas, though) of experiments and measurements; instead we concentrate on the physics of the processes of interest. Purely technical applications of gas discharges are not discussed for the same reason.

It would be impossible to give a comprehensive bibliography when covering such an immensely wide scope of topics; hence, original papers are cited only when recent results are discussed. In all other cases we refer to a book or review paper where more complete references are given.

The author is deeply grateful to Professors A. V. Eletsky and L. D. Tsendin, who read the Russian version of the manuscript, and Professor J. E. Allen, who read the English, for a number of useful comments. In addition, the author would like to thank the translator, Dr. V. I. Kisin, for a fruitful collaboration.

Moscow, April 1991 *Yu. P. Raizer*

Contents

1. Introduction

1.1 What Is the Subject of Gas Discharge Physics

The term "gas discharge" originates with the process of discharge of a capacitor into a circuit incorporating a gap between electrodes. If the voltage is sufficiently high, electric break down occurs in the gas and an ionized state is formed. The circuit is closed and the capacitor discharges. Later the term "discharge" was applied to any flow of electric current through ionized gas, and to any process of ionization of the gas by the applied electric field. As gases ionized to a sufficient degree emit light, it has become customary to say that a discharge "lights up," or is "burning."

As a rule, the flow of electric current is associated with the notion of a circuit composed of conductors. Actually, a closed circuit or electrodes are not needed for a directed motion of charges (electric current) in rapidly oscillating electric fields, and even less so in the field of electromagentic radiation. However, quite a few effects observed in gases subjected to oscillating electric fields and electromagnetic waves (breakdown, maintaining the state of ionization, dissipation of energy of the field) are not different, in principle, from dc phenomena. Nowadays all such processes are referred to as discharges and included within gas discharge physics. The fact that electric current flow in open circuits in the field of electromagnetic waves is of no general significance. In such cases, the dissipation of the energy of the field is described not as the release of the Joule heat by electric current, but as the absorption of radiation.

The modern field of gas discharge physics is thus occupied with processes connected with electric currents in gases and with generating and maintaining the ability of a gas to conduct electricity and absorb electromagnetic radiation.

Gas discharge physics covers a great variety of complex, multi-faceted phenomena; it is full of an enormous amount of experimental facts and theoretical models. Before we begin their analysis, it is expedient to single out the main types of discharge processes and clarify them.

1.2 Typical Discharges in a Constant Electric Field

A relatively simple experiment introduces us to several fundamental types of discharge. Two metal electrodes connected to a dc power supply are inserted into a glass tube (Fig. 1.1). The tube can be evacuated and filled with various

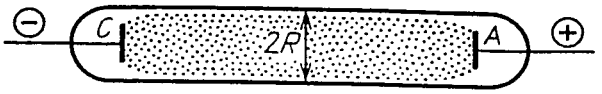

Fig. 1.1. Typical gas discharge tube

gases at different pressures. The quantities measured in the experiment are the voltage between the electrodes and the current in the circuit. This classical device served the study of discharge processes for nearly 150 years, and still remains useful.

If a low voltage is applied to the electrodes, say several tens of volts, no visible effects are produced, although a supersensitive instrument would record an extremely low current, on the order of 10^{-15} A. Charges are generated in the gas by cosmic rays and natural radioactivity. The field pulls them to the opposite-sign electrodes, producing a current. If the gas is intentionally irradiated by a radioactive or X-ray source, a current of up to 10^{-6} A can be produced. The resultant ionization is nevertheless too small to make the gas emit light. A discharge and an electric current that survive only while an external ionizing agent or the emission of electrons or ions from electrodes is deliberately maintained (e.g. by heating the cathode) are said to be *non-self-sustaining*. As the voltage is raised, the non-self-sustaining current first increases because most of the charges produced by ionization are pulled away to electrodes before recombination occurs. However, if the field manages to remove all new charges, the current ceases to grow and reaches saturation, being limited by the rate of ionization.

As the voltage is raised further, the current sharply increases at a certain value of V and light emission is observed. These are the manifestations of *breakdown*, one of the most important discharge processes. At pressure $p \sim 1$ Torr and interelectrode gap $L \sim 1$ cm, the breakdown voltage is several hundred volts. Breakdown starts with a small number of spurious electrons or electrons injected intentionally to stimulate the process: The discharge immediately becomes self-sustaining. The energy of electrons increases while they move in the field. Having reached the atomic ionization potential, the electron spends this energy on knocking out another electron. Two slow electrons are thus produced, which go on to repeat the cycle described above. The result is an electron *avalanche*, and electrons proliferate. The gas is appreciably ionized in 10^{-7} to 10^{-3} s, which is sufficient for the current to grow by several orders of magnitude.

Several conditions determine how the process develops at higher voltage. At low pressure, say 1 to 10 Torr, and high resistance of the external circuit (it prevents the current from reaching a large value), a *glow discharge* develops. This is one of the most frequently used and important types of discharge. It is characterized by low current, $i \sim 10^{-6} - 10^{-1}$ A in tubes of radius $R \sim 1$ cm, and fairly high voltage: hundreds to thousands of volts. A beautiful radiant column, uniform along its length, is formed in sufficiently long tubes of, say, $L \sim 30$ cm at $p \sim 1$ Torr. (This is how glowing tubes for street advertisements are made.) The ionized gas in the column is electrically neutral practically everywhere except in the regions close to the electrodes; hence, this is a *plasma*. The glow discharge

plasma is very weakly ionized, to $x = 10^{-8} - 10^{-6}$ (where x denotes the fraction of ionized atoms), and is nonequilibrium in two respects. Electrons that get energy directly from the field have a mean energy $\bar{\varepsilon} \approx 1\,\text{eV}$ and a temperature $T_e \approx 10^4\,\text{K}$. The temperature T of the gas, including the ions, is not much higher than the ambient temperature of 300 K. This state, with widely separated electron and gas temperatures, is sustained by a low rate of Joule heat release under conditions of relatively high specific heat of the gas and high rate of its natural cooling. Also as a result of the high rate of charge neutralization in a cold gas, its degree of ionization is many orders of magnitude lower than the thermodynamic equilibrium value corresponding to the electron temperature.

If the pressure in the gas is high (about the atmospheric level) and the resistance of the external circuit is low (the circuit allows the passage of a high current), an *arc discharge* usually develops soon after breakdown. Arcs typically burn at a high current ($i > 1\,\text{A}$) at a low voltage of several tens of volts; they form a bright column. The arc releases large thermal power that can destroy the glass tube: Arcs are often started in open air! Atmospheric-pressure arcs usually form thermodynamic equilibrium plasmas (the so-called low-temperature plasma), with $T_e \approx T \approx 10^4\,\text{K}$ and the ionization of $x = 10^{-3} \div 10^{-1}$ corresponding to such temperatures. The arc discharge differs essentially from the glow discharge in the mechanism of electron emission from the cathode, which is vital for the flow of dc current of the arc. In the glow discharge, electrons are knocked from the surface of the cold metal by impacts of positive ions. In the arc discharge, the high current heats up the cathode,and thermionic emission develops.

If $p \sim 1\,\text{atm}$, the interelectrode gap $L > 10\,\text{cm}$, and the voltage is sufficiently high, *sparking* occurs. The breakdown in the gap develops by rapid growth of the plasma channel from one electrode to another. Then the electrodes are as if short-circuited by the strongly ionized spark channel. Lightning, whose "electrodes" are a charged cloud and the ground, is a giant variety of the spark discharge. Finally, a *corona discharge* may develop in strongly nonuniform fields that are insufficient for the breakdown of the entire gap: A radiant corona appears at sharp ends of wires at sufficiently high voltage and also around power transmission line conductors.

1.3 Classification of Discharges

Discharges in a dc electric field can be classified into (a) non-self-sustaining and (b) self-sustaining types. The latter are more widespread, more diversified, and richer in physical effects; and they are the subject of this book. Steady and quasi-steady self-sustaining discharges contain (1) glow and (2) arc discharges. We have already mentioned in Sect. 1.2 that the cathode processes of two types differ in principle. A close relation of the glow discharge is (3) Townsend's dark discharge. It proceeds with a cold cathode and at very weak current. The (4) corona discharge, also self-sustaining and also at a low current, is a special case.

Corona has common features with glow and dark discharges. Among transient discharges, the (5) spark discharge stands out sharply, among others.

Many features of purely plasma processes, characterizing breakdown in a dc electric field, as well as the glow and arc discharges, are typical for discharges in rapidly oscillating fields, where electrodes are not necessary at all. It is therefore expedient to construct a classification avoiding the attributes related to electrode effects, and the following two properties will be basic for the classification: the state of the ionized gas and the frequency range of the field. The former serves to distinguish between (1) breakdown in the gas, (2) sustaining nonequilibrium plasma by the field, and (3) sustaining equilibrium plasma. Frequency serves to classify fields into (1) dc, low-frequency, and pulsed fields (excluding very short pulses), (2) radio-frequency fields ($f \sim 10^5 - 10^8$ Hz), (3) microwave fields ($f \sim 10^9 - 10^{11}$ Hz, $\lambda \sim 10^2 - 10^{-1}$ cm), and (4) optical fields (far from infrared to ultraviolet light). The field of any subrange can interact with each type of discharge plasma. In total, we have 12 combinations. All of them are experimentally realizable, and quite a few are widely employed in physics and technology. Typical conditions under which each of the combinations can be observed are summarized in Table 1.1.

Table 1.1. Classification of discharge processes

	Breakdown	Nonequilibrium plasma	Equilibrium plasma
Constant electric field	Initiation of glow discharge in tubes	Positive column of glow discharge	Positive column of high-pressure arc
Radio frequencies	Initiation of rf discharge in vessels filled with rarefied gases	Capacitively coupled rf discharges in rarefied gases	Inductively coupled plasma torch
Microwave range	Breakdown in waveguides and resonators	Microwave discharges in rarefied gases	Microwave plasmatron
Optical range	Gas breakdown by laser radiation	Final stages of optical breakdown	Continuous optical discharge

1.4 Brief History of Electric Discharge Research

Leaving lightning aside, man's first acquaintance with electric discharges was the observation, dating back to 1600, that friction-charged insulated conductors lose their charge. Coulomb proved experimentally in 1785 that charge leaks through air, not through imperfect insulation. We understand now that the cause of leakage is the non-self-sustaining discharge.

Occasional experiments were conducted in the 18th century with sparks produced by charging a body by an electrostatic generator, and with atmospheric electricity, experiments with lightning sometimes having tragic consequences.

Sufficiently powerful electric batteries were developed at the beginning of the 19th century to allow the discovery of the arc discharge. V.V. Petrov, who

worked in the Saint Petersburg Medical Surgery Academy in Russia, reported the discovery in 1803. The arc was obtained by bringing two carbon electrodes connected to battery terminals into contact and then separating them. Several years later Humphrey Davy in Britain produced and studied the arc in air. This type of discharge became known as "arc" because its bright horizontal column between two electrodes bends up and arches the middle owing to the Archimedes' force. In 1831–1835, Faraday discovered and studied the glow discharge. Faraday worked with tubes evacuated to a pressure $p \sim 1$ Torr and applied voltages up to 1000 V.

The history of physics of gas discharges in the late 19th and early 20th centuries is inseparable from that of atomic physics. After William Crookes's cathode ray experiments and J.J. Thomson's measurements of the e/m ratio, it became clear that the current in gases is mostly carried by electrons. A great deal of information on elementary processes involving electrons, ions, atoms, and light fields was obtained by studying phenomena in discharge tubes.

Beginning in 1900, J.S.E. Townsend, a student of J.J. Thomson and the creator of a school in the physics of gas discharges discovered the laws governing ionization and the gaseous discharge (known as the Townsend discharge) in a uniform electric field. Numerous experimental results were gradually accumulated on cross sections of various electron-atom collisions, drift velocities of electrons and ions, their recombination coefficients, etc. This work built the foundations of the current reference sources, without which no research in discharge physics would be possible. The concept of a plasma was introduced by I. Langmuir and L. Tonks in 1928. Langmuir made many important contributions to the physics of gas discharge, including probe techniques of plasma diagnostics.

As regards different frequency ranges, the development of field generators and the research into the discharges they produce followed the order of increasing frequencies. Radio frequency (rf) discharges were observed by N. Tesla in 1891. This kind of discharge is easily produced if an evacuated vessel is placed inside a solenoid coil to which high-frequency voltage is applied. The electric field induced by the oscillating magnetic field produces breakdown in the residual gas, and discharge is initiated. The understanding of the mechanism of discharge initiation came much latter, in fact, after the work of J.J. Thomson in 1926–1927. Inductively coupled rf discharges up to tens of kW in power were obtained by G.I. Babat in Leningrad around 1940.

The progress in radar technology drew attention to phenomena in microwave fields. S.S. Brown in the USA began systematic studies of microwave discharges in the late 1940s. Discharges in the optical frequency range were realized after the advent of the laser: A spark flashed in air when the beam of a ruby laser producing so-called giant pulses (of more than 10 MW in power) was focused by a lens, this success being achieved in 1963.

Continuously burning optical discharges, in which dense steady-state plasma is sustained by the energy of light radiation, were first initiated in 1970 by a cw CO_2 laser. Optical discharges (this term reflects a large degree of similarity with conventional discharges) immediately attracted considerable attention. Both

microwave and optical discharges have by now been studied with at least the same thoroughness that the discharges in constant electric fields has been during nearly 100 years of research.

The physics of the glow discharge, one of the oldest and, presumably, best-studied fields, has lived through an unparallel revival in the past 15–20 years, and numerous new aspects of this phenomenon have been revealed. This surge of attention was stimulated by the use of glow discharges in electric-discharge CO_2 lasers developed for the needs of laser technologies. Likewise, the application of plasmatrons (generators of dense low-temperature plasma) to metallurgy, plasma chemistry, plasma welding and cutting, etc. provided a stimulus for new extensive, detailed studies of arc plasma at $p \sim 1$ atm, $T \sim 10^4$ K, and of similar discharges in all frequency ranges. These, and many other practical applications of gas discharge physics place it within the range of sciences that lie at the foundation of modern engineering.

1.5 Organization of the Book. Bibliography

A long-standing tradition demands that a general-type book on gas discharges begin with a discussion of elementary processes: possible types of collisions of electrons and ions with atoms and molecules, the fundamentals of kinetic theory of gases, statistical physics, theory of radiation, and so forth. In this book, we mostly ignore these topics, wishing to use to maximum effect the severely limited space; besides, these topics are well represented in the literature, including some general textbooks. The reader is expected to have mastered a university general physics course, although some required information is cited in direct relation to processes to be studied.

The book starts by describing the behaviour of charged particles of an ionized gas in constant and oscillating electric fields. Chapters 2 and 3 treat the behavior of electrons in a field in terms of elementary theory. Its essential feature is that the attention is focused on one "mean" electron. Averaged behaviour of one electron is considered, and when a quantity characterizing the electron gas as a whole is to be calculated, all electrons are assumed to have the same mean free time between collisions. Chapter 4 briefly discusses the processes of creation and removal of charges in a gas placed in the field. This is necessary for avoiding later on an infinite number of digressions while presenting discharge phenomena. As we remarked previously, here we spend little time on physical details of collision processes and reactions. In fact, we have tried to compile a large amount of data useful in discharge research. Chapter 5 elaborates a rigorous approach based on the kinetic equation, to the velocity and energy distribution functions. Chapter 6 is devoted to the fundamental probe method of studying gas discharge plasma. These chapters prepare the ground for the following eight chapters, which discuss systematically and in detail the discharges of various types in fields belonging to different frequency ranges. The order in which this is done is clear from the elaboratory detailed table of contents, a list that hardly requires comment.

For reasons of restricted space, it was necessary to omit mentioning a large number of facts from discharge practice and discharge theory. Quite a few of them are discussed in available books, including the older ones. We will list several popular textbooks and general-type handbooks that treat a number of subjects of discharge physics and some elementary processes [1.1–1.10]. The Russian version of the present book [1.11] contains a modern treatise, dropped from the English edition, of collisions and radiation phenomena in plasmas, useful for discharge research. The kinetics and radiation of low-temperature plasmas ($T \sim 10^4$ K) are treated in [1.12, 13]. A number of fields in the physics of discharges are represented in recent volumes of collected papers [1.14, 15], in which each chapter was written by an appropriate specialist. The data book on electron collisions [1.16] is very useful in discharge work. The list of references to each chapter of the book cites monographs on elementary processes and on various types of discharge.

The book leaves out all aspects of discharges and plasma behavior in magnetic fields. This is also caused by shortage of space and also by the fact that magnetic fields are not much employed in traditional types of discharges; except in magnetohydrodynamic generators which are not discussed here (see [1.17]). Plasmas in magnetic fields as well as high-temperature plasmas for thermonuclear fusion ($T \sim 10^6$ K), have also become objects of a special science, viz. Plasma Physics represented by a copious literature (see, e.g., [1.18, 19]). We do not consider these aspects here, even though it is not very easy to draw a very clear-cut separation of the "spheres of influence" of gas discharge physics and plasma physics. Neither do we treat here the technical applications of gas discharges, except for CO_2 lasers and plasmatrons.

A survey of technical applications of gas discharges can be found in [1.9]; detailed discussion of applications to gas lasers is given in [1.10].

At present, there is a growing interest in radio-frequency discharge. Two major applications have stimulated its study: the use of moderate pressure capacitive discharges ($p \approx 10-100$ Torr) for high-efficiency, reliable and small size CO_2 lasers and the use of low-pressure discharges ($p \approx 10^{-3}-1$ Torr) for etching, deposition and other technologies. A detailed book about the physics and applications of radio-frequency discharges was recently published (see Further Reading [1]).

The units used in the book are traditional for gas discharge physics. Energy of particles is measured in eV, macroscopic energy and power – in J and W, respectively. Electrical quantities are measured in V, A, Ohm, etc.; pressure is measured in Torr (mm Hg) and atm, and temperature in K and eV.

2. Drift, Energy and Diffusion of Charged Particles in Constant Fields

2.1 Drift of Electrons in a Weakly Ionized Gas

In the interval between two collisions, an electron is accelerated along the line of force of the electric field $\boldsymbol{E}$. A collision changes the direction of motion sharply and in a random way, after which the electron is again accelerated, etc. Encounters of charged particles are rare in a weakly ionized gas; electrons mostly collide with neutral molecules. The systematic motion along the direction of the external force amid the random motion background is known as *drift*.

2.1.1 Equation of Averaged Motion

The duration of the act of scattering being very short in comparison with the average time τ_c between collisions, we can write the equation for the true velocity $\boldsymbol{v}_e$ of an electron in the form

$$m\dot{\boldsymbol{v}}_e = -e\boldsymbol{E} + \sum_i m\Delta\boldsymbol{v}_i\delta(t - t_i) \ , \quad \Delta\boldsymbol{v}_i = \boldsymbol{v}'_e - \boldsymbol{v}_e \ , \tag{2.1}$$

where $\Delta\boldsymbol{v}_i$ is the change in the velocity vector in the ith collision at a moment t_i, δ is the Dirac delta function, and $\boldsymbol{v}'_e$ is the velocity after collision. The equation has to be averaged because monitoring the trajectory of an individual particle would be a hopeless task. The true velocity $\boldsymbol{v}_e$ is then turned into the average velocity $\boldsymbol{v}$. The sum is also averaged over collision moments t_i and scattering angles θ between the vectors $\boldsymbol{v}'_e$ and $\boldsymbol{v}_e$. It is now interpretable as the mean change of momentum per unit time, $m\langle\Delta\boldsymbol{v}\rangle/\tau_c$. This is the *resistive force* ("*friction*") applied to the electron by the medium.

Let us decompose $\Delta\boldsymbol{v}$ into components that are perpendicular and parallel to the mean velocity $\boldsymbol{v}$ before the collision. In view of the collision symmetry, $\langle\Delta\boldsymbol{v}_\perp\rangle = \langle\boldsymbol{v}'_\perp\rangle = 0$. The electron and molecule masses, m and M, are so vastly different that the electron velocity v is almost unchanged in elastic collisiions. Hence,

$$\langle\boldsymbol{v}_\parallel\rangle = \langle\boldsymbol{v}'_\parallel\rangle - \boldsymbol{v} = \boldsymbol{v}\langle\cos\theta\rangle - \boldsymbol{v} \equiv -\boldsymbol{v}(1 - \overline{\cos\theta}) \ ,$$

where $\overline{\cos\theta}$ is the mean cosine of the scattering angle. Inelastic scattering events (those that change v) are much less frequent than elastic collisions, and will be neglected here.

As a result, (2.1) yields an equation for the mean velocity

$$m\dot{\boldsymbol{v}} = -e\boldsymbol{E} - m\boldsymbol{v}\nu_{\mathrm{m}} , \quad \nu_{\mathrm{m}} = \nu_{\mathrm{c}}(1 - \overline{\cos\theta}) , \tag{2.2}$$

where $\nu_{\mathrm{c}} = \tau_{\mathrm{c}}^{-1} = N v \sigma_{\mathrm{c}}$ is the frequency of collisions of the electron, N is the number of molecules in $1\,\mathrm{cm}^3$, σ_{c} is the cross section of elastic collisions, and v is the velocity of random motion. It will be shown in Sect. 2.3.6 that v is much greater than the drift velocity. The frequency ν_{m} is called the *effective collision frequency for momentum transfer,* and $\sigma_{\mathrm{tr}} = \sigma_{\mathrm{c}}(1 - \overline{\cos\theta})$ is the momentum transfer cross section. If the scattering is isotropic then, $\overline{\cos\theta} = 0$, $\sigma_{\mathrm{tr}} = \sigma_{\mathrm{c}}$, $\nu_{\mathrm{m}} = \nu_{\mathrm{c}}$. If electrons are scattered mostly forward, then $\overline{\cos\theta} \approx 1$, $\nu_{\mathrm{m}} \approx 0$, the momentum remains almost unchanged by the collision, and the resistive force is small. If the scattering is mostly backward, then $\overline{\cos\theta} \approx -1$ and $\nu_{\mathrm{m}} \approx 2\nu_{\mathrm{c}}$: the momentum change is doubled. In most gases at electron energies $\varepsilon \sim 1$–$10\,\mathrm{eV}$, typical for discharges, σ_{tr} is slightly less than σ_{c} (by up to 10%); at more high energies, it is less by a factor of about 1.5.

2.1.2 Drift Velocity

Integrating (2.2) results in

$$\boldsymbol{v}(t) = -(e\boldsymbol{E}/m\nu_{\mathrm{m}})[1 - \exp(-\nu_{\mathrm{m}}t)] + \boldsymbol{v}(0)\exp(-\nu_{\mathrm{m}}t) . \tag{2.3}$$

We find that the initial oriented velocity $\boldsymbol{v}(0)$ of the electron vanishes (is randomized) after several collisions. The mean velocity becomes

$$\boldsymbol{v}_{\mathrm{d}} = -e\boldsymbol{E}/m\nu_{\mathrm{m}} ; \tag{2.4}$$

this is the *drift velocity.* The electric force applied to drifting electrons compensates for the resistive force. The arguments above are valid for electrons having a definite random velocity v. Usually the cross section and frequency of collisions depend on the electron energy $\varepsilon = mv^2/2$ in a complicated manner [2.1], (Figs. 2.1, 2.2), so that (2.4) must be averaged over the spectrum.

A consistent approach to calculating the drift velocity is based on analyzing the *kinetic equation* for the electron velocity distribution function (Chap. 5). This approach shows how to average a formula of type (2.4) correctly. It is then found that the assumption of the independence of the effective collision frequency on velocity, which is quite acceptable in a number of cases, reduces the rigorous expression for $\boldsymbol{v}_{\mathrm{d}}$ exactly to (2.4); there is no need, then, to average (2.4). This fact is an obvious justification of the broadest use of the simplest formula (2.4) in theoretical models and estimates. The easiest way of numerical evaluation is to make use of the experimental data on $\sigma_{\mathrm{tr}}(v)$ [2.2, 4] and refer ν_{m} to the mean electron energy. Although this energy is field-dependent, the relevant reference data are available (see Sect. 2.3).

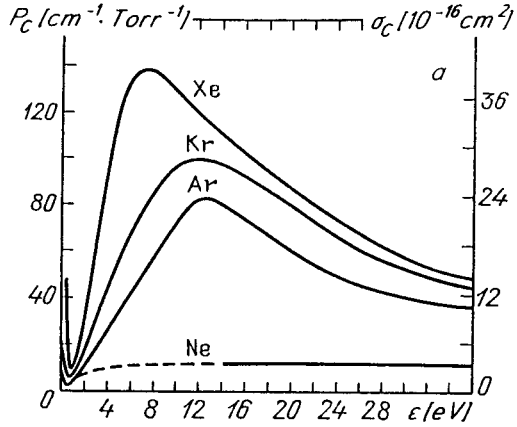

Fig. 2.1a–c. Experimental cross sections and probabilities of elastic collisions of electrons for different gases. The probability P_c is the number of collisions per cm or inverse free path length, at $p = 1$ Torr and $t = 0°$ C. From [2.3]

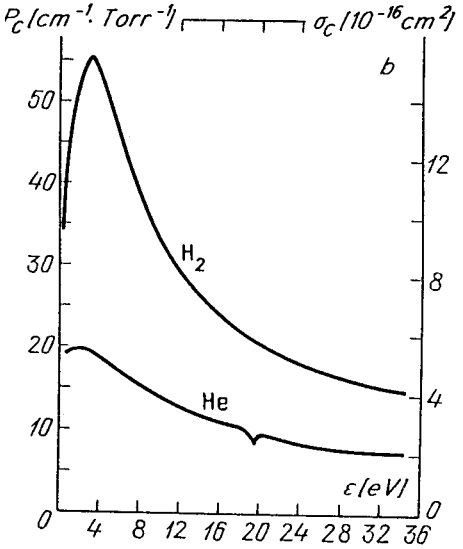

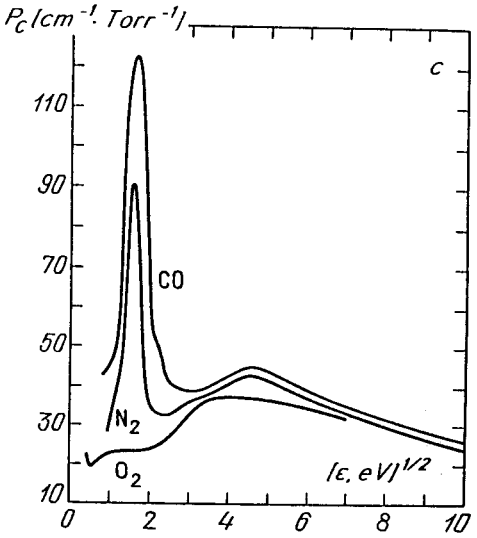

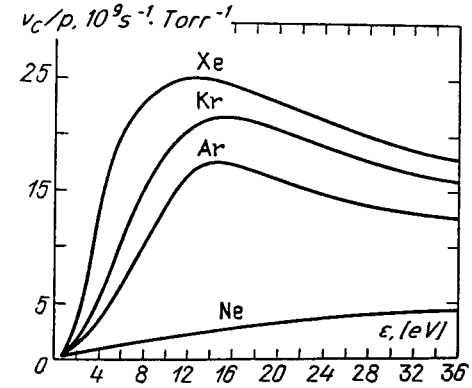

Fig. 2.2. Frequencies of elastic collisions of electrons for different gases

2.1.3 Mobility

Mobility is defined as the proportionality coefficient between the drift velocity of a charged particle and the field. The *mobility* of electrons is

$$\mu_e = \frac{e}{m\nu_m} = \frac{1.76 \cdot 10^{15}}{\nu_m[s^{-1}]} \frac{cm^2}{V \cdot s}, \quad v_d = \mu_e E . \tag{2.5}$$

The mean energy of electrons is field-dependent; hence, v_d is not a strictly linear function of E, and the mobility depends on field strength. However, the convenient linear relation (2.5) with μ_e = const is used for theoretical analysis of various discharge processes. A reasonable effective value of μ_e is chosen for numerical estimates (see Table 2.1). As a rule, this simplification does not interfere with the qualitative validity of the theory; nevertheless, in some cases the nonlinearity of the function $v_d(E)$ causes well-pronounced effects (Sect. 2.4.4).

Table 2.1. Estimated values of electron mobility, effective collision frequency for momentum transfer, conductivity, and mean free path length

Gas	$\mu_e p$, $10^6 \frac{cm^2\,Torr}{V \cdot s}$	ν_m/p, $10^9\,s^{-1}\,Torr^{-1}$	$\sigma p/n_e$, $10^{-13} \frac{Torr \cdot cm^2}{Ohm}$	range of E/p, $\frac{V}{cm \cdot Torr}$	lp, $10^{-2}\,cm \cdot Torr$
He	0.86	2.0	1.4	0.6–10	6
Ne	1.5	1.2	2.4	0.4–2	12
Ar	0.33	5.3	0.53	1–13	3
H_2	0.37	4.8	0.58	4–30	2
N_2	0.42	4.2	0.67	2–50	3
air	0.45	3.9	0.72	4–50	3
CO_2	1.1	1.8	1.8	3–30	3
CO	0.31	5.7	0.5	5–50	2

[Mobilities were found by approximating the experimental curves $v_d(E/p)$ with the function $v_d = \mu_e E$; ν_m and σ were calculated using the value of μ_e. Mean free path lengths, $l = (N\sigma_{tr})^{-1}$, refer to electron energies of 1 to 10 eV, typical for the positive column of glow discharges.]

2.1.4 Similarity, Results of Measurements, Drift in Mixtures

The collision frequency ν_m is proportional to the density N of the gas or to its pressure p.[1] If the frequency is constant, $\mu_e \propto p^{-1}$ and $v_d \propto E/p$. The energy spectrum and the mean electron energy also depend on E and N (or p) not independently, but in the combination E/p (Sect. 2.3; Chap. 5). Hence, the drift velocity is invariably a function of the ratio E/p. We will see that *similarity laws* manifest themselves in quite a few characteristics of gas discharge. Their importance is considerable. Similarity serves to reduce the amount of measurements and the results can be plotted not as functions of two variables (say, E and p),

[1] Traditionally, gas discharge physics operates with p instead of N; p is measured in Torr = 1 mm Hg – this is very convenient. At room temperature 20°C, $N = 3.295 \cdot 10^{16}\,p\,[Torr]\,cm^{-3}$. If the gas is heated, however, the N–p correspondence is not one-to-one: at low temperatures, $N = 3.3 \cdot 10^{16}\,p\,[Torr]\,(293/T\,[K])\,cm^{-3}$. Hereafter, p in numerical formulae is always expressed in Torr.

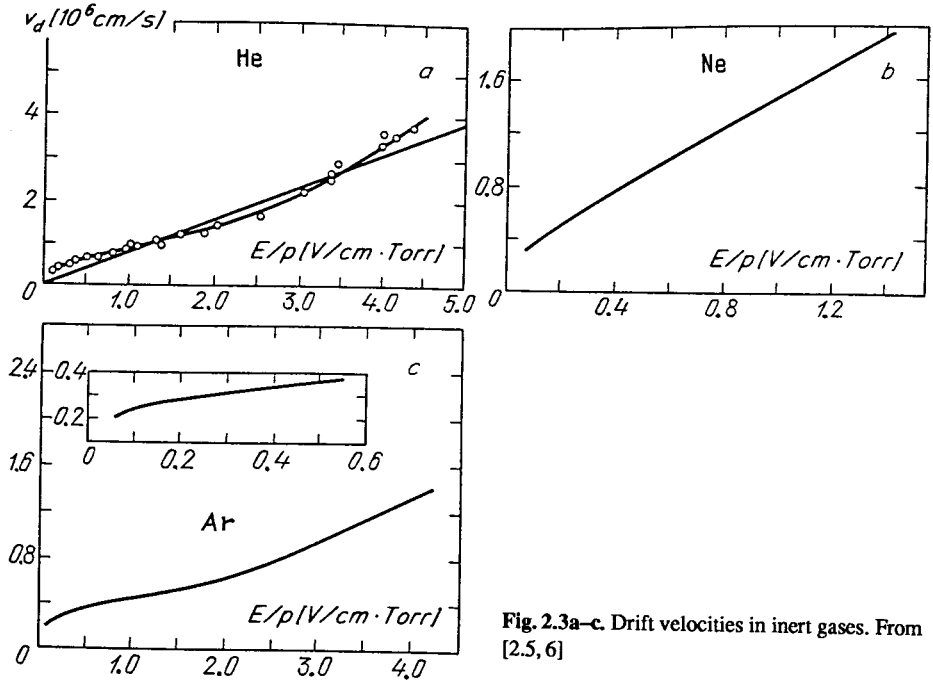

Fig. 2.3a–c. Drift velocities in inert gases. From [2.5, 6]

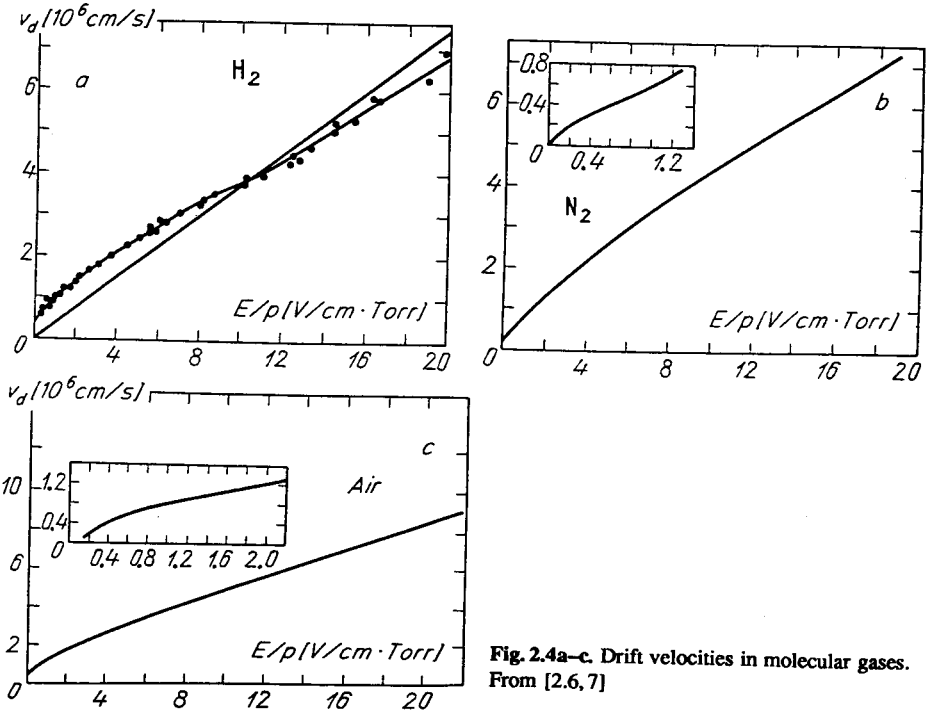

Fig. 2.4a–c. Drift velocities in molecular gases. From [2.6, 7]

but as functions of, say E/p, like $v_d = v_d(E/p)$. The drift velocity always increases with E/p (Figs. 2.3, 2.4) but this growth is not necessarily close to direct proportionality, since ν_m and v_d depend on the electron energy distribution. For example, anomalously fast drift is observed in argon at those values of E/p at which the characteristic electron energies fall in the range of the Ramsauer minimum of the collision cross section, $E/p \sim 10^{-3} - 10^{-1}$ V/(cm·Torr). When drift velocities are evaluated for gas mixtures, the averaging over percentage contents of the components must be carried out not for velocities or mobilities, but for their inverse values ("resistances") because the quantities that are summed in a mixture are collision frequencies. A small error is inevitable, since the electron spectrum of a mixture is different from those of the component gases.

2.2 Conduction of Ionized Gas

2.2.1 Weakly Ionized Plasma

The mobilities of massive ions are hundreds of times less than for light electrons. The contribution of ions to electric current is thus small, except in those rare cases when the ion densities n_+, n_- exceed by an appropriate number of times the electron density n_e. The current density j and conductivity σ in a plasma with $n_e \approx n_+$ are

$$j = -en_e v_d = en_e \mu_e E = \sigma E \,, \tag{2.6}$$

$$\sigma = e\mu_e n_e = \frac{e^2 n_e}{m\nu_m} = 2.82 \cdot 10^{-4} \frac{n_e[\mathrm{cm}^{-3}]}{\nu_m[\mathrm{s}^{-1}]} \mathrm{Ohm}^{-1}\,\mathrm{cm}^{-1} \,. \tag{2.7}$$

The conductivity of a weakly ionized gas is mostly determined by the degree of ionization n_e/N.

2.2.2 Strongly Ionized Plasma

The scattering of electrons by ions impedes their drift along the field as much as that by molecules. If ionization is not too weak and $n_+ = n_e$, then

$$\nu_m = Nv\sigma_{tr} + n_e v \sigma_{Coul} \,,$$

where σ_{Coul} is the cross section of electron-ion collisions dominated by Coulomb forces.

The scale of the *Coulomb cross section* is πr_{Coul}^2, where the *Coulomb radius* $r_{Coul} = (2/3)e^2/kT_e$ is found by equating the mean thermal energy of an electron to the energy of its interaction with the ion. An electron passing by the ion at an impact distance $r \lesssim r_{Coul}$ is deflected strongly, and if $r \gg r_{Coul}$, the deflection is small. Nevertheless, trajectories passing at a large distance give appreciable contributions to the momentum transfer cross section, owing to the long-range nature of Coulomb forces. For this reason, πr_{Coul}^2 is multiplied by the so-called *Coulomb logarithm*:

$$\sigma_{\text{Coul}} = \frac{4\pi}{9}\frac{e^4 \ln \Lambda}{(kT_e)^2} = \frac{2.87 \cdot 10^{-14} \ln \Lambda}{(T_e[\text{eV}])^2}\,\text{cm}^2\,, \tag{2.8}$$

$$\ln \Lambda = \ln\left[\frac{3}{2\sqrt{\pi}}\frac{(kT_e)^{3/2}}{e^3 n_e^{1/3}}\right] = 13.57 + 1.5\log\{T_e[\text{eV}]\} - 0.5\log n_e\,.$$

For example, if $T_e = 1\,\text{eV}$ (and $n_e = 10^{13}\,\text{cm}^{-3}$, $\ln \Lambda = 7.1$), then $\sigma_{\text{Coul}} \approx 2 \cdot 10^{-13}\,\text{cm}^2$, while $\sigma_{\text{tr}} \approx 10^{-16} - 10^{-15}\,\text{cm}^2$. As a result of a high Coulomb cross section, electron-ion collisions are already appreciable at ionizations greater than 10^{-3}.

These collisions become dominant at still higher degrees of ionization. In this case $\nu_m \propto n_e$, so that conductivity is independent of electron density (or rather, depends only weakly, via $\ln \Lambda$). The conductivity is

$$\sigma = \frac{e^2}{mv\sigma_{\text{Coul}}} = \frac{9(kT_e)^2}{4\pi e^2 mv \ln \Lambda}\,; \quad \sigma = 1.9 \cdot 10^2 \frac{\{T_e[\text{eV}]\}^{3/2}}{\ln \Lambda}\,\text{Ohm}^{-1}\,\text{cm}^{-1}\,. \tag{2.9}$$

The numerical formula was obtained with the mean thermal velocity of electrons and the coeffcient was refined by a factor of about 2 [2.8].

2.2.3 Why Electron-Electron Collisions Do not Contribute to Electric Resistance

The point is that the resistive force ("friction") in the drift of electrons is caused by the loss of momentum along the field in scattering events. As to the total momentum of any pair of interacting electrons, $m\boldsymbol{v}_1 + m\boldsymbol{v}_2$, it is conserved under scattering although the velocity of each one changes both in magnitude and in direction. This means that scattering preserves the total electric current of the pair, which is proportional to $-e\boldsymbol{v}_1 - e\boldsymbol{v}_2$. Hence, the motion of a group of electrons colliding only with electrons would be accelerated on average; this means that the electric resistance would be zero. Note that electron-electron collisions can affect the conductivity indirectly, namely, by changing the energy spectrum of the electron gas (by "Maxwellizing" it).

2.3 Electron Energy

2.3.1 Joule Heat

The work done by an electric field on an electron moving at a velocity $\boldsymbol{v}_e$ is $-e\boldsymbol{E} \cdot \boldsymbol{v}_e$ per unit time. Let us represent the electron's velocity as a sum of random $\boldsymbol{v}$ and drift $\boldsymbol{v}_d$ components: $\boldsymbol{v}_e = \boldsymbol{v} + \boldsymbol{v}_d$. By definition, averaging over a large number of electrons gives $\langle \boldsymbol{v} \rangle = 0$ and $\langle \boldsymbol{v}_e \rangle = \boldsymbol{v}_d$. The mean work of the field equals $-\langle e\boldsymbol{E} \cdot \boldsymbol{v}_e \rangle = eEv_d$. The energy released by the current in $1\,\text{cm}^3$ of the gas in 1 s is $eEv_d n_e = jE$. This is the *Joule heat* of the electric current. The field does work to overcome the resistive force. The Joule heat equals the energy of the field dissipated in response to resistance.

2.3.2 Mean Energy Gained by an Electron in One Effective Collision

This quantity equals

$$\Delta\varepsilon_E = \frac{eEv_d}{\nu_m} = \frac{e^2E^2}{m\nu_m^2} = mv_d^2 , \tag{2.10}$$

and coincides, in order of magnitude, with the "kinetic energy of drift motion", $mv_d^2/2$. On average, the total kinetic energy of an electron is composed of the random $\bar{\varepsilon}$ and drift components:

$$\left\langle \frac{m\boldsymbol{v}_e^2}{2} \right\rangle = \left\langle \frac{m\boldsymbol{v}^2}{2} \right\rangle + \frac{m\boldsymbol{v}_d^2}{2} = \bar{\varepsilon} + \frac{mv_d^2}{2} , \quad \langle \boldsymbol{v} \cdot \boldsymbol{v}_d \rangle = 0 .$$

Qualitatively, the result (2.10) can be given the following interpretation. On average, the velocity of the electron immediately after a collision ("effective" collision) is completely randomized: on average, its vector is zero. By the next collision, the electron has built up the drift velocity along the field, with the corresponding kinetic energy. The collision transfers this new portion of energy into the random part (the electron "heat") and the process starts anew.

2.3.3 True Change of Electron Energy in a Collision

Formula (2.10) reflects only the final result of various, sharply opposing situations that arise in different collisions. In fact, an electron in the interval between two collisions can be accelerated by the field or decelerated, it can store up energy or lose it. It depends on whether the motion after the collision started along or against the direction of the force, at a large or small velocity. A very simple example will be useful.

Let us fix our attention on two electrons that have velocities of identical magnitude v and start moving parallel to the field in opposite directions. Their initial kinetic energies are equal, $mv^2/2$. The electron moving along the force (against the field) reaches the velocity $v + eE/m\nu_m = v + v_d$ by the time of the next collision, picking up the additional energy

$$\Delta\varepsilon_+ = \frac{m(v+v_d)^2}{2} - \frac{mv^2}{2} = mvv_d + \frac{mv_d^2}{2} .$$

The electron that started moving along the field is decelerated some of the time (or all of it), and reaches the velocity $-v + v_d$ by the moment of collision. The additional energy is

$$\Delta\varepsilon_- = \frac{m(-v+v_d)^2}{2} - \frac{mv^2}{2} = -mvv_d + \frac{mv_d^2}{2} ;$$

if $v > v_d/2$, this increment is negative, that is, the electron loses energy. This is a typical situation: we will see in Sect. 2.3.6 that random velocities v are usually much greater than the drift velocity.

On average, the additional energy gained in these two scenarios is

$$\frac{\Delta\varepsilon_+ + \Delta\varepsilon_-}{2} = mv_d^2 ,$$

which is independent of v, is always positive, and coincides with (2.10). Clearly, electrons with arbitrary initial vectors $\boldsymbol{v}$ can be divided into similar pairs with oppositely directed velocities, producing the same result, at least to the order of magnitude.

We have already mentioned, referring to Sect. 2.3.6, that the mean random velocity $\bar{v} \gg v_d$; hence, the resulting average energy gained per one collision is a small net difference between large actual gains and losses; these are of order $|\Delta\varepsilon_\pm| \approx m\bar{v}v_d \gg \Delta\varepsilon_E = mv_d^2$. In their turn, the actual changes of energy $|\Delta\varepsilon_\pm|$ are small in comparison with the mean electron energy $\bar{\varepsilon} \approx m\bar{v}^2/2$. The ratio of these quantities is

$$\frac{\Delta\varepsilon_E}{|\Delta\varepsilon_\pm|} \sim \frac{|\Delta\varepsilon_\pm|}{\bar{\varepsilon}} \sim \frac{v_d}{\bar{v}} , \quad \frac{\Delta\varepsilon_E}{\bar{\varepsilon}} \sim \left(\frac{v_d}{\bar{v}}\right)^2 . \tag{2.11}$$

2.3.4 Equation of Electron Energy Balance

Electrons gain energy from the field and pass it on to atoms and molecules. The current density and Joule heat released are small when the ionization is low. The gas heats up slightly. But the mean energy and temperature of electrons in the discharge cannot be too low, since electrons would be unable to ionize atoms and sustain the conductive state in the gas. In such cases $T_e \gg T$ at low pressures, so that the energy exchange in elastic collisions is a one-way process: from electrons to the gas (if $T_e \sim T$, the exchange is mutual, on average). Let us find the mean energy lost by an electron in an elastic collision with a molecule.

When an electron loses momentum $\Delta\boldsymbol{p}$, the molecule gains the same momentum. If it was "at rest" before the collision, the energy gained is $(\Delta\boldsymbol{p})^2/2M$. The electron loses the same amount of energy; on the average, this amount is $(m^2/2M)\langle(\Delta\boldsymbol{v})^2\rangle$. Since

$$\langle(\Delta\boldsymbol{v})^2\rangle = \langle(\boldsymbol{v}' - \boldsymbol{v})^2\rangle = v^2 - 2v'v\overline{\cos\theta} + v^2 = 2v^2(1 - \overline{\cos\theta}) ,$$

the mean fraction of energy $\varepsilon = mv^2/2$ that the electron loses in an elastic collision is $(2m/M)(1-\overline{\cos\theta})$. We denote $\delta = 2m/M$ and can write the equation of energy balance for the "mean" electron undergoing only elastic collisions:

$$\frac{d\varepsilon}{dt} = (\Delta\varepsilon_E - \delta\varepsilon)\nu_m = \left(\frac{e^2E^2}{m\nu_m^2} - \delta\varepsilon\right)\nu_m . \tag{2.12}$$

The mean electron energies in discharge plasmas are usually quite low compared to the fairly high potentials of excitation and ionization of atoms, $I \sim 10\,\text{eV}$, and the corresponding energy losses are small. The gas is ionized by "super-energetic" electrons, and these are rare. For this reason, the main mechanism of energy transfer from electrons to the gas is the *elastic*

loss. Electrons in molecular gases mostly dissipate energy by exciting the *vibrational* (and *rotational*) energy levels of molecules. This case too can be described by (2.12), but the coefficient δ is not calculated as simply as for elastic losses. Inelastic losses are usually greater than elastic ones by one to two orders of magnitude; nevertheless, the corresponding coefficient δ is small: $\delta \sim 10^{-3} - 10^{-2} (2m/M \sim 10^{-4} - 10^{-5})$.

2.3.5 Mean Energy

The equilibrium value of energy of the "mean" electron corresponds to energy gains compensated for by losses; in the approximation above it can be treated as the mean energy of electrons, $\bar{\varepsilon}$, in the field (the rigorous calculation of this quantity requires the solution of the kinetic equation; see Chap. 5). Assume that the coefficient δ and scattering cross section σ_{tr} are independent of energy, that is, the free path of electrons, $l = 1/N\sigma_{tr}$, is energy-independent. Note that $\nu_m = \bar{v}/l \sim \sqrt{\bar{\varepsilon}}$. We also specify that $m\bar{v}^2 = (16/3\pi)\bar{\varepsilon}$, as in the case of the Maxwellian distribution. Equating the right-hand side of (2.12) to zero, we obtain

$$\bar{\varepsilon} = \frac{\sqrt{3\pi}}{4} \frac{eEl}{\sqrt{\delta}} \approx 0.8 \frac{eEl}{\sqrt{\delta}} \approx \frac{e}{\sigma_{tr}\sqrt{\delta}} \frac{E}{N} . \tag{2.13}$$

The mean energy is proportional to E/N and exceeds by a factor $1/\sqrt{\delta}$ the energy eEl that the electron builds up while moving along the direction of the electric force. The assumption of constant free path length corresponds to the square root dependence of drift velocity on the electric field. Indeed, substituting $\bar{v} = (16\bar{\varepsilon}/3\pi m)^{1/2}$ into $\nu_m = N\bar{v}\sigma_{tr}$ and defining $\bar{\varepsilon}$ by (2.13), we find from (2.5) that

$$v_d = \left(\frac{3\pi}{16}\delta\right)^{1/4} \left(\frac{eE}{m\sigma_{tr}N}\right)^{1/2} \approx 0.9\delta^{1/4} \left(\frac{eE}{m\sigma_{tr}N}\right)^{1/2} . \tag{2.14}$$

On the other hand, the assumption of constant collision frequency, with μ_e = const and $v_d \sim E/N$, corresponds to the quadratic dependence of energy on field strength (provided δ = const). In this case (2.12) implies

$$\bar{\varepsilon} = \frac{e^2E^2}{\delta m\nu_m^2} = \frac{e^2}{\delta m\tilde{\nu}_m^2} \left(\frac{E}{N}\right)^2 , \quad \tilde{\nu}_m \equiv \frac{\nu_m}{N} . \tag{2.15}$$

The choice of a particular model thus produces a dilemma: assume either

$$\nu_m, \mu_e = \text{const} , \quad v_d \sim E/N, \bar{\varepsilon} \sim \delta^{-1}(E/N)^2 ,$$

or

$$\sigma_{tr}, l = \text{const}, v_d \sim \delta^{1/4}(E/N)^{1/2}, \bar{\varepsilon} \sim \delta^{-1/2}(E/N) .$$

The actual dependence of v_d and $\bar{\varepsilon}$ on E/N found in experiment or obtained by solving the kinetic equation is usually quite complicated and, at best, is well

approximated by a specific model within certain intervals of E/N for specific gases. Consequently, for a theoretical analysis of various effects, for revealing characteristics of qualitative behavior and achieving more profound understanding of the physics of processes, one is forced to choose a version that is better suited for analysis. If an effect is determined by drift or electric current, it is expedient to choose constant mobility. If attention is focused on the energy aspects of electron behavior in the field as is the case in this section, it is better to use the approximation $l = \text{const}$ and the clearly descriptive formula (2.13); this is what we propose to do below.

Formula (2.13) gives reasonable numerical results. For instance, in helium ($\delta = 2.7 \cdot 10^{-4}$), the momentum transfer cross section changes little in the characteristic energy range and is approximately $\sigma_{\text{tr}} \approx 5.5 \cdot 10^{-16}\,\text{cm}^2$ ($l \approx 0.055/p[\text{Torr}]\text{cm}$); hence we find for $E/N = 3.3 \cdot 10^{-17}\,\text{V} \cdot \text{cm}^2$ [$E/p = 1\,\text{V}/(\text{cm} \cdot \text{Torr})$] that $\bar{\varepsilon} \approx 2.5\,\text{eV}$. Experiment gives $\bar{\varepsilon} \approx 2\,\text{eV}$. It did not prove possible to calculate $\bar{\varepsilon}$ in molecular gases in a simple manner because serious difficulties are encountered in finding the loss coefficient δ. However, this does not make (2.13) useless. Quite the opposite, it makes the estimation of δ possible because an independent way of determining $\bar{\varepsilon}$ is available (see Sect. 2.4). Thus $\bar{\varepsilon} \approx 1.5\,\text{eV}$ in nitrogen at $E/p = 3\,\text{V}/(\text{cm} \cdot \text{Torr})$; the cross section in the characteristic energy range is of order $\sigma_{\text{tr}} \approx 10^{-15}\,\text{cm}^2$ ($l \approx 0.03/p[\text{Torr}]\,\text{cm}$), and (2.13) yields $\delta \approx 2.1 \times 10^{-3}$, in agreement with the result obtained by an independent method. The elastic loss coefficient of nitrogen is much smaller, $2m/M = 3.9 \times 10^{-5}$.

2.3.6 Relation of Random to Drift Velocity

It is immediately implied by (2.5) and (2.13) that

$$\frac{v_{\text{d}}}{\bar{v}} = \frac{elE}{m\bar{v}^2} = \frac{\sqrt{3\pi}}{4}\sqrt{\delta} \approx 0.8\sqrt{\delta}\,, \quad \frac{\bar{v}}{v_{\text{d}}} \approx \frac{1.2}{\sqrt{\delta}}\,. \tag{2.16}$$

The random velocity that an electron develops in the field is greater than the drift velocity by a factor of $1/\sqrt{\delta}$, that is, of tens or hundreds. Relation (2.16), which clarifies the physical meaning of the smallness of $v_{\text{d}}/\bar{v}$, is closely tied to the parameters of smallness of the energy characteristics of electrons. In a collision, an electron gains or loses an energy of order $|\Delta\varepsilon_{\pm}| \approx \sqrt{\delta}\,\bar{\varepsilon} \approx eEl$, which corresponds to the potential difference traversed in an arbitrary direction across one free path length. The energy $\Delta\varepsilon_{+}$ is slightly greater than $|\Delta\varepsilon_{-}|$, by the amount $\Delta\varepsilon_E \approx \sqrt{\delta}|\Delta\varepsilon_{+}|$ that an electron picks up, on average, per one collision.

Now, several words on the limits of applicability of the relations above. On the side of very weak fields, it is restricted by the assumption of one-way energy exchange between electrons and the gas, $\bar{\varepsilon} \gg kT$. Indeed, in the absence of the field, electrons are thermalized and acquire the gas temperature T, unless they perish first! The condition $\bar{\varepsilon} \gg kT$ is usually met in weakly ionized discharge plasmas "many times over." Considerable inelastic losses become important in high-strength fields, at electron energies $\varepsilon \gtrsim 10\,\text{eV}$. Even the formal transition to

the limit of maximal possible losses $\delta \sim 1$ in (2.13,16) shows that the oriented and random components of velocity become comparable. Hence, strong asymmetry in motion and in true energy exchange between electrons and the field must develop. An electron builds up considerable energy between subsequent collisions, excites or ionizes an atom, losing energy and rushes forward again. This is not quite the picture that was taking shape before. Such phenomena may occur in the cathode layer of a glow discharge (Sect. 5.9, 8.4). Sometimes relatively high drift velocities are also observed outside the cathode layer. In low pressure mercury vapour the drift velocity is of one quarter of the random velocity [2.9].

2.3.7 Energy Relaxation; Criteria of Constant and Homogeneous Fields

We refer to the quantity $\nu_u = \delta\nu_m$ as the *frequency for energy losses*. If the field is instantaneously switched off, an electron dissipates its energy in a time of order

$$\tau_u = \nu_u^{-1} = \tau_m/\delta \,, \tag{2.17}$$

that is, after about $1/\delta$ effective collisions. A very slow electron picks up the appropriate energy in about the same time, because in one collision it acquires a fraction δ of it. As follows from (2.12), τ_u characterizes the rate at which equilibrium energy builds up in a given field. This is the *energy relaxation time*. If the field changes little over the time τ_u, the mean energy (and hence the electron energy distribution) track the changing field and is thus *quasi-steady*. If changes are fast, tracking becomes impossible. The field "constancy" criterion can thus be written as $(dE/dt)\tau_u \ll 1$.

On the average, the electrons are systematically displaced in the direction of the electric field, so that energy equilibration proceeds not only in time but in space as well. Over one relaxation time τ_u, electrons drift over a distance

$$\Lambda_u = v_d\tau_u \approx 0.8l/\sqrt{\delta} \,. \tag{2.18}$$

This quantity can be called the *energy relaxation length*. It is greater than the electron mean free path by a factor $1/\sqrt{\delta}$, not by the $1/\delta$ that characterizes the ratio of relaxation time to time between collisions. According to (2.13,18),

$$\bar{\varepsilon} = eE\Lambda_u \,, \tag{2.19}$$

that is, an electron builds up the mean energy in the potential difference across one Λ_u.

A dc field can be treated as homogeneous if it varies only slightly over distances of order Λ_u, that is, if $(dE/dx)\Lambda_u \ll 1$. The opposite case is that of strongly inhomogeneous fields in which the energy distribution and the mean energy of electrons cease to be functions of only the local ratio E/N. For instance, the energy may be determined by the potential difference crossed by electrons after being emitted from the atoms.

The loss term in parentheses in the energy balance equation (2.12) increases with increasing ε, while the energy gain generally decreases; under the assump-

tion l = const, it varies as $1/\varepsilon$. Therefore, electron energy always tends to the stationary value $\bar{\varepsilon}$. If $\varepsilon < \bar{\varepsilon}$, then $d\varepsilon/dt > 0$; if $\varepsilon > \bar{\varepsilon}$, then $d\varepsilon/dt < 0$. This shows that the stationary state is stable because energy invariably returns to $\bar{\varepsilon}$ (at the relaxation rate) after any random deviation of ε from $\bar{\varepsilon}$.

2.4 Diffusion of Electrons

2.4.1 Equation of Continuity

If the density of particles moving in a gas is spatially noniuniform, a *diffusion flux* appears that tends to level it off. The total flux consists of the drift and diffusion components. The flux densities of positively and negatively charged particles are

$$\boldsymbol{\Gamma}_{\pm} = \pm n\mu \boldsymbol{E} - D\nabla n \,. \tag{2.20}$$

(If the gas flows at a velocity $\boldsymbol{u}$, *convective* components $n\boldsymbol{u}$ are added to $\boldsymbol{\Gamma}$.) Note that subscripts $\pm$ with n, μ, and D are dropped. The diffusion coefficients are

$$D = \langle v^2/3\nu_{\mathrm{m}} \rangle \approx l\bar{v}/3 \,, \quad D \propto p^{-1} \,. \tag{2.21}$$

Particle number densities satisfy the *continuity equations*

$$\frac{\partial n}{\partial t} + \operatorname{div} \boldsymbol{\Gamma} = q \,, \tag{2.22}$$

which generalize the standard diffusion equation; q are the bulk sources of creation or annihilation of particles in $1\,\mathrm{cm}^3\,\mathrm{s}^{-1}$.

2.4.2 Relation Between Diffusion Coefficient, Mobility, and Mean Energy

Assuming that the collision frequency is constant, we find from (2.5) and (2.21) that

$$D_{\mathrm{e}}/\mu_{\mathrm{e}} = m\overline{v^2}/3e = (2/3)\bar{\varepsilon}/e \,, \tag{2.23}$$

where $\bar{\varepsilon}$ is the true mean energy of electrons, regardless of their energy spectrum. If the spectrum is Maxwellian, (2.23) is valid regardless of the dependence of ν_{m} on v. One only needs to substitute for μ_{e} a rigorous expression implied by the kinetic equation (Sect. 5.6.1). This is natural since here $\bar{\varepsilon} = (3/2)kT_{\mathrm{e}}$ and (2.23) reduces to the *Einstein relation*

$$D/\mu = kT/e \,, \tag{2.24}$$

which is thermodynamic in nature. Indeed, there are no fluxes in the state of thermodynamic equilibrium, and charge densities in the field $\boldsymbol{E} = -\nabla\varphi$ (φ is the potential) satisfy Boltzmann's law $n_{\pm} \propto \exp(\mp e\varphi/kT)$. This gives (2.24).

If the electron spectrum is non-Maxwellian and $\nu_m(v) \neq \text{const}$ (this is typical of weakly ionized gases in electric fields), the quantity $(3/2)D_e/\mu_e$ also characterizes the mean electron energy, but does not exactly coincide with it. The ratio D_e/μ_e, corresponding to the electron "temperature", is known as the *characteristic energy*. Like the spectrum, it is a function of E/p.

Experimentally, the ratio D_e/μ_e is measured by determining the spreading, due to diffusion, of electrons drifting in the field E. At a distance $x = v_d t$ from the point where electrons start, the beam has spread in the transverse direction to a radius $r \sim \sqrt{D_e t} = \sqrt{D_e x/v_d} \approx \sqrt{(D_e/\mu_e)(x/E)}$. Experimental curves of

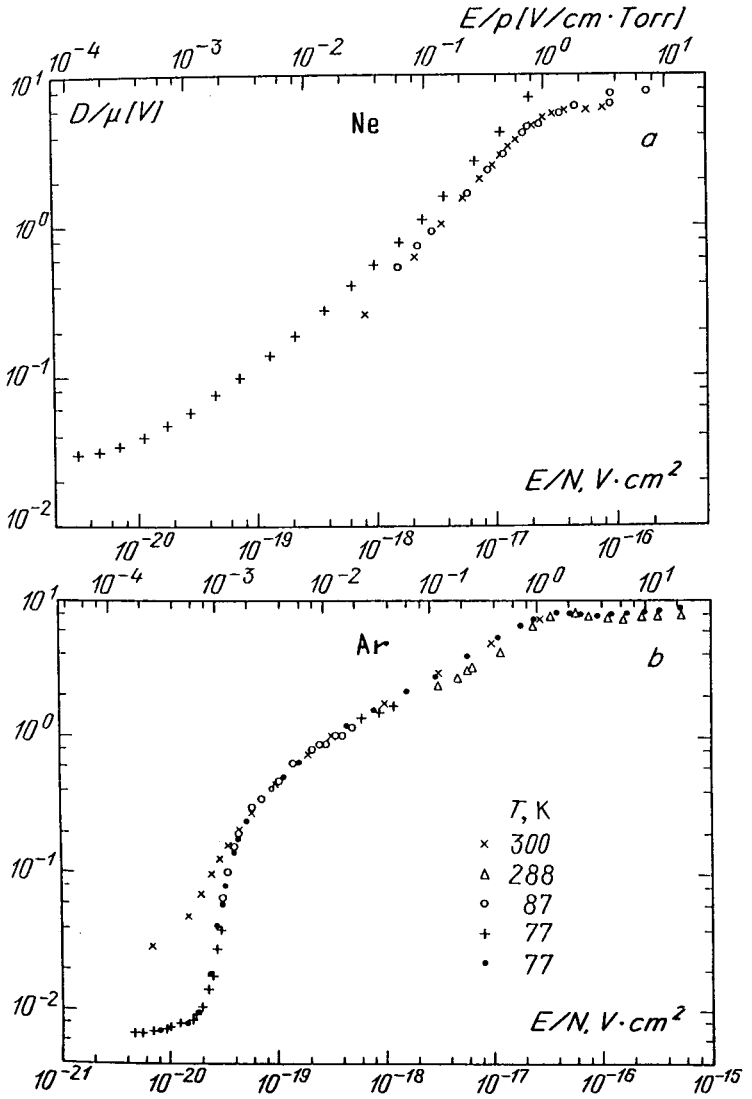

Fig. 2.5a,b. Characteristic energies in inert gases. From [2.10]

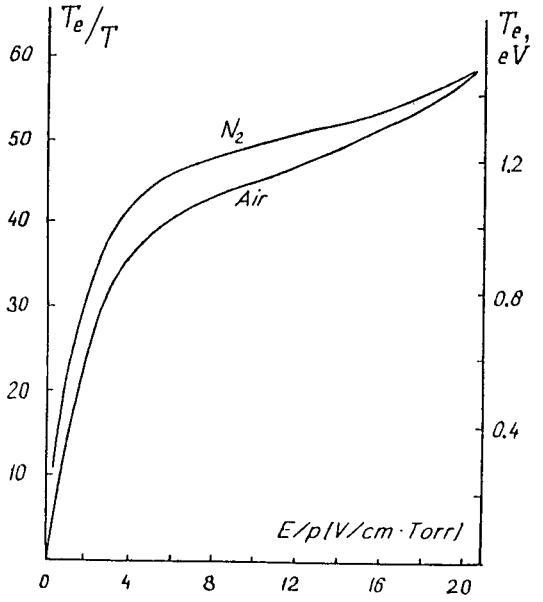

Fig. 2.6. The ratio of electron and gas temperatures in air and N_2. From [2.11]

D_e/μ_e as a function of E/p (Figs. 2.5, 2.6) can be successfully fitted for Ne and H_2, with reasonable accuracy, by a straight line through the origin in the ranges of E/p typical for glow discharges. Formula (2.19) then gives some idea about electron energy relaxation lengths Λ_u. Namely,

$$\text{Ne:}\quad \bar{\varepsilon} \approx 9.7\left(\frac{E}{p}\right)\text{eV}\,, \qquad \frac{E}{p} \sim 0.1 - 1.2\,\text{V/(cm}\cdot\text{Torr)}\,;$$

$$\Lambda_u \approx \frac{9.7}{p[\text{Torr}]}\text{cm}\,,$$

$$\text{H}_2\text{:}\quad \bar{\varepsilon} \approx 0.17\left(\frac{E}{p}\right)\text{eV} \qquad \frac{E}{p} \sim 0.5 - 13\,\text{V/(cm}\cdot\text{Torr)}\,;$$

$$\Lambda_u \approx \frac{0.17}{p[\text{Torr}]}\text{cm}\,.$$

2.4.3 Calculation of Diffusion Coefficients

The measurement of drift velocities and characteristic electron energies is perfectly feasible. On the other hand, it is exceptionally difficult to measure diffusion coefficients directly in the presence of an electric field. In fact, only diffusion coefficients of *thermalized* electrons that have come into thermal equilibrium with the gas in zero field have been measured in direct experiments. At room temperature, $D_{e,\text{therm}} = K \cdot 10^5/p\,[\text{Torr}]\,\text{cm}^2/\text{s}$, where

	He	Ne	Ar	H_2	N_2	O_2
$K =$	2	20	6.3	1.3	2.9	12

The value of D_e can be estimated using the data on v_d and D_e/μ_e. Thus in Ne at $E/p = 1$ V/(cm·Torr), we have $v_d = 1.46\times10^6$ cm/s, $T_e \approx 5.5$ eV [2.10], whence $D_e \approx v_d T_e/E \approx 8\times10^6/p\,\mathrm{cm}^2/\mathrm{s}$. In air at $E/p = 20$, we find $v_d = 8.5\times10^6$ cm/s, $T_e \approx 1.5$ eV[2.11], from this $D_e \approx 6.3\times10^5/p\,\mathrm{cm}^2/\mathrm{s}$.

2.4.4 Longitudinal and Transverse Diffusion

The ratio D_e/μ_e found from the measured diffusional spreading of electron packets along the direction of drift differs systematically from the results obtained by recording transverse spreading. The physical reason for the difference between the coefficients of *longitudinal* D_L and *transverse* D_T diffusion is the dependence of the collision frequency ν_m on electron energy [2.12]. According to (2.20), the mean electron flux consists of drift and diffusion components:

$$\boldsymbol{v} = \boldsymbol{\Gamma}_e/n_e = \boldsymbol{v}_d - D_e\nabla n_e/n_e \equiv \boldsymbol{v}_d + \boldsymbol{v}_{dif}\,;$$

in the zeroth approximation, D_e is the "ordinary" coefficient characterizing the diffusion perpendicular to the drift direction. If there is a gradient of n_e along the field, the field does additional work per second on the electrons, in comparison with the case of pure drift motion $-e\boldsymbol{E}\boldsymbol{v}_{dif} = eD_e(\boldsymbol{E}\nabla n_e)/n_e$. The mean electron energy $\bar{\varepsilon}$ gets an increment $\Delta\varepsilon$ proportional to the projection of the gradient on the direction of the vector $\boldsymbol{E}, \nabla_\parallel n_e$. If ν_m increases with increasing ε (this is the typical situation), the mobility reduces by $\Delta\mu_e$, which is proportional to $\nabla_\parallel n_e$. The effect of this response is equivalent to the drift velocity remaining unchanged but the velocity due to longitudinal diffusion, $\boldsymbol{v}_{dif,\parallel} = -D_e\nabla_\parallel n_e/n_e$, getting an increment proportional to $\Delta\mu_e \sim \nabla_\parallel n_e$. In its turn, this effect means a drop in the longitudinal diffusion coefficient. In the first approximation, in a small gradient, we find [2.12] that

$$D_T = D_e,\ D_L = \left(1 - \frac{\hat{\nu}_m}{1+2\hat{\nu}_m}\right) D_e\,,\quad \hat{\nu}_m \equiv \frac{\partial \ln \nu_m}{\partial \ln \varepsilon}\,. \tag{2.25}$$

The logarithmic derivative $\hat{\nu}_m$ characterizes the steepness of the function. Thus for $\nu_m \sim \varepsilon^k$, we have $\hat{\nu}_m = k$. Experimentally, D_L is seen to diminish by a factor of up to 2 in comparison to D_T.

2.5 Ions

2.5.1 Collisions with Molecules

An ion of mass M_i comparable with that of a gas molecule M exchanges larges portions of energy with molecules. If the field is not strong, an ion gets from the field an energy less than kT; ions then reach the gas temperature T. These conditions are typical for the positive column of a glow discharge. The cross section of elastic scattering of slow ions is determined by *polarization forces*. An ion at a distance r from a molecule induces in it a dipole moment $d = \alpha e/r^2$,

where α is the polarizability of the molecule, and is attracted to the molecule with a force $2ed/r^3$. The ion is scattered strongly if it passes at a distance $r \lesssim \varrho_0$, where $\varrho_0 \approx (\alpha e^2/2\varepsilon')^{1/4}$ corresponds to the equality of the potential energy of interaction $|U| = \alpha e^2/2r^4$ and the kinetic energy of relative motion of the particles ε'. To an order of magnitude, therefore, the scattering cross section is $\sigma_{tr} \approx \pi\varrho_0^2$. Including the corrective factor of $2\sqrt{2}$ [2.13], we have

$$\sigma_{tr} \approx 2\pi\sqrt{\alpha e^2/\varepsilon'} = 2\sqrt{2}\pi a_0^2\sqrt{(\alpha/a_0^3)\,(I_H/\varepsilon')}\,. \tag{2.26}$$

To indicate the scale, we have substituted $e^2 = 2a_0 I_H$ into σ_{tr} (a_0 is the Bohr radius and I_H is the ionization potential of the hydrogen atom; see Appendix). In the polarization interaction, $\sigma_{tr} \propto 1/v'$ and the collision frequency is $\nu_m \propto v'\sigma_{tr} = \text{const}$, where v' is the relative velocity of the particles.

When the "radius" of polarization foces ϱ_0 becomes less than the molecular size, scattering occurs only when particles come into "contact." The polarization cross section is replaced with the gas-kinetic one, which weakly depends on v'; now $\nu_m \propto v'$. In Ar, N_2, and O_2 (where $\alpha/a_0^3 \approx 10-12$), as well as in He, this occurs when $\varepsilon' > \varepsilon_k \approx 0.5-0.6\,\text{eV}$, in Ne when it is 0.15 eV, and in H_2 when it is 0.9 eV.

Ions moving in their own gases, (e.g., He^+ in He, N_2^+ in N_2) lose momentum intensively via charge transfer. An ion accelerated by the field appropriates an electron from a neutral molecule. This happens so quickly that the new ion (the former neutral) fails to move at all. The charge transfer cross section, $\sigma_{c.t.}$, is usually even greater than the elastic scattering cross section [2.4] (Fig. 2.7). In the center-of-mass reference frame, the molecule and the ion move towards each other at equal velocities, while after charge transfer the charge moves at the same velocity but in the opposite direction. This is equivalent to scattering by 180°, so that in charge transfer, $\sigma_{tr} = 2\sigma_{c.t.}$. Charge transfer considerably reduces the mobility of ions in their own gas.

2.5.2 Drift in Weak and Moderate Fields

In the general case, the mean rate of momentum loss by a particle in a collison (resistive force) is determined by the reduced mass $M' = M_i M/(M_i+M)$ and the relative velocity $\boldsymbol{v}'$. The quantity $M'\langle \boldsymbol{v}'\nu_m(v')\rangle$ is averaged over the velocities of molecules for a fixed ion velocity $\boldsymbol{v}$. The situation looks simpler when electrons are considered (Sect. 2.1.1) because $m \ll M$ and $M' \approx m$, $\boldsymbol{v}' \approx \boldsymbol{v}_e$. There is also no need for averaging if the ion cross section is determined by polarization forces and charge transfer, since $\nu_m(v') \approx \text{const}$ and $\langle \boldsymbol{v}'\nu_m\rangle = \boldsymbol{v}\nu_m$, where $\boldsymbol{v}$ is the mean velocity of ions. Equating the resistive forces and fields, we obtain the drift velocity and ion mobilities similar to (2.4, 5):

$$\boldsymbol{v}_{id} = e\boldsymbol{E}/M'\nu_m\,, \quad \mu_i = e/M'\nu_m\,. \tag{2.27}$$

If no charge transfer occurs and the cross section is purely polarization-induced, then

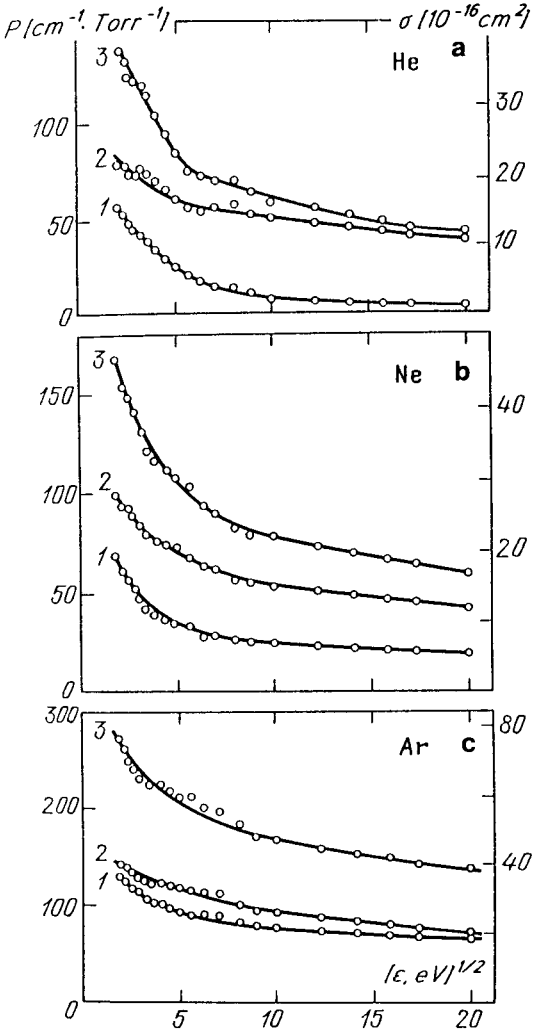

Fig. 2.7a–c. Cross sections and probabilities of collisions of atomic ions in inert gases. (1) – elastic scattering, (2) – charge transfer, (3) — sum of (1) and (2). From [2.14, 15]

$$\mu_i = \frac{2.7 \times 10^4 \sqrt{1 + M/M_i}}{p\,[\text{Torr}]\sqrt{(\alpha/a_0^3)A}} = \frac{36\sqrt{1 + M/M_i}}{p\,[\text{atm}]\sqrt{(\alpha/a_0^3)A}} \frac{\text{cm}^2}{\text{V} \cdot \text{s}}, \tag{2.28}$$

where A is the molecular weight of the gas. Formula (2.28), with a slightly different coefficient, was derived by Langevin in 1905. It is in good agreement with experimental data [2.1]. Ions often tend to join with molecules and atoms into complexes of the type N_4^+, O_4^+, Ne_2^+ and He_2^+ (in contrast to Ne_2 and He_2, these complexes are sufficiently stable). This process affects mobility since it eliminates charge transfer (Fig. 2.8). As an example, consider the drift of Ne_2^+ in Ne. For Ne, $\alpha/a_0^3 = 2.76$. From (2.28), we have $\mu_i = 4.5 \times 10^3/p\,[\text{Torr}]\,\text{cm}^2/(\text{V}\cdot\text{s})$. The experimental value is $\mu_i = 5 \times 10^3/p$. In a field typical of glow discharges,

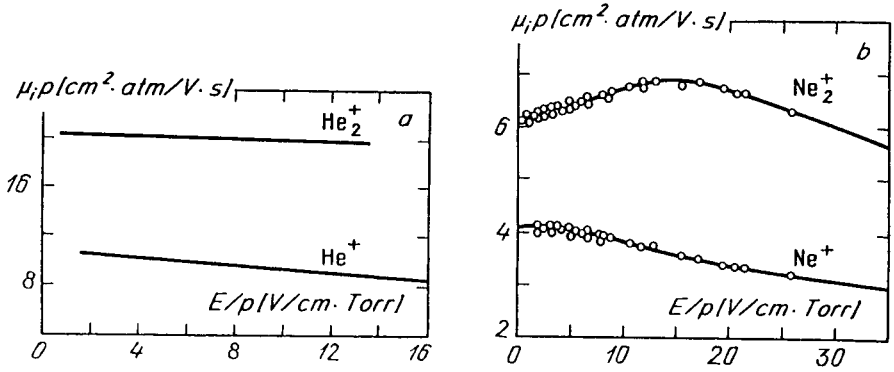

Fig. 2.8. Mobility of (a) Ne^+ and Ne_2^+ in Ne; (b) He^+ and He_2^+ in He; $p = 1$ atm, $T = 300$ K. From [2.16]

$E/p = 1\,\mathrm{V/(cm \cdot Torr)}$, we have $v_{id} = 50\,\mathrm{m/s}$. The corresponding thermal velocity at $T = 300\,\mathrm{K}$ is $v_{iT} \approx 400\,\mathrm{m/s}$.

2.5.3 Mean Energy

The equation for the mean ion energy $\bar{\varepsilon}_i$ in the approximation $\nu_m = \text{const}$, in which the problem of averaging over the particle velocities is greatly simplified, is

$$\frac{d\bar{\varepsilon}_i}{dt} = \left[\frac{e^2E^2}{M'\nu_m^2} - \frac{2M'}{M+M_i}(\bar{\varepsilon}_i - \bar{\varepsilon}_M)\right]\nu_m\,, \quad M' = \frac{M_iM}{M+M_i}\,. \tag{2.29}$$

If the mean energy of molecules $\bar{\varepsilon}_M = (3/2)kT \ll \varepsilon_i$ and $M_i \ll M$, then (2.29) is identical to (2.12) for electrons undergoing only elastic energy loss ($\delta = 2m/M$). The equilibrium energy of ions is

$$\bar{\varepsilon}_i = \frac{3}{2}kT + \frac{(1+M_i/M)^3}{2(M_i/M)}\frac{e^2E^2}{M_i\nu_m^2}\,. \tag{2.30}$$

If the field is not too strong, this energy is only slightly greater than the thermal value $3kT/2$. Electrons exchange energy very poorly with a gas and are thermalized only in extremely weak fields of $E/p \lesssim 10^{-3} - 10^{-2}\,\mathrm{V/(cm \cdot Torr)}$. The masses M_i and M being comparable, ions reach the temperature of the gas in fields that are not necessarily weak, say $E/p \sim 1 - 10\,\mathrm{V/(cm \cdot Torr)}$.

If the field is strong, an ion acquires in a free path length l an energy eEl much greater than $\bar{\varepsilon}_M$, so that its energy $\bar{\varepsilon}_i$ runs much ahead of the thermal energy. The collision cross section becomes close to the gas-kinetic value and $l \approx \text{const}$. For example, if $\sigma = 3 \times 10^{-15}\,\mathrm{cm^2}$, then $l = 10^{-2}/p\,[\mathrm{Torr}]\,\mathrm{cm}$. For room temperature and $E/p > 40\,\mathrm{V/(cm \cdot Torr)}$, we find $eEl > 10\bar{\varepsilon}_M \approx 0.4\,\mathrm{eV}$. Such conditions are characteristic of the cathode layer of a glow discharge. We now approximate (2.30) for the case of $l = \text{const}$ and $\nu_m = v/l \sim v$. Replacing v with the approximation $\sqrt{2\bar{\varepsilon}_i/M_i}$, we find

$$\bar{\varepsilon}_i = \frac{(1+M_i/M)^{3/2}}{2(M_i/M)^{1/2}}eEl\,. \tag{2.31}$$

In the limit $M_i \ll M$, (2.31) transforms into (2.13). In contrast to electrons, an ion with a mass $M_i \sim M$ does not store energy pumped by the field: it sheds it in each collision, so that $\bar{\varepsilon}_i \sim eEl$.

2.5.4 Drift in Strong Field

Assuming $\nu_m = v/l$ and $l = \text{const}$, expressing velocity v through $\bar{\varepsilon}_i$ [as in deriving (2.31)] and substituting it into (2.27), we find v_{id}:

$$v_{id} \approx \left(\frac{M_i}{M}\right)^{1/4} \left(1 + \frac{M_i}{M}\right)^{1/4} \sqrt{\frac{eEl}{M_i}} \,. \tag{2.32}$$

This is proportional not to E/p, as in moderate fields, but to $\sqrt{E/p}$. If $M_i \approx M$, v_{id} is approximately equal to the ion velocity $\bar{v} \approx \sqrt{2\bar{\varepsilon}_i/M_i}$ that corresponds to its mean energy, because the motion of the ion is sharply oriented. Ions in a heavy gas, however, drift more slowly than they move randomly: $v_{id}/\bar{v} = [M_i/(M_i + M)]^{1/2} \sim \sqrt{M_i/M}$ [cf. (2.16)]. Like electrons, they store energy $\bar{\varepsilon}_i \approx (M/M_i)^{1/2} eEl$.

The transition from the mobility law $v_{id} \propto E/p$ to the law $v_{id} \propto \sqrt{E/p}$ is gradual (Fig. 2.9). It begins usually in fields in which ion energies reach about 1 eV and the polarization forces are replaced with short-range forces and the cross section becomes gas-kinetic. If ions move in their own gas and charge transfer dominates, this occurs when the ion energy is appreciably greater than the thermal energy.

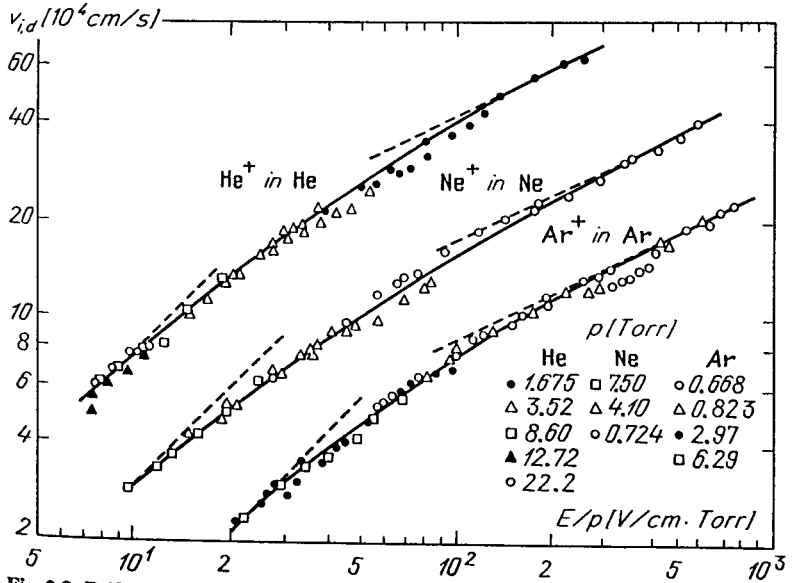

Fig. 2.9. Drift velocities of ions in inert gases. Change in mobility laws: from $v_{id} \sim E$ (*dashed line* on the left) to $v_{id} \sim \sqrt{E}$ (*dashed line* on the right); $T = 300$ K. From [2.17]

2.5.5 Diffusion

The Einstein relation (2.24) is valid in not too strong fields when ions are in thermal equilibrium with the gas and their energy is $\bar{\varepsilon}_i \approx 3kT/2$. Direct studies of ion diffusion are much less numerous than mobility measurements, so that the diffusion coefficients D_i are typically found in this way. In the case of moderate E/p, D_i varies with E/p as little as μ_i does. For instance, in the case of nitrogen ions in nitrogen, $\mu_i \approx 1.5 \times 10^3/p\,[\mathrm{Torr}]\,\mathrm{cm}^2/(\mathrm{V}\cdot\mathrm{s})$, $D_i \approx 40/p\,\mathrm{cm}^2/\mathrm{s}$.

2.6 Ambipolar Diffusion

When the density of charged particles, n_e and n_+, is very low, the charges of opposite signs diffuse independently of each other. This is known as *free diffusion*. Electrons are more mobile and thus diffuse faster; if there is a charge density gradient in the plasma, electrons may leave their less mobile partners far behind. If, however, the densities n_e and n_+ are not low, a considerable space charge is formed as a result of charge separation, and the generated polarization field impedes further violation of charge neutrality (Fig. 2.10). Charge separation and the field so adjust to each other that the field restrains the run-away electrons and pulls forward the heavy ions, making them diffuse only as a team. This diffusion is known as *ambipolar*; the concept was introduced by Schottky in 1924.

2.6.1 Ambipolar Diffusion Coefficient

Let us turn to the general expressions (2.20) for charge particle fluxes. We will be interested in the cases of no external field or of diffusion in the direction normal to it. Then the field $\boldsymbol{E}$ entering these formulas is connected exclusively with the polarization of the plasma. It satisfies the electrostatics equation

$$\operatorname{div} \boldsymbol{E} = 4\pi e\left(n_+ - n_e\right) . \tag{2.33}$$

Let the separation of charges be small: $|n_+ - n_e| \ll n_e \approx n_+ \approx n$. For the separation not to grow appreciably, the electron and ion fluxes must be almost

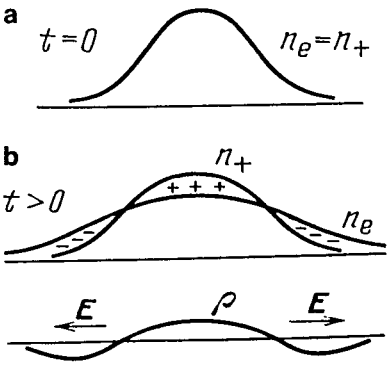

Fig. 2.10a,b. Plasma polarization in the presence of electron and ion density gradients. **(a)** Initial distributions $n_e = n_+$; **(b)** distributions n_e, n_+, and space-charge density $\varrho = e(n_+ - n_e)$ some time later. *Arrows* indicate the direction of the polarization field

equal: $\Gamma_{ex} \approx \Gamma_{+x} \approx \Gamma_x$, where the x axis is chosen to be perpendicular to the external field, provided it exists. In order to eliminate the polarization field from the expressions

$$\Gamma_x \approx -\mu_e E_x n - D_e \frac{\partial n}{\partial x}\,, \quad \Gamma_x \approx +\mu_+ E_x n - D_+ \frac{\partial n}{\partial x}\,, \tag{2.34}$$

we divide the first by μ_e, the second by μ_+, and add up the results. We find that the flux of charged particles of both signs is written in the form standard for diffusion:

$$\Gamma_x = -D_a \frac{\partial n}{\partial x}\,, \quad D_a = \frac{D_+\mu_e + D_e\mu_+}{\mu_e + \mu_+}\,, \tag{2.35}$$

with an effective coefficient D_a, the *ambipolar diffusion coefficient*. Since $\mu_e \gg \mu_+$ and $D_e \gg D_+$, the quantity $D_a \approx D_+ + D_e(\mu_+/\mu_e)$ is greater than D_+ but less than D_e, in accord with the remarks on "speeding-up of the ions" and "restraining" electrons. For an equilibrium plasma, where the electron, T_e, and ion, T, temperatures are equal, the Einstein relations (2.24) yield $D_a = 2D_+$. For a nonequilibrium plasma, where the electron temperature is much higher than that of the ions (the latter is equal to the gas temperature), we have

$$D_a \approx D_e \frac{\mu_+}{\mu_e} = D_+ \frac{T_e}{T} = \mu_+ \frac{kT_e}{e} = \frac{2}{3}\mu_+ \bar{\varepsilon}_e\,[\mathrm{eV}]\,. \tag{2.36}$$

2.6.2 What Are the Conditions Under Which the Diffusion Is Ambipolar?

This question is very important because the free and ambipolar diffusion coefficients differ by a factor of ten and more. For the flux Γ_{ex} of (2.34) not to exceed Γ_{+x} despite the strong inequalities $D_e \gg D_+$ and $\mu_e \gg \mu_+$, the diffusion and drift terms of Γ_{ex} with opposite signs must compensate each other to within the relatively small flux Γ_{+x}. Hence, the polarization field that appears automatically in ambipolar diffusion equals

$$E_x \approx -\frac{D_e}{\mu_e}\frac{1}{n}\frac{\partial n}{\partial x} = -\frac{kT_e}{e}\frac{1}{n}\frac{\partial n}{\partial x} \sim \frac{kT_e}{eR}\,, \tag{2.37}$$

where R is the length characterizing the scale of the charge density gradient. This is the distance over which the electron density varies considerably. For example, R is the radius of plasma in a tube because the density at the axis is much greater than at the tube walls, where the charges are neutralized.

The *polarization field* is a result of charge separation; in its turn, the separation is caused by the random (thermal) motion of the faster (electron) component and stems from the electron thermal energy. Indeed, where the polarization field exists, its potential difference over the entire length R is such that the electric energy to which the charge is accelerated over it is of the order of the thermal energy of electrons: $e\delta\varphi \sim eE_xR \sim kT_e$. The polarization field is generated by the space charge $e\delta n = e(n_+ - n_e)$; according to (2.33), this charge is determined,

to within an order of magnitude, from the relation $E_x/R \sim 4\pi e\delta n$. Using (2.37), we find

$$\frac{\delta n}{n} \approx \frac{kT_e}{4\pi e^2 n}\frac{1}{R^2} = \left(\frac{d}{R}\right)^2 , \quad d = \left(\frac{kT_e}{4\pi e^2 n}\right)^{1/2} . \tag{2.38}$$

The quantity d is the *Debye radius* of a plasma.[2] It gives the distance characterizing strong charge separation and plasma polarization. If $R \gg d$, that is, if large density differences appear over distances greater than the Debye radius, then $\delta n/n \ll 1$, deviations from charge neutrality are small, and the diffusion is ambipolar. If $R \lesssim d$, electrons and ions diffuse independently. For example, for $T_e = 1\,\text{eV}$, $n_e = 10^8\,\text{cm}^{-3}$, and $R = 1\,\text{cm}$, we have $d = 0.052\,\text{cm}$ and $\delta n/n = 2.5 \cdot 10^{-3}$, that is, the diffusion is clearly ambipolar. If T_e and R are the same but $n_e < 10^6\,\text{cm}^{-3}$, the diffusion of charges is free.

2.6.3 Definition of "Plasma"

The condition $(d/R)^2 \ll 1$, where R is the characteristic size of the region of large density difference, gives the quantitative criterion that distinguishes between *plasma* as an electrically neutral ionized medium and other cases of the presence of charges in a gas.

2.7 Electric Current in Plasma in the Presence of Longitudinal Gradients of Charge Density

2.7.1 Continuity Equation for Charges and Currents

If plasma is placed in an external electric field and if the current is nonzero, then in contrast to Sect. 2.6.1 the densities of electron and ion fluxes are not equal, and the current density is $\boldsymbol{j} = e(\boldsymbol{\Gamma}_+ - \boldsymbol{\Gamma}_e)$. The continuity equation (2.22) for particles of a given species and the fact that positive and negative charges are created and annihilated *only in pairs* (if negative ions are absent, $q_e = q_+$) imply the following continuity equation:

$$\frac{\partial \varrho}{\partial t} + \operatorname{div} \boldsymbol{j} = 0 , \quad \varrho = e\left(n_+ - n_e\right) . \tag{2.39}$$

In electrically neutral media, and under steady-state conditions in all media, the current has no source:

$$\operatorname{div} \boldsymbol{j} = 0 . \tag{2.40}$$

---

[2] The Debye radius of an equilibrium plasma ($T_e = T$) is less than (2.38) by a factor of $\sqrt{2}$. When considering charge screening in plasmas with $T_+ \ll T_e$, one should not subject the density of low-mobility ions around a charge to Boltzmann's law $n_+ = n_{+\infty}\exp(-e\varphi/kT_+)$, but assume it to be constant, $n_+ = n_{+\infty}$. Then d is given by (2.38).

In the one-dimensional plane case $dj/dz = 0$ along the current direction z, $j(z) = \text{const}$, and the current density does not change. It is usually determined not by local characteristics, but by conditions of the entire system, including the circuit external to the discharge.

2.7.2 Diffusion Current and the Distortion of the Field by Gradients

Under the conditions of quasineutrality ($n_e \approx n_+ \approx n$), formulas (2.20) yield

$$j/e = e(\Gamma_+ - \Gamma_e) = (D_e - D_+)\nabla n + (\mu_e + \mu_+)En\,, \tag{2.41}$$

$$E = \frac{j}{e(\mu_e + \mu_+)n} \frac{D_e - D_+}{\mu_e + \mu_+} \frac{\nabla n}{n}\,. \tag{2.42}$$

The electric field is made up of the external one, which drives the current, and the polarization field due to the presence of gradients (in fact, temperature gradients generate additional, thermodiffusion currents but their role is usually minor). Of course, these components are indistinguishable: measuring a field, say, by a probe (Chap. 6), we determine the total field (2.42).

If the charge density falls steeply in the direction opposite to that of the external field, the total field may be completely suppressed or may even reverse in direction with respect to the current (such effects are observed in glow discharges, low-voltage arcs, etc.). The electric current cannot be affected by this [see (2.40)] and is carried through by electron diffusion: if $E \approx 0$, then (2.41), taking into account that $D_e \gg D_+$, yields $j \approx D_e \nabla n$. The diffusion is then free (ambipolar diffusion cannot transfer charge). Indeed, electrons in zero field do not pull ions behind. In gases, this situation cannot, however, exist on too long a path, as we see from (2.42). Note that the diffusion coefficient D_e depends on the electron energy distribution, which reaches a state corresponding to the field after an energy relaxation length $\Lambda_u = l/\sqrt{\delta} \gg l$ (Sect. 2.3.7). Strictly speaking, it strengthens the usual condition of applicability of diffusion concepts, namely, a small drop in n over a length l; at any rate, it calls for very careful analysis in treating diffusion in highly nonuniform fields.

2.7.3 Plasma Density Equation

Using (2.42) in the formulas (2.20) for Γ_e and Γ_+ and recalling definition (2.35), we find that

$$\Gamma_e = -D_a \nabla n - \frac{\mu_e}{\mu_e + \mu_+} \frac{j}{e}\,, \quad \Gamma_+ = -D_a \nabla n + \frac{\mu_+}{\mu_e + \mu_+} \frac{j}{e}\,. \tag{2.43}$$

Electron and ion fluxes are made up of identical ambipolar diffusion fluxes (they can also have a component along the current) and fluxes due to the electric current. In contrast to ambipolar fluxes, these latter fluxes differ greatly, by a factor of $\mu_e/\mu_+ \gg 1$. Substituting any of expressions (2.43) into the appropriate continuity equation (2.22) and recalling (2.40), we arrive at *the general balancing equation for the number of charged particles*:

$$\frac{\partial n}{\partial t} - D_a \Delta n = q\,, \quad n \approx n_e \approx n_+\,. \tag{2.44}$$

This looks like an ordinary diffusion equation (with ambipolar coefficient) for a problem with bulk sources of charge; it manifests no signs of the possibility of electric current in the medium. This current affects charge fluxes (2.43), not the balance. The balance is current-independent because, metaphorically speaking, the amount of electricity flowing into somewhere is exactly equal, in view of (2.40), to the amount flowing out of it.

2.7.4 Charge Neutrality Criterion

This requires different descriptions for two different situations. If the drift current is zero or small in comparison with the electron diffusion current [the polarization field is greater than the external one in (2.42)], we return to the situation treated in Sect. 2.6.2 and the criterion $(d/R)^2 \ll 1$ [see (2.38)]. If the drift current is greater than the diffusion current, then (2.42) implies that $\boldsymbol{j} \approx e\mu_e \boldsymbol{E} n$ and we have, in accord with (2.40, 33),

$$
\begin{aligned}
&-\boldsymbol{E}\cdot\nabla n = n\,\mathrm{div}\,\boldsymbol{E} = 4\pi e n\left(n_+ - n_e\right) = 4\pi e n \delta n\,, \\
&\frac{\delta n}{n} \sim \frac{E}{4\pi e n L} \sim \frac{kT_e}{4\pi e^2 n}\,\frac{eE}{kT_e L} \sim \frac{d^2}{L\Lambda_u} \sim \left(\frac{d}{L}\right)^2 \frac{L}{\Lambda_u}\,,
\end{aligned}
\tag{2.45}
$$

where Λ_u is the electron temperature relaxation length (or that of the mean electron energy) of (2.18) and (2.19), and L is the characteristic length of strong variation of n_e and conductivity. The Debye radius must be compared with the geometric mean of L and Λ_u. The actual conditions decide whether the criterion based on (2.45) is stronger or weaker than that based on (2.38) and whether the gradient along the current or transverse to it violates charge neutrality more strongly.

2.7.5 Ambipolar Flow of Charges Along a Nonuniform Field

In contrast to the diffusion flux, this flow is of a drift nature, and is caused by a space charge [2.18]. Let us use in the continuity equations (2.22) for n_e and n_+ the expressions (2.20) for the fluxes $\boldsymbol{\Gamma}_e$ and $\boldsymbol{\Gamma}_+$. Multiplying the equation for n_e by μ_+/μ_e and assuming, for simplification, that μ_e and μ_+ are constant, we then add the result to the equation for n_+. When summing up the drift fluxes, we retain the "small" difference δn because we are interested in the effect of space charge; this charge may be considerable even in quasineutral plasma (in the sense of $\delta n/n \ll 1$). Substituting $\delta n = (4\pi e)^{-1}\,\mathrm{div}\,\boldsymbol{E}$ and neglecting the terms proportional to μ_+/μ_e (this ratio is less than 10^{-2}), we arrive at the equation

$$
\frac{\partial n}{\partial t} + \mathrm{div}\left(-D_a \nabla n + \frac{\mu_+}{4\pi e}\boldsymbol{E}\,\mathrm{div}\,\boldsymbol{E}\right) = q\,, \quad n \approx n_+ \approx n_e\,,
\tag{2.46}
$$

which is a refinement of (2.44). The ambipolar diffusion flux is now supplemented with the "ambipolar drift" flux.

In the one-dimensional case, the latter term equals $\mu_+/8\pi e \times \partial E^2/\partial x$. It is not related directly to charge density. However, the current is constant along its direction x, $j \approx e n_e \mu_e E = \mathrm{const}$, so that a field gradient is invariably accompa-

nied with a plasma density gradient. The ambipolar drift flux is thus equivalent to a diffusion flux,

$$\frac{\mu_+}{8\pi e}\frac{\partial E^2}{\partial x} \approx -\frac{\mu_+ E^2}{4\pi en}\frac{\partial n}{\partial x} = -D_E\frac{\partial n}{\partial x}\,, \quad D_E = \frac{\mu_+ E^2}{4\pi en}\,, \tag{2.47}$$

with effective diffusion coefficient D_E to be added to D_a [2.19]. The relative roles of the two fluxes are characterized by the ratio of the energy density of electric field to the density of the thermal energy of electrons,

$$D_E/D_a = E^2/4\pi nkT_e = \{E[\mathrm{V/cm}]\}^2/\{1.8\times 10^{-6} nT_e[\mathrm{eV}]\}\,. \tag{2.48}$$

For example, for $n = 6\times 10^9\,\mathrm{cm}^{-3}$ and $T = 1\,\mathrm{eV}$, the *ambipolar drift* dominates ambipolar diffusion if $E > 10^2\,\mathrm{V/cm}$ or, in view of the E/p values typical for plasma, 1–10 V/(cm·Torr) if $p > 10^2$–10 Torr. As a result of the two effects, plasma is pumped from regions of weaker field and higher density to those of stronger field and lower density. Details concerning the application of (2.46) are given in Sect. 8.6.6.

2.8 Hydrodynamic Description of Electrons

A partially ionized gas is a three-component mixture of electrons, ions, and neutral particles. Its behavior in a field can be described in terms of the ordinary equations of gas dynamics. We will consider here a simplified and more frequently used (for discharge conditions) version of equations, assumming the gas to be at rest as a whole, weakly ionized, and quasineutral. Actually, it is then sufficient to write the equations only for the electron gas. Its state is characterized by the electron density n_e, the vector of macroscopic velocity $\boldsymbol{v}_e$, and temperature T_e (or pressure $p_e = n_e kT_e$).

2.8.1 Equations of Continuity and Motion

The former has already been written out, see (2.22). The latter is

$$mn_e\frac{d\boldsymbol{v}_e}{dt} = -n_e e\boldsymbol{E} - \nabla p_e - n_e m\boldsymbol{v}_e\nu_m\,, \quad \frac{d\boldsymbol{v}_e}{dt} = \frac{\partial \boldsymbol{v}_e}{\partial t} + (\boldsymbol{v}_e\cdot\nabla)\,\boldsymbol{v}_e\,. \tag{2.49}$$

In fact, this result has already been used above. The inertia term can be dropped from (2.49) because of the smallness of the electron mass. Then (2.49) reduces to (2.20) for the flux density $\boldsymbol{\Gamma}_e = n_e\boldsymbol{v}_e$, considered together with (2.21) and (2.24), and differs from (2.20) only in the additional *thermodiffusion* flux proportional to $-\nabla T_e$. This last term is usually smaller than the diffusion term, and has been accordingly neglected.

2.8.2 Energy Equation

This equation is of the form [2.20]

$$\frac{\partial}{\partial t}\left(\frac{3}{2}n_e k T_e\right) + \operatorname{div} \boldsymbol{F} = -n_e e \boldsymbol{E}\cdot\boldsymbol{v}_e - \frac{3}{2}n_e k T_e \nu_u - qI\,, \tag{2.50}$$

$$\boldsymbol{F} = \tfrac{5}{2}n_e k T_e \boldsymbol{v}_e - \lambda_e \nabla T_e\,, \quad \lambda_e = \tfrac{5}{2}k n_e D_e\,. \tag{2.51}$$

The flux density of electron energy $\boldsymbol{F}$ is composed of the hydrodynamic flux of enthalpy and the *heat conduction* flux; λ_e is its coefficient.[3] The terms containing the electron kinetic energy of drift motion, $mv_e^2/2 \ll kT_e$, are neglected; according to (2.16), $v_e \sim v_d \ll \bar{v}$. Electron energy losses in collisions with molecules are written in (2.50) in accordance with (2.12, 17). The last term in (2.50) describes energy spent to create new electrons, q is the resultant creation rate that enters the continuity equation (2.22), and I is the ionization potential.

The combination of (2.22, 49–51) implies that the equation for the rate of heating of a moving particle of the electron gas is

$$\frac{3}{2}k\frac{dT_e}{dt} = -e\boldsymbol{E}\cdot\boldsymbol{v}_e - \frac{3}{2}kT_e\nu_u - \frac{1}{n_e}\operatorname{div}(p_e\boldsymbol{v}_e) + \frac{1}{n_e}\operatorname{div}(\lambda_e\nabla T_e) - \left(I + \frac{3}{2}kT_e\right)\frac{q_e}{n_e}\,, \tag{2.52}$$

where dT_e/dt is the total derivative with respect to time, as in (2.49).

Equation (2.52) generalizes (2.12), covering the effects caused by *spatial inhomogeneity*: work of pressure forces and the contribution of heat conduction. The last term describes energy spent on ionization and passing thermal energy to the created electron; it is usually small in comparison with the term proportional to $\nu_u = \delta\nu_m$ in (2.12).

2.8.3 Current-Carrying Plasma

It is convenient to present the velocity $\boldsymbol{v}_e$ or $n_e\boldsymbol{v}_e$ in (2.22, 50–52) in the form (2.43), where the current $\boldsymbol{j}$ satisfying (2.40) is singled out of $\boldsymbol{\Gamma}_e$. Ignoring the ambipolar thermodiffusion flux and taking into account that $\mu_+ \ll \mu_e$, we obtain

$$n_e\boldsymbol{v}_e = -\boldsymbol{j}/e - D_a\nabla n_e\,, \quad \operatorname{div}\boldsymbol{j} = 0\,. \tag{2.53}$$

According to (2.24, 42), the field $\boldsymbol{E}$ in (2.50, 52) is, to the same accuracy,

$$\boldsymbol{E} = \boldsymbol{j}/e\mu_e n_e - \left(kT_e/e\right)\nabla n_e/n_e\,. \tag{2.54}$$

The outlined system of equations will be employed in Sect. 9.7.

---

[3] The expression for $n_e\boldsymbol{v}_e$, derived from (2.49), and expression (2.51) for $\boldsymbol{F}$ and λ_e stem from the kinetic equation for electrons (Chap. 5), assuming Maxwellian distribution functions and $\nu_m(\varepsilon)$ = const. If $l(\varepsilon)$ = const, $\nu_m \sim \sqrt{\varepsilon}$, and the coefficients in $\boldsymbol{F}$ and λ_e, $\frac{5}{2}$, are set equal to 2; the thermal diffusion coefficient is found to be twice as small.

3. Interaction of Electrons in an Ionized Gas with Oscillating Electric Field and Electromagnetic Waves

3.1 The Motion of Electrons in Oscillating Fields

Both the equations of electrodynamics and the equations of motion of electrons are linear with respect to the fields $\boldsymbol{E}$, $\boldsymbol{H}$ and the velocity $\boldsymbol{v}$ of the electron. For this reason, the *superposition principle* holds. Any periodical field can be resolved into harmonic components, so that it is sufficient to consider only the *sinusoidal* field, all the more so because one normally deals with *monochromatic* fields and waves. In the case of nonrelativistic motion, the magnetic force of the wave, $e(v/c)H$, is much less than the electric force eE. Furthermore, the amplitude of electron oscillations in discharge processes is usually small in comparison with wavelength λ. We assume, therefore, that the electron is in a spatially uniform electric field $\boldsymbol{E} = \boldsymbol{E}_0 \sin \omega t$, $\boldsymbol{E}_0 = \text{const}$.

3.1.1 Free Oscillations

Assume that an electron moves without collisions, an assumption that is meaningful if the electron performs a large number of oscillations in the interval between collisions, $\omega \gg \nu_m$. We integrate the equation of collisionless motion,

$$m\dot{\boldsymbol{v}} = -e\boldsymbol{E}_0 \sin \omega t \,, \quad \dot{\boldsymbol{r}} = \boldsymbol{v} \,,$$

to give

$$\boldsymbol{v} = \frac{e\boldsymbol{E}_0}{m\omega} \cos \omega t + \boldsymbol{v}_0 \,, \quad \boldsymbol{r} = \frac{e\boldsymbol{E}_0}{m\omega^2} \sin \omega t + \boldsymbol{v}_0 t + \boldsymbol{r}_0 \,. \tag{3.1}$$

An electron oscillates at the frequency of the field; these oscillations are superimposed onto an arbitrary translation velocity $\boldsymbol{v}_0$. The displacement and oscillation velocities are

$$a = \frac{eE_0}{m\omega^2} \,, \quad u = \frac{eE_0}{m\omega} \,. \tag{3.2}$$

The displacement is in phase with the field, while the velocity is out of phase by $\pi/2$. The limiting case of "collisionless" oscillations is approximately realized at optical frequencies, and also at microwave frequencies at low pressures, $p \lesssim 10\,\text{Torr}$.

3.1.2 Effect of Collisions

Collisions "throw off" the phase, thereby disturbing the purely harmonic course of the electron's oscillations. A sharp change in the direction of motion after

scattering stops the electron from achieving the full range of displacement (3.2) that the applied force can produce; the electron starts oscillating anew after each collision, with a new phase and new angle relative to the instantaneous direction of velocity. In order to take this factor into account, we add the rate of loss of momentum due to collisions to the equation of motion of the "mean" electron. As in the case of constant fields (Sect. 2.1.1), we have the equation for the mean velocity:

$$m\dot{\boldsymbol{v}} = -e\boldsymbol{E}_0 \sin\omega t - m\boldsymbol{v}\nu_m \,, \quad \dot{\boldsymbol{r}} = \boldsymbol{v} \,. \tag{3.3}$$

The solution of (3.3), valid after several collisions, is

$$\begin{aligned} \boldsymbol{v} &= \frac{e\boldsymbol{E}_0}{m\sqrt{\omega^2+\nu_m^2}} \cos(\omega t+\varphi) \,, \quad \varphi = \arctan\frac{\nu_m}{\omega} \,, \\ \boldsymbol{r} &= \frac{e\boldsymbol{E}_0}{m\omega\sqrt{\omega^2+\nu_m^2}} \sin(\omega t+\varphi) \,. \end{aligned} \tag{3.4}$$

The amplitudes of displacement and velocity of the electron are less by a factor of $\sqrt{1+\nu_m^2/\omega^2}$ than those for free oscillations. The higher the effective collision frequency ν_m, the smaller they are (ν_m is determined by the velocity of random motion, which is much greater in discharges than the oscillation velocity; see Sect. 3.2). The displacement is shifted in phase relative to the field, the phase shift increasing from 0 to $\pi/2$ as the relative role of collisons ν_m/ω increases from 0 to ∞.

The oscillation displacement and velocity (3.4) can always be resolved into two components, one proportional to the magnitude of the field $\boldsymbol{E} = \boldsymbol{E}_0 \sin\omega t$, and the other to its rate of change, $\dot{\boldsymbol{E}} = \omega\boldsymbol{E}_0 \cos\omega t$:

$$\begin{aligned} \boldsymbol{r} &= \frac{e\boldsymbol{E}_0}{m(\omega^2+\nu_m^2)} \sin\omega t + \frac{\nu_m}{\omega}\frac{e\boldsymbol{E}_0}{m(\omega^2+\nu_m^2)} \cos\omega t \,, \\ \boldsymbol{v} &= \frac{\omega e\boldsymbol{E}_0}{m(\omega^2+\nu_m^2)} \cos\omega t - \frac{\nu_m e\boldsymbol{E}_0}{m(\omega^2+\nu_m^2)} \sin\omega t \,. \end{aligned} \tag{3.5}$$

The ratio of the components is determined by the relative role of collisions and is unambiguously related to the phase shift φ. This form of presenting the solution adds visual clarity to the results of the subsequent sections.

Expressions (3.4,5) show that the role of collisions is characterized by the ratio of the effective frequency ν_m and the circular frequency of the field $\omega = 2\pi f$, which is greater than the frequency f by nearly an order of magnitude.[1] In the limit $\nu_m^2 \ll \omega^2$, formulas (3.4,5) are close to (3.1) for free oscillations. To illustrate numerical values, consider an example of microwave radiation at frequency $f = 3\,\mathrm{GHz}$; $\lambda = 10\,\mathrm{cm}$, $\omega = 1.9 \times 10^{10}\,\mathrm{s}^{-1}$. Let $p \approx 1\,\mathrm{Torr}$, then $\nu_m \approx 3 \times 10^9\,\mathrm{s}^{-1} \ll \omega$; $E_0 = 500\,\mathrm{V/cm}$, roughly corresponding to the threshold

[1] When the degree of spatial uniformity of the field is evaluated, the displacement amplitude must be compared not with wavelength $\lambda = c/f$, but with $\lambda\!\!\!^{-} = \lambda/2\pi$: $a/\lambda\!\!\!^{-} = e E_0/m\omega^2 \lambda\!\!\!^{-} = u/c$.

of microwave breakdown at such pressures. Formulas (3.2) show that $a = 2.5 \times 10^{-3}$ cm, $u = 4.7 \times 10^7$ cm/s. We find that $a \ll \lambda = 1.6$ cm, that is, the field in the electromagnetic wave is "uniform".

3.1.3 Drift Oscillations

In the limit of very frequent collisions or relatively low frequencies, $\nu_m^2 \gg \omega^2$, the oscillation velocity drops to

$$\boldsymbol{v} \approx -\frac{e\boldsymbol{E}_0}{m\nu_m} \sin\omega t = -\frac{e\boldsymbol{E}(t)}{m\nu_m} = -\mu_e \boldsymbol{E}(t) = \boldsymbol{v}_d(t) \,. \tag{3.6}$$

At each moment of time, the oscillation velocity coincides with the drift velocity that corresponds to the field vector at this moment. For brevity, we refer to such oscillations in the *mobility regime* as *drift oscillations*.

An electron behaves as it would in a constant field, responding to relatively slow changes of the field. Its displacement,

$$\boldsymbol{r} \approx \boldsymbol{A}\cos\omega t \,, \quad \boldsymbol{A} = \frac{e\boldsymbol{E}_0}{m\nu_m\omega} = \frac{\mu_e \boldsymbol{E}_0}{\omega} \,, \tag{3.7}$$

has an amplitude A less than that of free oscillations in the same field by a factor of $\nu_m/\omega \gg 1$.

The oscillations of electrons in rf fields (and of course, at lower frequencies) are of drift type. For example, the collision frequency at $f \approx 10$ MHz, $\nu_m \approx 3 \times 10^9\, p\,\mathrm{s}^{-1}$, exceeds $\omega \sim 10^8\,\mathrm{s}^{-1}$ even at fairly low pressures of $p \sim 0.03$ Torr. In order to maintain a low-pressure, weakly ionized plasma by an rf field, one usually needs the values of E_0/p of the same order as E/p in a constant field. Therefore, at $f \approx 10$ MHz and $E_0/p \approx 10\,\mathrm{V/(cm \cdot Torr)}$, we have $A \sim 0.1$ cm regardless of pressure.

3.2 Electron Energy

3.2.1 Collisionless Motion

If collisions do not occur, the field does no work, on the average, on an electron; indeed, (3.1) implies that

$$\langle -e\boldsymbol{E} \cdot \boldsymbol{v} \rangle = -\frac{eE_0^2}{m\omega} \langle \sin\omega t \cos\omega t \rangle - e\boldsymbol{E}_0 \cdot \boldsymbol{v}_0 \langle \sin\omega t \rangle = 0 \,,$$

where angle brackets denote time averaging.

The electric field pumps up the motion of the electron only once, when it is switched on; then the electron's energy $mv^2/2$ pulsates but remains unchanged on the average. The time averaged energy $\langle mv^2/2 \rangle$ is made up of the energy of translational motion $mv_0^2/2$, corresponding to the mean velocity $\boldsymbol{v}_0 = \langle \boldsymbol{v}(t) \rangle$, and that of oscillations. In the case of free oscillations, the latter energy is

$$\varepsilon_{\text{fr.osc.}} = \frac{e^2 E_0^2}{4m\omega^2} = mu^2/4 \,. \tag{3.8}$$

In the example given at the end of Sect. 3.1.2, $f = 3\,\text{GHz}$, $E_0 = 500\,\text{V/s}$, and the oscillation energy $\varepsilon_{\text{fr.osc.}} = 0.31\,\text{eV}$, which is much less than the mean energy of random motion (1–10 eV) necessary to sustain a discharge. The absence of collisions thus means no dissipation of the energy of the field and no deposition of energy in the matter.

3.2.2 Gaining of Energy From the Field

The collisions lead to a net transfer of energy to the electrons, via the electric field. According to (3.5), the mean work per unit time that the field performs on an electron,

$$\langle -e\boldsymbol{E} \cdot \boldsymbol{v} \rangle = \frac{e^2 E_0^2}{2m(\omega^2 + \nu_\text{m}^2)} \nu_\text{m} = \Delta\varepsilon_\text{E} \nu_\text{m} \,, \tag{3.9}$$

is determined by that component of velocity that oscillates in phase with the field and is proportional to ν_m. The term shifted in phase by $\pi/2$ does no work, on the average, over one period. The random motion is not associated with any transfer of energy. In one effective collision an electron gains the mean energy $\Delta\varepsilon_E$, equal to twice the mean kinetic energy of oscillations:

$$\Delta\varepsilon_E = \frac{e^2 E_0^2}{2m(\omega^2 + \nu_\text{m}^2)} = 2\left\langle \frac{m\boldsymbol{v}^2}{2} \right\rangle = 2\varepsilon_\text{osc} \,. \tag{3.10}$$

This result can be given the following interpretation. In the interval between two collisions, the electric field imparts to an electron an average kinetic energy ε_osc. If the electron goes through a large number of oscillations in this period, then ε_osc is of the order of the free oscillation energy (3.8). An act of elastic scattering of an electron by an atom sharply changes the direction of motion but leaves the absolute value of velocity unaltered. Then the field starts swinging the electron in a new direction with respect to its velocity, that is, imparts to it an energy of order ε_osc as if anew. The mean amount of energy gained from the field in each scattering event following the preceding collision is thus transformed into the energy of translational random motion. Microscopically, the field does work on overcoming the friction due to collisions of the electron. Everything proceeds as in a constant field (see Sect. 2.3.2), but the role of the drift energy is played by that of oscillations.

3.2.3 Balancing of the Electron Energy

The balance is made up of gaining energy from the field and transferring it to heavy particles as a result of elastic and inelastic losses. If an electron loses in each collision a fraction δ of its energy ε, then

$$\frac{d\varepsilon}{dt} = (\Delta\varepsilon_E - \delta\varepsilon)\nu_\text{m} = \left[\frac{e^2 E^2}{m(\omega^2 + \nu_\text{m}^2)} - \delta\varepsilon\right] \nu_\text{m} \,, \tag{3.11}$$

where the amplitude E_0 is replaced with the mean-square field E defined by the equality $E^2 = \langle E^2(t)\rangle = E_0^2/2$. If $\omega^2 \ll \nu_m^2$, then (3.11) transforms into (2.12). In the $\omega \to 0$ limit, the R.M.S. of E plays the role of a constant field.

3.2.4 Mean Equilibrium Energy

The mean energy reached by electrons under stationary conditions, when they transfer the entire energy gained from the field, is

$$\bar{\varepsilon} = \Delta\varepsilon_E/\delta = 2\varepsilon_{osc}/\delta = e^2E^2/m\delta\left(\omega^2 + \nu_m^2\right) . \tag{3.12}$$

Low-frequency fields ($\omega^2 \ll \nu_m^2$) behave indistinguishably from constant fields; the similarity $\bar{\varepsilon} = f(E/p)$ holds. At high frequencies, $\omega^2 \gg \nu_m^2$, the mean electron energy is independent of ν_m, p, and the similarity in field frequency holds: $\bar{\varepsilon} = f_1(E/\omega)$. If $\delta = \text{const}$, $\bar{\varepsilon} \propto (E/\omega)^2$. In equivalent situations, $E \propto \omega$. This is the reason why gas breakdown at optical frequencies ($\omega \sim 10^{15}\,\text{s}^{-1}$) requires enormous fields ($E \sim 10^7\,\text{V/cm}$) in the light wave, realizable only when giant laser pulses are focused (Sect. 7.6). Indeed, electron avalanches can develop only if the electron energies are of the order of 10 eV.

3.2.5 Actual Change in Electron Energy in a Collision

The situation in ac fields is also similar in this respect to that found in dc fields (Sect. 2.3.3). An electron may either gain energy from the field or lose energy to it, in amounts that much exceed the mean change $\Delta\varepsilon_E$ averaged over a large number of collisions. The relative directions of the motion and the field and the phase of field oscillations at the moment of collision decide whether the electron is to gain or lose energy. This is a fact of fundamental importance, which contains a classical analogue of such purely quantum phenomena as the *true absorption* and *stimulated emission* of photons.

To illustrate this, we calculate directly the change in the energy of an electron in a collision. Let an electron undergo its most recent collision at a moment t_1 and have, immediately after scattering, a velocity $\boldsymbol{v}_1$ and energy $\varepsilon_1 = mv_1^2/2$. Effective collisions occurring at a frequency ν_m each time give the velocity a completely random direction; hence, ε_1 is the energy of random motion at the moment of collision t_1. In the time $t \geq t_1$ and until the next collision, the electron is driven by the force $-e\boldsymbol{E}_0 \sin\omega t$ at a velocity $\boldsymbol{v}(t) = \boldsymbol{u}(\cos\omega t - \cos\omega t_1) + \boldsymbol{v}_1$, $\boldsymbol{u} = e\boldsymbol{E}_0/m\omega$. Its energy $\varepsilon = mv^2/2$ at each moment of this period is

$$\varepsilon(t) = \frac{m}{2}\left[v_1^2 + 2\boldsymbol{v}_1\boldsymbol{u}\left(\cos\omega t - \cos\omega t_1\right) + u^2\left(\cos^2\omega t - 2\cos\omega t\cos\omega t_1 + \cos^2\omega t_1\right)\right] .$$

At the moment t_2 of the next collision, the velocity is again directed in an arbitrary direction but remains virtually unchanged in magnitude. The electron resumes motion at an energy $\varepsilon(t_2)$, which is also the energy of random motion. Therefore, between two collisions the random-motion energy changes by

$$\Delta\varepsilon(t_1, t_2) = \varepsilon(t_2) - \varepsilon_1 \approx m\boldsymbol{v}_1 \cdot \boldsymbol{u}\left(\cos\omega t_2 - \cos\omega t_1\right) .$$

This last (approximate) transition takes into account that the random-motion velocity v_1 is much greater than the oscillation velocity u; hence, we can ignore the specific form of the small term of order mu^2.

For the sake of simplicity, assume that collisions are rare: $\nu_m \ll \omega$. Then many oscillations occur in the time $t_2 - t_1$ between two collisions, and the correlation between the field phases at the moments of collisions ωt_1 and ωt_2 vanishes owing to the random nature of collisions, i.e., the phases may be arbitrary. The value of $\Delta\varepsilon$ then varies in this interval from the maximum gain $\Delta\varepsilon_+ = 2mv_1u$ and the maximum loss $\Delta\varepsilon_- = -2mv_1u$, the extremal values corresponding to parallel velocities $\boldsymbol{v}_1$ and $\boldsymbol{u}$ and certain phases, ωt_1, ωt_2. When averaged over many collisions, however, that is, over moments t_1 and t_2, an electron gains the energy

$$\Delta\varepsilon_E = \langle \Delta\varepsilon(t_1, t_2)\rangle_{t_1, t_2} = mu^2/2 = 2\varepsilon_{\text{fr.osc.}}$$

which we found above by calculating the mean work done by the field.[2] Since $u/v \ll 1$, the actual changes that the electron energy experiences in collisions, be they positive or negative, are of first order of smallness in u/v, $|\Delta\varepsilon_\pm|/\varepsilon \sim u/v$, while the resulting positive $\Delta\varepsilon_E/\varepsilon \sim (u/v)^2$ is of second order. This latter quantity is a small difference of two relatively large ones; in symbolic form, $\Delta\varepsilon_E \sim (\Delta\varepsilon_+ - |\Delta\varepsilon_-|)$.

3.2.6 Why Electron-Electron Collisions Do not Dissipate the Energy of the Field

Electrons of a weakly ionized gas collide with atoms and molecules. In a strongly ionized gas they collide with ions and other electrons with nearly equal frequency. However, only electron-ion collisions need to be taken into account in considering the effects of the interaction with the field.

To reveal the reason, consider an electron gas (an even more general case can be taken: a gas of particles with an identical e/m ratio) and assume that electrons collide only with electrons. Sum up over all electrons the equation of motion $m\dot{\boldsymbol{v}} = -e\boldsymbol{E}_0 \sin\omega t + \dot{\boldsymbol{p}}_{\text{col}}$, where $\dot{\boldsymbol{p}}_{\text{col}}$ is the rate of change of an electron's momentum due to collisions. As the total momentum of interacting particles is conserved, the total momentum $\sum m\boldsymbol{v}$ of the gas oscillates as $\cos\omega t$, with a $\pi/2$ phase shift. Recalling that the total energy of particles is also conserved under elastic collisions, we can find the rate of change of the gas energy:

$$\frac{d}{dt}\sum\frac{mv^2}{2} = \sum m\boldsymbol{v}\cdot\boldsymbol{v}^2 = -\left(\frac{e}{m}\boldsymbol{E}_0\sin\omega t\right)\left(\sum m\boldsymbol{v}\right)$$
$$\propto \sin\omega t\cos\omega t \propto \sin 2\omega t\,.$$

[2] In the general case of $\nu_m \sim \omega$, only one of the phases is arbitrary because the moments of consecutive collisions are correlated. The probability of the interval $t_2 - t_1$ is $\exp[-\nu_m(t_2 - t_1)]\nu_m dt_2$. Correlations add an additional factor to $\Delta\varepsilon_E$ of (3.10): $\omega^2/(\omega^2 + \nu_m^2)$ [3.1].

The total energy of particles oscillates at double frequency, as in collisionless motion, and remains unchanged on average. No dissipation of the field energy occurs. Recall that electron-electron collisions in a dc field do not contribute to resistance and Joule heat release (Sect. 2.2.3), though as in dc fields, electron-electron collisions may affect dissipation indirectly, by changing the electron energy distribution and ν_m.

3.3 Basic Equations of Electrodynamics of Continuous Media

Sections 3.1 and 3.2 outlined what happens with electrons of an ionized gas placed in an ac electric field. Let us turn to a different aspect of the electron-field interaction: the effect of the ionized state on the behavior of ac fields and the propagation of electromagnetic waves.

3.3.1 Maxwell's Equations

The electromagnetic field and the state of the medium are described in terms of field strengths $\boldsymbol{E}$, $\boldsymbol{H}$ and inductions $\boldsymbol{D}$, $\boldsymbol{B}$. By definition, $\boldsymbol{D} = \boldsymbol{E} + 4\pi\boldsymbol{P}$ and $\boldsymbol{B} = \boldsymbol{H} + 4\pi\boldsymbol{M}$, where $\boldsymbol{P}$ and $\boldsymbol{M}$ are the electric and magnetic moments, respectively, per unit volume. The vectors $\boldsymbol{E}$, $\boldsymbol{H}$, $\boldsymbol{D}$, $\boldsymbol{B}$ satisfy the system of Maxwell's equations:

$$\operatorname{curl} \boldsymbol{H} = \frac{4\pi}{c}\boldsymbol{j} + \frac{1}{c}\frac{\partial \boldsymbol{D}}{\partial t}\,, \tag{3.13}$$

$$\operatorname{curl} \boldsymbol{E} = -\frac{1}{c}\frac{\partial \boldsymbol{B}}{\partial t}\,, \tag{3.14}$$

$$\operatorname{div} \boldsymbol{B} = 0\,, \tag{3.15}$$

$$\operatorname{div} \boldsymbol{D} = 4\pi\varrho\,. \tag{3.16}$$

This system is not completely closed because the electric current $\boldsymbol{j}$, polarization $\boldsymbol{P}$, and magnetization $\boldsymbol{M}$ generated by the field, depend on material properties. Both experience and theory indicate that direct proportionality reigns in constant fields and fields that vary not too rapidly: $\boldsymbol{j} = \sigma\boldsymbol{E}$, $\boldsymbol{P} = \chi_e\boldsymbol{E}$, $\boldsymbol{M} = \varkappa\boldsymbol{H}$. Instead of the electric χ_e and magnetic susceptibility $\varkappa$, one introduces the permittivity $\varepsilon = 1 + 4\pi\chi_e$ and magnetic permeability $\mu = 1 + 4\pi\varkappa$. Together with the equations

$$\boldsymbol{j} = \sigma\boldsymbol{E}\,, \quad \boldsymbol{D} = \varepsilon\boldsymbol{E}\,, \quad \boldsymbol{B} = \mu\boldsymbol{H}\,, \tag{3.17}$$

where the material constants ε, μ and conductivity σ are assumed to be known, system (3.13–17) is closed. In gases and plasmas, the approximation $\mu = 1$ can be used with extremely high accuracy.

3.3.2 Displacement, Polarization, Conduction, and Charge Currents

The right-hand side of (3.13) can be treated as a current density

$$\boldsymbol{j} + \frac{1}{4\pi}\frac{\partial \boldsymbol{D}}{\partial t} = \boldsymbol{j} + \frac{\partial \boldsymbol{P}}{\partial t} + \frac{1}{4\pi}\frac{\partial \boldsymbol{E}}{\partial t}\,, \tag{3.18}$$

times $4\pi/c$. Maxwell called the term $(1/4\pi)\partial \boldsymbol{D}/\partial t$, which he postulated should be added to the conduction current, the *displacement current*. Without the displacement current, (3.13, 16) contradict the unassailable law of charge conservation, (2.39).

A variable field changes the polarization of matter with time, namely, displaces negative charges relative to positive ones by applying the electric force. In fact, any displacement of charges in space is a current, so that the term $\partial \boldsymbol{P}/\partial t$ in the displacement current is indeed a current density: that of the *polarization current*. Together with the conduction current $\boldsymbol{j}$, it forms the total charge current $\boldsymbol{j}_t$. The term $(1/4\pi)\partial \boldsymbol{E}/\partial t$ is in no way connected with the motion of charge and therefore, is not literally a current. (Its meaning will be discussed in Sect. 13.5.)

The total charge current was divided into the conduction and polarization components only to facilitate the application of the equations to ideal dielectrics, where $\sigma, \boldsymbol{j} = 0$. This partition is by no means mandatory. The total polarization vector $\boldsymbol{P}_t$ can be defined for any electrically neutral medium; $\boldsymbol{P}_t$ is related to the total charge current $\boldsymbol{j}_t$, so that it is sufficient to operate with just one of these quantities. Indeed, by definition

$$\boldsymbol{P}_t = \sum e_i \boldsymbol{r}_i\,, \quad \sum e_i = 0\,, \quad \boldsymbol{j}_t = \sum e_i \boldsymbol{v}_i = \frac{\partial \boldsymbol{P}_t}{\partial t}\,, \tag{3.19}$$

where $\boldsymbol{r}_i$ is the radius vector of the charge e_i, $\boldsymbol{v}_i = \dot{\boldsymbol{r}}_i$ is its velocity, and summation is extended to absolutely all charges (free, bound, electrons, nuclei) within a unit volume.

3.3.3 Expansion into Harmonics

Equations (3.17) fail in rapidly varying fields. Owing to the inertia of the processes that produce polarization and current, they cease to track the variations of the field. The polarization and current at t_1 are now determined less by the value of $\boldsymbol{E}(t_1)$ than by the evolution of $\boldsymbol{E}(t)$ in the preceding period $t < t_1$. For instance, if the field $\boldsymbol{E}$ pointed for a long time in one direction and then was suddenly reversed, the current would flow for some time in the former direction, against the new field, until the charges are brought to rest.

Obtaining the material equations (like $\boldsymbol{D} = \varepsilon \boldsymbol{E}$) that take into account retardation effects is greatly facilitated because the motion of charges in matter is described by equations linear in $\boldsymbol{E}$, $\boldsymbol{r}$, $\boldsymbol{v}$. Since Maxwell's equations are also linear, all time-dependent quantities can be expanded into Fourier series or integrals; in view of the superposition principle, one can operate only with harmonic components, as we have already done in Sects. 3.1, 2. Three parameters completely determine the evolution of harmonic quantities: amplitude, frequency, and phase, so that the entire retardation effect is contained in the relation between these parameters for material characteristics and the field. If the field for some harmonic is $\boldsymbol{E}_\omega = \boldsymbol{E}_{\omega 0} \sin \omega t$, then the total current is $\boldsymbol{j}_{t\omega} = \boldsymbol{j}_{t\omega 0} \sin(\omega t + \varphi_\omega)$, with $\boldsymbol{j}_{t\omega 0}$ and φ_ω being the functions of $\boldsymbol{E}_{\omega 0}$ and ω.

3.3.4 Material Equations for Harmonic Components

These can be given a convenient and lucid form if we retain the concepts of conductivity and dielectric permittivity, which are familiar from working with constant fields. The total current $\boldsymbol{j}_{t\omega}$ is given by a linear combination of $\sin\omega t$ and $\cos\omega t$, which corresponds to a linear combination of $\boldsymbol{E}$ and $\partial\boldsymbol{E}/\partial t$. Returning to the original concepts of conduction current $\sigma\boldsymbol{E}$ and polarization current $\partial\boldsymbol{P}/\partial t$, which is equal to $[(\varepsilon-1)/4\pi]\partial\boldsymbol{E}/\partial t$ if the field varies slowly, and equipping the new coefficients σ and ε with the subscript ω (because now they are frequency-dependent), we rewrite the material equation in the form

$$\boldsymbol{j}_{t\omega} = \sigma_\omega \boldsymbol{E}_\omega + \frac{\varepsilon_\omega - 1}{4\pi}\frac{\partial \boldsymbol{E}_\omega}{\partial t}\,, \quad \boldsymbol{E}_\omega = \boldsymbol{E}_{\omega_0}\sin\omega t\,. \tag{3.20}$$

The quantities σ_ω and ε_ω are called the *high-frequency conductivity* and *dielectric permittivity* of the medium. It is these characteristics of the medium that affect the behavior of variable fields in it.

3.3.5 Energy Equation

We now form the scalar products of (3.13) with $\boldsymbol{E}$ and of (3.14) with $\boldsymbol{H}$, and subtract the resulting equations from each other. In view of the fact that $\boldsymbol{H}\,\mathrm{curl}\,\boldsymbol{E} - \boldsymbol{E}\,\mathrm{curl}\,\boldsymbol{H} = \mathrm{div}[\boldsymbol{E}\times\boldsymbol{H}]$, assuming the relations between $\boldsymbol{D}$ and $\boldsymbol{E}$, $\boldsymbol{B}$ and $\boldsymbol{H}$ are linear, we obtain the relation

$$\frac{\partial}{\partial t}\frac{\boldsymbol{E}\cdot\boldsymbol{D} + \boldsymbol{H}\cdot\boldsymbol{B}}{8\pi} + \mathrm{div}\frac{c}{4\pi}[\boldsymbol{E}\times\boldsymbol{H}] = -\boldsymbol{j}\cdot\boldsymbol{E}\,. \tag{3.21}$$

This formula expresses the law of conservation of energy of the electromagnetic field. The quantity $\boldsymbol{E}\cdot\boldsymbol{D}/8\pi$ is the electric energy density, and $\boldsymbol{H}\cdot\boldsymbol{B}/8\pi$ is that of magnetic energy;

$$\boldsymbol{S} = \frac{c}{4\pi}[\boldsymbol{E}\times\boldsymbol{H}] \tag{3.22}$$

is the electromagnetic energy flux density (Poynting vector); and $\boldsymbol{j}\cdot\boldsymbol{E}$ is the energy released per second in $1\,\mathrm{cm}^3$ of the medium, equal to the decrease in electromagnetic energy. As a time average, the dissipation of energy in harmonic fields in a plasma is caused only by the conduction current. The polarization current does not result in dissipation because it is shifted by $\pi/2$ with respect to the field, and $\langle\sin\omega t\cos\omega t\rangle = 0$ (cf. the results of Sects. 3.2.1, 2).

3.4 High-Frequency Conductivity and Dielectric Permittivity of Plasma

The results of Sect. 3.1 permit the immediate calculation of these quantities, but two qualifications will be made first. We assume that ions do not move and make a negligible contribution to conduction and polarization currents. Next, we

single out the term $\varepsilon_M - 1$ in $\varepsilon_\omega - 1$ due to the electrons bound in molecules and ions. This term is of the same order of magnitude as in nonionized gases (unless the polarizability of the excited molecules in the plasma is greater than that of nonexcited ones). Under normal conditions, $\varepsilon_M - 1 = 5.28 \times 10^{-4}$ in air, 2.65×10^{-4} in H_2, and 0.67×10^{-4} in He; it is even smaller at low pressure because $\varepsilon_M - 1$ is proportional to density. These figures refer to the visible part of the spectrum and to lower frequencies. The contribution of the molecular part to the bulk polarizability of plasma is very small for any appreciable ionization.

3.4.1 Calculation of σ_ω and ε_ω

First we substitute the general expression (3.5) of the mean electron velocity v into (3.19) for the charge current j_t. Replacing the summation over all electrons with the multiplication by n_e (the term with random velocity vanishes upon averaging) and comparing the obtained expression with (3.20), we find:

$$\sigma_\omega = e^2 n_e \nu_m / m \left(\omega^2 + \nu_m^2\right) , \tag{3.23}$$

$$\varepsilon_\omega = 1 - 4\pi e^2 n_e / m \left(\omega^2 + \nu_m^2\right) . \tag{3.24}$$

These formulas are of fundamental importance for the physics of interaction between plasma and electromagnetic fields. The ratio of the amplitudes of conduction and polarization currents,

$$\frac{j_{\text{cond},0}}{j_{\text{polar},0}} = \frac{4\pi\sigma_\omega}{\omega|\varepsilon_\omega - 1|} = \nu_m/\omega , \tag{3.25}$$

is determined by the ratio of collision and field frequencies.

3.4.2 The High-Frequency Limit (Collisionless Plasma)

This regime is reached when $\omega^2 \gg \nu_m^2$, that is, at not particularly high frequencies, i.e., the microwave or very far IR range, even at atmospheric pressure. In fact, the molecular polarizability of most dielectrics and nonionized gases retains the value typical for dc fields up to optical frequencies. In the high-frequency limit,

$$\sigma_\omega = \frac{e^2 n_e}{m\omega^2}\nu_m , \quad \varepsilon_\omega = 1 - \frac{4\pi e^2 n_e}{m\omega^2} , \tag{3.26}$$

that is, conductivity is proportional to collision frequency, while dielectric permittivity is independent of ω. According to (3.25), the conduction current is small compared with the polarization current. This limit corresponds to the collisionless plasma model (Sects. 3.1, 3.2.1).

3.4.3 Static Limit

If $\omega^2 \ll \nu_m^2$, then

$$\sigma_\omega = \frac{e^2 n_e}{m\nu_m} , \quad \varepsilon_\omega = 1 - \frac{4\pi e^2 n_e}{m\nu_m^2} . \tag{3.27}$$

The conductivity is indistinguishable from the ordinary dc conductivity of the ionized gas. The dielectric permittivity also reaches a value independent of frequency. The polarization current is small in comparison with the conduction current, and vanishes completely in the limit $\omega \to 0$.

3.4.4 Why Dielectrics Usually Have $\varepsilon > 1$, and Plasma $\varepsilon < 1$

Electrons in atoms and molecules are bound, while in plasmas (and metals, where also $\varepsilon < 1$) some of them are free. An absolutely free electron, moving without collisions, oscillates in phase with the field [see (3.1)]. It shifts away from the center of equilibrium along $\boldsymbol{E}$, against the direction of the electric force; having a negative charge, it induces the negative polarizability of the medium, so that $\varepsilon < 1$.

Electrons in molecules are like particles that feel an elastic restoring force in response to displacement. If ω_0 is the frequency of natural vibrations of an elastically bound electron, then

$$\ddot{\boldsymbol{r}} + \omega_0^2 \boldsymbol{r} = -\frac{e\boldsymbol{E}_0}{m} \sin \omega t \,, \quad \boldsymbol{r} = -\frac{e\boldsymbol{E}_0}{m(\omega_0^2 - \omega^2)} \sin \omega t \,.$$

The displacement in a static field and at frequencies less than the natural frequency (the latter usually lie in the optical range) is directed against $\boldsymbol{E}$, so that polarizability is positive (the situation at $\omega > \omega_0$ is reversed; this results in the anomalous dispersion of light). In solid and liquid dielectrics ε has usually a value between 1 and 10.

3.5 Propagation of Electromagnetic Waves in Plasmas

In ideal dielectrics, where the conduction current is zero and free charges are absent, the system of Maxwell's equations yields equations for $\boldsymbol{E}$ and $\boldsymbol{H}$ that describe the propagation of electromagnetic waves. Similar equations are obtained for a monochromatic field in an electrically neutral conducting medium such as a plasma. The simplest way to do this is to represent harmonic quantities in complex form. In general, this is expedient in the presence of phase shifts, because it removes the need to operate constantly with combinations of sines and cosines.

3.5.1 Complex Dielectric Permittivity

In the case of a monochromatic field [$\boldsymbol{E}$, $\boldsymbol{H} \propto \exp(-\mathrm{i}\omega t)$], the first Maxwell equaiton (3.13), taken together with the material equation (3.20), transforms to

$$\operatorname{curl} \boldsymbol{H} = (4\pi/c)\sigma \boldsymbol{E} - \mathrm{i}(\omega\varepsilon/c)\boldsymbol{E} \,, \quad \sigma \equiv \sigma_\omega \,, \quad \varepsilon \equiv \varepsilon_\omega \tag{3.28}$$

(hereafter we drop the subscript ω with σ_ω, ε_ω). It is convenient to eliminate the conduction current in (3.28), introducing the complex dielectric permittivity

$$\varepsilon' = \varepsilon + \mathrm{i}4\pi\sigma/\omega \,. \tag{3.29}$$

The resulting equation,

$$\text{curl}\, \boldsymbol{H} = -\mathrm{i}(\omega\varepsilon'/c)\boldsymbol{E}\,, \tag{3.30}$$

is apparently identical to the corresponding equation for dielectrics, where $\sigma = 0$, $\varepsilon' = \varepsilon$.

3.5.2 Plane Electromagnetic Wave

First we substitute $\partial \boldsymbol{B}/\partial t = -\mathrm{i}\omega \boldsymbol{H}$ into (3.14) and take the curl of the resulting equation, using the formula $\text{curl}\,(\text{curl}\,\boldsymbol{E}) = -\Delta \boldsymbol{E} + \text{grad}(\text{div}\,\boldsymbol{E})$, remarking that for $\varrho = 0$ (3.16) implies that $\text{div}\,\boldsymbol{E} = 0$, and replacing $\text{curl}\,\boldsymbol{H}$ with (3.30), we arrive at the equation

$$\Delta \boldsymbol{E} + \left(\varepsilon'\omega^2/c^2\right)\boldsymbol{E} = 0\,. \tag{3.31}$$

In fact, this is a result of substituting $\exp(-\mathrm{i}\omega t)$ for $\boldsymbol{E}$ into the wave equation. Eliminating $\boldsymbol{E}$, instead of $\boldsymbol{H}$, from (3.13, 14) and using (3.15), we obtain for $\boldsymbol{H}$ an equation similar to (3.31). Equation (3.31) admits a travelling-wave type solution, $\boldsymbol{E}$, $\boldsymbol{H} \propto \exp(-\mathrm{i}\omega t + \mathrm{i}\boldsymbol{k}\cdot\boldsymbol{r})$, where $\boldsymbol{k}$ is the wave vector. The pre-exponential coefficients are certain complex numbers that characterize the amplitudes of the fields and the phase shifts between them. Substitution of these expressions into the original equations (3.13) or (3.30) and (3.14) yields

$$[\boldsymbol{k} \times \boldsymbol{H}] = -(\omega\varepsilon'/c)\boldsymbol{E}\,, \quad [\boldsymbol{k} \times \boldsymbol{E}] = (\omega/c)\boldsymbol{H}\,. \tag{3.32}$$

These equalities imply that if $\varepsilon' \neq 0$, all three vectors $\boldsymbol{E}$, $\boldsymbol{H}$, and $\boldsymbol{k}$ are mutually perpendicular, that is, the wave is transverse. If $\varepsilon' = 0$ (meaning that $\varepsilon = 0$ in weakly conducting media, where $\sigma \approx 0$), the equations admit the existence of longitudinal purely electric waves with $\boldsymbol{H} = 0$, $\boldsymbol{E} \| \boldsymbol{k}$: these are the plasma waves (see Sect. 3.6.3).

3.5.3 Refractive Index and Attenuation of Waves

Equations (3.32) imply that the wave vector is a function of frequency (the dispersion relation) and give a relation between the complex amplitudes of the fields,

$$k = (\omega/c)\sqrt{\varepsilon'}\,, \quad H = \sqrt{\varepsilon'}E\,. \tag{3.33}$$

The wave vector is a complex quantity because ε' is complex. In order to find $k = k_1 + \mathrm{i}k_2$, we introduce the dimensionless numbers n and $\varkappa$ via the formula $ck/\omega = n + \mathrm{i}\varkappa = \sqrt{\varepsilon'}$. Squaring this quantity, substituting ε' from (3.29), and equating the real and imaginary parts, we find that

$$n^2 - \varkappa^2 = \varepsilon\,, \quad 2n\varkappa = 4\pi\sigma/\omega\,,$$
$$n = \sqrt{\frac{\varepsilon + \sqrt{\varepsilon^2 + (4\pi\sigma/\omega)^2}}{2}}\,, \quad \varkappa = \sqrt{\frac{-\varepsilon + \sqrt{\varepsilon^2 + (4\pi\sigma/\omega)^2}}{2}}\,. \tag{3.34}$$

The physical meaning of the quantities n and $\varkappa$ follows from the expression for the travelling wave:

$$E,\, H \propto \mathrm{e}^{-\mathrm{i}\omega t + \mathrm{i}kx} = \exp\left[-\mathrm{i}\omega\left(t - n\frac{x}{c}\right) - \varkappa\frac{\omega}{c}x\right] .$$

The number n determines the *phase velocity* c/n and wavelength $\lambda = \lambda_0/n$ in the medium ($\lambda_0 = 2\pi c/\omega$ is the wavelength in vacuum) and corresponds to the *refractive index*. The number $\varkappa$ characterizes the *attenuation* of the wave: its amplitude is reduced by a factor e over the path length $\Delta x = \lambda_0/2\pi\varkappa$ or by a factor $\mathrm{e}^{\varkappa}$ over a path length λ_0. The numbers n and $\varkappa$ determine the relation between the amplitudes of the field and the phase shift between them:

$$H = (n + \mathrm{i}\varkappa)E = \sqrt{n^2 + \varkappa^2}\,\mathrm{e}^{\mathrm{i}\psi}E\,, \quad \psi = \arctan(\varkappa/n) .$$

3.5.4 The Law of Attenuation of the Energy Flux

Only the value of the energy flux density averaged over one period is of practical importance. In order to calculate the mean value of two harmonic variables given in complex form, we have to multiply one variable by the complex conjugate of the other and divide by two.[3] In a homogeneous medium, the energy flux of a wave decays exponentially,

$$S = \frac{c}{4\pi}\frac{1}{2}\mathrm{Re}\{EH^*\} = \frac{cn}{8\pi}EE^* = \frac{cn}{8\pi}|E(0)|^2\,\mathrm{e}^{-\mu_\omega x}\,, \tag{3.35}$$

where the averaging subscript with S is dropped, $E(0)$ is the amplitude at the point $x = 0$, and

$$\mu_\omega = 2\varkappa\omega/c = 4\pi\sigma/nc \tag{3.36}$$

is the absorption coefficient. The energy flux decreases by a factor e over the length μ_ω^{-1}.

It follows from (3.35) and also from the general equation for energy (3.21), that if (3.35) is averaged over one period of time, the Bouguer law is valid:

$$\frac{dS}{dx} = -\mu_\omega S\,. \tag{3.37}$$

The electromagnetic energy dissipated per second in 1 cm^3 (the energy deposited in the medium) is $\langle \boldsymbol{j}\cdot\boldsymbol{E}\rangle = \sigma\langle E^2\rangle = \mu_\omega S$. The proportionality between the absorption coefficient and conductivity is in perfect agreement with the proportionality of the rate of Joule heat release to the conductivity of the medium.

---

[3] Indeed, if $A = A_0\cos(\omega t + \varphi_A)$ and $B = B_0\cos(\omega t + \varphi_B)$, then $\langle AB\rangle = (1/2)A_0B_0\cdot\cos(\varphi_B - \varphi_A)$. In the complex representation, $A = A_0\exp(-\mathrm{i}\omega t + \mathrm{i}\varphi_A)$ and $B = B_0\exp(-\mathrm{i}\omega t + \mathrm{i}\varphi_B)$. Hence,

$$\tfrac{1}{2}\mathrm{Re}\{AB^*\} = \tfrac{1}{2}A_0B_0\,\mathrm{Re}\{\exp[-\mathrm{i}(\varphi_B - \varphi_A)]\} = \tfrac{1}{2}A_0B_0\cos(\varphi_B - \varphi_A) = \langle AB\rangle\,.$$

In the limit of a nonconducting medium ($\sigma = 0$), the dielectric permittivity $\varepsilon' = \varepsilon$ is a real quantity, $n = \sqrt{\varepsilon}$, $\varkappa = 0$, and $\mu_\omega = 0$, i.e., the medium is absolutely transparent. Waves in it are not damped, because on the average the polarization current does not dissipate any Joule heat within one period.

3.5.5 Wave Absorption Coefficient in Plasma

If the imaginary part of ε' is much less than the real part, $4\pi\sigma/\omega\varepsilon \ll 1$, and ε is positive, then equations (3.34) yield $n \approx \sqrt{\varepsilon}$ and $\varkappa \approx 2\pi\sigma/\omega n \ll 1$. The refractive index of the medium is typical for a dielectric, but the absorption is weak, in the sense that the wave is only slightly attenuated over a path length of order λ. The absorption coefficient is given by (3.36), where we use $n = \sqrt{\varepsilon}$. This situation is normally realized in the propagation of light, and partly in the propagation of microwave radiation in laboratory plasmas.

According to (3.23, 36), the absorption coefficient of an electromagnetic wave in an ionized gas is

$$\mu_\omega = \frac{4\pi e^2 n_e \nu_m}{mc(\omega^2 + \nu_m^2)} = 0.106 n_e \frac{\nu_m}{\omega^2 + \nu_m^2} \mathrm{cm}^{-1} . \tag{3.38}$$

Here we assume $n \approx \sqrt{\varepsilon} \approx 1$, since this is the most typical case under the conditions (weak ionization, weak absorption) in which (3.38) is definitely valid. The absorption coefficient is proportional to the electron density. In the high-frequency limit ($\omega^2 \gg \nu_m^2$), absorption is characterized by inverse square frequency dependence: $\mu_\omega \propto \omega^{-2} \propto \lambda^2$; hence short waves are better transmitted through plasma than long waves.

3.5.6 Quasistationary Field and the Skin Layer

Assume that the imaginary part of ε' is much greater than the real part (or more accurately, than the absolute value of the real part, because typically for such cases $\varepsilon < 0$). This is the case, for example, in good conductors if the field frequency is not excessively high. The conduction current then dominates the displacement current:

$$\frac{|j_{\mathrm{cond}}|}{|j_{\mathrm{disp}}|} = \frac{\varepsilon'_{\mathrm{im}}}{|\varepsilon'_{\mathrm{re}}|} = \frac{4\pi\sigma}{\omega|\varepsilon|} \gg 1 .$$

In this limiting case, (3.34) gives $n \approx \varkappa \approx \sqrt{2\pi\sigma/\omega}$, and the field is strongly damped over a distance of order λ. It is then meaningless to speak of a travelling wave or wave propagation, although these, formally, still exist. Electromagnetic waves are possible because of the displacement current. In the absence of this term, Maxwell's equation (3.13) is identical to the equation for the magnetic field of a dc current. This gives the limit of the quasistationary field.

The effective depth of penetration of the quasisteady field into a conductor can also be found from the formulas for the electromagnetic wave, as the distance over which the amplitude of a wave with purely imaginary ε' is reduced by a factor e

$$\delta = \frac{c}{\omega \varkappa} = \frac{c}{\sqrt{2\pi\sigma\omega}} = \frac{5.03}{\{\sigma[\mathrm{Ohm}^{-1}\,\mathrm{cm}^{-1}] f[\mathrm{MHz}]\}^{1/2}} \mathrm{cm} \,. \tag{3.39}$$

This quantity is called the *skin depth*, and ac current in good conductors flows only in this surface (skin) layer. For example, in copper ($\sigma = 6 \times 10^5\,\mathrm{Ohm}^{-1}\,\mathrm{cm}^{-1}$) at $f = 10\,\mathrm{MHz}$, we have $\delta = 2 \times 10^{-3}\,\mathrm{cm}$. However, the limiting case we discuss here is realized not only in metals but also in plasmas in the rf range (Sect. 11.3).

3.6 Total Reflection of Electromagnetic Waves from Plasma and Plasma Oscillations

3.6.1 Nonabsorbing Medium with Negative Dielectric Permittivity

Let a medium have $\varepsilon < 0$ and the conductivity σ be, if not zero, then so small that $4\pi\sigma/\omega|\varepsilon| \ll 1$. As follows from (3.34), this medium has $n \approx 0$, $\varkappa \approx \sqrt{|\varepsilon|}$. Electromagnetic waves cannot penetrate into such a medium, as in the case of purely imaginary ε', albeit for a different reason. The phase velocity and wavelength tend to infinity as $\sigma \to 0$, the field oscillates only in time, and its amplitude decreases exponentially into the medium. However, the energy of the field is not dissipated, in contrast to the case of a good conductor, where the amplitude decreases away from the boundary owing to the strong absorption of energy. The depth of penetration into a medium with $\varepsilon < 0$ and $\sigma \approx 0$ is independent of σ and equals $\lambda_0/\sqrt{|\varepsilon|}$. This situation corresponds to the total reflection of the electromagnetic wave and is frequently realized in the collisionless plasmas when $\nu_m^2 \ll \omega^2$. For example, let the wave frequency be $f = 3\,\mathrm{GHz}$, $\lambda_0 = 10\,\mathrm{cm}$, $p = 0.1\,\mathrm{Torr}$ ($N = 3.3 \times 10^{15}\,\mathrm{cm}^{-3}$). In the case of weak ionization, $\nu_m \approx 3 \times 10^8\,\mathrm{s}^{-1}$ and $\nu_m^2/\omega^2 \sim 10^{-4}$.

3.6.2 Critical Electron Density

Let us rewrite the dielectric permittivity (3.24) for a collisionless plasma in the form

$$\varepsilon = 1 - \omega_p^2/\omega^2 \,, \quad \omega_p = \sqrt{4\pi e^2 n_e/m} = 5.65 \times 10^4 n_e^{1/2}\,\mathrm{s}^{-1} \,. \tag{3.40}$$

It is negative if $\omega < \omega_p$ or if the electron density is greater than the critical value

$$n_{e,cr} = m\omega^2/4\pi e^2 = 1.24 \times 10^4 \{f[\mathrm{MHz}]\}^2 = 1.11 \times 10^{13} \{\lambda_0[\mathrm{cm}]\}^{-2}\,\mathrm{cm}^{-3} \,. \tag{3.41}$$

In the example above, $n_{e,cr} = 1.1 \times 10^{11}\,\mathrm{cm}^{-3}$. The wave with $\lambda_0 = 10\,\mathrm{cm}$ cannot penetrate the region with high electron density: it undergoes total reflection.

If n_e in a plasma increases in the direction of the x axis, and an electromagnetic wave propagates through the plasma in the same direction, it will reach roughly the point of $n_e = n_{e,cr}$, be reflected, and travel back. If plane symmetry holds, then the geometrical optics law is obeyed: the angle of incidence is equal

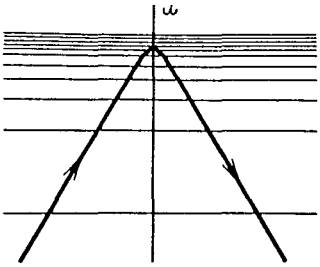

Fig. 3.1. Reflection of electromagnetic waves from plasma. Increasing electron density is shown by crowding of *horizontal lines*. The beam is turned back approximately at the point where the electron density reaches the critical value for the given wave frequency

to that of reflection (Fig. 3.1). This effect is of enormous practical importance and is widely used in experimental work and in technology. It lies at the foundation of one of the most efficient methods of both laboratory and ionospheric diagnostics of plasmas. The plasma is irradiated with signals of various frequencies, and one records which frequencies are transmitted ($\omega > \omega_p$) and which are stopped ($\omega < \omega_p$). The value of n_e is found from (3.40) once the cutoff frequency $\omega = \omega_p$ is known. A low-pressure (collisionless) laboratory plasma with $n_e \sim 10^{11}$–$10^{15}\,\mathrm{cm}^{-3}$ may be investigated in this way with microwave radiation of $\lambda_0 \sim 10 - 0.1\,\mathrm{cm}$.

3.6.3 Plasma Frequency

Longitudinal electric waves with $\boldsymbol{E} \| \boldsymbol{k}$ and $\boldsymbol{H} = 0$ in collisionless plasma are realized if $\varepsilon' = \varepsilon = 0$; from (3.40), this corresponds to $\omega = \omega_p$. The bulk charge density ϱ also undergoes oscillations. Indeed, if the polarization due to free electrons (which is described by oscillations of ϱ) is eliminated from $\boldsymbol{D}$, we find from (3.16) that $(\boldsymbol{k} \cdot \boldsymbol{E}) = 4\pi\varrho/\varepsilon_{\text{bound}}$, where $\varepsilon_{\text{bound}}$ is the dielectric permittivity due to bound electrons. The frequency ω_p defined by (3.40) is called the *plasma*, or *Langmuir, frequency*. This is the natural oscillation frequency of electrons in plasma established by *Tonks* and *Langmuir* in 1929. Strictly speaking, ω_p corresponds to the oscillations of the gas as a whole, that is, to waves of "infinite" wavelength.

Let all the electrons be initially shifted, for some reason, to the right with respect to the ion, which we assume to be at rest (Fig. 3.2). The separation of charges produces the attractive force that tends to return the electrons to where they "belong". Being accelerated by this force, the electrons overshoot the equilibrium position and move to the left of the ions, and so forth. If Δx

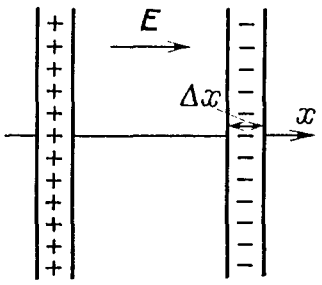

Fig. 3.2. Plasma oscillations. Electrons are displaced rightward with respect to ions by a distance Δx

is the displacement of electrons from the equilibrium, then the surface charge density at the boundaries of the plasma layers is $en_e\Delta x$, the strength of the field of polarization being $E = 4\pi en_e\Delta x$. Therefore, the equation of electron motion,

$$m(\Delta\ddot{x}) = -eE = -4\pi e^2 n_e \Delta x\ , \quad (\Delta\ddot{x}) + \omega_p^2 \Delta x = 0\ ,$$

describes harmonic oscillations at a frequency ω_p as implied by (3.40). The plasma frequency, Debye radius, and mean electron velocity are related by the formula

$$\omega_p d = \left(\frac{4\pi e^2 n_e}{m} \cdot \frac{kT_e}{4\pi e^2 n_e}\right)^{1/2} = \left(\frac{kT_e}{m}\right)^{1/2} = 0.62\bar{v}\ .$$

The velocity of the oscillating electrons is randomized at a rate given by the collision frequency ν_m, which determines the rate of damping of free oscillations. The notion of oscillations remains meaningful as long as $\nu_m \ll \omega_p$ or $n_e \gg 2 \times 10^9\ (p\ [\text{Torr}])^2\ \text{cm}^{-3}$. *Plasma oscillations* were discovered experimentally by *Penning* in 1926.

4. Production and Decay of Charged Particles

4.1 Electron Impact Ionization in a Constant Field

4.1.1 Ionization Frequency

Ionization of atoms and molecules by electron impact is the most important mechanism of charge generation in the bulk of a gas discharge. The rate of this process, $(dn_e/dt)_i = \nu_i n_e = k_i N n_e$, is characterized by the *ionization frequency* ν_i, that is, the number of ionization events performed by an electron per second, or by the *reaction rate constant* k_i. If $n(\varepsilon)$ is the electron energy distribution function (density-normalized), and $\sigma_i(\varepsilon)$ is the ionization cross section of atoms in their ground state (Fig. 4.1), then

$$\nu_i = N \int n(\varepsilon) v \sigma_i(\varepsilon) d\varepsilon \Big/ \int n(\varepsilon) d\varepsilon = N \langle v \sigma_i \rangle \equiv N k_i \,. \tag{4.1}$$

The electron energy distribution of a weakly ionized plasma in an electric field depends on a number of elastic and inelastic collision processes. Under these conditions, the ionization frequency is found either by solving the kinetic equation for $n(\varepsilon)$ (Chap. 5) or experimentally. If the ionization by electrons proceeds under unvarying conditions, so that ν_i = const., and the removal of electrons can be

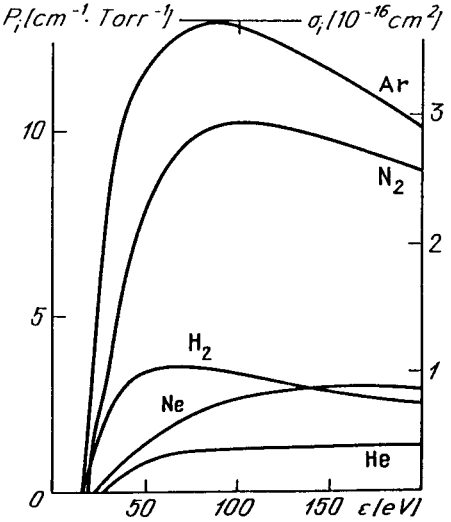

Fig. 4.1. Cross sections and probabilities of electron impact ionization. From [4.1]

neglected, electrons proliferate exponentially: $n_e = n_e(0)\exp(\nu_i t)$: an *electron avalanche* develops.

4.1.2 Maxwellian Distribution

This distribution arises when the degree of ionization is not too small and electron-electron collisions are important. The dependence of ν_i on the field and collisions with molecules in the case of a Maxwellian distribution (see Appendix) is contained implicitly in the electron temperature that determines the ionization frequency. As a rule, the temperature of a gas discharge plasma is substantially lower than the ionization potential I, because strong ionization occurs when kT_e is less than I by a factor in the range of 5 to 10. Atoms are ionized by high-energy electrons in the tail of the Maxwellian distribution. In this energy range, $n(\varepsilon) \propto \exp(-\varepsilon/kT_e)$ falls off steeply, so that a linear function can be used for the cross section, $\sigma_i(\varepsilon) = C_i(\varepsilon - I)$, in integral (4.1); the linearity is valid if ε is slightly greater than the ionization threshold I, which gives

$$\nu_i = N\bar{v}C_i\left(I + 2kT_e\right)\exp\left(-I/kT_e\right), \quad \bar{v} = \left(8kT_e/\pi m\right)^{1/2}. \tag{4.2}$$

For example, in argon, $C_i = 2 \cdot 10^{-17}\,\mathrm{cm^2/eV}$. If $T_e = 1\,\mathrm{eV}$, then $\bar{v} = 6.7 \cdot 10^7\,\mathrm{cm/s}$ and $k_i = \langle v\sigma_i \rangle = 3 \cdot 10^{-16}\,\mathrm{cm^3/s}$. If $p = 50\,\mathrm{Torr}$ and $T = 300\,\mathrm{K}$, then $N = 1.7 \cdot 10^{18}\,\mathrm{cm^{-3}}$. This gives $\nu_i = 510\,\mathrm{s^{-1}}$. At these T_e and N, the equilibrium degree of ionization is $(n_e)_{eq}/N = 0.021$. The values of C_i for several other gases (in $10^{-17}\,\mathrm{cm^2/eV}$) are

$$\mathrm{He} - 0.13\,,\ \mathrm{Ne} - 0.16\,,\ \mathrm{Hg} - 7.9\,,\ \mathrm{N_2} - 0.85\,,\ \mathrm{O_2} - 0.68\,,\ \mathrm{H_2} - 0.59\,.$$

4.1.3 Townsend's Ionization Coefficient

An electron avalanche generated by an electron in a dc field evolves not only in time but also in space, along the direction of drift of the knocked-out electrons. It is more convenient, therefore, to characterize the rate of ionization not by frequency $\nu_i\,\mathrm{s^{-1}}$, but by the *ionization coefficient* $\alpha\,\mathrm{cm^{-1}}$, that is, the number of ionization events performed by an electron in a 1 cm path along the field. Obviously,

$$\alpha = \nu_i/v_d\,, \quad \nu_i = \alpha v_d\,. \tag{4.3}$$

Note that the primary and complete characteristic of the rate of ionization is the frequency ν_i, not α. The distribution function gives us this frequency, as well as the drift velocity. The ionization coefficient α is a derived quantity, found from (4.3). Actually, α is not very meaningful in fast-oscillating fields. However, dc measurements give us α, not ν_i.

4.1.4 Measurement of α and Similarity Laws

If we place plane electrodes at a separation d, apply a voltage V, and irradiate the cathode with UV light, knocking out $\mathcal{N}_0$ electrons in 1 s, the number of electrons in the avalanche grows towards the anode:

$$d\mathcal{N}/dx = \alpha\mathcal{N}\,, \quad \mathcal{N}(x) = \mathcal{N}_0\exp(\alpha x)\,. \tag{4.4}$$

The electron current at the anode is $i = e\mathcal{N}_0 \exp(\alpha d)$. In the steady state, the positive ions produced in the discharge gap arrive at the cathode in the same numbers as the electrons at the anode. The current in the closed circuit is everywhere identical and equal to i. The low-mobility ions accumulate in the gap between the electrodes in much larger numbers than the electrons, which are removed more quickly by the field. As a result, the gap contains positive space charge. However, this space charge causes little distortion of the field at small currents, and the field is known: $E = V/d$. If i is measured with varying d, and $\ln i$ is plotted as a function of d for constant E, the coefficient is found from the slope of the straight line $\ln i = \text{const} + \alpha d$.

The energy distribution, mean electron energy, and drift velocity are functions of the ratio E/p. Hence, a similarity law of the type $\alpha = pf(E/p)$ holds for both ν_i and α. Experimentally, therefore, one can vary p instead of d, keeping E/p constant: $\ln i = \text{const} + (\alpha/p)(pd)$. Experimental data show that points fall on straight lines quite well up to a certain limit of pd (see Sect. 4.7.1); the values of α for a number of gases were measured in this way (Figs. 4.2–5).

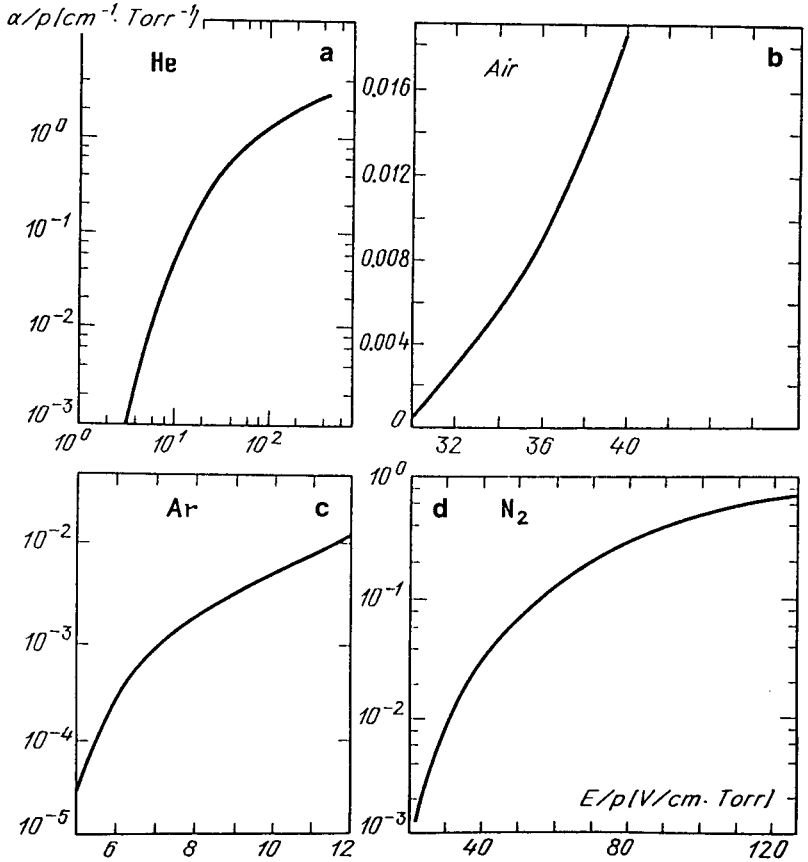

Fig. 4.2. Ionization coefficient in **a)** He, **b)** air, **c)** Ar, **d)** N_2. From [4.2]

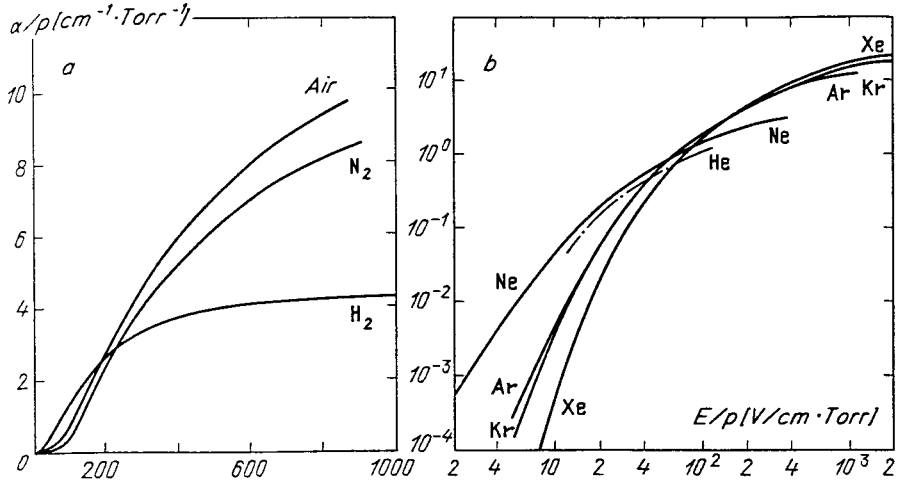

Fig. 4.3. Ionization coefficients for a wide range of E/p values (**a**) in molecular gases, (**b**) in inert gases. From [4.3]

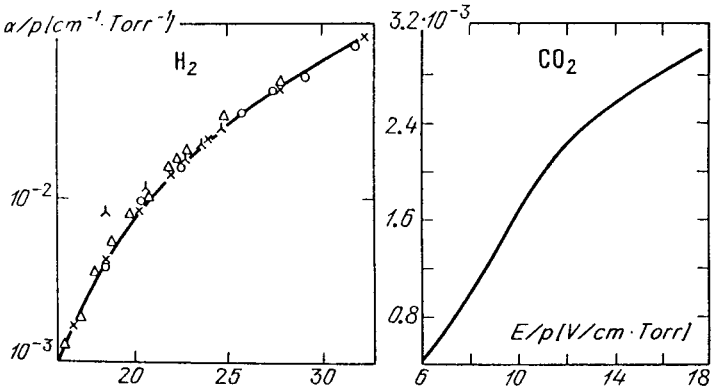

Fig. 4.4. Ionization coefficients in H_2 and CO_2. From [4.2]

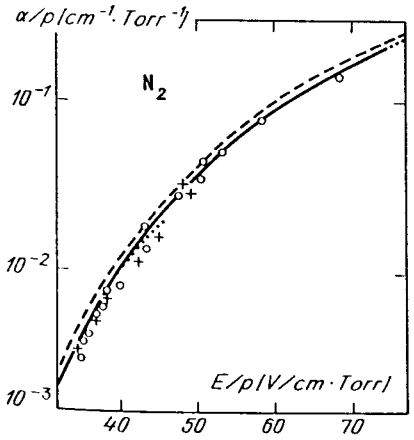

Fig. 4.5. Ionization coefficient in N_2 from the data of a number of authors. From [4.2]

4.1.5 Interpolation Formula for α

The theoretical and numerical analysis of discharges widely uses a conventional empirical formula suggested by Townsend:

$$\alpha = Ap\exp(-Bp/E) \,. \tag{4.5}$$

The constants A and B are determined by approximating the experimental curves (Table 4.1). In a number of cases the relation (4.5) can be attributed a certain physical meaning. Assume, for example, that an electron undergoes only ionizing collisions. (This assumption may be realistic at high E/p and moderate energies.) The energy picked up by an electron along a free path length x is slightly greater than the ionization potential I. The probability that it will move the distance $x = I/eE$ without collisions and then be involved in an ionizing collision in a distance dx is $\alpha\, dx = dx\, l^{-1} \exp(-I/eEl)$, where $l = l_1/p$ is the mean-free-path length. This gives us (4.5) with $A = l_1^{-1}$, $B = I/el_1$. If $\sigma = 5 \cdot 10^{-16}\,\mathrm{cm}^2$, then $l_1 = 0.06\,\mathrm{cm} \cdot \mathrm{Torr}$; if $I = 15\,\mathrm{eV}$, then $A = 17$, $B = 250$, which is quite close to tabulated values.

The fraction of electrons in a Maxwellian spectrum that are capable of ionizing an atom is proportional to $\exp(-I/kT_e)$. If $T_e \propto E/p$ (see Sect. 2.3.5), we again arrive at a dependence of ν_i and α on E of type (4.5), but now the constant B has a different meaning. It will be shown in Sect. 7.4.7 that an approximate solution of the kinetic equation that takes into account the large role of inelastic losses of electron energy on excitation also leads to a relation of type (4.5), but again with a changed meaning of B. For inert gases, the formula

$$\alpha = Cp\exp\left[-D(p/E)^{1/2}\right] \tag{4.6}$$

Table 4.1. Constants in the formulas for the ionization coefficient, and regions of applicability [4.4, 5]

Gas	A	B	E/p	C	D	$E/p <$
	$\mathrm{cm}^{-1}\mathrm{Torr}^{-1}$	V/(cm · Torr)	V/(cm · Torr)	$\mathrm{cm}^{-1}\mathrm{Torr}^{-1}$	$\mathrm{V/(cm \cdot Torr)^{1/2}}$	V/(cm · Torr)
He	3	34	20–150	4.4	14	100
Ne	4	100	100–400	8.2	17	250
Ar	12	180	100–600	29.2	26.6	700
Kr	17	240	100–1000	35.7	28.2	900
Xe	26	350	200–800	65.3	36.1	1200
Hg	20	370	150-600			
H_2	5	130	150-600			
N_2	12	342	100–600			
N_2	8.8	275	27–200			
Air	15	365	100–800			
CO_2	20	466	500–1000			
H_2O	13	290	150–1000			

[4.4] is sometimes used since it gives a better fit to experimental data then (4.5), even though it is less convenient for the theory (Table 4.1). Note also a useful empirical formula for air at relatively high E/p (see also Table 12.1):

$$\alpha/p = 1.17 \cdot 10^{-4}(E/p - 32.2)^2\,\mathrm{cm}^{-1}\,\mathrm{Torr}^{-1}\,,$$
$$E/p \approx 44 - 176\,\mathrm{V/(cm \cdot Torr)}\,. \tag{4.7}$$

4.1.6 Optimal Conditions for Ionization

An electron passing through a potential difference of 1 V generates α/E electrons (pairs of ions). In order to create one pair, it must be accelerated by the field to an energy $W = eE/\alpha$. The function $W(E/p)$ has a minimum, which, when using approximation (4.5), is given by $W_{\min} = \bar{e}eB/A$ at $(E/p)_m = B$, where $\bar{e} = 2.718\ldots$. Even under these most favorable conditions for proliferation, the creation of one pair of ions consumes the energy $W_{\min}$ (*Stoletov's constant*), which is several times the ionization potential. Electrons have to devote much energy to the excitation of atoms: In air, $W_{\min} = 66\,\mathrm{eV}$/pair of ions for $(E/p)_m = 365\,\mathrm{V/(cm \cdot Torr)}$.[1]

Note that (4.5) implies that as $E/p \to \infty$, $\alpha \to \mathrm{const} = Ap$. Indeed, at $E/p > 2000 - 3000$, α decreases as E/p increases, because the ionization cross section at high energies falls off with increasing ε (Fig. 2.1). However, such high values of E/p are not typical for discharges.

4.1.7 Stepwise Ionization

The atoms of a weakly ionized gas are mostly ionized from the ground state. Many excited atoms and molecules may be formed if the gas is highly ionized, and stepwise ionization may be predominant. Atoms are first excited by electron impact and then ionized by subsequent collisions. Long-lived metastable excited particles play an important role in this process (Table 4.2); their ionization cross sections are rather high (Fig. 4.6).

4.2 Other Ionization Mechanisms

4.2.1 Photoionization

This mechanism cannot compete with electron impact ionization under discharge conditions. Sometimes, however, it supplies seed electrons that start electron avalanches, as they do in streamer propagation (Chap. 12). Photoionization cross sections close to the threshold are rather high (see Table 4.3) but as a rule, a gas has few quanta of $\hbar\omega > I$ capable of photoionization.

[1] This figure must not be confused with another frequently encountered quantity: 33 eV/ion pair. This the energy dissipated by a fast electron with energy $\varepsilon > 4\,\mathrm{keV}$ when it is being stopped in air. Fast electrons have smaller energy losses.

Table 4.2. Energies of the lower resonance and metastable levels, lifetimes of metastable states, and excitation cross sections

Atom, molecule	Excitation energy, E^* eV (metastable levels: *)	Lifetime, s	Interpolation of the total excitation cross section at the threshold, $\sigma^* = C^*(\varepsilon - E^*)$	
			C^*, 10^{-18} cm^2/eV	E^*_{eff}, eV
H(2s)	10.20*	0.142	25	10
H(2p)	10.20			
He(2^3S_1)	19.82*	$6 \cdot 10^5$		
He(2^1S_0)	20.6*	$2 \cdot 10^{-2}$	4.6	20
He	21.21			
Ne	16.62*			
	16.7*		1.5	16
	16.85			
Ar$(4^3P_2^0)$	11.55*	> 1.3		
	11.61		7	11.5
	11.72*	> 1.3		
H_2	8.7*		7.6	8.7
	11.5			
N_2 $(A^3\Sigma_u^+)$	6.2*	1.3–2.6		
N_2 $(a^1\Sigma_u^-)$	8.4*	0.5		
O_2 $(^1\Delta_g)$	0.98*	$2.7 \cdot 10^3$		
O_2 $(b^1\Sigma_g^+)$	1.64*	12		
Hg(6^3P_0)	4.65*			
(6^3P_1)	4.87		$\sigma^*_{\max} = 1.7 \cdot 10^{-16}$ cm^2	
	5.4*		for $\varepsilon = 6.5$ eV	
	6.7			

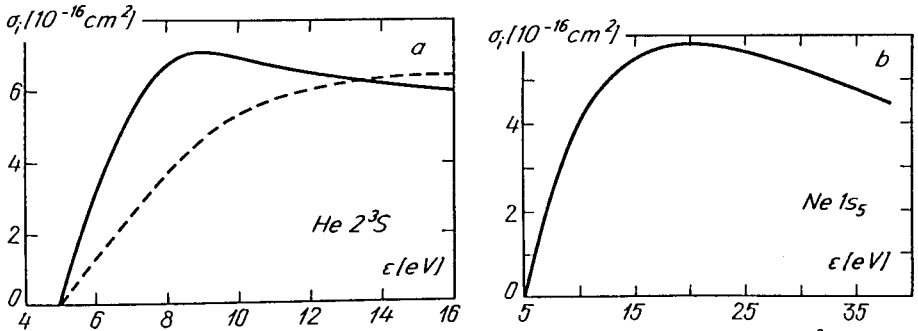

Fig. 4.6. Cross sections of ionization of excited metastables by electron impact: **(a)** He 2^3S; experimental data [4.6] – *solid curve*; theory [4.7] – *dashed curve*; **(b)** Ne $1s_5$ – theory. From [4.7]

Table 4.3. Cross sections of photoionization of atoms and molecules from the ground state close to the threshold

Gas	$\hbar\omega = I$, eV	λ, Å	σ_ν, 10^{-18} cm^2
H	13.6	912	6.3
He	24.6	504	7.4
Ne	21.6	575	4.0
Ar	15.8	787	35
Na	5.14	2412	0.12
K	4.34	2860	0.012
Cs	3.89	3185	0.22
N	14.6	852	9
O	13.6	910	2.6
O_2	12.2	1020	~ 1
N_2	15.58	798	26
H_2	15.4	805	7

4.2.2 Ionization by Excited Atoms

Even the high kinetic energy of slow heavy particles is not effective in ionization processes. Ionization requires the velocities of atoms and molecules to be comparable to the electron velocity in atoms, 10^8 cm/s, which corresponds to energies of 10 to 100 keV, not realizable in discharge conditions. On the other hand, the atomic excitation energy E^* is easily spent on liberating an electron from another atom, provided, of course, that it exceeds the ionization potential I. Resonance-excited atoms are especially effective in this respect. Thus the ionization cross sections of Ar, Kr, Xe, N_2, and O_2 in impacts by He(2^1P) atoms with $E^* = 21.2$ eV is $\sigma \approx 2 \cdot 10^{-14}$ cm^2, which is much greater than the gas-kinetic value [4.8]. Cross sections for ionization by metastable atoms, also with $E^* > I$ (*Penning effect*), are smaller but metastable atoms are much more numerous than short-lived resonance-excited atoms. Cross sections for ionization of Ar, Xe, N_2, CO_2 by metastable He(2^3S) atoms with $E^* = 19.8$ eV reach 10^{-15} cm^2, and that of Hg is exceptionally large: $1.4 \cdot 10^{-14}$ cm^2 [4.8].

4.2.3 Associative Ionization

This process of type $A + A^* \rightarrow A_2^+ + e$, discovered by Hornbeck and Molnar in 1951, is sometimes important in inert gases. The separation of an electron is facilitated by the release of a small binding energy of order 1 eV in the association of an ion and an atom into a molecular ion. A reaction in helium involves atoms excited to states with the principal quantum number $n = 3$; their electron binding energies are from 1.52 to 1.62 eV. The binding energy of He_2^+ is somewhat higher, 2.23 eV, so that the electron can be ejected. At $T = 400$ K, the reaction cross sections are $2 \cdot 10^{-16} - 2 \cdot 10^{-15}$ cm^2. The *associative ionization* in mercury vapor involves two excited atoms,

$$\mathrm{Hg}\,(6^3P_1,\ E^* = 4.9\,\mathrm{eV}) + \mathrm{Hg}\,(6^3P_0,\ E^* = 4.7\,\mathrm{eV}) \rightarrow \mathrm{Hg}_2^+ + e\,,$$

the first atom being in a resonance and the second, in a metastable state. The total energy is 9.6 eV, less than that required to ionize an Hg atom ($I_{Hg} = 10.4\,eV$); together with the binding energy of an Hg_2^+ molecular ion, however (0.15 eV), it is sufficient to ionize the molecule ($I_{Hg_2} = 9.7\,eV$).

4.3 Bulk Recombination

4.3.1 Decay of Plasma

In the absence of an electric field, the charge densities $n_e = n_+$ in a plasma without electronegative components decay with time according to the law

$$\left(\frac{dn_e}{dt}\right)_r = -\beta n_e n_+ , \quad n_e = \frac{n_e^0}{1+\beta n_e^0 t} \underset{t\to\infty}{\longrightarrow} \frac{1}{\beta t} . \tag{4.8}$$

For example, if the *electron-ion recombination coefficient* $\beta = 10^{-7}\,cm^3/s$ and the initial plasma density $n_e^0 = 10^{10}\,cm^{-3}$, then the characteristic decay time $\tau_r = (\beta n_e^0)^{-1} = 10^{-3}\,s$. The recombination coefficient can be determined experimentally, by measuring $n_e(t)$ and plotting n_e^{-1} as a function of t. The slope of the straight line gives β.

4.3.2 Dissociative Recombination

This mechanism follows the scheme $A_2^+ + e \rightarrow A + A^*$. This is the fastest mechanism of bulk recombination in weakly ionized plasma, for example, in a glow discharge. In this case the gas is cold and the plasma usually includes molecular ions. The released energy is mostly transformed into the excitation energy of the atom. The dissociative recombination coefficients $\beta_{dis} \sim 10^{-7}\,cm^3/s$; at temperatures from room to several kK, β_{dis} decreases with increasing T_e as $T_e^{-1/2}$, and as $T_e^{-3/2}$ at still higher temperatures (Fig. 4.7). This is the way recombination proceeds, even in weakly ionized inert gases. Molecular ions are formed from atomic ones, generated in the course of the *conversion reaction* $A^+ + A + A \rightarrow A_2^+ + A$. The rate of conversion, $(dN_{A_2^+}/dt)_{conv} = k_{conv} N_{A^+} \cdot N_A^2$, is far from small (Table 4.4). Thus the atomic ion lifetime at $p = 10\,Torr$ with respect to the conversion is $\tau_{conv} = (k_{conv} N_A^2)^{-1} \sim 10^{-4}\,s$, and at 100 Torr it is $10^{-6}\,s$. If $n_e = 10^{10}\,cm^{-3}$ and $\beta_{dis} = 10^{-7}\,cm^3/s$, then $\tau_{conv} \ll \tau_{dis,r} = 10^{-3}\,s$. Conversion replenishes the amount of molecular ions almost instantaneously, without impeding the dissociative recombination. In helium, β_{dis} is less by a factor of 10 to 100 than in other gases. Conversion can also produce *complicated ion complexes* O_4^+, N_4^+, and some others that have large coefficients up to $10^{-6}\,cm^3/s$.

4.3.3 Radiative Recombination

Cross sections of the process $A^+ + e \rightarrow A + h\nu$ are very small: $\sigma_c \sim 10^{-21}\,cm^2$. The recombination coefficient is correspondingly small [4.9]

$$\beta_{rr} = \langle v\sigma_c \rangle \approx 2.7 \cdot 10^{-13} \{T_e[eV]\}^{-3/4}\,cm^3/s \sim 10^{-12}\,cm^3/s . \tag{4.9}$$

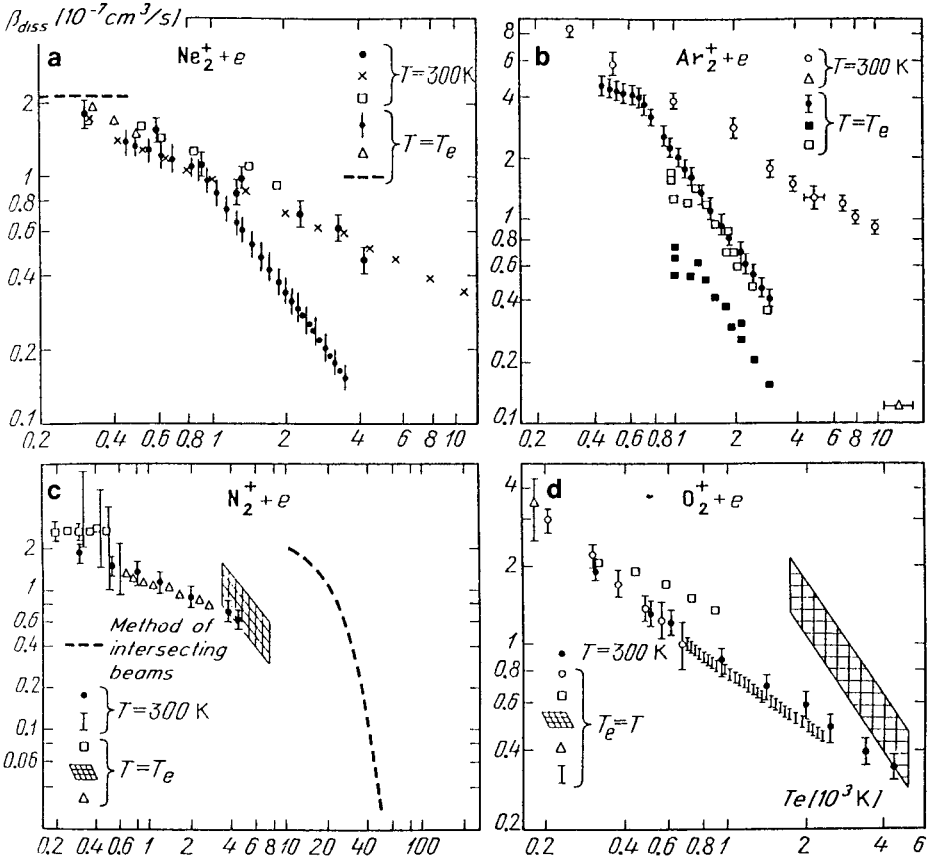

Fig. 4.7a–d. Dissociative recombination coefficients from the data of a number of authors. From [4.8]

Table 4.4. Measured reaction rate constants for the conversion of A^+ into A_2^+ in triple collisions with atoms A at $T = 300$ K [4.8]

Gas A	k_{conv}, 10^{-31} cm^6/s
He	0.63–1.15
Ne	0.42–0.79
Ar	1.46–3.9
Kr	1.9 –2.7
Xe	3.6
Hg	1 ($T = 700$ K)
Cs	150

Electrons are more often captured by the ground state of an atom, emitting a quantum $\hbar\omega \approx 10$ eV in the VUV range, $\lambda \lesssim 1000$ Å. However, capture by excited states, with subsequent photon emission in the visible at $\lambda \approx 4000 - 7000$ Å is also possible. Radiative recombination in gas discharge plasma may happen to be important, not as a channel for electron removal but as a mechanism for light emission.

4.3.4 Radiative Recombination in Three-Body Collisions

This process follows the scheme $A^+ + e + e \rightarrow A + e$; it is the main process in high-density low-temperature equilibrium plasma where $T \approx T_e \sim 10^4$ and the concentration of molecular ions is too low for dissociative recombination to be significant. In three-body collisions, electrons are captured by ions to form very high by excited atoms with a binding energy of order kT. An excited atom is then gradually deactivated by subsequent electron impacts, it "cascades" down the level staircase, and finally falls to the ground state from the lower excited state by radiative transition. This completes the process of recombination; its coefficient is [4.9]

$$\beta_{crr} = 8.75 \cdot 10^{-27} \{T[eV]\}^{-9/2} n_e$$
$$= 5.2 \cdot 10^{-23} \{T[kK]\}^{-9/2} n_e \, cm^3/s \, . \quad (4.10)$$

According to (4.9, 10), β_{crr} exceeds the radiative recombination coefficient if

$$n_e > 3.1 \cdot 10^{13} \{T[eV]\}^{3.75} = 3.2 \cdot 10^9 \{T[kK]\}^{3.75} \, cm^{-3} \, . \quad (4.11)$$

The recombination rate constant of triple collisions involving an atom as a third particle, β/N, is less than β_{crr}/n_e of (4.10) by a factor of $10^7 - 10^8$. This process is not typical for discharge conditions and can manifest itself only at very weak ionization and high pressures.

4.3.5 Ion-Ion Recombination

This is the main mechanism of charge neutralization in gases where electron attachment is important. In this process, $(dn_-/dt)_r = (dn_+/dt)_r = -\beta_i n_- n_+$. If $n_e \ll n_-$, then $n_- \approx n_+ \approx n_+^0/(1 + \beta_i n_+^0 t)$. Recombination at low pressure takes place through binary collisions of the type $A^- + B^+ \rightarrow A + B^*$ (Table 4.5). The process is similar to charge transfer. The energy thus released goes to excite the former ion B, the excitation later being released in collisions.

Table 4.5. Coefficients of binary ion-ion recombination at room temperature [4.8]

Ions	β_i, 10^{-7} cm^3/s
$H^+ + H^-$	3.9
$O^+ + O^-$	2.7
$N^+ + O^-$	2.6
$O_2^+ + O_2^-$	4.2
$N_2^+ + O_2^-$	1.6
$O^+ + O_2^-$	2.0
$O_2^+ + O^-$	1.0
$NO^+ + O^-$	4.9
$NO^+ + NO_2^-$	5.1–1.8
$SF_5^+ + SF_6^-$	0.39

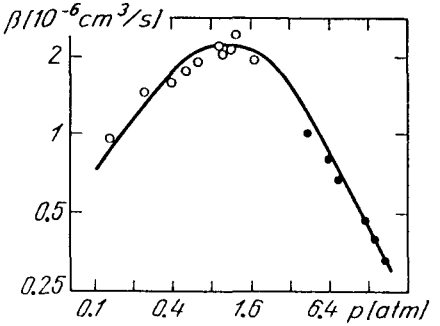

Fig. 4.8. Coefficient of ion-ion recombination in air. From [4.8]

At moderate pressures, recombination proceeds through triple collisions of the type $A^- + B^+ + C \rightarrow A + B + C$ (Thomson's theory, developed in 1924). The recombination coefficient is $\beta_i = k_{ii} N_c \propto p$. The recombination rate constant for the ions O_2^- and O_4^+ in oxygen is $k_{ii} \approx 1.55 \cdot 10^{-25}\,\mathrm{cm^6/s}$ at $p \sim 100\,\mathrm{Torr}$. For the ions NO^+ and NO_2^-, $k_{ii} \approx 3.4 \cdot 10^{-26}$ in oxygen and $1.0 \cdot 10^{-25}$ in N_2 (both at $T = 300\,\mathrm{K}$). Frequent collisions of ions with molecules at high pressures impede an ion from approaching another ion with opposite charge required for mutual neutralization. The $\beta_i \propto p$ law is replaced with the $\beta_i \propto p^{-1}$ law (Langevin's theory, developed in 1903). The maximum $\beta_{i,max} \sim 10^{-6}\,\mathrm{cm^3/s}$ is reached at $p \sim 1\,\mathrm{atm}$ (Fig. 4.8).

4.4 Formation and Decay of Negative Ions

4.4.1 Attachment

Atoms and molecules, such as O, H, O_2, H_2O, Hg, Cs, halogens, Cl, Cl_2, or halogen-containing compounds CCl_4, SF_6, have an electrons affinity of 0.5–3 eV. *Attachment* is an important, sometimes the main, mechanism of removing electrons in *electronegative* gases and gases with electronegative additives. Attachment impedes break-down and makes it difficult to sustain the ionized state and the current. Sometimes this may be useful: to improve the insulating properties of the gas, or to speed up the removal of electrons in counters of nuclear particles.

The process in cold air in the absence of an electric field is $e + O_2 + M \rightarrow O_2^- + M$ ($M = O_2$, N_2, H_2O), with reaction rate constants $k_M = k_{O_2} = 2.5 \cdot 10^{-30}\,\mathrm{cm^6/s}$, $k_{N_2} = 0.16 \cdot 10^{-30}$, $k_{H_2O} = 14 \cdot 10^{-30}$ at $T = T_e = 300\,\mathrm{K}$. The electron density decreases according to the law $(dn_e/dt)_a = -\nu_a n_e$, $n_e = n_e^0 \exp(-\nu_a t)$. The attachment frequency of electrons in dry air at $p = 1\,\mathrm{atm}$ is $\nu_a = k_{O_2} N_{O_2}^2 + k_{N_2} N_{N_2} N_{O_2} = 0.9 \cdot 10^8\,\mathrm{s^{-1}}$. The electron lifetime with respect to attachment is $\tau_a = \nu_a^{-1} = 1.1 \cdot 10^{-8}\,\mathrm{s}$.

When an electron attaches itself to a complex molecule, the binding energy is immediately distributed over its vibrational degrees of freedom. As a result, each electron capture in a binary collision forms a stable negative ion.

For an electron energy $\varepsilon = 0.05\,\text{eV}$, most active molecules of CCl_4 and SF_6 have $\sigma_{\text{capt}} \approx 1.2 \cdot 10^{-14}\,\text{cm}^2$, and $\sigma_{\text{capt}} \propto 1/\varepsilon$. The attachment rate constant corresponding to this is $k_a = \nu_a/N \approx 1.6 \cdot 10^{-7}\,\text{cm}^3/\text{s}$. The dissociation potentials of halogen molecules are very low (1.5–2.5 eV). The electron affinity energy is sufficient for the dissociative attachment $e + A_2 \rightarrow A + A^-$. In iodine at 300 K, the attachment cross section is $\sigma_a \approx 3.2 \cdot 10^{-15}\,\text{cm}^2$ and $k_a \approx \bar{v}_e \sigma_a \approx 3.4 \cdot 10^{-8}\,\text{cm}^3/\text{s}$. In triple collisions, in which $\nu_a \sim p^2$, attachment can exceed the dissociative recombination with $\nu_a \sim p$ only at $p \gtrsim 100\,\text{atm}$.

In contrast, the molecules O_2, CO_2, H_2O are strongly bound; a fairly high energy is then required for the dissociative attachment of an electron:

$$e + O_2 + 3.6\,\text{eV} \rightarrow O + O^-\,,$$
$$e + CO_2 + 3.85\,\text{eV} \rightarrow CO + O^-\,,$$
$$e + H_2O + 4.25\,\text{eV} \rightarrow OH + H^-\,,$$
$$e + H_2O + 3.6\,\text{eV} \rightarrow H_2 + O^-\,,$$
$$e + H_2O + 3.2\,\text{eV} \rightarrow H + OH^-\,.$$

However, an electric field produces enough energetic electrons in discharges, so that such processes are usually faster than attachment in triple collisions (Figs. 4.9–11). Attachment in triple collisions involving a second electron and radiative attachment ($\sigma_{ra} \sim 10^{-21} - 10^{-23}\,\text{cm}^2$) both play insignificant roles in laboratory plasmas.

4.4.2 Attachment Coefficient

Like ionization, the attachment of electrons in dc fields occurs in the course of drift. The attachment coefficient $a = \nu_a/v_d$, similar to α, gives the number of attachment events per 1 cm of path along the field. Dissociative attachment mostly occurs in not too weak fields and obeys the same similarity law, $a = pf(E/p)$. In the case of triple collisions, dominating in very weak fields, $a =$

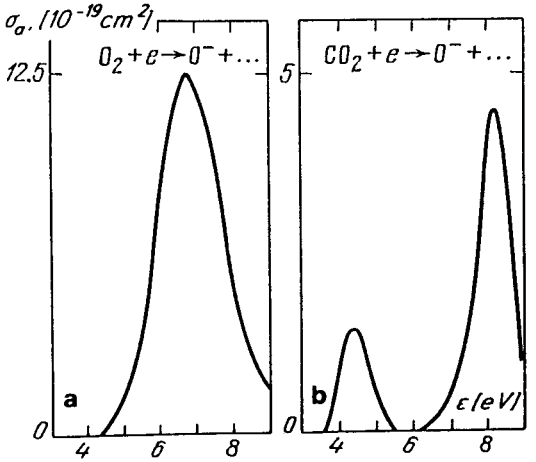

Fig. 4.9. Dissociative attachment cross section of electrons in a) O_2 and b) CO_2. From [4.10]

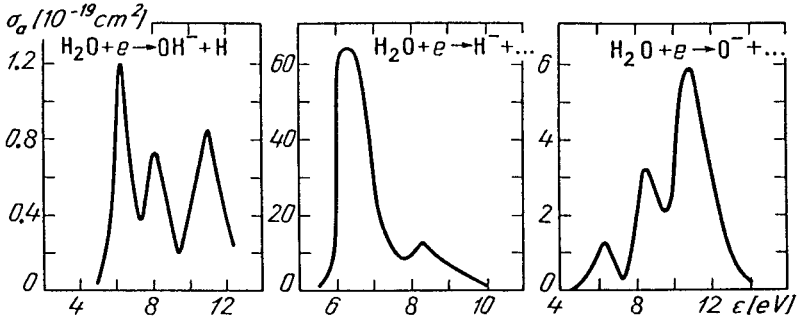

Fig. 4.10. Dissociative attachment cross sections of electrons in H_2O for three possible channels. From [4.11]

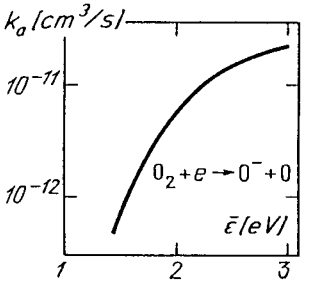

Fig. 4.11. Dissociative attachment rate constant of O_2 as a function of mean electron energy. From [4.12]

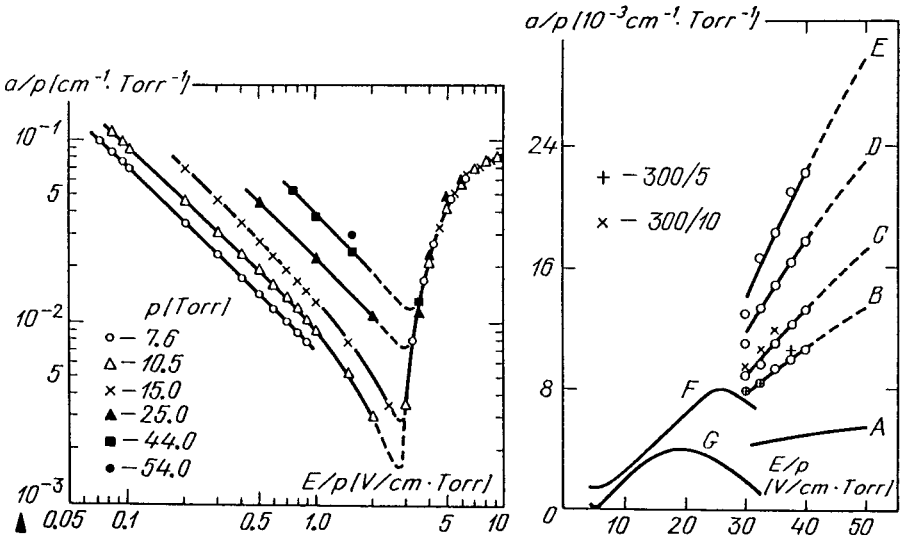

Fig. 4.12. Electron attachment coefficient in pure oxygen at T = 300 K and various pressures. From [4.12]

Fig. 4.13. Electron attachment coefficient in moist air, for various air humidity values: *A*: dry air; *B*: total pressure 150 Torr, water vapor pressure 2.5 Torr (150/2.5); *C* (150/5); *D* (150/9); *E* (150/15); *F* and *G* – air with negligible amount of water vapor. From [4.13, 14]

$p^2 f_1(E/p)$ (Figs. 4.12, 13). A change of mechanism is apparent in Fig. 4.12. The multiplication of electrons in an avalanche is determined by the effective coefficient $\alpha_{\text{eff}} = \alpha - a$. If $\alpha < a$ (this happens at E/p less than a certain value for a given gas, see Sect. 7.2.5), multiplication becomes impossible.

4.4.3 Detachment

Experiments show that steady-state weakly ionized plasma is sustainable in electronegative gases at much lower values of E/p than short pulsed discharges require. This observation indicates that a discharge sustained for a long time accumulates active particles (in all likelihood, excited molecules) that release electrons upon collisions with negative ions. The detachment frequency ν_d and rate constant k_d are determined by the equations $(dn_e/dt)_d = -(dn_-/dt)_d = \nu_d n_- = k_d N n_-$. The constant per active molecule is $k_{d,act} \sim 10^{-10}\,\text{cm}^3/\text{s}$ (Table 4.6). Metastable molecules $N_2(A^3\Sigma_u^+)$, and also $O_2(b^1\Sigma_d^+)$ in air, are presumably efficient in air and laser mixtures of CO_2, N_2, and He (Table 4.2). The constants $k_{d,act}$ are unknown for them but are assumed to be of the same order of magnitude. Indirect estimates (Sect. 8.8.4) show that discharges are characterized by $k_d \sim 10^{-14}\,\text{cm}^3/\text{s}$ per any molecule. If $k_{d,act} \sim 10^{-10}$, the concentrations of active particles are about 10^{-4}.

The O^- ions formed in laser mixtures and in air in the reactions

$$O^- + CO_2 + M \rightarrow CO_3^- + M\,, \quad k = 1.1 \cdot 10^{-27}\,\text{cm}^6/\text{s} \quad \text{for} \quad M = CO_2\,,$$

$$O^- + O_2 + M \rightarrow O_3^- + M\,, \quad k = 1.05 \cdot 10^{-30}\,\text{cm}^6/\text{s} \quad \text{for} \quad M = O_2\,,$$

Table 4.6. Rate constants for the decay of negative ions at room temperature [4.8]

Reaction	Release of energy, eV	Rate constant k_d, 10^{-10} cm^3/s
$O^- + O \rightarrow O_2 + e$	3.6	2
$O^- + N \rightarrow NO + e$	5.1	2
$O^- + NO \rightarrow NO_2 + e$	1.4	1.6
$O^- + CO \rightarrow CO_2 + e$	4	4
$O^- + CO_2 \rightarrow CO_3 + e$	< 0	10^{-3}
$O^- + O_2\,(^1\Delta_g) \rightarrow O_3 + e$ [a]	0.5	3
$O_2^- + O_2 \rightarrow O_2 + O_2 + e$	−0.43	$2.2 \cdot 10^{-8}$; $3 \cdot 10^{-4}$ ($T = 600\,\text{K}$)
$O_2^- + N_2 \rightarrow O_2 + N_2 + e$	−0.43	$1.8 \cdot 10^{-6}$ ($T = 600\,\text{K}$)
$O_2^- + N \rightarrow NO_2 + e$	4.1	5
$O_2^+ + O_2\,(^1\Delta_g) \rightarrow O_2 + O_2 + e$	0.6	2
$H^- + H \rightarrow H_2 + e$	3.8	13
$H^- + O_2 \rightarrow H_2O + e$	1.25	12
$OH^- + O \rightarrow HO_2 + e$	0.9	2
$OH^- + H \rightarrow H_2O + e$	3.2	10

[a] $O_2(^1\Delta_g)$; see Table 4.2.

are transformed into more stable complexes, namely, O_3^- and CO_3^- *clusters*. It was established that CO molecules are efficient in destroying O^- ions but very inefficient in destroying CO_3^- (this is important for laser discharges).

4.5 Diffusional Loss of Charges

Breakdown and low-pressure discharges are usually greatly affected by electron losses due to the electron diffusion toward walls. These losses are irreversible: electrons go into the metal or attach to dielectrics and there recombine with ions. Obviously, the mean electron lifetime with respect to the diffusional loss is $\tau_{\text{dif}} = \Lambda^2/D$, where Λ is a length of the order of the minimal size of the vessel and D is the diffusion coefficient (for free or ambipolar processes). The value of Λ can be elaborated by solving the stationary diffusion equation of type (2.44) taking into account ionization sources, $D\Delta n_e + \nu_i n_e = 0$ (without attachment). Assume the field to be homogeneous, that is, $\nu_i(\boldsymbol{r}) = \text{const}$, with $n_e = 0$ at the walls. This gives us an eigenvalue problem, solvable by the method of separation of variables. For example, in a cylinder of radius R and length L, we have $n_e \propto J_0(2.4r/R)\cos(\pi z/L)$; J_0 is the Bessel function and z has its origin at the center of the cylinder's axis. The solution exists only if $\nu_i = \nu_{\text{dif}} \equiv D/\Lambda^2$, where

$$\begin{array}{lll} \text{(cylinder)} & (1/\Lambda)^2 & = (2.4/R)^2 + (\pi/L)^2 \\ \text{(sphere)} & (1/\Lambda)^2 & = (\pi/R)^2\,,\ \Lambda = R/\pi \\ \text{(parallelepiped)} & (1/\Lambda)^2 & = (\pi/L_1)^2 + (\pi/L_2)^2 + (\pi/L_3)^2 \end{array} \qquad (4.12)$$

($L_{1,2,3}$ are the lengths of the sides). Obviously, $\nu_{\text{dif}} = \tau_{\text{dif}}^{-1}$ is the mean frequency of diffusional removal of electrons; Λ is known as the *characteristic diffusion length.*

For example, the ambipolar diffusion coefficient in the positive column of a nitrogen glow discharge at $p = 10\,\text{Torr}$ is $D_a = 200\,\text{cm}^2/\text{s}$. If the discharge is sustained in a long tube of radius $R = 1\,\text{cm}$, then $\Lambda = R/2.4 = 0.42\,\text{cm}$. The diffusion frequency is $\nu_{\text{dif}} = 1.1 \cdot 10^3\,\text{s}^{-1}$. Charges diffuse to the wall in a mean time $\tau_{\text{dif}} = 0.9 \cdot 10^{-3}\,\text{s}$. The rate of diffusional losses $(dn_e/dt)_{\text{dif}} = -\nu_{\text{dif}} n_e$ can be evaluated for more complicated and nonsteady cases as well, using the formula $\nu_{\text{dif}} = D/\Lambda^2$ with Λ given by (4.12). Thus, if the source is distributed uniformly on the axis of a long cylinder, the diffusion time is only $(2.4/2)^2 = 1.44$ times longer than the average value above.

4.6 Electron Emission from Solids

4.6.1 Work Function

A dc current in a gas discharge is sustained by the emission of electrons from the surface of the cathode. To extract an electron from a metal, it is necessary to spend a certain amount of energy; its minimum value is called the *work function* (Table 4.7). It is a function of the state of the surface, its contamination and roughness; on single crystals, it varies from face to face within 1 eV. The binding of electrons to a metal, $e\varphi$, can be interpreted as the work $e^2/4a$ against the attractive image force $e^2/4r^2$; this work is done to remove an electron from a distance a of the order of one interatomic spacing to infinity. If there is an external field E, the force applied to an electron is $F = e^2/4r^2 - eE$. The electron breaks loose of the metal if it is pulled to a distance r_K at which $F = 0$ and reverses its sign. The work function is reduced in comparison with $e\varphi = e^2/4a$ by a quantity

$$e\Delta\varphi = e\varphi - \int_a^{r_K} F dr = e^{3/2}E^{1/2} = 3.8 \cdot 10^{-4}\,\{E[\mathrm{V/cm}]\}^{1/2}\,\mathrm{eV}\,. \qquad (4.13)$$

This is the so-called *Schottky effect* established in 1914.

Table 4.7. Work function of polycrystalline materials and the constant of thermionic emission. (The values of φ recommended in the handbook [4.15] on the basis of an analysis of measurements reported by numerous authors.)

Element	φ, eV	A_1, A/(cm$^2 \cdot$ K^2)
C	4.7	30–170
Al	4.25	
Fe	4.31	60–700
Ni	4.5	30– 50
Cu	4.4	60–100
Mo	4.3	60–150
Ba	2.49	60
W	4.54	40–100
Pt	5.32	10–170

4.6.2 Thermionic Emission

This occurs when a metal is heated: some electrons acquire sufficient energy to escape from the potential well that the metal represents for them. In the absence of an external field, the escaping electrons accumulate near the surface, and the field of this space charge prevents other electrons from escaping from the metal. The space charge is easily removed by a weak accelerating field. Unimpeded emission corresponds to the *saturation current*

$$j_T = A_0 D T^2 \exp\left(-\frac{e\varphi}{kT}\right)\,, \quad A_0 = \frac{4\pi mek^2}{h^3} = 120\,\mathrm{A/(cm^2\,K^2)}\,. \qquad (4.14)$$

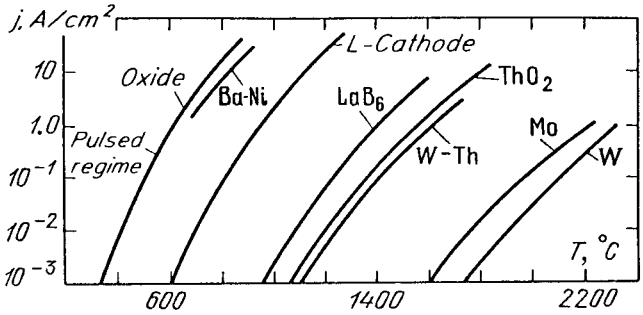

Fig. 4.14. Current density of thermionic emission as a function of cathode temperature for a number of materials. From [4.16]

The factor D in this Dushman-Richardson formula covers the quantum-mechanical effect of the reflection of electrons into the metal from the wall of the potential well, and $A_1 = A_0 D$ is in the range from 15 to 300 (Table 4.7, Fig. 4.14). Electrons leave the metal with a mean energy of $2kT$. The Schottky effect can greatly affect the *thermionic current* (Table 4.8). Thermionic emission is present in arc discharges.

Table 4.8. The currents of the thermionic (j_T), field electron (j_F), and thermionic field (j_{TF}) emission. (The following parameters were used in the computations: $T = 3000\,\mathrm{K}$, $\varphi = 4\,\mathrm{V}$, $A_1 = 80\,\mathrm{A/(cm^2 \cdot K^2)}$, $\varepsilon_F = 7\,\mathrm{eV}$.)

E, 10^7 V/cm	$\Delta\varphi$, V	j_T, A/cm^2	j_F, A/cm^2	j_{TF}, A/cm^2
0	0	$1.3 \cdot 10^2$	0	0
0.8	1.07	$8.2 \cdot 10^3$	$2.0 \cdot 10^{-20}$	$1.2 \cdot 10^4$
1.7	1.56	$5.2 \cdot 10^4$	$2.2 \cdot 10^{-4}$	$1.0 \cdot 10^5$
2.3	1.81	$1.4 \cdot 10^5$	$1.3 \cdot 10^0$	$2.1 \cdot 10^5$
2.8	2.01	$3.0 \cdot 10^5$	$1.3 \cdot 10^2$	$0.8 \cdot 10^6$
3.3	2.18	$6.0 \cdot 10^5$	$4.7 \cdot 10^3$	$2.1 \cdot 10^6$

4.6.3 Field Electron Emission

The field that pulls the electrons away transforms the potential well into a potential barrier of finite width (Fig. 4.15); as a result, electrons can escape from the metal by tunneling. The result is *field electron emission* and the emission current is given by the Fowler-Nordheim formula. In numerical form,

$$j_F = 6.2 \cdot 10^{-6} \frac{(\varepsilon_F/\varphi)^{1/2} E^2}{\varepsilon_F + \varphi} \exp\left(\frac{-6.85 \cdot 10^7 \varphi^{3/2} \xi}{E}\right) \mathrm{A/cm^2}\,. \qquad (4.15)$$

Here ε_F[V] is the Fermi energy, φ[V]is the work function nonperturbed by the field, $\xi(\Delta\varphi/\varphi)$ is a correction factor for its reduction (Table 4.9), and E is measured in V/cm. In reality, appreciable current is obtained at $E \sim 10^6$ V/cm, which is less than implied by (4.15) and Table 4.8 by an order of magnitude. The

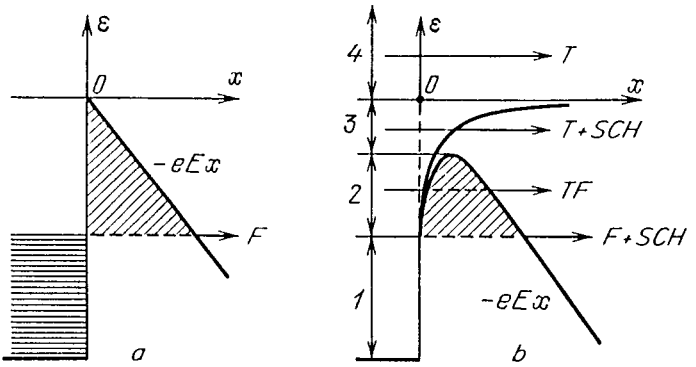

Fig. 4.15. Electron potential energy when an external field is applied to the metal. F – field emission, T – thermionic emission, T+SCH – Schottky-affected thermionic emission, TF – thermionic field emission, F+SCH – Schottky-affected field emission; (a) Mirror forces neglected; (b) mirror forces taken into account. The diagrams illustrate the nature of field-electron and thermionic-field emission, T+SCH – Schottky-affected thermionic emission, TF – thermionic field emission, F+SCH – Schottky-affected field emission

Table 4.9. Correction factor for the reduced work function in the Fowler-Nordheim formula

$\Delta\varphi/\varphi$	0	0.2	0.3	0.4	0.5	0.6	0.7	0.8	0.9	1
ξ	1	0.95	0.90	0.85	0.78	0.70	0.60	0.50	0.34	0

reason is a dramatic enhancement of the applied field at the microscopic protrusions that always exist on real metal surfaces (see Sect. 12.6.1). Field emission results in the breakdown of vacuum gaps.

4.6.4 Thermionic Field Emission

When a strong extracting field is applied to a heated metal surface, both factors (high temperature and field) affect the emission of electrons, in ways not restricted to the mechanisms discussed above. In Fig. 4.15, all allowed energy states of electrons in a metal are classified into four groups. At $T = 0$, electrons occupy states 1 with $\varepsilon \leq \varepsilon_F$. At $T > 0$, all four groups fill up, although the number of electrons falls off rapidly as the excess $\varepsilon - \varepsilon_F$ becomes greater. Electrons of group 1 undergo field emission as at $T = 0$. Electrons of group 4 would escape by thermionic emission even if the field were zero. Electrons of group 3 jump over the barrier, lowered thanks to the field, at the expense of thermal energy. As for the electrons of group 2, which exist only if the metal is heated, they face a narrower and lower barrier that they can cross by tunneling at a higher probability than group-1 electrons.

These are the electrons that generate the current of the *thermionic field emission* [4.17, 18] which is not expressible by simple formulas. The values of j_{TF} given in Table 4.8 are taken from the results of computer simulation [4.19] for the cathode spot of an arc discharge. At $T = 3000\,\mathrm{K}$ and $E > 0.8 \cdot 10^7\,\mathrm{V/cm}$,

thermionic field emission is predominant, the more so at higher fields. If $E < 0.5 \cdot 10^7\,\mathrm{V/cm}$, mostly group-3 electrons are emitted; this is described by (4.14, 13).

4.6.5 Secondary Emission

This is caused by various particles: positive ions, excited atoms, electrons, and also photons. *Secondary emission* from a cold cathode produces breakdown of discharge gaps and also sustains small dc currents that are incapable of substantial heating of the cathode or of creating such a strong field at the cathode that thermionic field emission develops.

The most important among the various secondary mechanisms is the *ion-electron emission*. It is characterized by a coefficient γ_i: the number of electrons emitted per incident positive ion. The relatively small kinetic energies that ions acquire in discharges are ineffective for knocking out electrons, and the main mechanism, as established by *Penning* in 1928 is that the field of an ion approaching a surface to within a distance of atomic dimensions transforms a potential well on the surface into a potential barrier. The barrier is low and narrow because the field is tremendously strong, on the order of that around nuclei. An electron from the metal immediately tunnels into the ion and neutralizes it. If the energy released thereby, $I - e\varphi$, is greater than $e\varphi$, it may be spent on ejecting another (emission) electron. An empirical formula $\gamma_\mathrm{i} \approx 0.016(I - 2e\varphi)\mathrm{eV}$ holds for clean surfaces (with an accuracy of about 50%). Thus $\gamma_\mathrm{i} \approx 0.21$ for tungsten and He^+, 0.30 for Ne^+, 0.09 for Ar^+, and 0.02 for Xe^+; γ_i is almost independent of ε_i up to ion energies $\varepsilon_\mathrm{i} \sim 1\,\mathrm{keV}$ [4.16]. For platinum and the ions H^+, H_2^+, we have $\gamma_\mathrm{i} \approx 3 \cdot 10^{-3}$, for N^+, N_2^+ it is $5 \cdot 10^{-3}$, and for O^+, O_2^+ it is $5 \cdot 10^{-4}$ (for $\varepsilon_\mathrm{i} \sim 0 - 10\,\mathrm{eV}$)[4.20].

Metastable atoms of inert gases are very efficient: $\gamma_\mathrm{m} \approx 0.24$ for $He(2^3S)$ and Pt, 0.4 for $He(2^1S)$ and Pt, 0.4 for Ar^* and Cs. The difference $E^* - e\varphi$ goes to the released electron. In the case of Hg and Ni, $\gamma_\mathrm{m} \sim 10^{-2}$. The photoeffect from the surface at $\hbar\omega > e\varphi$ is characterized by its *quantum yield*, that is, the number of electrons per photon γ_ν (Fig. 4.16). The yield in the visible and near-UV regions is $\sim 10^{-3}$, and in the far-UV region it is $\sim 10^{-2} - 10^{-1}$. In the first two regions, γ_ν is very sensitive to the state and contamination of the surface, and is considerably reduced by reflection. Photoemission often plays the crucial role in breakdown. *Secondary electron emission* is essential in the case of vacuum breakdown by high-frequency fields: the oscillating electron strikes the gap walls alternatingly, one after the other. The secondary emission coefficients γ_e for different metals with ε_e up to several keV vary from 0.4 to 1.6 [4.16]. Secondary electrons are also knocked out of dielectric surfaces. In glass and quartz, $\gamma_\mathrm{e} \sim 1 - 3$ and the maxima are at $\varepsilon_\mathrm{e} \approx 300$–$400\,\mathrm{eV}$. If $\varepsilon_\mathrm{e} < 40$–$60\,\mathrm{eV}$, then $\gamma_\mathrm{e} < 1$ [4.21]. The incident electrons attach to the dielectric, so that the surface is charged negatively if $\gamma_\mathrm{e} < 1$ and positively if $\gamma_\mathrm{e} > 1$.

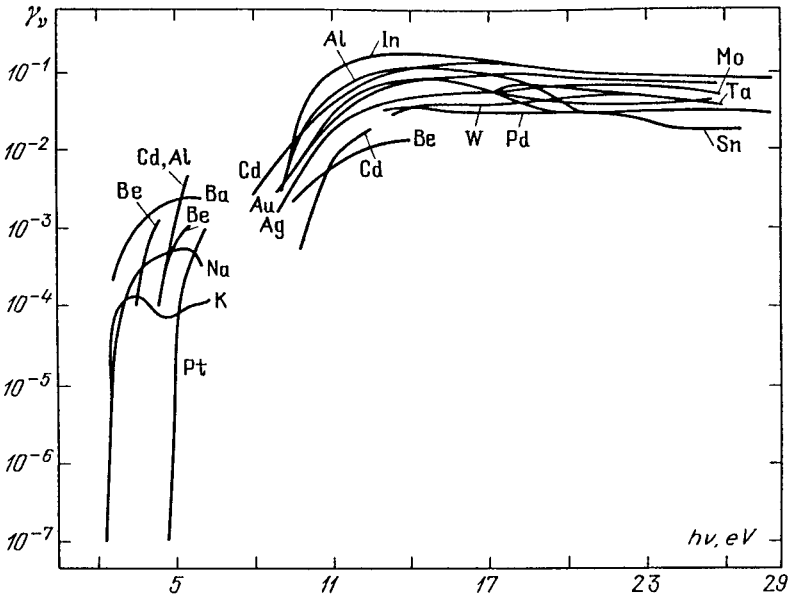

Fig. 4.16. Photoelectron emission coefficients (quantum yield) for various metals as functions of photon energy. From [4.2]

4.7 Multiplication of Charges in a Gas via Secondary Emission

4.7.1 Effect of Secondary Emission on the Enhancement of Primary Electron Current

Let us turn to the experiment for measuring the ionization coefficient α (Sect. 4.1.4). If the photocurrent from the cathode is $i_0 = e\mathcal{N}_0$, then the current recorded at the anode in the absence of secondary emission is $i = i_0 \exp(\alpha d)$. An electron leaving the cathode generates $\exp(\alpha d) - 1$ positive ions in the gap; all of them arrive at the cathode. The current at the cathode in the stationary state can be written $i = i_{el} + i_{ion} = i_0 + i_0[\exp(\alpha d) - 1]$. The dependence of $\ln i$ on d at p, E = const is linear. As E or d is increased, multiplication rapidly intensifies and the secondary electron emission from the cathode begins to affect the total current. Assume that this is the ion-electron emission. Each of the $\exp(\alpha d) - 1$ ions generated by a single electron leaving the cathode knocks out γ_i electrons from the cathode; this secondary electron current is added to the primary current i_0 of the external source. The electronic part of the cathode current i_1 is given by the equation $i_1 = i_0 + \gamma_i i_1[\exp(\alpha d) - 1]$. The current at the anode and in the external circuit is

$$i = i_1 \exp(\alpha d) = i_0 \exp(\alpha d)/\{1 - \gamma[\exp(\alpha d) - 1]\} \tag{4.16}$$

(we have dropped the subscript of γ).

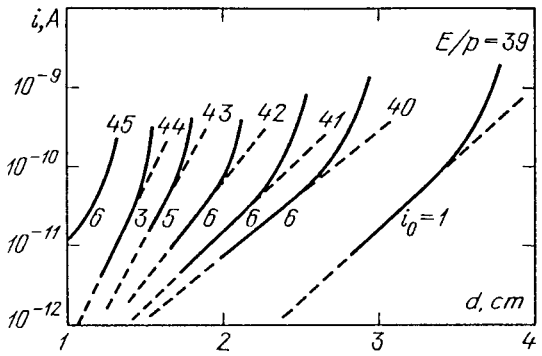

Fig. 4.17. Effect of secondary emission on current enhancement in a discharge gap of length d in air at p = 200 Torr. The *curves* are marked with the values of E/p, V/(cm·Torr), and cathode photocurrent i_0 in 10^{-15} A. From [4.22]

A formula of this type was first derived by *Townsend* in 1902 to explain the process of the ignition of a self-sustaining discharge. As a result of secondary emission, the region of linear growth of $\ln i$ with d turns steeply upward (Fig. 4.17). This process occurs when the denominator of (4.16), which is very close to unity at small enhancement coefficients αd, tends to zero as αd increases. When the denominator becomes zero, breakdown takes place and a self-sustaining discharge is formed: formally, $i = 0/0 \neq 0$ at $i_0 = 0$ (Sect. 7.2.2). Experimentally, this is achieved by raising the voltage between the electrodes. In order to follow a certain E = const curve in Fig. 4.17, one needs to increase V and d simultaneously and proportionally. By analyzing this plot using (4.16) and a known value of α (found from the slope of the linear segment of the curve), one can determine γ.[2]

4.7.2 Photoemission and Effective Coefficient γ

A cold cathode under discharge conditions may emit electrons in response to a large number of agents; it is not always possible to identify a specific agent. For this reason, one usually employs an effective secondary emission coefficient γ per ion. This coefficient characterizes the entire complex process and replaces the elementary-process characteristics γ_i, γ_ν, etc., that are found by bombarding a target with beams of particles or photons of a specific energy.

Let an electron excite along 1 cm of the field such a number of atoms that they later emit α_ν cm^1 photons capable of generating emission. The total number of

[2] Townsend was of the opinion that the secondary process that makes it possible for a non-self-sustaining discharge with exponential amplification of photocurrent i_0 to transform into self-sustaining discharge was the ionization of gas atoms by impact of positive ions. In addition to α, the theory had a second ionization coefficient β for ions. Numerous experiments later proved that ionization of a gas by ions is impossible in a discharge (for the reason given at the beginning of Sect. 4.2.2). The 'α, β'-theory was replaced with an 'α, γ'-theory.

such photons, which are in fact the progeny of one electron leaving the cathode, equals

$$\int_0^d \exp(\alpha x)\alpha_\nu \, dx = (\alpha_\nu/\alpha)[\exp(\alpha d) - 1] \, .$$

If emitted quanta are weakly absorbed by the gas (this happens if pressure is low) and ζ is the mean probability of their reaching the cathode, then the number of secondary electrons emitted from the cathode per primary electron is $(\gamma_\nu \zeta \alpha_\nu/\alpha)[\exp(\alpha d) - 1]$. Adding this quantity to the $\gamma_i[\exp(\alpha d) - 1]$ caused by positive ions, we arrive at the same formula, (4.16), with effective coefficient $\gamma = \gamma_i + \gamma_\nu \zeta \alpha_\nu/\alpha$. The contribution of metastable atoms can likewise be added to γ.

4.7.3 Results of γ Measurements. Positive Ions or Photons?

The results of determining the effective γ by the method outlined in Sect. 4.7.1 are summarized in [4.20, 23] and are illustrated in Fig. 4.18 and Table 4.10. They are not easy to interpret. The coefficient γ depends on E/p in an irregular manner and is very sensitive to the state of the cathode surface. In a number of cases, γ is found to be of the same order of magnitude as γ_i reported in experiments with

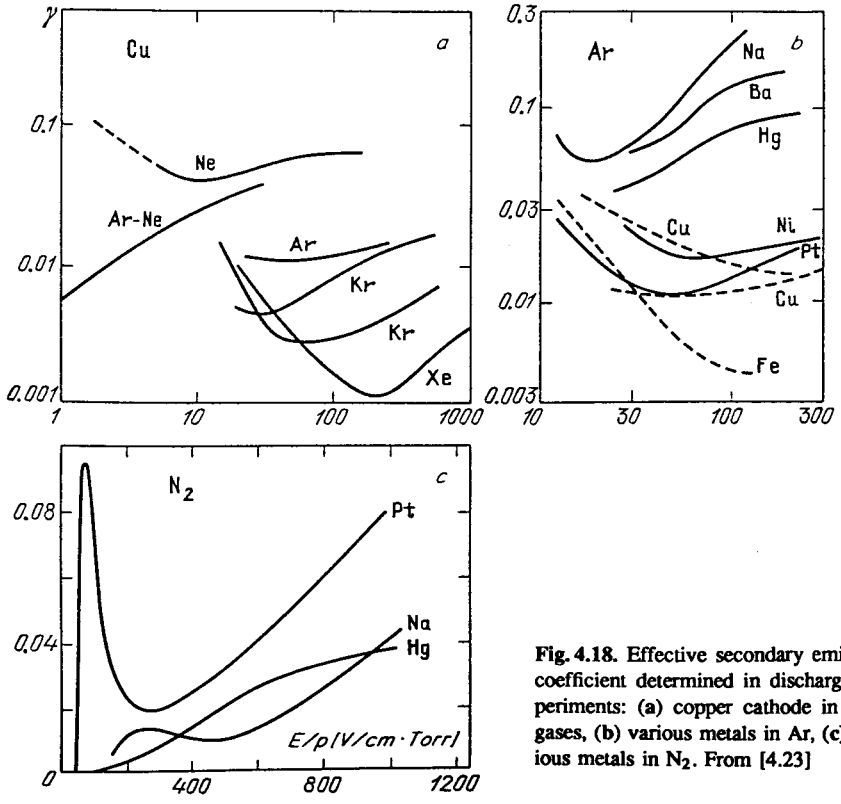

Fig. 4.18. Effective secondary emission coefficient determined in discharge experiments: (a) copper cathode in inert gases, (b) various metals in Ar, (c) various metals in N_2. From [4.23]

Table 4.10. Effective secondary emission coefficients at medium ($\sim$ 100 Torr) and high ($\sim$ 1 atm) pressures, see the references given in [4.21]

Gas	Cathode	State of surface	Conditions in the gas E/p V/(cm·Torr)	pd cm·Torr	γ	Mechanism
Air	Ni	cleaned	39–45		$8.0 \cdot 10^{-6} - 1.5 \cdot 10^{-4}$	
N_2	Ni	cleaned	39–45		$1.3 \cdot 10^{-4} - 3.7 \cdot 10^{-4}$	
N_2	Cu	cleaned		50	$1.5 \cdot 10^{-6}$	ions
N_2	Cu	oxidized		50	$> 10^{-3}$	ions
O_2	Ni		35.4		$4.5 \cdot 10^{-2}$	
O_2	Cu	cleaned		50	$\sim 10^{-7}$	
O_2	Cu	oxidized		50	10^{-6}	ions, photons
H_2	Ni	cleaned	20.3–25.1	$d = 2$	$1.0 \cdot 10^{-3} - 2.4 \cdot 10^{-3}$	
H_2	Cu	cleaned		50	10^{-6}	photons
H_2	Cu	oxidized		50	$5.0 \cdot 10^{-5}$	photons
organics: alcohol, methane, methylal					$\sim 10^{-9}$	

targets bombarded by ion beams. An indication of the emission mechanism may be obtained by studying the nonsteady-state process of generation of secondary, tertiary, etc., electrons (or avalanches, rather) after the primary ones have started, because the arrival times of ions and photons at the cathode are very different (Sect. 12.1.2).

The following preliminary conclusions can be drawn from the available data. Ion-electron emission with $\gamma \sim 10^{-1} - 10^{-3}$ seems to be predominant at $pd \sim 1 - 10$ cm Torr, where $E/p \gtrsim 100$–200 V/(cm Torr) are typical. This is the case for the breakdown of rarefied gases and for the cathode layer of glow discharges. In inert gases on a clean (annealed) cathode, $\gamma \approx \gamma_i$ at high pressures as well. On a contaminated surface, the γ_i are sharply reduced and photoemission is often predominant. Photoemission is dominant in most gases, except inert ones, at about atmospheric pressure and $E/p \approx 30$–40 V/(cm Torr), typical for the breakdown of dense gases. Secondary electrons may appear owing to photoprocesses in the gas itself (Sect. 12.1.3). The data on γ are incomplete and often contradictory. The uncertainty that usually mars the selection of γ for designing or analyzing an experiment is partly alleviated by the fact that γ is normally found in the formulas only within the logarithm (Sects. 7.2 and 8.3). As a rule, one assumes that $\gamma \sim 10^{-1} - 10^{-2}$.

5. Kinetic Equation for Electrons in a Weakly Ionized Gas Placed in an Electric Field

5.1 Description of Electron Processes in Terms of the Velocity Distribution Function

The behavior of electrons in an ionized gas placed in a constant or oscillating electric field was treated in Chaps. 2 and 3 in the framework of *elementary theory*. This concentrates all attention on a single electron, assuming that all electrons behave identically in the transition to macroscopic quantities. This approach allows an approximate calculation of a number of important characteristics of ionized gases: electric conductivity and dielectric permittivity, absorption coefficient for electromagnetic waves, and heating of electrons in the field. These results permit an analysis of various concrete processes: different types of discharge, propagation of radio and light waves in plasma, etc.; we will frequently resort to simple and illustrative notions of elementary theory. This approach is nevertheless quite imperfect, especially if one needs to analyze subtler and more complex effects: ionization and excitation of atoms by electron impact, excitation of molecular oscillations in molecular lasers, etc. These problems cannot be solved without knowing the *electron distribution function* which makes it possible to describe various effects of electron interaction, not only with atoms and molecules but also with the field, much more completely and in finer detail.

The velocity distribution function of electrons, $f(t, \boldsymbol{r}, \boldsymbol{v})$, is defined as follows. The quantity $f\,d\boldsymbol{r}\,d\boldsymbol{v}$ is the number of electrons at a moment t in an element of volume $d\boldsymbol{r} = dx\,dy\,dz$ around a point $\boldsymbol{r}$, with velocity components from v_x to $v_x + dv_x$, etc., so that $d\boldsymbol{v} \equiv dv_x dv_y dv_z$. The integral of f over all velocity components equals the electron density $n_e(t, \boldsymbol{r})$. Recalling that we have a preferred direction in space, defined by the electric vector $\boldsymbol{E}$, it is expedient to express velocity in terms of spherical, not Cartesian, coordinates. The vector $\boldsymbol{v}$ is characterized by its magnitude v, the angle ϑ it makes with the polar axis $\boldsymbol{E}$, and the azimuthal angle φ (Fig. 5.1). Besides, $d\boldsymbol{v} = v^2\,dv\,d\Omega'$, where $d\Omega = \sin\vartheta\,d\vartheta\,d\varphi$ is an element of solid angle around the direction of $\boldsymbol{v}$.

It is easy to pass from the function $f(\boldsymbol{v})$ to distribution functions in absolute values of v, $\varphi(v)$, and in energies, $n(\varepsilon)$:

$$n(\varepsilon)d\varepsilon = \varphi(v)dv = v^2 dv \int f(\boldsymbol{v})d\Omega\ . \tag{5.1}$$

These are also normalized to the density n_e, and the relation between them follows from the equality $\varepsilon = mv^2/2$:

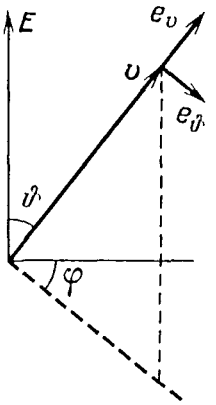

Fig. 5.1. Velocity vector in spherical coordinates

$$n(\varepsilon) = \varphi(v)/mv\ ; \quad \varphi(v) = n(\varepsilon)\sqrt{2m\varepsilon}\ . \tag{5.2}$$

With the distribution function known, any quantity characterizing the electron gas can in principle be calculated. The frequency of ionization of atoms and molecules is given by (4.1). Frequencies of all inelastic collisions, of any reactions, are given by similar formulas. The density of the total electric current carried by electrons is

$$j_t = -e \int v f(v) dv\ . \tag{5.3}$$

The theory of kinetic equation gives expressions for the conductivity and the dielectric permittivity. They are free of the uncertainty in choosing the electron collision frequency inherent in formulas (3.23) and (3.24) of the elementary theory.

5.2 Formulation of the Kinetic Equation

The kinetic equation for electrons is a particular case of the general *kinetic Boltzmann equation* for the distribution function of particles in a gas. In fact, it gives the balancing of the number of particles in an elementary volume in *phase space*.

5.2.1 Balancing Equation

Let us take an elementary volume in the form of a cube around a fixed point in phase space $\boldsymbol{r}$, $\boldsymbol{v}$. One cannot draw a six-dimensional cube, so we trace an ordinary cube (Fig. 5.2) and, appealing to our imagination, think of a six-dimensional cube; one of its vertices has the coordinates x, y, z, v_x, v_y, v_z. At a moment t, the cubic volume $d\Gamma = dx\, dy\, dz\, dv_x dv_y dv_z$ contains $f\, d\Gamma$ particles, so that the distribution function f is interpreted as the *density* in phase space.

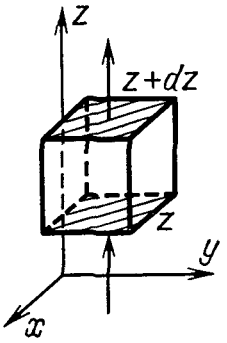

Fig. 5.2. Cube in three-dimensional space: Derivation of the balance equation for particle numbers in phase space

Even with no collisions, the number of particles in the cube changes. A particle moving at a velocity $\boldsymbol{v} = \dot{\boldsymbol{r}}$ changes its position $\boldsymbol{r}$; if subjected to a force $\boldsymbol{F}$, it undergoes acceleration $\boldsymbol{w} = \dot{\boldsymbol{v}}$ and changes its velocity $\boldsymbol{v}$. The particle moves in the phase space where the density f, in general, changes from point to point; hence, the number of particles entering the cube through one face may be greater or smaller than that leaving through the opposite face. Particles may thus accumulate in the volume or be depleted in it. Collisions produce the same effect. Some particles go out of $d\Gamma$ because their velocity vector sharply changes or because they disappear, others enter $d\Gamma$ after a collision or as a result of creation.

The number of particles entering the volume $d\Gamma$ per second through a specific face of the cube, say the lower one in Fig. 5.2 (there are 12 such faces), is $(fv_z)_z dx\, dy\, dv_x dv_y dv_z$. The subscript z with the z-component fv_z of the flux density signifies that the value of the flux is taken at a point z of the axis perpendicular to the face. The product of the five differentials is the area of the face (a face is *five*-dimensional). The number of particles per second leaving through the opposite (upper) face is $(fv_z)_{z+dz} dx\, dy\, dv_x dv_y dv_z$. The difference between the inflow and outflow,

$$\left[(fv_z)_z - (fv_z)_{z+dz}\right] dx\, dy\, dv_x dv_y dv_z = -\left[\partial(fv_z)/\partial z\right] d\Gamma\,,$$

contributes to the rate of particle accumulation in the cube, $(\partial f/\partial t)d\Gamma$. A similar procedure is applied to the other five faces.

As for the collisions, their contribution to the rate of change of the number of particles in the volume $d\Gamma$ is proportional to the volume itself; we denote it by $(df/dt)_c d\Gamma$. Collecting the terms and cancelling the common factor $d\Gamma$, we arrive at the balancing equation for the number of particles:

$$\frac{\partial f}{\partial t} + \left[\frac{\partial}{\partial x}(fv_x) + \ldots + \frac{\partial}{\partial v_x}(fw_x) + \ldots\right] = \left(\frac{df}{dt}\right)_c . \tag{5.4}$$

This is quite similar to the ordinary continuity equation in the presence of sources (represented by the collision term). The sum in brackets is the six-dimensional divergence of the "flux density". Let us introduce into (5.4) the derivative df/dt *along the trajectory* of a specific group of particles in the phase space. This can be done by treating f as a composite function of time,

$$\frac{df}{dt} = \frac{\partial f}{\partial t} + \frac{\partial f}{\partial x}\frac{dx}{dt} + \ldots + \frac{\partial f}{\partial v_x}\frac{dv_x}{dt} + \ldots$$
$$= \frac{\partial f}{\partial t} + v_x\frac{\partial f}{\partial x} + \ldots + w_x\frac{\partial f}{\partial v_x} + \ldots \quad .$$

(The operation d/dt corresponds to the total derivative in hydrodynamics.) We obtain

$$\frac{df}{dt} + f\left[\frac{\partial v_x}{\partial x} + \ldots + \frac{\partial w_x}{\partial v_x} + \ldots\right] = \left(\frac{df}{dt}\right)_c \quad . \tag{5.5}$$

The pairs of quantities v_x and x, and so on, are independent coordinates in phase space, v_x not being a function of x. If the ordinary space contains a field of force $\boldsymbol{F}(\boldsymbol{r})$, the accleration $\boldsymbol{w} = \boldsymbol{F}/m$ is a function of coordinates x, y, z. Even in the presence of a magnetic field, the Lorentz force $\boldsymbol{F} \propto \boldsymbol{v} \times \boldsymbol{H}$, and the component w_x depends on v_y and v_z but is independent of v_x, etc. Hence, the divergence of velocity vanishes: $[\partial v_x/\partial x + \ldots + \partial w_x/\partial v_x + \ldots] = 0$, so that (5.5) reduces to the equality

$$df/dt = (df/dt)_c \quad . \tag{5.6}$$

In the absence of collisions, the number density in a specific group of particles does not change with time while the particles move along the trajectory in the phase space: $df/dt = 0$. The medium in the phase space is "incompressible".

5.2.2 Liouville's Theorem

Let us follow an ensemble of particles that occupy a small volume $\Delta\Gamma$ at a moment t. Without collisions, the number of particles in the group remains constant: $d(f\Delta\Gamma)/dt = 0$. However, $df/dt = 0$ and hence, $d\Delta\Gamma/dt = 0$. The phase volume occupied by a given set of particles travels through the phase space, undergoes deformation, but retains unchanged in volume. This statement is known as *Liouville's theorem*. It is clearly illustrated by Fig. 5.3, drawn for the one-dimensional case x, v_x in which the phase space is represented by the plane of the figure.

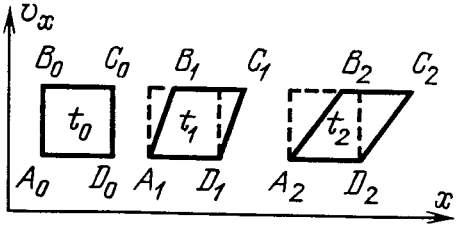

Fig. 5.3. Illustration of Liouville's theorem. A region that is rectangular at a moment t_0 transforms at subsequent moments t_1, t_2 into parallelograms of the same area

5.2.3 Application to Electrons in a Field

We shall not consider the cases with a strong magnetic field, even though this would not be difficult: The Lorentz force is small in the field of electromagnetic waves in comparison with the electric force (Sect. 3.1). Using $\boldsymbol{F} = -e\boldsymbol{E}$, we can rewrite the balance equation (5.6) in the form

$$\frac{\partial f}{\partial t} + \boldsymbol{v} \cdot \mathrm{grad} f - \frac{e\boldsymbol{E}}{m} \cdot \mathrm{grad}_v f = \left(\frac{df}{dt}\right)_c , \tag{5.7}$$

where the symbol "grad_v" denotes the gradient in velocity space. In spherical coordinates we have

$$\mathrm{grad}_v \equiv \boldsymbol{e}_v \frac{\partial}{\partial v} + \boldsymbol{e}_\vartheta \frac{1}{v} \frac{\partial}{\partial \vartheta} + \boldsymbol{e}_\varphi \frac{1}{v \sin\vartheta} \frac{\partial}{\partial \varphi} ;$$

here $\boldsymbol{e}_v$, $\boldsymbol{e}_\vartheta$, and $\boldsymbol{e}_\varphi$ are the unit vectors along the three directions (Fig. 5.1). Let us consider only spatially uniform fields, an approximation justified for electromagnetic waves because the amplitude of electronic oscillations is usually small in comparison with the wavelength (Sect. 3.1). The dependence of f on space coordinates in a uniform field can be caused only by the presence of walls and diffusion flows due to gradients. To avoid distracting attention from our main objective (to find the effect of field and collisions on the distribution function), we assume the entire space to be uniform (the effects of diffusion fluxes being taken into account later by simple techniques), which gives

$$\frac{\partial f}{\partial t} - \frac{eE}{m} \left[\cos\vartheta \frac{\partial f}{\partial v} + \frac{\sin^2\vartheta}{v} \cdot \frac{\partial f}{\partial(\cos\vartheta)} \right] = \left(\frac{df}{dt}\right)_c . \tag{5.8}$$

The function $f(t, v, \vartheta)$ is independent of the angle φ because $\boldsymbol{E}$ defines an axis of symmetry.

5.2.4 Classification of Collisions into Elastic and Inelastic

Let us look at the right-hand side of (5.8). Assume the gas to be weakly ionized and neglect the collisions of electrons with other electrons and with ions, taking into account only those with neutrals. This is a very important assumption, greatly facilitating the problem of solving the kinetic equation by making it *linear*. The general Boltzmann equation for a gas is nonlinear because the right-hand side includes the collisions of particles of a given species with one another. These terms contain, of course, the products of distribution functions of the colliding particles. In our case, electrons collide with foreign particles, that is, heavy atoms "at rest", which are assumed here to have no distribution. The contributions of collisions of each type to the change in distribution function are simply added up. Let us divide all collisions into *elastic* and *inelastic*:

$$\left(\frac{df}{dt}\right)_c = \left(\frac{df}{dt}\right)_{el} + \left(\frac{df}{dt}\right)_{inel} = I(f) + Q(f) . \tag{5.9}$$

We subsume into the group of inelastic collisions, in addition to the processes of excitation of atoms and molecules, the creation of new electrons as a result of ionization and the possible annihilation processes. Inelastic collisions are important for the formation of the *energy spectrum* of electrons but, being much less frequent than elastic collisions, they have practically no influence on the field-electron interaction and on the change in electron velocity and energy caused by the field. Hence, inelastic processes do not affect the build-up of the *asymmetric* part of the distribution function that reflects the oriented action of the field and frequent elastic collisions. For these reasons, we do not yet specify the expression $Q(f) \equiv (df/dt)_{\text{inel}}$; this will be done only after we pass from the velocity vector distribution function to the distribution in electron energy.

5.2.5 Collision Integral

This name is applied to the term $I(f)$ representing the effect of elastic collisions. Assume that the atoms are at rest and, in addition, neglect the quantities of order m/M, assuming $M = \infty$. Under this approximation, the absolute value of the electron velocity v and its energy ε are exactly conserved in scattering. We will take elastic losses into account later, after having derived the final equation for the electron velocity distribution. It will be possible to use a simple line of reasoning to add to the equation an elastic loss term, and obtain an accurate result. If, however, the change in v due to scattering is introduced from the very beginning, this not too significant refinement makes the derivation of the collision integral considerably more complex.

The *collision integral* $I[f(\boldsymbol{v})]$ takes into account the change in the number of electrons with a given velocity vector $\boldsymbol{v}$, caused by the loss of electrons to the points of the phase space with a different vector $\boldsymbol{v}'$ as a result of scattering by atoms, and also by the arrival to $\boldsymbol{v}$ from all other points $\boldsymbol{v}'$. According to our assumption, the magnitude of velocity is conserved in scattering, so that it is sufficient to characterize $\boldsymbol{v}$ by a unit vector of direction, $\boldsymbol{\Omega}$. Since f has for argument the same absolute value of velocity v, we write simply $f(\boldsymbol{\Omega})$ instead of $f(\boldsymbol{v}) = f(v, \boldsymbol{\Omega})$. Owing to scattering, $f(\boldsymbol{\Omega})d\Omega\nu_c(v)$ electrons move in one second out of a given solid angle $d\Omega$ around the given direction $\boldsymbol{\Omega}$ of velocity, ν_c being the collision frequency. The electrons are lost to all other allowed directions $\boldsymbol{\Omega}'$. Let $q(v, \boldsymbol{\Omega}, \boldsymbol{\Omega}')d\Omega'$ be the probability for a colliding electron, moving in the direction $\boldsymbol{\Omega}$, to change its direction to $\boldsymbol{\Omega}'$ in the interval $d\Omega'$. The electron has to move in some direction, so that

$$\int q(\boldsymbol{\Omega}, \boldsymbol{\Omega}')d\Omega' = 1 \, .$$

The number of electrons leaving $d\Omega$ can be written in the form of a detailed expression:

$$f(\boldsymbol{\Omega})d\Omega\nu_c = \nu_c \int_{\boldsymbol{\Omega}'} f(\boldsymbol{\Omega})d\Omega q(\boldsymbol{\Omega}, \boldsymbol{\Omega}')d\Omega' \, .$$

The number of electrons arriving per second in the same volume $d\Omega$ and the given direction Ω from other directions Ω' is

$$\nu_c \int_{\Omega'} f(\Omega')d\Omega' q(\Omega', \Omega)d\Omega .$$

The difference between the gain and loss gives us $I[f(\Omega)]d\Omega$. Before we write out this expression, note that the probability of scattering from one direction to another depends not on the directions as such, but only on the angle between them: the scattering angle θ (Fig. 5.4). Hence, $q(\Omega, \Omega') = q(\Omega', \Omega) = q(\theta)$, and the probability can be integrated, with the same result, in final directions Ω' or in initial ones, Ω. Then we can cancel the differential $d\Omega$ not involved in integration and finally obtain

$$I(f) = \nu_c(v) \int_{\Omega'} [f(\Omega') - f(\Omega)]q(\theta)d\Omega' . \tag{5.10}$$

Integration is carried out here in all directions Ω' at a fixed Ω. Equation (5.8) with the right-hand side (5.9), where the collision integral I is given by (5.10) and the inelastic collisions term Q is to be specified later, is the required kinetic equation.

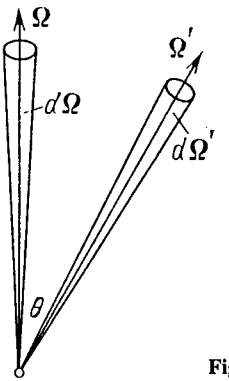

Fig. 5.4. Scattering angle θ

5.3 Approximation for the Angular Dependence of the Distribution Function

The kinetic equation is integro-differential in the angle ϑ and hence is mathematically very unwieldy. The factor that makes the distribution function depend on the direction of velocity, that is, on ϑ, is the field. In zero field, the distribution is isotropic. The field accelerates negative charges in the opposite direction to E, therefore producing an excess of electrons moving in this direction and a shortage of those moving in the opposite direction.

5.3.1 Symmetric and Asymmetric Parts of the Distribution Function

Assume the field to be moderately strong, and the *anisotropy* caused by it to be small. (We take this into account approximately, as a correction to the main, *symmetric* part of the function.) If this operation is to be mathematically rigorous, the angular dependence $f(t, v, \vartheta)$ must be written as a series expansion, so as to describe in an accurate manner the detailed departure from symmetry. Only a system of orthogonal and normalized functions may be used for the expansion. Such a system satisfying the angular dependence is that of Legendre polynomials: $P_0 = 1$, $P_1 = \cos\vartheta$, etc. Our approximation limits the series to the first two terms,

$$f(t, v, \vartheta) = f_0(t, v) + f_1(t, v) \quad \cos\vartheta \,, \tag{5.11}$$

where f_0 and f_1 are the new sought-after functions; equations for finding these are to be formulated.

The new functions have a definite physical meaning, the first of them, the *symmetric* part, determines the electron *energy* spectrum. According to (5.1), we have

$$n(\varepsilon)d\varepsilon = \varphi(v)dv = 4\pi v^2 f_0(v)dv \,. \tag{5.12}$$

The *asymmetric* part $f_1 \cos\vartheta$ determines the *electric current*. In view of the axial symmetry $f(v)$ the current points along the field. Formulas (5.3) and (5.11) imply that its magnitude is

$$j_t = -e \int\int v(\cos^2\vartheta)\, f_1 2\pi v^2\, dv \sin\vartheta\, d\vartheta = -\frac{4\pi}{3} e \int v^3 f_1\, dv \,. \tag{5.13}$$

Approximation (5.11) is admissible only if the anisotropy of the distribution function is sufficiently small, that is, if the field is not too strong. The quantitative criterion of the notion "not too strong" will be clear after we find the correction f_1 to the main part of f and demand that $f_1 \ll f_0$ (Sect. 5.5.1). Approximation (5.11) is attributed to H. Lorentz, who formulated the kinetic equation for electrons in a dc field, and elaborated formula (2.7) for conductivity using approximation (5.11).

5.3.2 Equations for the Functions f_0 and f_1

The simplest way to derive these functions is to make use of the method of moments. The original equation for f is multiplied by a Legendre polynomial and integrated over the angles taking into account the properties of polynomials. In the case in question, it is sufficient to do it twice: first simply integrate (5.8) over the solid angle $d\Omega$ because the zeroth polynomial P_0 is equal to 1, and then multiply (5.8) by $P_1 = \cos\vartheta$ and integrate for the second time. As a result of the first integration (rather, of averaging, i.e., of the operation $\int d\Omega/4\pi$), taking into account that $\langle\cos\vartheta\rangle = 0$, $\langle\cos^2\vartheta\rangle = 1/3$, $\langle\sin^2\vartheta\rangle = 2/3$, we find

$$\frac{\partial f_0}{\partial t} - \frac{eE}{m}\left(\frac{1}{3}\frac{\partial f_1}{\partial v} + \frac{2f_1}{3v}\right) = Q(f_0) \,.$$

The integral $\int I d\Omega$ on the right-hand side vanishes automatically since it gives the change in the number of electrons moving in all directions as a result of elastic collisions and elastic collisions do not change the total number of electrons. Of course, the inelastic-collisions term is linear in f; in general, the effect of inelastic collisions is independent of the direction of velocity, being a function only of energy spectrum. Hence, Q becomes a function of the symmetric part of f. The obtained equation can be rewritten in the form

$$\frac{\partial f_0}{\partial t} = \frac{eE}{m}\frac{1}{3v^2}\frac{\partial (v^2 f_1)}{\partial v} + Q(f_0) \,. \tag{5.14}$$

The second averaging of the kinetic equation with the weight $\cos\vartheta$ yields

$$\frac{1}{3}\frac{\partial f_1}{\partial t} - \frac{1}{3}\frac{eE}{m}\frac{\partial f_0}{\partial v} = \frac{\nu_c}{4\pi}\int \cos\vartheta \, d\Omega \int [f(\Omega') - f(\Omega)] q(\theta) d\Omega' \,, \tag{5.15}$$

where we have so far simply copied (5.10) without substituting (5.11) there, and neglected the contribution of inelastic collisions in comparison with that of elastic ones.

Let us take the right-hand side of (5.15). The inner integral in $d\Omega'$ is taken over all directions Ω' at a fixed Ω. In fact, when integrating over the angle Ω', one need not choose the vector E as the polar axis, as we did in constructing the original kinetic equation. Now it is more convenient to direct the polar axis along Ω (Fig. 5.5) and describe the direction of Ω' by the angles θ and φ', the azimuth φ' being measured from a fixed plane passing through the vectors Ω and E. In these coordinates, an element of the solid angle is $d\Omega' = d\varphi' \sin\theta \, d\theta$; this is very convenient because the factor q in the integrand is a function of θ. Now we substitute (5.11) and rewrite the inner integral, with a fixed angle ϑ:

$$J = \int [f(\Omega') - f(\Omega)] q(\theta) \, d\Omega' = f_1 \int (\cos\vartheta' - \cos\vartheta) q(\theta) \times d\varphi' \sin\theta \, d\theta \,.$$

Expressing $\cos\vartheta'$ via the familiar formula of spherical trigonometry,

$$\cos\vartheta' = \cos\vartheta\cos\theta + \sin\vartheta\sin\theta\cos\varphi' \,,$$

and taking into account that the term with $\cos\varphi'$ vanishes in the integration in φ', we find

$$J = f_1 \cos\vartheta \int (\cos\theta - 1) q(\theta) d\varphi' \sin\theta \, d\theta = f_1 \cos\vartheta (\overline{\cos\theta} - 1) \,.$$

Here $\overline{\cos\theta}$ is, by definition, the *mean cosine of the scattering angle* because $\cos\theta$ is averaged on the basis of the scattering probability $q(\theta)$ normalized to unity over all angles. The second of the sought equations is obtained by introducing the effective collision frequency $\nu_m = \nu_c(1 - \overline{\cos\theta})$ (note that we have just derived this expression rigorously), substituting the inner integral J into (5.15), and again integrating over $d\Omega$:

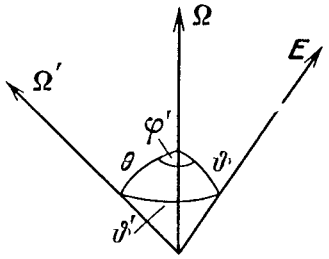

Fig. 5.5. Directions of field and velocities before and after scattering

$$\frac{\partial f_1}{\partial t} + \nu_m f_1 = \frac{eE}{m} \frac{\partial f_0}{\partial v} . \tag{5.16}$$

We have thus obtained, instead of the integro-differential equation (5.8), two differential equations for the functions f_0 and f_1 that approximate the true distribution function by (5.11). These equations hold for arbitrary dependence $E(t)$, that is, both for dc and for oscillating fields.

5.4 Equation of the Electron Energy Spectrum

5.4.1 Approximate Integration of the Equation for f_1

In order to proceed further, we have to specify the dependence of the field on time. Let us take a harmonic field $E = E_0 \sin \omega t$. It is obviously impossible to find the exact solution of the system (5.14, 16), so we make the following approximation. The correction f_1 to the symmetric part of the distribution function is caused by the field, which changes its direction periodically. The correction oscillates with the same frequency: first a greater number of electrons move along the field, and after half a cycle more electrons move in the opposite direction. As follows from (5.14), the dependence of the main (symmetric) function f_0 on time consists of two parts. On one hand, this is a relatively slow dependence due to the buildup of the electron energy spectrum as a result of various inelastic processes, creation and loss of electrons, and energy gain from the field. Since f_1 is also a harmonic function and is proportional to E_0, the first term in the right-hand side of (5.14) has a component, averaged over a period, that is proportional to E_0^2, and an oscillating component. The accumulation of energy is provided by the averaged component. On the other hand, f_0 contains an oscillating component due to the oscillating part of the first term in the right-hand side of (5.14). It resembles a ripple imposed on the slowly changing $f_0(t)$. Obviously, the variations of the spectrum during one period, that is, the ripple, need not bother us if we are interested in the electron energy spectrum at sufficiently high frequencies (see the criterion in Sect. 5.5.2). The object of physical interest is the smoothed function $\langle f_0 \rangle$ averaged over one period of field oscillations.

When integrating equation (5.16), we substitute the function $\langle \partial f_0 / \partial v \rangle$ averaged over a period. The high-frequency component would contribute to f_1 a term

of higher order in E. Neglecting the slow dependence of $\langle \partial f_0/\partial v \rangle$ on time in comparison with $\sin \omega t$, we integrate (5.16) as a linear equation, where $\langle \partial f_0/\partial v \rangle$ is independent of time. We find that

$$f_1 = -\frac{eE_0}{m(\omega^2 + \nu_m^2)} \left\langle \frac{\partial f_0}{\partial v} \right\rangle (\omega \cos \omega t - \nu_m \sin \omega t) , \tag{5.17}$$

and this expression can be rewritten in the form

$$f_1 = \frac{eE_0}{m\sqrt{\omega^2 + \nu_m^2}} \left\langle \frac{\partial f_0}{\partial v} \right\rangle \sin(\omega t - \alpha) , \tag{5.18}$$

where $\alpha = \arctan(\omega/\nu_m)$.

We conclude that $f_1 \propto E_0$; it oscillates at a frequency ω but its phase is shifted with respect to the field. In the limiting case of high frequencies ($\omega^2 \gg \nu_m^2$), the phase shift is $\alpha \approx \pi/2$, and

$$f_1 \approx -\frac{eE_0}{m\omega} \left\langle \frac{\partial f_0}{\partial v} \right\rangle \cos \omega t = -u \left\langle \frac{\partial f_0}{\partial v} \right\rangle \cos \omega t .$$

To an order of magnitude, $\partial f_0/\partial v \sim f_0/v$, where v is some characteristic, average velocity of random motion. According to (3.2), $eE_0/m\omega = u$ is the amplitude of the varying velocity of an electron in the oscillating field, so that to an order of magnitude,

$$f_1 \sim (u/v) f_0 . \tag{5.19}$$

In the opposite limiting case of low frequencies ($\omega^2 \ll \nu_m^2$), the phase shift α is small and

$$f_1 \approx \frac{eE_0}{m\nu_m} \left\langle \frac{\partial f_0}{\partial v} \right\rangle \sin \omega t \underset{\omega \to 0}{\longrightarrow} \frac{eE}{m\nu_m} \frac{\partial f_0}{\partial v} .$$

It is readily seen that the same result is implied directly by (5.16) if the field is assumed to be constant *ab initio*. The asymptotic constant value of f_1 that is reached after a time of about one collision period is

$$f_1 = \frac{eE}{m\nu_m} \frac{\partial f_0}{\partial v} \sim \frac{v_d}{v} f_0 , \tag{5.19'}$$

where, in view of (2.4), $v_d = eE/m\nu_m$ is the absolute value of the electron drift velocity. The smallness criterion f_1/f_0 is implied by (5.19, 19') (Sect. 5.5.1).

5.4.2 Equation for f_0

Now that we have expressed the correction f_1 in terms of the main function f_0, we may take the last step: to substitute it into (5.14) and thus obtain an equation for the symmetric part of the distribution function which is unambiguously related to the energy spectrum. If the field is harmonic, we substitute (5.17) into (5.14)

and average the equation so obtained over one period of oscillation in order to eliminate the ripples and reveal the slow time-dependence of the spectrum, it being the only one of interest. Remarking that

$$\langle \cos \omega t \sin \omega t \rangle = 0 , \quad \langle \sin^2 \omega t \rangle = \tfrac{1}{2} ,$$

and dropping the averaging brackets $\langle \ \rangle$ with f_0, we arrive at an equation for the function $f_0(t, v)$:

$$\frac{\partial f_0}{\partial t} = \frac{1}{v^2} \frac{\partial}{\partial v} \left[\frac{e^2 E^2}{3m^2} \left(\frac{\nu_m(v) v^2}{\omega^2 + \nu_m^2} \right) \frac{\partial f_0}{\partial v} \right] + Q(f_0) . \tag{5.20}$$

Here we have substituted for E_0 the root-mean-square field $E = E_0/\sqrt{2}$. In the case of a dc field, the substitution of (5.19′) into (5.14) gives the same equation (5.20) but with $\omega = 0$. In other words, the exact limiting transition is possible from the case of the harmonic field to that of a dc field, provided we replace the root-mean-square field with a constant one as $\omega \to 0$; note that this appears to be intuitively natural.

5.4.3 Equation for $n(\varepsilon)$

If we recast (5.20) to a new independent variable $\varepsilon = mv^2/2$, $d\varepsilon = mv\,dv$, and replace the function $f_0(t, v)$ with the energy distribution function $n(t, \varepsilon)$ via (5.12), the result is an equation for the energy spectrum:

$$\frac{\partial n}{\partial t} = \frac{\partial}{\partial \varepsilon} \left(A \varepsilon^{3/2} \frac{\partial}{\partial \varepsilon} \frac{n}{\varepsilon^{1/2}} \right) + Q(n) ,$$

$$A = \frac{2e^2 E^2}{3m} \frac{\nu_m}{\omega^2 + \nu_m^2} = \frac{e^2 E_0^2}{3m} \frac{\nu_m}{\omega^2 + \nu_m^2} . \tag{5.21}$$

The case of a dc field is also obtained if we set $\omega = 0$ and replace the root-mean-square field by the constant field.

5.4.4 Diffusion Nature of the Equation

Carrying out the differentiation of $n\varepsilon^{-1/2}$ in (5.21) and introducing new notation for combinations of variables, we rewrite this equation:

$$\frac{\partial n}{\partial t} = -\frac{\partial J}{\partial \varepsilon} + Q , \quad J = -\mathcal{D} \frac{\partial n}{\partial \varepsilon} + nU ,$$
$$\mathcal{D} = A\varepsilon , \quad U = A/2 . \tag{5.22}$$

The structure of (5.22) is quite similar to that of the equation of *one-dimensional diffusion* of particles. Indeed, ε is the coordinate, n is the density of particles, J is the flux, Q is the source, $\mathcal{D}$ is the diffusion coefficient that, in fact, is position dependent (this is also imaginable: say, the density of the main gas through which particles diffuse varies with the coordinate), and U is the velocity of the "kinematic" flow, that is, of the systematic motion in one direction, for instance, a drift that may be caused by the flow of the medium.

The physical meaning of the diffusion nature of energy accumulation in the field, that is, of the diffusive motion of electrons along the "energy axis," is very lucid. We have indicated in Sects. 2.3.3 and 3.2.5 that collisions can either increase or decrease the energy of electrons, in portions that equal, to an order of magnitude, mvu, where v is the velocity of random motion and u is the velocity of oriented motion caused by the field. In the high-frequency case, u is the amplitude of the oscillating electron velocity, and in the dc field, u equals the drift velocity v_d. Since on average, energy is gained or lost with almost equal probability, the change in electron energy resembles a random walk along the axis ε. The coefficient of ordinary diffusion, which manifests itself in treating the one-dimensional random walk of a particle, is approximately $D \approx \overline{\Delta x^2}/\tau$, where Δx is a step along the x axis and τ is the mean time interval between steps. In our case,

$$\mathcal{D} \approx (mvu)^2 \nu_m .$$

Substituting here $u = eE_0/m\omega$ in the high-frequency range $\omega^2 \gg \nu_m^2$, or $u = v_d = eE/m\nu_m$ (drift velocity) in the low-frequency range $\omega^2 \ll \nu_m^2$, and recalling that $\varepsilon = mv^2/2$, we find for these limiting cases the diffusion coefficient defined by (5.22) and (5.21) (to within an unimportant numerical factor).

The kinematic velocity U also has a physical meaning. The positive kinematic flux directed towards increasing ε is mostly related to the predominant energy gain in collisions, in contrast to energy losses. We have seen in Sects. 2.3.3 and 3.2.5 that on the average the energy gained is greater than the energy lost by a quantity $\Delta\varepsilon_E \propto mu^2$, which is less by a factor v/u than a mean increment in any direction, mvu. The rate of systematic upward motion on the energy axis, $U \sim \Delta\varepsilon_E \nu_m$, is indeed on the order of

$$U \sim mu^2 \nu_m \sim (mvu)^2 \nu_m / mv^2 \sim \mathcal{D}/\varepsilon ,$$

as we have formally obtained in deriving (5.22).

5.4.5 Elastic Loss Term

Following the remarks on the diffusion along the energy axis, it is not difficult to add to the energy spectrum equation a term describing elastic energy loss. Indeed, elastic losses also produce a flux along the energy axis, always pointing toward decreasing ε. The mean energy that an electron loses in an elastic collision, calculated in Sect. 2.3.4, is

$$\Delta\varepsilon_{el} = (2m/M)(1 - \overline{\cos\theta})\varepsilon .$$

This is the quantity by which an electron slides "downward" on the ε axis after each collision. The time between collisions is $\tau_c = \nu_c^{-1}$. Hence, the corresponding velocity of downward motion is

$$U_{el} = -\Delta\varepsilon_{el}/\tau_c = -(2m/M)\nu_m \varepsilon ;$$

the kinetic flux corresponding to this velocity is nU_{el}. We add it to the flux J in (5.22). Returning now from (5.22) to the original equations (5.20,21), we write them out, now taking into account the elastic loss term:

$$\frac{\partial f_0}{\partial t} = \frac{1}{v^2}\frac{\partial}{\partial v}\left[\frac{e^2E^2}{3m^2}\frac{\nu_m v^2}{\omega^2+\nu_m^2}\frac{\partial f_0}{\partial v} + \frac{m}{M}\nu_m v^3 f_0\right] + Q(f_0)\,, \tag{5.23}$$

$$\frac{\partial n}{\partial t} = \frac{\partial}{\partial \varepsilon}\left(A\varepsilon^{3/2}\frac{\partial}{\partial \varepsilon}\frac{n}{\varepsilon^{1/2}} + \frac{2m}{M}\varepsilon\nu_m n\right) + Q(n)\,,$$
$$A = \frac{2e^2E^2}{3m}\frac{\nu_m}{\omega^2+\nu_m^2}\,. \tag{5.24}$$

Note that our simple reasoning has led to the exact result covering elastic losses. If the finite mass of atoms has been introduced from the very beginning into the collision integral, we would have arrived at the same equations, (5.23) and (5.24).

5.4.6 Inelastic Collision Term

Let us specify the quantity Q that was to include all processes not related to the field and elastic collisions. The loss of electrons per second in 1 cm^3 from the energy interval $d\varepsilon$ due to the excitation and ionization of atoms equals $n(\varepsilon)d\varepsilon\nu^*(\varepsilon)$ and $n(\varepsilon)d\varepsilon\nu_i(\varepsilon)$, respectively, where $\nu^*(\varepsilon)$ and $\nu_i(\varepsilon)$ are, respectively, the frequencies of excitation of corresponding levels and of ionization at a given electron energy ε. The energy E^* lost by an electron in an act of excitation equals the excitation potential plus a small energy needed to impart to the atom the velocity necessary for the total momentum of the electron and the atom to remain unaltered. This additional energy loss is very small, as it is in elastic scattering; it is negligible in comparison with E^*. If the inelastic collision involved an electron with energy $\varepsilon' = \varepsilon + E^*$ in the interval $d\varepsilon' = d\varepsilon$, then the loss of energy shifts it into the interval $d\varepsilon$ at the point ε. Hence, the term in $Q(n)$ due to the excitation of a certain level can be expressed approximately in the form

$$Q^*(n) = -n(\varepsilon)\nu^*(\varepsilon) + n(\varepsilon + E^*)\nu^*(\varepsilon + E^*)\,, \tag{5.25}$$

where $\nu^*(\varepsilon) = 0$ if $\varepsilon \leq E^*$. The excitation of vibrational levels in molecules is described by expressions of similar type. The total amount Q is the sum of this type of term over all relevant levels of atoms and molecules.

The term representing ionizing collisions, $Q_i(n)$, is more complicated. Let an electron have energy $\varepsilon' > I$. The electron spends energy I on liberating an electron from an atom; the remainder, $\varepsilon' - I$, is divided between the primary and the secondary electrons (the energy transferred to the ion being negligible). Let $\Phi(\varepsilon', \varepsilon)d\varepsilon$ be the probability for the energy of the electron knocked out of the atom to be between ε and $\varepsilon + d\varepsilon$ ($\int_0^{\varepsilon'-I}\Phi(\varepsilon', \varepsilon)d\varepsilon = 1$). The ionizing electron falls into the same interval if the new one acquires an energy from $\varepsilon' - I - \varepsilon - d\varepsilon$ to $\varepsilon' - I - \varepsilon$, and the probability of such an event is $\Phi(\varepsilon', \varepsilon' - I - \varepsilon)d\varepsilon$. Forming

$Q_i d\varepsilon$ from the terms due to electrons arriving at and leaving the interval ε to $\varepsilon + d\varepsilon$ and then dividing by $d\varepsilon$, we obtain

$$Q_i = -n(\varepsilon)\nu_i(\varepsilon) + \int_{\varepsilon+I}^{\infty} n(\varepsilon')\nu_i(\varepsilon')[\Phi(\varepsilon', \varepsilon) + \Phi(\varepsilon', \varepsilon' - I - \varepsilon)]d\varepsilon' . \tag{5.26}$$

Expression (5.26) transforms to (5.25) if we assume that all new electrons appear with identical energy ε_0 and $\varepsilon' > I + \varepsilon_0 \equiv I_1$. Then $\Phi(\varepsilon', \varepsilon) = \delta(\varepsilon - \varepsilon_0)$, where δ is the Dirac delta function. In this case

$$Q_i = -n(\varepsilon)\nu_i(\varepsilon) + n(\varepsilon + I_1)\nu_i(\varepsilon + I_1) + \delta(\varepsilon - \varepsilon_0)\int_{I_1}^{\infty} n(\varepsilon')\nu_i(\varepsilon')d\varepsilon' . \tag{5.26'}$$

The additional term when compared with (5.25) describes the source of new electrons.

The losses due to recombination or attachment of electrons are extremely easy to introduce into Q, for example, by a term $-n(\varepsilon)\nu_a(\varepsilon)$, where $\nu_a(\varepsilon)$ is the frequency of attachment to atoms or molecules.

5.4.7 Spatial Diffusion of Electrons

This can be rigorously calculated if the term $\boldsymbol{v}\,\mathrm{grad}\,f$ found in (5.7) is left in the left-hand side of the original equation (5.8). We have not done this in the preceding paragraphs in order to avoid complicating the manipulations and to focus the attention on the effects of interaction with the field. In the final equation for the spectrum, the diffusional losses of electrons can be taken into account approximately, adding to Q a term of type

$$Q_d = -n(\varepsilon)\nu_d(\varepsilon) ,$$

where $\nu_d = D/\Lambda^2$ is the "diffusion frequency", that is, a quantity reciprocal to the characteristic time of diffusional removal of an electron from the chosen volume, $D = v^2/3\nu_m$ is the diffusion coefficient (in ordinary space!), and Λ is the characteristic diffusion length (Sect. 4.5).

5.5 Validity Criteria for the Spectrum Equation

5.5.1 With Respect to Field Magnitude

The Lorentz approximation (5.11), on which the derivation of the equation was based, is valid if the asymmetry of the distribution function $f(\boldsymbol{v})$ is small: $f_1/f_0 \ll 1$. According to (5.19, 19'), this happens if the velocity of the electron directed along the field (amplitude u in the case of rapidly oscillating field or the drift velocity v_d in the case of dc field) is much less than the random velocity v. The terms with higher-order harmonics in the expansion of f in Legendre polynomials are proportional to the appropriate powers of the ratios u/v

and v_d/v. These ratios serve as the small parameters for series expansion of the distribution function f. The indicated conditions are satisfied in most practically interesting cases. Indeed, in a uniform not very high dc field in which an electron loses only a small fraction δ of its energy, $v_d/v \approx \sqrt{\delta} \ll 1$ [see (2.16)]. A quite similar relation, $u/v \approx \sqrt{\delta}$, is implied by (3.2) and (3.12) in the case of a rapidly oscillating field.

If a colliding electron loses a considerable fraction of its energy (formally, $\delta \sim 1$), the conditions are violated and the distribution function becomes essentially asymmetric (electrons move mostly along the field). This happens when an electron gains from the field in one free path length l (or in oscillations) the energy greater than that necesssary for the excitation of electron levels or for ionization of atoms, say, $eEl \gtrsim I$. Such situations occur mainly in exceptionally strong fields: in the cathode layer of the glow discharge, in focusing superpowerful optical pulses etc. Equations (5.23) and (5.24) have limited applicability on the side of small E, as well. The electron temperature in a very weak field may be comparable to the gas temperature T, which we assumed to be zero. The kinetic equation with $T \neq 0$ was discussed by *B.I. Davydov* in 1936.

5.5.2 With Respect to Field Frequency

The calculations of Sect. 5.4.1 ignored the modulation of the spectrum at the field frequency ω, since the symmetric part of the distribution function, f_0, was averaged over the oscillation period. This is admissible if the field oscillates rapidly in comparison with the time necessary for the buildup of the electron energy spectrum. Then only the root-mean-square field affects the spectrum and the gaining of energy from the field. In other words, the condition of applicability of the approximation used is the inequality $\omega \gg \nu_u = \nu_m \delta$, where $\tau_u = \nu_u^{-1}$ is the spectrum relaxation time, equal to the characteristic time of energy transfer from electrons to molecules (Sect. 2.3.7). In atomic gases this inequality is satisfied better than in molecular ones. It is satisfied practically always in the microwave and, of course, in the optical range of frequencies; almost always in the radiofrequency range in atomic gases; and sometimes also in the radiofrequency range in molecular gases. For example, in nitrogen $\nu_m \approx 4.2 \cdot 10^9 p[\text{Torr}]\,\text{s}^{-1}$, $\delta = 2.7 \cdot 10^{-3}$, $\nu_u \approx 1.1 \cdot 10^7 p[\text{Torr}]\,\text{s}^{-1}$; at a frequency $f = 13.7\,\text{MHz}$, $\omega = 0.86 \cdot 10^8\,\text{s}^{-1}$, the approximation holds only if $p \ll 10\,\text{Torr}$.

In the opposite limiting case, $\omega \ll \nu_m \delta$, the energy spectrum and the mean electron energy oscillate together with the field, tracking its relatively slow variations. The range $f \sim 10\,\text{kHz}$ is employed in discharge devices, for instance, in "ac" lasers (Sect. 14.4.6). The field is quasistationary in this case. The limiting transition from oscillating to dc field produced by imposing a weaker condition $\omega \ll \nu_m$ instead of $\omega \ll \nu_m \delta$ in Sect. 5.4.1 was a purely formal operation.

5.5.3 With Respect to Spatial Nonuniformity

When a group of electrons drift in a dc field, the energy spectrum builds up over one energy relaxation length $\Lambda_u \approx l/\sqrt{\sigma}$ (Sect. 2.3.7). The dc field must therefore be uniform over this length, otherwise the spectrum depends, not only on the field magnitude, but also on the distribution of potential in space (this *nonlocal* nature of the spectrum manifests itself in the cathode layer of the glow discharge). A field that is quasistationary in the sense $\omega \ll \nu_u$ is definitely uniform with respect to wavelength λ, because $\lambda = \lambda/2\pi \gg \Lambda_u(c\sqrt{\delta}/v) \gtrsim \Lambda_u$. The effect of field variation over one wavelength on the energy spectrum of electrons in electromagnetic waves of high frequencies is often negligible, but one must nevertheless be vigilant.

5.5.4 With Respect to the Degree of Ionization

One of the most important assumptions made in the analysis of the kinetic equation is that of neglecting collisions between electrons and thus making the equation linear. As in an ordinary gas, collisions between like particles lead to the Maxwellian distribution ("Maxwellization" of electrons). This is the situation in a sufficiently strongly ionized, dense low-temperature plasma. Colliding electrons exchange portions of energy that are of the order of the electron energies themselves. Electrons colliding inelastically with atoms and molecules also lose large amounts of energy, comparable with their energies. Hence, if inelastic collisions are possible, electron-electron collisions can be neglected if their frequency ν_{ee} (Sect. 2.2.2) is much less then ν_{inel}. At electron energies $\varepsilon \gtrsim 5$–$10\,\mathrm{eV}$, sufficient for the impact excitation of atoms and molecules (and for their ionization), the condition $\nu_{ee} \ll \nu_{inel}$ in weakly ionized plasma is satisfied up to quite considerable degrees of ionization, $n_e/N \sim 10^{-4}$–10^{-3}. The same estimate is valid at smaller energies, $\varepsilon \sim 1$–$5\,\mathrm{eV}$, in the case of molecular gases where electron impact excites molecular vibrations. Generally speaking, inelastic collisions distort the Maxwellian distribution by reducing the number of high-energy electrons.

The situation in atomic gases at energies below the excitation potential of atoms E^* ($E^* \approx 10\,\mathrm{eV}$ in inert gases) is different. Here only very weak elastic energy losses are efficient, especially if atoms are heavy, so that energy exchange in electron-electron collisions is active in spectrum formation process at much lower degrees of ionization. The condition of applicability of the linear kinetic equation in the energy range $\varepsilon < E^*$ is something like $\nu_{ee} \ll (m/M)\nu_m$, $n_e/N < 10^{-6}/A$, where A is the atomic mass. The spectrum in the range $\varepsilon < E^*$ may approach the Maxwellian form in steady-state conditions at not too weak ionization; only if $\varepsilon > E^*$, does it fall off much more steeply than the latter. If we wish the kinetic equation to describe these effects, it needs refinement, that is, the addition of electron-electron collisions.

5.6 Comparison of Some Conclusions Implied by the Kinetic Equation with the Results of Elementary Theory

5.6.1 Conductivity and Dielectric Permittivity

If we substitute f_1 of (5.17) into (5.13), the part of the current in phase with the field, that is, the part proportional to $\sin\omega t$ and E, gives the conduction current. The component proportional to $\cos\omega t$, that is, $\partial E/\partial t$, is the polarization current. Let us compare the result with the phenomenological formula (3.20) and equate separately the terms proportional to $\sin\omega t$ and $\cos\omega t$, as we did in Sect. 3.4.1. The rigorous expressions for the high-frequency conductivity σ_ω and dielectric permittivity ε_ω, derived in this way, are

$$\sigma_\omega = \frac{4\pi e^2}{3m}\int_0^\infty \frac{\nu_m(v)v^3}{\omega^2+\nu_m^2}\left(-\frac{\partial f_0}{\partial v}\right)dv\,, \tag{5.27}$$

$$\varepsilon_\omega = 1 - \frac{16\pi^2 e^2}{3m}\int_0^\infty \frac{v^3}{\omega^2+\nu_m^2}\left(-\frac{\partial f_0}{\partial v}\right)dv\,. \tag{5.28}$$

In the general case, these quantities depend on the electron energy spectrum. If, however, the collision frequency $\nu_m(v)$ is independent of velocity, the factors containing ν_m can be factored out from the integral. Integrating the resulting expression by parts and taking into account that there are no electrons with infinite energy, that is, $f_0 \to 0$ as $v \to \infty$, and the normalization condition for the function $f_0(v)$,

$$\int_0^\infty 4\pi v^2 dv\, f_0(v) = n_e\,, \tag{5.29}$$

we arrive at the formulas (3.23,24) of the elementary theory. We conclude that the latter formulas are valid for any spectrum provided $\nu_m(v) = \text{const}$. The dc conductivity is obtained automatically from (5.27) if we set $\omega = 0$:

$$\sigma = \frac{4\pi e^2}{3m}\int_0^\infty \frac{v^3}{\nu_m(v)}\left(-\frac{\partial f_0}{\partial v}\right)dv\,. \tag{5.30}$$

In practice, however, one normally resorts to elementary formulas (3.23, 24, 27), selecting on the basis of pertinent arguments a value of the characteristic collision frequency that is the most plausible for the real spectrum. But once the spectrum is known, formulas (5.27, 28, 30) make it possible to choose this quantity correctly: They are employed in exact theories and for determining the correction coefficients to elementary formulas.

5.6.2 Rate of Change of the Mean Energy of the Spectrum

By definition, the mean electron energy is

$$\bar{\varepsilon} = \int_0^\infty \varepsilon n(\varepsilon) d\varepsilon \Big/ \int_0^\infty n(\varepsilon) d\varepsilon = n_e^{-1} \int_0^\infty \varepsilon n(\varepsilon) d\varepsilon \,. \tag{5.31}$$

Let us construct an equation for the rate of change of $\bar{\varepsilon}$, neglecting the effect of inelastic losses and taking into account only the effects of the field and elastic losses. Correspondingly, we multiply (5.24) [better still, (5.22) with an additional term nU_{el} in the expression for the flux J] by ε and integrate the product over the entire spectrum. The inelastic collisions term Q is omitted. Now we integrate twice by parts, recalling that $n \to 0$, $J \to 0$ as $\varepsilon \to \infty$, divide by n_e, and obtain

$$\frac{d\bar{\varepsilon}}{dt} = \frac{d\bar{D}}{d\varepsilon} + \bar{U} + \bar{U}_{el} = \frac{e^2 E^2}{m} \overline{\left(\frac{\nu_m}{\omega^2 + \nu_m^2} \right)} - \frac{2m}{M} \overline{(\nu_m \varepsilon)} \,, \tag{5.32}$$

where a bar means averaging over the spectrum. If $\nu_m(\varepsilon) = \text{const}$, this expression coincides exactly with the formula (3.11) of the elementary theory for the rate of change of the energy of the "mean" electron [in (3.11), $\delta = 2m/M$ because we include only elastic losses]. The condition of constancy of collision frequency again ensures the rigorousness of the elementary theory.

5.6.3 Similarity Laws

Similarity relations for drift velocity (Sect. 2.1.4), mean electron energy (Sects. 2.3.5 and 3.2.4), ionization coefficient (Sect. 4.1.4), etc., find confirmation and stringent justification in the kinetic equation. Consider the case of a dc field, $\omega = 0$. The frequencies of all inelastic, as well as elastic, collisions are proportional to the gas density N. Assume that there are no spatial gradients. If ionization is low, recombination is unimportant; then $Q \propto N$. Dividing (5.23) and (5.24) by N, we find that the distribution functions $f_0(v)$ and $n(\varepsilon)$ include E and N only as a combination E/N. In the non-steady-state case, $n(t, \varepsilon, E, N) = n(Nt, \varepsilon, E/N)$. As the gas density increases, the time of evolution is correspondingly reduced; this is natural because all processes are related to collisions.

In a high-frequency field $\omega^2 \gg \nu_m^2$ $n(t, \varepsilon, E, N, \omega) = n(Nt, \varepsilon, E/\omega)$, that is, the steady-state spectrum is completely independent of density and is determined by the ratio E/ω. If the collision frequency is assumed constant, $\nu_m(v) = \text{const}$, and $\omega \gg \nu_m \delta$ (Sect. 5.5.2), the kinetic equation and the spectrum for an oscillating field with root-mean-square magnitude E and amplitude $E_0 = \sqrt{2}E$ are identical to the equation and the spectrum in a dc field of effective strength

$$E_{eff} = E \left[\nu_m^2 / \left(\omega^2 + \nu_m^2 \right) \right]^{1/2} < E \,. \tag{5.33}$$

Thus it is sometimes possible to make use of the richer store of computational and experimental dc data when studying discharge in rapidly varying fields. What is needed is an appropriate recalculation via (5.33).

5.7 Stationary Spectrum of Electrons in a Field in the Case of only Elastic Losses

On the whole, the results of Sects. 5.6.1 and 5.6.2 pointed to a high accuracy of the elementary theory. Now we will analyze an example revealing its imperfections and limited capabilities in comparison with those offered by the kinetic equation.

Imagine an ionized gas in an oscillating or dc field, and ignore the effects of inelastic collisions. Consider a stationary electron spectrum that is finally established as a result of exact balancing of energy gain in the field and elastic energy loss. This situation cannot be described as too abstract, since something like this is implemented if a monatomic weakly ionized gas occupying a large volume is placed in a weak field (the gas is monatomic in order to avoid the excitation of molecular vibrations). If the volume is large, the diffusion loss of electrons is small, especially because appreciable ionization leads to ambipolar electron diffusion (Sect. 2.6), which is much slower than free diffusion. In order to compensate for the small loss of electrons (so as to maintain the steady state), low-rate ionization by the relatively weak field is sufficient. Hence, electron energies are mostly low and very few electrons gain enough energy for the excitation or ionization of an atom. The effect of inelastic collisions on the spectrum is therefore not very significant.

5.7.1 What the Elementary Theory Has to Say

Let us look first at what the elementary theory predicts for this situation. This theory considers the behavior of a single, mean electron and assumes the states of all electrons to be identical. The electron energy ε varies in time as given by (2.12), for $\delta = 2m/M$:

$$\frac{d\varepsilon}{dt} = \left(\Delta\varepsilon_E - \Delta\varepsilon_{\mathrm{el}}\right)\nu_{\mathrm{m}} = \left[\frac{e^2E^2}{m(\omega^2+\nu_{\mathrm{m}}^2)} - \frac{2m}{M}\varepsilon\right]\nu_{\mathrm{m}} .$$

The energy $\Delta\varepsilon_E$ gained from the field in one collision is independent of ε (if $\nu_{\mathrm{m}}(\varepsilon) = \mathrm{const}$), while $\Delta\varepsilon_{\mathrm{el}} \propto \varepsilon$. Hence, the electron energy reaches the value $\varepsilon_{\max}$ found from the equality $\Delta\varepsilon_E = \Delta\varepsilon_{\mathrm{el}}$,

$$\varepsilon_{\max} = \frac{M}{2m}\,\frac{e^2E^2}{m(\omega^2+\nu_{\mathrm{m}}^2)} , \tag{5.34}$$

and then remains constant. Indeed, if the energy of an electron drops by chance to less than $\varepsilon_{\max}$, it immediately starts to gain energy, $d\varepsilon/dt > 0$; if it grows above $\varepsilon_{\max}$, the electron starts losing energy, $d\varepsilon/dt < 0$. A steady (and stable) state corresponds to $d\varepsilon/dt = 0$ and to a delta distribution function: all electrons have identical energies $\varepsilon = \varepsilon_{\max}$. In view of the initial assumption, $\varepsilon_{\max}$ must be less than the excitation potential or, even more so, the ionization potential of atoms; otherwise inelastic losses will determine the behavior, instead of elastic

ones. This leads to a question, however: how is ionization to occur if the gas has not a single electron with sufficient energy? Indeed, at least very low-rate ionization is necessary, otherwise unavoidable losses would gradually remove all electrons and the steady state would be impossible. Here the elementary theory is at a dead end.

5.7.2 Solution of Kinetic Equation (5.23)

In the stationary case, $\partial f_0/\partial t = 0$ and the expression in brackets (the flux) is constant if inelastic processes are neglected ($Q = 0$). However, as $v \to \infty$, f_0 and the flux vanish; hence, this constant equals zero. There is no flux at each point of the energy axis; the energy gained from the field is exactly balanced out by elastic losses at each energy ε. The second integration yields

$$f_0 = C \exp\left[-\frac{3m^3}{Me^2E^2}\int_0^v v\left(\omega^2 + \nu_m^2\right) dv\right] , \tag{5.35}$$

where the integration constant C is determined by the normalization condition (5.29). The distribution function (5.35) is especially simple (Maxwellian) in the case $\nu_m(v) = \text{const}$:

$$f_0 = C \exp - \left[\frac{3m^2(\omega^2 + \nu_m^2)}{Me^2E^2}\,\frac{mv^2}{2}\right] = C \exp\left(-\frac{\varepsilon}{kT_e}\right) , \tag{5.36}$$

with temperature T_e and mean energy $\bar{\varepsilon}$ equal to

$$\bar{\varepsilon} = \frac{3}{2}kT_e = \frac{M}{2m}\,\frac{e^2E^2}{m(\omega^2 + \nu_m^2)} = \varepsilon_{max} . \tag{5.37}$$

The mean energy coincides with the single energy ε_{max} given by the elementary theory. The exact coincidence is more or less accidental. If different assumptions about the function $\nu_m(v)$ are chosen, $\bar{\varepsilon}$ coincides with ε_{max} only to an order of magnitude.

The "true" spectrum is thus spread around ε_{max}; it contains high-energy electrons (the tail of the Maxwell distribution) that produce ionization and sustain the stationary state. Electrons with $\varepsilon < \varepsilon_{max}$ are also present. Electrons with energies not equal to ε_{max} appear in the stationary spectrum because the kinetic equation takes into account rigorously the force exerted by the field on the electrons; we have already seen in Sect. 3.2.5 that this field admits the possibility of gaining an energy in excess of $\Delta\varepsilon_E$ and of losing large portions of energy in collisions. Energetic electrons with $\varepsilon > \varepsilon_{max}$ "survive" at the expense of gaining $\Delta\varepsilon \gg \Delta\varepsilon_E$ in this individual fashion, while slow electrons with $\varepsilon < \varepsilon_{max}$ make use of high individual losses.

5.7.3 Margenau and Druyvesteyn's Distributions

The particular case of distribution (5.35) that is more often considered in gas discharge physics is the one where not the collision frequency but the free path

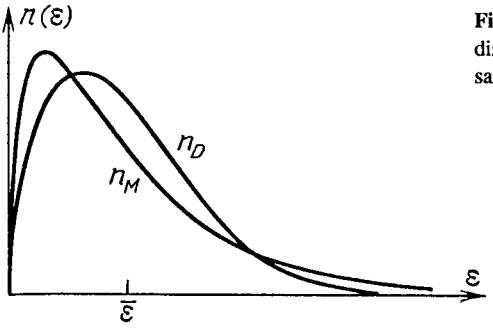

Fig. 5.6. Maxwell (n_M) and Druyvesteyn (n_D) distribution functions in energy, $n(\varepsilon)$, for the same mean energy $\bar{\varepsilon}$

length of electrons, $l = v/\nu_m$ (i.e., cross section for momentum transfer), is assumed to be independent of energy. Under this approximation, $\nu_m \propto v \propto \sqrt{\varepsilon}$ and the integration of (5.35) gives

$$f_0 = C \exp\left[-\frac{3m^3}{4Me^2E^2l^2}\left(v^4 + 2v^2\omega^2l^2\right)\right] . \tag{5.38}$$

This is the so-called *Margenau distribution* (1946); we shall not dwell on it here. In the dc case, the Margenau distribution transforms into *Druyvesteyn's distribution*

$$f_0 = C \exp\left[-\frac{3m}{M}\frac{\varepsilon^2}{\varepsilon_0^2}\right] ; \quad \varepsilon_0 = eEl \tag{5.39}$$

which was derived directly by Druyvesteyn in 1930. The parameter ε_0 is the energy gained by an electron from the field over a free path length. As follows from (5.39), the mean energy $\bar{\varepsilon}$ is gained over approximately $\sqrt{M/m}$ free paths [cf. (2.13)]. It is easy to see that $\bar{\varepsilon}$ also coincides, to an order of magnitude, with that unique energy ε'_{max} an electron is allowed to gain in the elementary theory. However, the quantity ε'_{max} is now different from (5.34) because $\Delta\varepsilon_E = e^2E^2/m\nu_m^2 \propto 1/\varepsilon$, in contrast to the high-frequency case where $\Delta\varepsilon_E = \text{const}$. Druyvesteyn's distribution is characterized by a considerably steeper decrease of the number of electrons in the "tail" than that of the Maxwell distribution (ε^2 in the exponential instead of ε); see Fig. 5.6.

5.7.4 Remark on Approximate Solution for Inert Gases in the Case of Predominant Inelastic Losses

The solution will be obtained in Sect. 7.5 in the analysis of electrical breakdown: it is unusual in that it employs the "infinite sink" approximation. In a certain sense, this case is the opposite of that treated in Sect. 5.7.

5.8 Numerical Results for Nitrogen and Air

Analytic solutions of the kinetic equation (5.23) are always obtained at the cost of considerable simplifications and assumptions, as in Sect. 5.7 (see also Sect. 5.8.1). In the case of molecular gases, any analytic solution would be hopeless, because of the need to take into account the vibrational and rotational excitations, in addition to the electron excitation. Advances in computer technology make it possible, however, to perform numerical integration, even though the computations require certain skill and are time-consuming. The most prominent physical aspect is the analysis of the processes to be taken into account and the choice of the most reliable data on cross sections. Considerable discrepancies exist between the results of various authors, which is connected with the complexity of the corresponding experiments. It is the shortage of cross section data that constitutes the main source of error in solving the kinetic equation.

The needs of modern molecular laser techniques provided a strong impetus for the computations. Numerical modeling was carried out for many mixtures of the type $CO_2 + N_2 + He$ (see Sect. 8.8). In addition to laser mixtures, such gases as nitrogen and air, widely used in discharge work, have also been studied. Here we will give the results of computations for N_2 [5.1] and for air [5.2] both as illustrations of the application of the kinetic equation and as material of interest for discharge research.

Equation (5.23) (slightly transformed for reasons of convenience) was integrated numerically for stationary conditions and a dc field. In Fig. 5.7, a function $\psi = \varepsilon^{-1/2} n(\varepsilon)/n_e$ for nitrogen is plotted on a semilogarithmic scale. The mean-

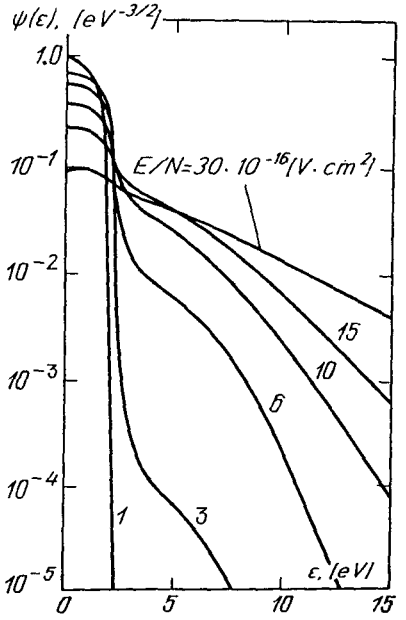

Fig. 5.7. Electron distribution function $\psi(\varepsilon) = n(\varepsilon)/n_e\sqrt{\varepsilon}$ in nitrogen

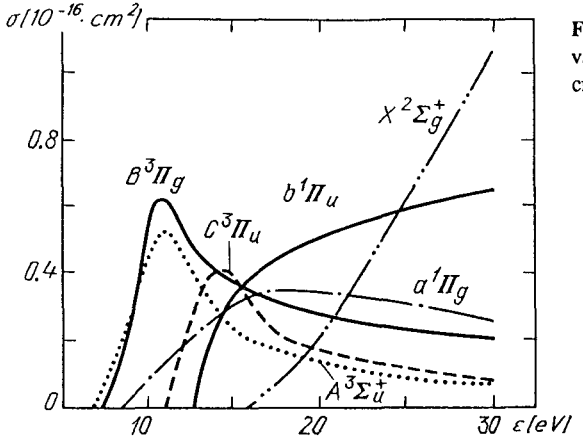

Fig. 5.8. Excitation cross sections of various energy levels, and ionization cross section of nitrogen molecule

ing of ψ becomes clearer if we take into account that in the case of the Maxwell distribution, $\psi_M(\varepsilon) = 2\pi^{-1/2}(kT_e)^{-3/2}\exp(-\varepsilon/kT_e)$ is the Boltzmann exponential up to the normalizing factor. Its semilogarithmic plot would be a straight line. The cross sections of excitation of a number of electron levels and ionization cross sections, employed in the computation, are shown in Fig. 5.8.

Figure 5.9 plots drift velocity, electron temperature, and characteristic energy given by (5.30) and (5.31) (see Sect. 2.4.2). (The diffusion coefficient was found by averaging $l_m v/3 = v^2/\nu_m$ over the spectrum; the mobility is found as v_d/E.) If the spectrum is Maxwellian, the characteristic energy coincides with temperature. The difference between T_e (given in volts) and D_e/μ_e is caused by the non-Maxwellian nature of the spectrum; this is seen in Fig. 5.7. Figure 5.10 plots the ionization rate constant k_i found from (4.1), and Fig. 5.11 shows the fractions of energy transferred from electrons to different degrees of freedom. The curves demonstrate that a predominant part of the work done by the field transforms into the energy of molecular vibrations in a wide range of E/N. This fact is

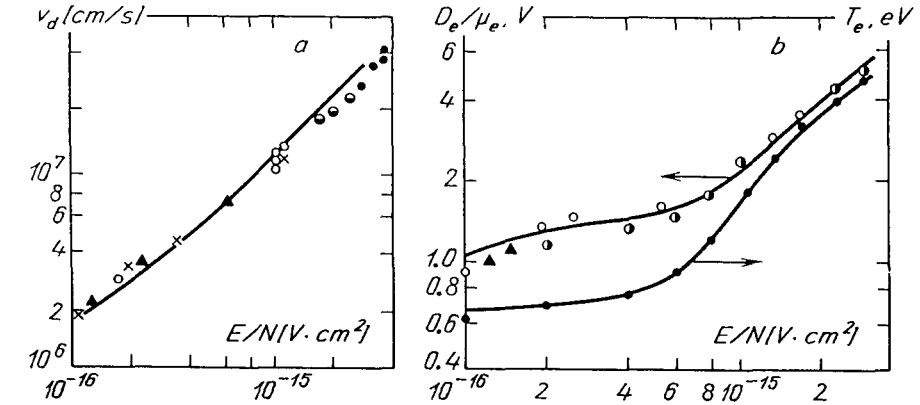

Fig. 5.9. (a) Drift velocity of electrons in nitrogen, (b) electron temperature as 2/3 of mean energy of the spectrum, and the characteristic energy D_e/μ_e in nitrogen

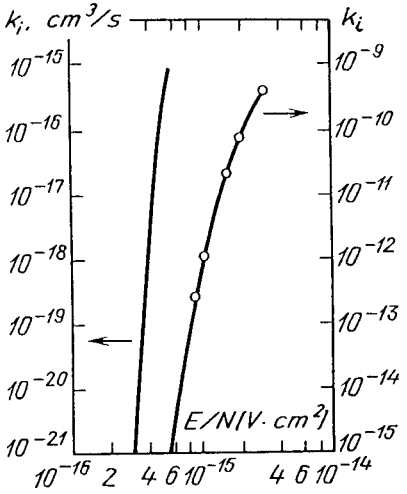

Fig. 5.10. Ionization rate constant $k_i \equiv \langle \sigma_{ion} v \rangle$ in nitrogen. *Dots* represent experimental data. Townsend's coefficient $\alpha/N = k_i/v_g$

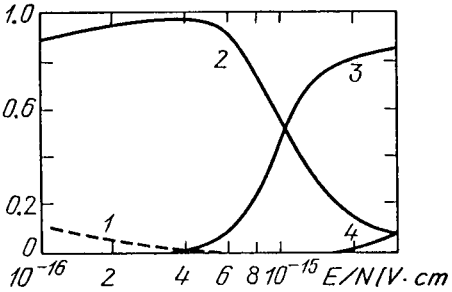

Fig. 5.11. Fraction of energy transferred by electrons to (*1*) rotation, (*2*) oscillations, (*3*) electronic excitation, and (*4*) ionization

of principal importance. This property of weakly ionized plasma in the field is essential for the operation of electric discharge molecular lasers. The calculated constants of the rate of ionization of nitrogen molecules from the ground and metastable $A^3\Sigma_u^+$ states, k_i, k_{iA}, and the rates of excitation of levels $A^3\Sigma_u^+$ and $B^3\Pi_g$ (Fig. 5.8), k_A^*, and k_B^* are approximated by the formulas [5.3]

$$\log k_i = -8.3 - 34.8(N/E)\,, \quad \log k_{iA} = -6.1 - 27.5(N/E)\,,$$
$$\log k_A^* = -8.35 - 14.9(N/E)\,, \quad \log k_B^* = -8.2 - 15.6(N/E)\,, \tag{5.40}$$

where E/N is given in 10^{-16} V cm^2, and k in cm^3/s. The rate constants increase in the case of strong vibrational excitation, which is typical of glow discharge in nitrogen, owing to the lower rate of vibrational relaxation. This is connected both with reduced reaction thresholds and with the enrichment of the spectrum with higher-energy electrons. If T_v is the vibrational temperature characterizing the ratio of populations of the levels with $v = 1$ and $v = 0$, and $Z = \exp(-\hbar\omega_k/kT)$, then we approximately have

$$\log[k(T_v)/k(0)] = 43.5(N/E)^2 Z\,, \quad Z = \exp(-3360/T)\,. \tag{5.41}$$

The formula is the same for all k and is valid up to $T_v = 5000$ K. Figures 5.12–14 plot the results of computations for dry air (in practice the water vapor content may vary from one experiment to another). The distribution functions qualitatively resemble those for nitrogen.

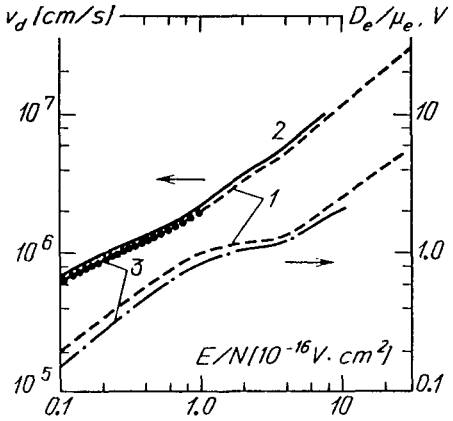

Fig. 5.12. Drift velocity (*upper curves*) and characteristic energy D_e/μ_e (*lower curves*) in air. (*1*) calculated values, (2) and (3) experimental data

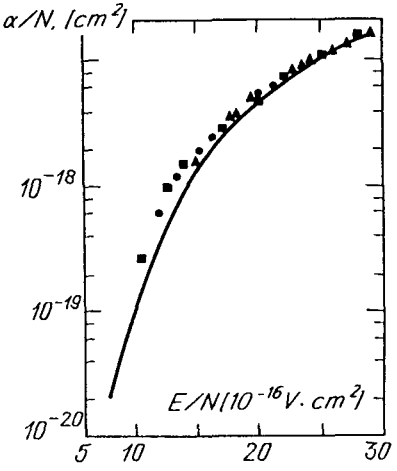

Fig. 5.13. Townsend's ionization coefficient α/N in air. *Dots* represent experimental data

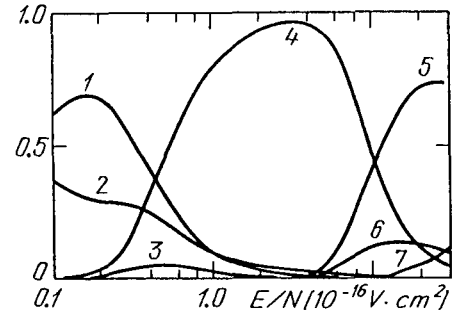

Fig. 5.14. Fraction of energy transferred by electrons in air to (*1*) vibrations of O_2, (2) rotations of O_2 and N_2, (*3*) elastic losses, (*4*) vibrations of N_2, electronic excitation of N_2 (*5*) and of O_2 (*6*), and (*7*) ionization of O_2 and N_2

5.9 Spatially Nonuniform Fields of Arbitrary Strength

Strongly nonuniform fields are produced in weakly ionized gases in the cathode layer of a glow discharge, in the electrode layers of a radio-frequency capacitively coupled discharge, in high-voltage pulsed discharges, and possibly in other situations. The Lorentz approximation fails in these cases (Sect. 5.5) and we have to return to the original kinetic equation. At present, the *Monte Carlo method* is regarded as the most efficient and accurate method of solving this equation. This is a computational procedure in which a computer simulates the process of random walk of a particle implied by the kinetic equation. These computations [5.4, 5] are very complicated, require considerable computer time, and are rarely worthwhile. As an alternative to Monte Carlo simulations, an approximate approach can be used in which the problem is reduced to equations that are *no*

more complicated than the equations of the Lorentz approximation. The simplified method is a more manageable tool, in comparison with the Monte Carlo techniques, for studying discharge phenomena when moderate accuracy is acceptable. It is suitable for analyzing the behavior of electrons in any, strong or weak, uniform or nonuniform, fields, with all the qualitative features and corollaries of the exact equation retained.

5.9.1 "Forward-Backward" Approximation

We shall assume that electrons move only along the field. They are scattered in elastic collisions either forward or, with probability ξ, backwards. In inelastic collisions (with excitation or ionization) they lose energy but do not change the direction of motion. Let $\varphi_1(v,x,t)dv$ electrons move at velocities from v to $v+dv$ in the positive direction of the x axis ($E \equiv E_x < 0$), and $\varphi_2(v,x,t)dv$ move in the negative direction. Functions φ_1, φ_2 obey equations which are easily obtained from (5.7, 9, 10):

$$\begin{aligned} \frac{\partial\varphi_1}{\partial t} + v\frac{\partial\varphi_1}{\partial x} - \frac{eE}{m}\frac{\partial\varphi_1}{\partial v} &= \frac{1}{2}\nu_m(\varphi_2-\varphi_1) + Q(\varphi_1) \\ \frac{\partial\varphi_2}{\partial t} - v\frac{\partial\varphi_2}{\partial x} + \frac{eE}{m}\frac{\partial\varphi_2}{\partial v} &= \frac{1}{2}\nu_m(\varphi_1-\varphi_2) + Q(\varphi_2)\ . \end{aligned} \tag{5.42}$$

The effective frequency of elastic collisions is $\nu_m = 2Nv\sigma_c(v)\xi$, where $\xi = (1/2)(1-\overline{\cos\theta})$. Adding and subtracting equations (5.42), we now use the functions $\Phi_{0,1} = \varphi_1 \pm \varphi_2$. They characterize the spectral density and the flux of electrons and correspond to $f_{0,1}$ of the Lorentz approximation. In the weak field limit, equations for $\Phi_{0,1}$ become similar to (5.14, 16). If $\nu_m(v) = \text{const}$, the exact value of the drift velocity is obtained, while that of the diffusion coefficient is three times the true value, reflecting the "one-dimensionality" of the random motion. For details and the application to the *cathode layer of a glow discharge* see [5.6] and Sect. 8.4.10; see also [5.7].

5.9.2 Runaway Electrons

In very strong and sufficiently extended fields, electrons reach high energies. Inelastic collisions are then more frequent than elastic ones, and electrons are mostly scattered forward. Of the two equations in (5.42), only the first survives with ξ, $\nu_m = 0$. The resulting equation for the mean energy of the spectrum corresponds to the equation for a "monoenergetic" beam,

$$\frac{d\varepsilon}{dx} = e|E(x)| - L(\varepsilon)\ , \quad L = N\sigma_i I + N\sum \sigma_k^* E_k^*\ . \tag{5.43}$$

As with all cross sections $\sigma_i(\varepsilon)$, $\sigma_k^*(\varepsilon)$, the inelastic loss function $L(\varepsilon)$ goes through a maximum, at $\varepsilon \sim 20$–$50\,\text{eV}$. Therefore, an electron moving in the field $|E| > E_{crit} = L_{max}/e$ will be continuously accelerated (will "run away"), in spite of inelastic losses. In N_2, $(E/p)_{crit} = 365\ \text{V/(cm·Torr)}$, and in He, $63\ \text{V/(cm·Torr)}$.

6. Electric Probes

6.1 Introduction. Electric Circuit

The main objectives in experimental determination of plasma parameters are to measure the density n_e of electrons, their temperature T_e (provided they have temperature), and, in the general case, the distribution function $f_0(v)$. The distributions of potential and electric field in space are of considerable interest in discharge research. The *probe method* developed by Langmuir in 1923 solves these problems if conditions are favourable. The probe method is unique among all diagnostic techniques in making it possible to determine directly the local plasma characteristics, that is, the spatial distribution of parameters; this is the reason for the special value of probe techniques.

To conduct a probe study, one introduces into a chosen place in the plasma an electrode and connects it to various potentials. The probe is a metal conductor coated with insulation almost to the tip. The naked surface of the probe, in contact with the plasma, may be given a plane, cylindrical, or spherical shape. The probe potential imposed by a power supply is determined with respect to a *reference* electrode: the anode, the cathode, or the grounded metal wall of the discharge chamber if one is present. The measurement circuit is shown in Fig. 6.1. In this circuit the current closes the probe circuit via the anode, so that the polarity of the probe current supply is chosen so as to have the probe potential lie between those of the anode and the cathode (as in the plasma). The probe potential is varied by a potentiometer. The experiment consists in measuring the current through the probe and the voltage applied to it, that is, in recording its *current-voltage* $(V - i)$ *characteristic*. Figure 6.2 shows several probe geometries. Probes are

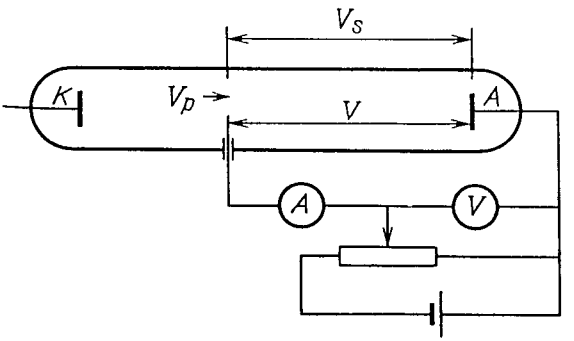

Fig. 6.1. Circuit for probe measurements

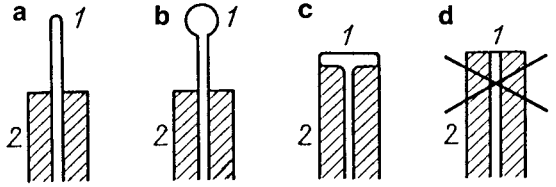

Fig. 6.2. (**a–c**) probe design, (**d**) wrong design; *(1)* probe, *(2)* insulator

usually made of refractory metals: tungsten, molybdenum, tantalum. Cylindrical probes are made of wire 0.5–0.05 mm in diameter. Special glass coatings of wire, ceramics, quartz, alumina (99 % Al_2O_3), etc. are used as probe insulators. In contrast to the wrong geometry in *d*, the probe geometry in *c* reduces edge effects. Indeed, data processing operates with the *current-collecting* surface area. The characteristic size of spherical and plane probes is about 1 mm.

The simplicity of equipment and experiment constitute the advantages of the probe method. The disadvantages lie in the complexities of the theory used to extract the plasma characteristics from probe measurement data. To put it more correctly: there is only a limited range of conditions under which the theory is only moderately complicated and thus does not lead to a considerable probability of obtaining erroneous results and faulty interpretations. In measuring the quantity, one must strive for a method based on a simple, reliable theory with a minimal number of assumptions and fuzzy constraints. In this respect, the probe method is sufficiently reliable only in rarefied gases where the free path length is greater than the characteristic size of the probe and the perturbed region around it.[1] In principle, though, probes can be used to study plasma in a very wide range of conditions: $p \sim 10^{-5} - 10^{2}$ Torr $n_e \sim 10^{6} - 10^{14}\,\mathrm{cm}^{-3}$.

If the plasma is placed in a magnetic field, the theory becomes very complicated and measurements are only interpreted with considerable difficulty. The same is true if negative ions are present. If there is no reference electrode (e.g., in electrodeless high-frequency discharge or in a decaying plasma after the field has been switched off), a *single probe* is useless. In such cases, *double-probe* circuits are used (Sect. 6.6).

6.2 Current-Voltage Characteristic of a Single Probe

Figure 6.3 shows a somewhat idealized *probe characteristic,* that is, the electric current i through a plane probe is plotted as a function of its potential V. The choice of the reference point is immaterial as long as it is strictly fixed. This is

[1] This is the case for which Langmuir's theory is valid. Probes were introduced into discharge plasma much earlier, at the beginning of this century. The potential difference between the probe and the cathode was measured electrostatically. But it soon become clear that the probe and plasma potentials do not coincide, although the potential difference between neighbouring points can be determined in this way. Only with Langmuir's theory did probes turn into an efficient method of quantitative diagnostics

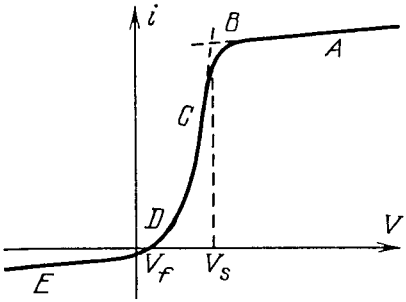

Fig. 6.3. Typical probe characteristic

why a reference electrode is introduced. Let us give a qualitative interpretation to the curve $i(V)$. Assume that the plasma is electroneutral in the absence of the probe: $n_e = n_+ = n_0$. We denote its potential at the point where the probe is located by V_S. The plasma (space) potential V_S is measured with respect to the reference electrode. Let V_S change only slightly within the region perturbed by the probe, that is, the potential of the nearby unperturbed plasma around the probe is V_S. The experimentally measured probe potential with respect to the reference electrode is $V = V_p + V_S$, where V_p is the probe potential with respect to the unperturbed plasma in the surrounding space (Fig. 6.1).

A probe does not emit charged particles, it only collects them from the plasma. We will operate with the absolute values of the electron and ion currents to the electrode, i_e and i_+, and use the following convention of probe current sign: $i = i_e - i_+$; it corresponds to the curve orientation in Fig. 6.3. If the probe and space potentials are identical, and the current-collecting surface is parallel to the direction of the external field between the anode and cathode, the charges reach the probe only owing to their thermal motion. In fact, electrons move much faster than ions, all the more so because their temperature in the weakly ionized plasma is much higher than the ionic (gas) temperature T. As a result, at $V = V_S$ the probe current is practically equal to the electronic one: $i \approx i_e$. Let us emphasize the fact that the conductor *collects* the electric current of electrons *in the absence* of potential difference between the conductor and the surrounding plasma.

When the potential applied to the probe is positive with respect to the plasma, $V > V_S$, ions are repelled by the probe so that the ionic current vanishes, and electrons are attracted. A *layer* of negative *space charge* (known as the sheath), screening the potential V_p, develops around the probe. The potential drop from V to V_S and the probe field are concentrated within the space charge layer, vanishing asymptotically in the transition to the unperturbed plasma. The effect is quite similar to plasma *polarization* around a charge and to the screening of the field of a charge by plasmas at distances greater than the *Debye radius* (2.38).

Let us introduce the exterior surface of the sheath, that is, the boundary beyond which the plasma can be considered approximately neutral and the field absent. Electrons are brought to the boundary from the outside and then transferred to the probe mostly via *thermal* motion; this factor determines their flux, which is only weakly dependent on probe potential. The probe current coincides with the more or less constant *saturation* electronic current $i_{e,sat}$. It corresponds

to the *upper plateau* AB of the current-voltage characteristic. In the ideal case of an "infinite" plane, $i_{e,sat} = \text{const}$, so that this part of $V - i$ curve would be horizontal. If the probe is small, the current grows with increasing positive potential, though more slowly than on the steep segment of the $V - i$ curve.

If the potential applied to the probe is negative with respect to the plasma, the electronic current drops sharply as $|V_p|$ increases, because the fraction of electrons with velocities sufficient for overcoming the decelerating field diminishes. Thus is the *steep* part C of the characteristic formed. The upper knee of the current-voltage characteristic, B, fixes the space potential V_S, corresponding to $V_p \approx 0$. It is in this way that it is determined experimentally. The probe is moved and the electric field is found from the difference between the potentials V_S at the neighbouring points.

The *current vanishes* at a certain negative potential $V_p = V_f$ (D in Fig. 6.3). The flux of a small number of energetic electrons, capable of overcoming the decelerating potential, to the probe is compensated in this state by the ion flux. This potential V_f (known as the *floating* potential) develops on an *insulated* body placed in the plasma. Returning to the footnote in Sect. 6.1, we can say that experiments with probes not connected to a current source yielded, not the plasma potential, but the more negative floating potential.

At still more negative potentials, the probe repels practically all the electrons but attracts ions. The probe is surrounded with an *ionic sheath* of positive space charge that screens the high negative potential V_p. The probe current is then purely ionic, determined by the flux of ions reaching the sheath boundary from the surrounding plasma. This flux is nearly independent of the probe potential, which is screened off, that is, the probe current varies slowly and coincides with the *ionic saturation current*. This current corresponds to the *lower plateau* of the current-voltage characteristic.

6.3 Theoretical Foundations of Electronic Current Diagnostics of Rarefied Plasmas

6.3.1 Electron Temperature

Consider the steep segment of the probe characteristic C, where the current is electronic and the potential decelerates electrons. Let the electrons cross the positive space-charge layer *without collisions*. When the probe voltage corresponds to the steep segment, the sheath thickness is of the order of the Debye radius. If $T_e \approx 1\,\text{eV}$, $n_e \approx 10^9\,\text{cm}^{-3}$, formula (2.38) yields $d \approx 10^{-2}\,\text{cm}$. If the free path length of electrons l_e is such that $l_e p \approx 0.03 - 0.01\,\text{cm·Torr}$, then $l_e > d$ if $p < 10^{-1} - 1\,\text{Torr}$. We now calculate the electronic current to the probe, assuming for simplicity that the layer is thin in comparison with the curvature radius or size of the current-collecting surface. The problem can then be considered *plane*. In Sect. 6.3.4, it is shown that the result obtained below is true for any *convex* surface, for example, for a small spherical probe. Let us assume that the metal surface totally absorbs (does not reflect) the charges.

An electron impinging on the outer boundary of the sheath at a thermal velocity is decelerated by the field normal to the surface, $E_x = -d\varphi/dx$. As prescribed by the equation of motion, $m\dot{v}_x = d(mv_x^2/2)dx = e\,d\varphi/dx$, an electron can reach the probe surface only if at the beginning its velocity component v_x is such that $mv_x^2/2 \geq e|V_p|$ or $v_x \geq v_t = (2e|V_p|/m)^{1/2}$. If the electron distribution function at the outer boundary of the layer is $f(v_x, v_y, v_z)$, then the probe current density is

$$j_e = e\int_{-\infty}^{\infty} dv_y \int_{-\infty}^{\infty} dv_z \int_{v_t}^{\infty} f(v_x, v_y, v_z) v_x dv_x \,. \tag{6.1}$$

Integrating (6.1) for the Maxwell distribution (see Appendix) and multiplying the result by the surface area S, we find the probe current

$$i = S(en_0\bar{v}_e/4)\exp(eV_p/kT_e)\,, \quad \bar{v}_e = (8kT_e/\pi m)^{1/2}\,. \tag{6.2}$$

This formula, describing the steep fragment of the current-voltage characteristic, was derived by Langmuir and is widely employed in practical work. Having found the probe characteristic and then plotted $\ln i$ as a function of V, one can determine the electron temperature T_e from the slope of the obtained straight line. At the same time, the linearity of the $\ln i$ vs. V curve is evidence of the maxwellian distribution of electrons.

6.3.2 Saturation Current; the Potential and Charge Density in Plasmas

We have already mentioned that the space potential V_S is determined by the point of the upper knee on the $V - i$ curve. If $V > V_S$ (the field accelerating the electrons), formula (6.2) is invalidated because now one has to integrate v_x in (6.1) from zero, regardless of V_p. The probe current then coincides with the electronic saturation current corresponding to zero field, that is, $V_p = 0$ in (6.2):

$$i = i_{e,sat} = Sen_0\bar{v}_e/4\,. \tag{6.3}$$

This quantitity correspends to the flux density of particles of the gas, crossing the area element from one side: $n\bar{v}/4$. One of the two factors of 1/2 in the 1/4 appears because only one half of the particles move in the necessary direction, and the other results from averaging over the hemisphere the cosine of the angle ϑ between the direction of the velocity v and the normal to the area element. Having found the thermal velocity $\bar{v}_e$ of electrons by measuring T_e on the steep segment of the current-voltage characteristic, and the current at the knee of the $V - i$ curve, one can find the electron density n_0 in the plasma from formula (6.3).

6.3.3 Criteria of "Rarefaction" of a Plasma

In order to justify the interpretation of n_0 as the electron density in nonperturbed plasmas, it is necessary that the presence of the probe not violate n_0 at the point of the last collision before electrons reach the probe. These points are at a distance of about one free path length from the probe. However, the density at a

point is created by particles arriving from the sphere of a radius of the order of l. The surface of the probe, S, "eclipses" the fraction $S/4\pi l^2$ of this sphere and thus weakens the source of density formation. This fraction must be small, that is, $S/4\pi l^2 \ll 1$, for the free path length l to exceed the characteristic linear size of the probe, $\sqrt{S}$. Another condition of rerefaction is the smallness of the size of the space-charge layer in comparison with l.

6.3.4 How to Find the Electron Distribution Function

In the case of an arbitrary, nearly isotropic electron distribution in an unperturbed plasma, $f(v_x, v_y, v_z) \approx f_0(v)$, it is expedient to introduce into expression (6.1) for the electronic current to the probe surface the magnitude of velocity v and the angle between $\boldsymbol{v}$ and the inward normal to the surface, ϑ. Remarking that $v_x = v \cos \vartheta$, we rewrite (6.1) in the form

$$j_e = e \int_0^{\pi/2} \cos \vartheta \, 2\pi \sin \vartheta \, d\vartheta \int_{v_t/\cos \vartheta}^{\infty} v^3 f_0(v) dv \, . \tag{6.4}$$

Changing the sequence of integration but retaining the domain covered by the double integral, we integrate (6.4) over $\mu = \cos \vartheta$:

$$\begin{aligned} j_e &= 2\pi e \int_0^1 \mu \, d\mu \int_{v_t/\mu}^{\infty} v^3 f_0(v) dv = 2\pi e \int_{v_t}^{\infty} v^3 f_0(v) dv \int_{v_t/v}^1 \mu \, d\mu \\ &= \frac{2\pi e}{m} \int_{v_t}^{\infty} \left(\frac{mv^2}{2} - e|V_p| \right) v f_0(v) dv \, . \end{aligned} \tag{6.5}$$

The Maxwell function, $f_0 = (m/2\pi kT_e)^{3/2} \exp(-mv^2/2kT_e)$, transforms (6.5) into (6.2). Both (6.2) and (6.5) are valid only if $V_p \leq 0$. If $V_p > 0$, the integration in v in (6.4) must begin from zero, regardless of V_p. This gives the saturation current (6.3) with non-maxwellian mean velocity $\bar{v}_e$.

Now we twice differentiate (6.5) with respect to V_p and obtain

$$\frac{d^2 i}{dV_p^2} = -S \frac{2\pi e^3}{m^2} f_0(v_t) \, , \quad v_t = \sqrt{\frac{2e|V_p|}{m}} \, . \tag{6.6}$$

In order to find the electron distribution function, one has to obtain the probe characteristic, differentiate it twice at each point of the steep segment, and assign to the point the potential V_p measured from the point B of the upper knee. The second derivative gives a number $f_0(v)$ for $v = (2e|V_p|/m)^{1/2}$. This method, first employed by *Druyvesteyn* in 1930, is still used nowadays, with certain improvements (Sect. 6.4).

6.3.5 The Applicability of the Theory of the Steep Segment of the $V - i$ Characteristic to Small-Sized Probes

Let us show that the fundamental diagnostics formula (6.5), derived above for the case of plane geometry, holds just as well for probes that are small in comparison with the size of the space-charge region. The only necessary condition is for the

probe surface to be *convex*. The possibility of using small probes is extremely desirable, because such probes disturb the natural conditions in the plasma to be studied only slightly. The need to *intrude* into the plasma is one of the essential *drawbacks* of the probe technique.

Not every electron entering the space-charge layer around a finite-size probe reaches its surface. Some of them fly by the probe (Fig. 6.4). This is not a plane problem; therefore the derivation of formula (6.5) must be reconsidered. This shall do, following [6.1]. Denoting by $\boldsymbol{r}_\mathrm{p}$ the coordinates of a point on the probe surface, and by $\boldsymbol{v}_\mathrm{p}$ and $f(\boldsymbol{r}_\mathrm{p}, \boldsymbol{v}_\mathrm{p})$ the velocity and electron distribution function at the surface, the probe current density at a point $\boldsymbol{r}_\mathrm{p}$ is

$$j_\mathrm{e} = e \int_0^{\pi/2} \int_0^{\infty} v_\mathrm{p} \cos \vartheta f(\boldsymbol{r}_\mathrm{p}, \boldsymbol{v}_\mathrm{p}) 2\pi \sin \vartheta \, d\vartheta v_\mathrm{p}^2 dv_\mathrm{p} \,. \tag{6.7}$$

The surface being conves, electrons arrive at it from the entire hemisphere $0 \leq \vartheta \leq \pi/2$.[2]

For an electron to arrive at a surface point $\boldsymbol{r}_\mathrm{p}$ without collisions and with a velocity $\boldsymbol{v}_\mathrm{p}$, it has to leave a point $\boldsymbol{r}$ of nonperturbed plasma at a velocity $\boldsymbol{v}$. The force of deceleration has a potential, so that the change in the kinetic energy of electrons over this distance is independent of the spatial distribution of the potential and the shape of the trajectories:

$$mv_\mathrm{p}^2/2 = mv^2/2 - e|V_\mathrm{p}| \,. \tag{6.8}$$

According to (5.6), however, the distribution function cannot change along the trajectory of a particle in phase space. In nonperturbed plasma, it is isotropic and equal to $f_0(v)$. Hence, $f(\boldsymbol{r}_\mathrm{p}, \boldsymbol{v}_\mathrm{p}) = f(\boldsymbol{r}, \boldsymbol{v}) = f_0(v)$. After replacing f in (6.7) with $f_0(v)$, v_p^2 with the expression derived from (6.8), $v_\mathrm{p} dv_\mathrm{p}$ with $v\,dv$, and integrating over ϑ, we arrive at the last expression in (6.5). The current density

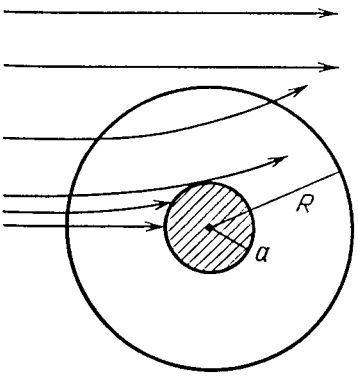

Fig. 6.4. Trajectories of particles near a repulsing spherical or cylindrical probe

[2] Some corners of concave areas are in the "shadow" of nearby protrusions, and thus have to be singled out of the integral.

is the same for all surface elements of a convex probe, that is, $i_e = Sj_e$, where S is the total probe surface area.

6.3.6 Why the Current to a Small Probe Does Not Saturate

For the electronic current to reach the potential-independent value (6.3) corresponding to saturation, it is sufficient to apply to the probe a small positive potential V_p both in the ideal plane case and in real situations, provided the space-charge thickness is small in comparison with the radius of curvature and the size of the current-collecting surface. If the probe size is small in comparison with the size (radius) of the space-charge region, the electronic current continues to increase with increasing positive potential, although it grows less steeply than on the steep part of the $V-i$ curve, which corresponds to decreasing deceleration potential. The reason for this behaviour of the $V-i$ curve is that not all electrons entering the space-charge layer (where they are in the attracting field) reach the probe. Some of them *pass by* the probe and escape from the layer without touching the probe. But it is obvious that the higher the accelerating potential V_p, the stronger the attractive force pulling electrons to the probe, the greater the fraction of electrons in the layer that are collected by the probe; hence, the current grows.

This situation is illustrated in Fig. 6.5, which represents a spherical and a long cylindrical probe. In the latter case, it shows projections of trajectories on the plane perpendicular to the axis. If a particle approaches the layer with an impact parameter ϱ greater than the layer radius R (the effective boundary beyond which the field vanishes), its straight path does not bend. If a particle enters the layer ($\varrho \leq R$), it can either pass or hit the probe. The outcome depends on the initial velocity v_0, the impact parameter ϱ, and the magnitude and radial distribution $V(r)$ of potential. The more energetic the electron, the smaller its impact parameter must be, or the higher the potential, for the electric force to be able to attract it to the probe. Very slow electrons with any $\varrho < R$ are collected by the probe.

This behavior is implied by the energy and angular momentum conservation laws:

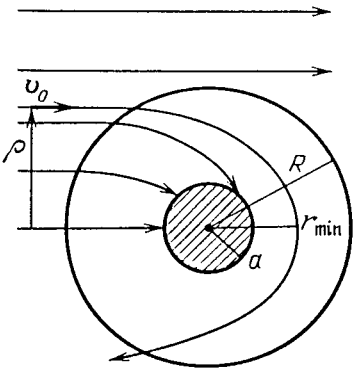

Fig. 6.5. Trajectories of particles near an attracting spherical or cylindrical probe

$$\frac{mv_0^2}{2} = \frac{mv^2}{2} - eV(r)\,, \quad mvr\,\sin\theta = mv_0\varrho\,, \tag{6.9}$$

where r is the distance from the center to a point moving along the trajectory, v is the velocity of the point, and θ is the angle between the direction of motion (tangent to the trajectory) and the radius vector $\boldsymbol{r}$ connecting the center to the moving piont. The minimum distance of approach $r_{\min}$ of the particle to the center satisfies (6.9) for $\sin\theta = 1$, because the tangent to the trajectory is perpendicular to $\boldsymbol{r}_{\min}$. If $r_{\min}$ is less than the probe radius a, the particle inevitably strikes its surface, and if $r_{\min}$ is greater, it goes by the probe.

Note that these effects, characterizing charges of both signs, are of greater importance for ions. In practical work, the electronic part of the probe characteristic ($V_p > 0$), corresponding to attraction, is rarely used. In order to reduce the effect of a probe on the plasma, small probes are preferable; electronic current in the range $V > V_S$ is very high, melting the probe. Consequently, the *ionic* part of the $V - i$ curve is typically employed for measuring the charge density in plasma (Sect. 6.5).

6.4 Procedure for Measuring the Distribution Function

6.4.1 Application of a Low ac Voltage

Direct differentiation of an experimental $i(V)$ curve, let alone double differentiation, involves considerable errors. For this reason, d^2i/dV^2 is found by indirect means. Thus it is advisable to superpose on the constant probe voltage V_c a small ac component: $V = V_c + V_a \sin\omega t$. If $V_a \ll V_c$, then

$$i(t) \approx i(V_c) + \left(\frac{di}{dV}\right)_{V_c} V_a \sin\omega t + \frac{1}{2}\left(\frac{d^2i}{dV^2}\right)_{V_c} V_a^2 \sin^2\omega t$$

for each value of V_c. Averaging over time gives

$$\Delta i = \langle i\rangle - i(V_c) = \frac{1}{4}\left(\frac{d^2i}{dV^2}\right)_{V_c} V_a^2\,.$$

To achieve greater accuracy, the main component $i(V_c)$ is cancelled out by a balancing circuit. Then the time-averaged increment to current, with known amplitude V_a, immediately yields the second derivative.

A small, constant increment in the current can be measured only if the discharge parameters are highly stable. The method can be improved by modulating the amplitude of a high-frequency (ω) the ac voltage with a low frequency ω_1, i.e. $V_a = V_{a0}(1 + \cos\omega_1 t)$. The second derivative is then related to the low-frequency oscillating component of current:

$$\Delta i = \frac{1}{2}\left(\frac{d^2i}{dV^2}\right)_{V_c} V_{a0}^2 \cos\omega_1 t\,.$$

This component is easier to measure. High-frequency-oscillations of current are automatically averaged by the instrument because it cannot resolve them. In the experiments to be described below, the carrier frequency was $\omega/2\pi = 8.4 \cdot 10^4$ Hz, and the modulation frequency was $\omega_1/2\pi = 500$ Hz.

6.4.2 A Typical Result

To illustrate the applications of probe techniques, we will give the results obtained for the electron distribution function in the positive column of a glow discharge. The discharge was produced in a glass tube 2.5 cm in diameter and 50 cm long. Cylindrical probes 0.03 and 0.06 mm in diameter and 6 mm long were sealed into the central part of the tube, parallel to the axis. Figure 6.6 shows a typical current-voltage characteristic (on a semilogarithmic scale) and gives the second derivative of current. At the knee of the $V-i$ curve, d^2i/dv^2 reverses its sign (see Fig. 6.3); this fact rather facilitates the determination of the bend point and of the space potential. Figure 6.7 plots energy distribution functions $n(\varepsilon)$ recalculated on the basis of $f_0(v)$. They are given in arbitrary units, the quantity 100 being assigned to the maximum. The corresponding Maxwell distributions are also shown. The distribution temperatures were found from straight segments in the range of low electron energies $\varepsilon = eV_p$ present on the plots of ln i vs. V. The contribution of energetic electrons to the spectrum is seen to drop in comparison with the maxwellian curve, as a result of electron energy loss to excitation.

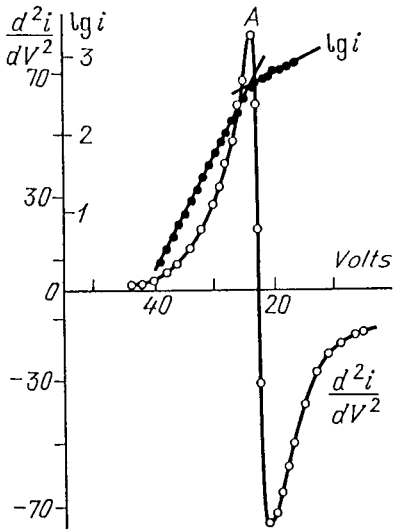

Fig. 6.6. Example of probe measurements. Discharge in mercury vapor. Wire probe on the tube axis, 0.03 mm in diameter, 6 mm in length [6.2]

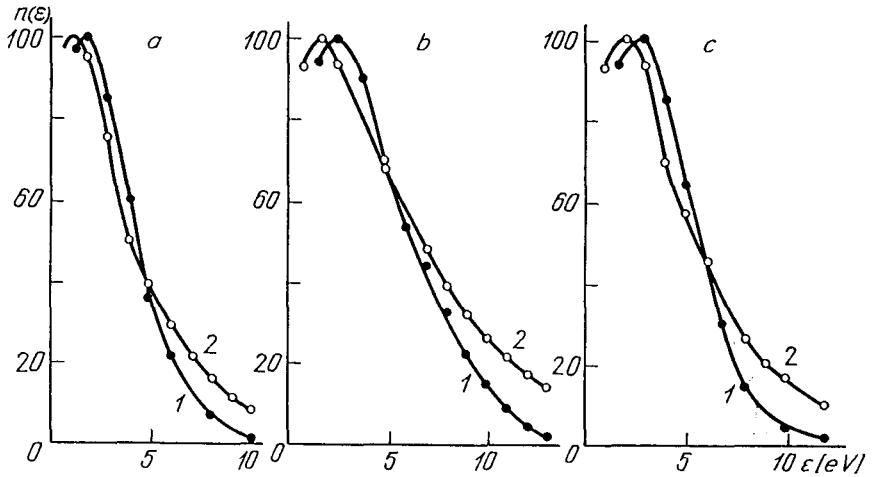

Fig. 6.7. Examples of distribution functions in neon, obtained by probe measurements. **(a)** p = 1 Torr, i = 100 mA; **(b)** p = 1 Torr, i = 25 mA; **(c)** p = 1.6 Torr, i = 25 mA. *(1)* Measured distribution, *(2)* Maxwell distribution of the same mean energy [6.2]

6.5 Ionic Current to a Probe in Rarefied Plasma

Let a probe be connected to a negative potential so much higher than the electron temperature (say, by an order of magnitude) that all electrons are repelled from the probe and make no contribution to the probe current. The probe is surrounded by a layer of positive space charge. Assume that the layer is thin, so that the surface area of its outer boundary differs only slightly from the probe area S. If the mean-free-path length of ions is much greater than the probe size (and hence, than the layer thickness), the surrounding plasma is only slightly perturbed and the ionic current can seemingly be evaluated using (6.3) after $\bar{v}_e$ is replaced with the thermal velocity of ions, $\bar{v}_+ = (8kT/\pi M)^{1/2}$. However, if the charge density n_0 of weakly ionized plasma is determined in this way from the measured ionic current at the lower low-slope part of the $V - i$ curve, it is found to be systematically *greater* than the value calculated by using (6.3) and the electronic saturation current (at the upper break point B).

Much theoretical work, including that of Langmuir himself and his coworkers, was devoted to clarifying this situation. The clear answer was given by *Bohm, Burhop,* and *Massey* in 1949. Varous versions of the detailed theory, which includes the analysis of ion trajectories in the space-charge layer (Sect. 6.3.6) and of the potential distribution in it, are very complicated [6.1, 6.3, 6.4]. We will describe the process in the simplest possible way, aiming only at clarifying the physical essence of the phenomenon and finding an evaluation formula for the ionic current.

6.5.1 Saturation Current

The gas and ion temperature T in a weakly ionized plasma is less, by more than an order of magnitude than the electron temperature $T_e \approx 1\,\text{eV}$. The charge neutrality of plasma far from the probe begins to be violated where electrons are appreciably decelerated in the repulsive field, that is, where the negative potential with repsect to the nonperturbed plasma equals roughly $|V_b| \approx kT_e/e$. This is the external boundary of the space-charge layer (Fig. 6.8). The electron density at the boundary is given by the Boltzmann law: $n_b = n_0 \exp(-e|V_b|/kT_e) \approx n_0/\bar{e}$, where $\bar{e}$ is the base of natural logarithms. On the outside of this boundary, low-energy ions manage to "keep up" with more energetic electrons so as to maintain quasineutrality, that is, the ion density at the boundary is quite close to n_b. However, since $kT \ll kT_e \approx e|V_b|$, ions are relatively strongly influenced by the field outside the layer as well, namely, in the outer *pree-sheath*, where the potential V lies in the interval $kT < |eV| < kT_e$. Inside it the plasma is quasineutral but the field imparts to ions a velocity much higher than their thermal value. They enter the layer from the pre-layer with a velocity normal to the boundary surface given by

$$v_+ \approx (2e|V_b|/M)^{1/2} \approx (2kT_e/M)^{1/2} \approx (T_e/T)^{1/2}\bar{v}_+ .$$

As a result, the ionic saturation current in the idealized plane case is approximately equal to

$$i_{+\text{sat}} \approx Sen_b v_+ \approx \left(\sqrt{2}/\bar{e}\right) Sen_0 \sqrt{kT_e/M} . \tag{6.10}$$

More detailed calculations give the same result, and even a very close value for the numerical coefficient that in (6.10) equals $\sqrt{2}/\bar{e} = 0.52$. In the case of a spherical or thin cylindrical probe, the ionic current grows with increasing negative potential, for reasons described in Sect. 6.3.6.

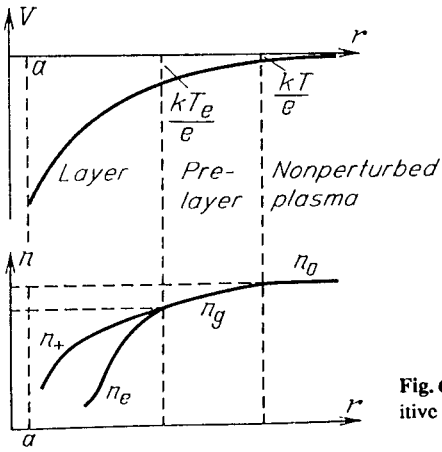

Fig. 6.8. Variation of potential, electron density, and positive ion density near a negative probe

6.5.2 Measurement of Charge Density in Plasma

This quantity is conveniently determined from T_e and the measured ionic current at the lower low-slope part of current-voltage characteristic, using (6.10) or corrected, more complex formulae provided by the small probe theory.[3] This is the method that is mostly used in practice for finding n_0, especially if the ionic current is weakly dependent on potential, the $V - i$ curve has a low-slope, and the simple formula (6.10) is valid. As a comparison of (6.3) and (6.10) shows, the electronic saturation current exceeds the ionic current by a factor of about $\sqrt{M/m} \sim 10^2$. We have mentioned already that the former produces greater plasma perturbations and melts small probes. Formula (6.10) is used for the rapid evaluation of spatial electron density distributions in plasmas. Typically, the electron temperature is uniform in space and need not be measured at each point.

6.5.3 Floating Potential

In the case of the Maxwell distribution of electrons, the electronic current at a negative probe potential is given by (6.2) and the ionic current by (6.10). The negative probe potential with respect to plasma, corresponding to zero probe current, is found by equating the two expressions:

$$e|V_f|/kT_e \approx \ln\left[\left(\bar{e}/\sqrt{4\pi}\right)\sqrt{M/m}\right] \approx \ln\left(0.77\sqrt{M/m}\right) . \tag{6.11}$$

The floating potential V_f [V] is about $-3.3T_e$ [eV] in hydrogen and $-6.3T_e$ in argon. The simplest way to measure the spatial plasma potential distribution V_S is to determine at each point the probe potential V at which the probe current vanishes. The space potential is found by adding $|V_f|$ of (6.11) to the measured potential. If the electron temperature (in a more general case, the mean energy) is spatially uniform, that is, $V_f \approx$ const, a constant potential bias does not affect the electric field distribution, determined by the differences of V between neighbouring points.

6.6 Vacuum Diode Current and Space-Charge Layer Close to a Charged Body

Estimates of the possibility of working with the simplest formulae of the probe theory obtained for the plane case are based on comparing the space-charge layer thickness with the probe size. We will evaluate the layer thickness in the simplest situations, but those of main interest to probe diagnostics, in the extreme situations in which the sign of particles flowing to the probe coincides with that

[3] In fact, difficulties are encountered in estimating the correspondence of the experimental conditions to the limits of applicability of a specific approximate formula; these limits are not always clearly defined.

of the space charge. These are the cases of positive or sufficiently high negative potentials, that is, of saturation currents. In the range of the steep part of the $V-i$ curve, where the space charge at the probe repelling electrons is positive and the current is electronic, this current is independent of layer geometry (Sect. 6.3.5). The classical problem of current in the *vacuum diode* can be used as a suitable model fo considering a layer at the probe and a number of other situations, such as the cathode layer of arc discharges (Sect. 10.5.3).

6.6.1 Space-Charge-Limited Current in the Vacuum Gap

Let a voltage V be applied to plane electrodes separated by a distance h. External factors cause the emission of charges from one electrode, so that dc current flows through the circuit. This model represents an actual device, namely, the vacuum diode with a heated cathode emitting thermionic current. If the heater current is low and so is the emission current, the number of electrons in the surrounding space is also small. They do not produce an apprciable field, so that the potential φ is distributed in the gap exactly as in the absence of charges: $\varphi = -Ex$, where $E = -V/h$ is the field; φ and x are measured from the cathode (curve 1 in Fig. 6.9). If the voltage is not too low, the field transports all the electrons to the anode. The current coincides with the emission current (of density j_{em}) and is independent of V.

If the emission current is considerable, the gap fills up with a large number of charges that produce their own field. The potential distribution $\varphi(x)$ is affected by the space charge. The electron density distribution, in its turn, depends on $\varphi(x)$. This *self-consistent* picture is described by Poisson's equation, current continuity equations, and the equation for electron energy, $mv^2/2 = mv_0^2 + e\varphi$, that determines their velocity $v(x)$. An electron leaves the cathode at a velocity v_0. If one assumes for simplicity that all electrons have identical velocities, the absolute value of current density is $j = en_e v = \text{const}$. Therefore

$$\frac{d^2\varphi}{dx^2} = 4\pi e n_e = \frac{4\pi j}{v} = \frac{4\pi j}{v_0(1 + 2e\varphi/mv_0^2)^{1/2}}\ ; \tag{6.12}$$

note that $\varphi(0) = 0$, which has already been used in writing the equality for $v(x)$, and $\varphi(h) = V$.

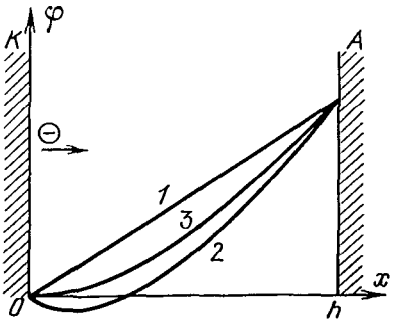

Fig. 6.9. Potential distribution in plane vacuum gap when electrons are emitted by the cathode. *(1)* very low emission current, the field is not distorted by space charge; *(2)* potential barrier is formed for electrons when they leave the cathode at a finite velocity; *(3)* electrons are ejected at zero velocity

Let us look at the behaviour of $\varphi(x)$. Electrons accumulate in the vicinity of the cathode, while the field has not yet accelerated them. This negative charge repels the electrons of the metal away from the surface, forming a *double layer*: plus on the metal and minus in its vicinity. A reverse field $E > 0$ appears at the cathode, decelerating the emerging electrons, so that the potential φ falls below the potential $\varphi = 0$ of the cathode itself. However, $\varphi > 0$ at the anode, and hence, $\varphi(x)$ passes through a minimum $\varphi_m < 0$ (curve 2 in Fig. 6.9). Electrons face a potential barrier, $-e\varphi_m$, that they have to overcome at the expense of the initial energy $mv_0^2/2$.

How high can this barrier be? Assume that $|e\varphi_m| > mv_0^2/2$. Then none of the electrons could cross it and the current is zero. This is possible only at very low V; this case holds no interest for us. Let $|e\varphi_m| < mv_0^2/2$. Then all (assumed to be monoenergetic) emerging electrons cross the barrier; the current is that of saturation, j_{em}. The case of interest is intermediate: the space charge limits, but does not cut off, the current, $0 < j < j_{em}$; a case that is realized if the barrier height (assuming electron energies to be identical) is exactly equal to the initial energy of the electrons. Formally, electrons pass across the barrier peak at zero velocity, their density at this point being infinite although $j =$"$0 \cdot \infty$" is finite. The solution of (6.12) that satisfies the condition $d\varphi/dx = 0$ for $\varphi = \varphi_m = -mv_0^2/2e$ selects the value of current that the gap can let through at the voltage V when the space charge does not let all the emitted electrons reach the anode.[4]

Let us introduce a dimensionless potential $\psi = 2e\varphi/mv_0^2$ into (6.12):

$$\frac{d^2\psi}{dx^2} = \frac{4}{9x_0^2}\frac{1}{\sqrt{1+\psi}}, \quad x_0 = \left(\frac{mv_0^3}{18\pi ej}\right)^{1/2}. \tag{6.13}$$

The physical meaning of the length scale x_0 will be clear immediately. Note that $d^2\psi/dx^2 = (1/2)d(d\psi/dx)^2/d\psi$ and integrate (6.13). To find the arbitrary constant, we make use of the condition $d\psi/dx = 0$ for $\psi = -1$. We obtain

$$\frac{d\psi}{dx} = \mp\frac{4}{3x_0}(1+\psi)^{1/4}, \quad (\mp) \text{ for } x \lessgtr x_{(\min)}.$$

Let us integrate these two equations. The constant in the equation with the sign $(-)$ is found from the condition $\psi = 0$ at $x = 0$. The result shows that the minimum $\psi_m = -1$ is attained at a distance $x_{(\min)} = x_0$ from the cathode. The constant in the solution of the equation with $(+)$ is found by stipulating that the solution pass through the same point x_0, $\psi = -1$. This gives the potential distribution plotted by curve 2 in Fig. 6.9:

$$\frac{2e\varphi}{mv_0^2} = \left[\pm\left(\frac{x}{x_0} - 1\right)\right]^{4/3} - 1, \quad (\pm) \text{ for } x \gtrless x_0. \tag{6.14}$$

[4] Real emitted electrons possess various velocities and a quite definite barrier is formed: $|e\varphi_m|$. The electrons with higher initial energy overcome the barrier while the slower ones are turned back. The correct solution is obtainable only by numerical integration; actually, the same result is obtained in the limit $V \gg |\varphi_m|$ [6.5].

Assigning (6.14), with the sign (+), to the anode coordinate $x = h$, where $\varphi = V$, we find the relation defining the current $j(V, h, v_0)$. Nearly always $eV \gg mv_0^2/2 \sim kT$, where T is the cathode temperature (several tenths of a volt). Hence, $h \gg x_0$ and the "1"s in (6.14) can be neglected everwhere except in the immediate vicinity of the cathode. Hence, $\varphi \propto x^{4/3}$, $E \propto x^{1/3}$, $v \propto x^{2/3}$, $n_e \propto x^{-2/3}$, and the current is

$$j = \frac{1}{9\pi}\sqrt{\frac{2e}{m}} \cdot \frac{V^{3/2}}{h^2} = 2.34 \cdot 10^{-6} \frac{\{V[\mathrm{V}]\}^{3/2}}{\{h[\mathrm{cm}]\}^2} \frac{\mathrm{A}}{\mathrm{cm}^2} . \tag{6.15}$$

This relation, giving the space-charge-limited current in a planar vacuum diode, is known as the Child-Langmuir equation derived in 1913 or the *law of three-halves power*: the current is proportional to $V^{3/2}$. In this approximation, the vanishingly small minimum of φ sits on the cathode. Law (6.15) can be derived in an elementary manner, by integrating (6.12) under an additional condition $E = 0$ for $x = 0$, which is equivalent to assuming that electrons leave the cathode at zero velocity. The independence of j from j_{em} must be interpreted as the unlimited emission capability of the cathode. On the side of high voltages and currents, the validity of (6.15) is limited by the condition $j < j_{\mathrm{em}}$, and on the side of low values, by the condition $V \gg kT/e$ and the stipulation that space charge strongly affects the current.

We will illustrate this with a numerical example. If $T \approx 1000\,\mathrm{K} \approx 0.1\,\mathrm{eV}$, an oxide cathode emits $j_{\mathrm{em}} \sim 1\,\mathrm{A/cm^2}$. If a voltage $V = 100\,\mathrm{V}$ is applied to a gap $h = 1\,\mathrm{cm}$, the current will be only $j \approx 2.3 \cdot 10^{-3}\,\mathrm{A/cm^2}$; only two electrons out of 1000 will break through the barrier raised by the electrons themselves.

The $i \propto V^{3/2}$ equation (6.15) holds for spherical and cylindrical diodes, but h^2 is replaced with the product of one radius squared by a function of the ratio of the radii; these functions are tabulated in [6.5]. Formula (6.15) also holds for ion emitters after m is replaced with M, and V with $|V|$.

6.6.2 Evaluation of Plane Layer Thickness

This can be evaluated using the result above (and the relations for the appropriate diodes in the cases of the spherical and cylindrical probes). The probe acts as a charge-collecting electrode. The boundary of the quasineutral plasma, from which particles are injected into the space-charge region, acts as the emitting electrode. Note that the dependent variable changes. In a diode, the gap width is fixed and the current "tunes up" to the applied voltage. The layer at the probe receives a certain saturation current, imposed by the thermal gas-kinetic electron flux in the case of positive probe potential, and by the V_{p}-independent ion flux from the pre-layer to the layer in the case of high negative potentials. As for the layer, its thickness h adjusts itself to the probe potential.

For $V_{\mathrm{p}} > 0$ and the Maxwell electron distribution, formulas (6.3) and (6.15) yield

$$h \approx (8/9)^{1/2}(eV_{\mathrm{p}}/kT_{\mathrm{e}})^{3/4} d\,, \quad d = (kT_{\mathrm{e}}/4\pi e^2 n_0)^{1/2}\,.$$

The thickness scale for the negative space-charge layer is the *Debye radius* d, but the thickness increases with increasing potential. If the negative potential is high, so that the current is due only to ions, (6.10) and (6.15) (with m replaced by M) give the same thickness of the positive charge layer:

$$h \approx (4\bar{e}/9)^{1/2}(e|V_p|/kT_e)^{3/4}d\,.$$

But in this case the potential $|V_p|$ is much higher. It exceeds the electron temperature by about an order of magnitude, so as to have the electron current smaller than the ion current. The ionic layer thickness is therefore an order of magnitude greater than the Debye radius. Qualitatively similar results are obtained for the sphere and cylinder, but the theory gets very complicated when these cases deviate very much from the plane case, that is, when h is much greater than the probe radius [6.3, 4].

6.7 Double Probe

A double probe designed for plasma diagnostics in the absence of a reference electrode was first used in [6.6, 7]. Two Langmuir probes are introduced into the plasma and connected via a potentiometer to a dc supply unit so as to vary not only the voltage V between the probes but its polarity as well (Fig. 6.10).

6.7.1 Probe Characteristic

The current-voltage characteristic of a double probe in an electrodeless high-frequency discharge is shown in Fig. 6.11. Let us discuss its physical meaning under the assumption of *identical probes* and *identical plasma parameters* at the points where the probes are located. The characteristic in the figure is *symmetric,* which demonstrates that in this particular experiment the above conditions were

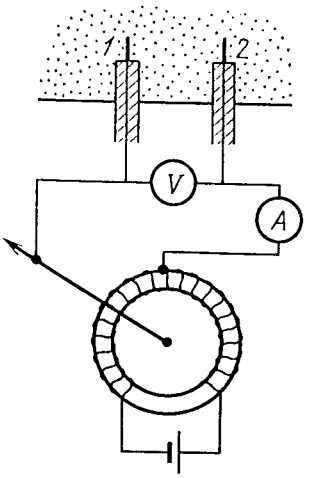

Fig. 6.10. Double probe circuit with circular potentiometer [6.4]

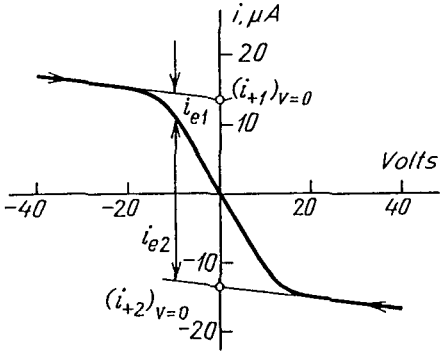

Fig. 6.11. Characteristic of symmetric double probe. Recorded by the circuit of Fig. 6.10 in electrodeless rf discharge [6.4]

satisfied with high accuracy. If the plasma potentials V_S at the two probes are equal, then no current flows through the probe circuit at zero voltage, $V = 0$: $i = 0$. This condition has also been met in this experiment: apparently, the probes were placed very close, and the potential gradient in the plasma was small. The two probes are at the same floating potential $V_f < 0$ (Fig. 6.12a).

Let us denote the potential of the left-hand probe with respect to the plasma by V_{p1}, and that of the right-hand probe by V_{p2}. For the direction of the voltage axis, we set: $V = V_{p1} - V_{p2}$. The electric current i is assumed positive if it flows from the plasma into the left-hand probe; as before, i_e and i_+ are the magnitudes of the electronic and ionic probe currents (the signs of i and V are in accord with the orientation of the curve in Fig. 6.11). The amount of positive charge flowing from the plasma into one of the probes equals the amount flowing into the plasma from the other probe; hence,

$$i = i_{+1} - i_{e1} = -(i_{+2} - i_{e2}) \ , \quad i_{+1} + i_{+2} = i_{e1} + i_{e2} \ . \tag{6.16}$$

The potential of neither of the probes can be positive. Indeed, if V_p were positive the probe would receive the electronic saturation current. According to (6.16), the electric circuit must be closed at the other probe where a substantially smaller ionic current flows. Therefore, not only is the entire probe system floating, that is, negatively charged with respect to the plasma, but each of the probes is necessarily negative. Let the negative side of the power supply be connected to the left-hand probe and the positive terminal to the right-hand one ($V < 0$). The current in the plasma flows from (+) to (−). Therefore, the ionic curent dominates at the left-hand probe and the electronic current at the right-hand one. If the voltage $|V|$ is high (in comparison with kT_e/e), the left-hand probe is strongly negative, while the right-hand one is less negative than the floating potential (Fig. 6.12b). The left-hand probe receives the purely ionic saturation current. The dependence $i(V)$ is then weak, corresponding to the left-hand low-slope part of $V - i$ curve. If V is small and negative, the ionic current to the left-hand probe is partly compensated for by the electronic current. However, the latter strongly depends on the probe potential, [namely, by Boltzmann's law (6.2)]. This is the steep segment of the $V - i$ curve; the current drops sharply to

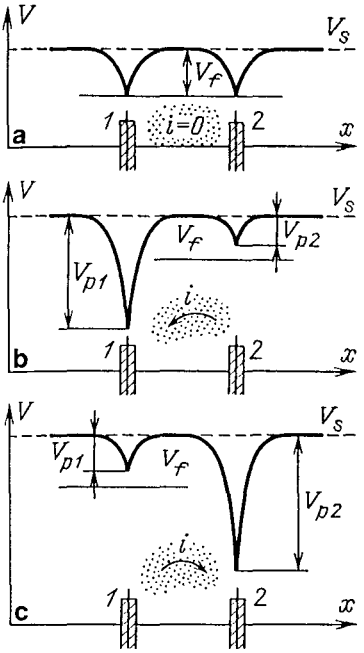

Fig. 6.12. Double probe potential: (a) Floating potential, no current through the probes; (b) Left-hand probe is strongly negative, and receives ionic saturation current; (c) Polarity reversal; the right-hand probe is strongly negative

zero as $V \to 0$. The right-hand part of the $V - i$ curve exactly retraces the left-hand one, corresponding to polarity reversal: "plus" connected to the left-hand probe and "minus" to the right-hand probe (Fig. 6.12c).

Langmuir's formula (6.2) is applicable to electronic currents i_{e1} and i_{e2}, because the potentials of both probes are negative with respect to the plasma. In view of (6.16),

$$i = i_{+1}(V_{p1}) - i_{e,sat} \exp(eV_{p1}/kT_e) = -i_{+2}(V_{p2}) + i_{e,sat} \exp(eV_{p2}/kT_e) , \tag{6.17}$$

where ionic currents weakly depend on the negative probe potential that accelerates ions.

6.7.2 Measurement of Plasma Parameters

Differentiating the first equation of (6.17) with respect to V, and then considering the symmetry point of the $V - i$ characteristic, where $i = 0$ by setting $i_{e1}(V_f) = i_{+1}(V_f) \equiv (i_+)_0$ results in

$$\left(\frac{di}{dV}\right)_0 = \left[\left(\frac{di_{+1}}{dV_{p1}}\right)_0 - \frac{e}{kT_e}(i_+)_0\right]\left(\frac{dV_{p1}}{dV}\right)_0 . \tag{6.18}$$

If the probe current vanishes at zero potential difference V, polarity reversal simply changes the roles of the two probes. As a result, in addition to the relation $V = V_{p1} - V_{p2}$, the probe potentials are related by the equation $V_{p1}(V) = V_{p2}(-V)$.

Differentiating these equations with respect to V, we obtain

$$1 = (dV_{p1}/dV)_V - (dV_{p2}/dV)_V \ , \quad (dV_{p1}/dV)_V = -(dV_{p2}/dV)_{(-V)} \ .$$

Hence, at the symmetry point, $(dV_{p1}/dV)_0 = 1/2$. Now (6.18) implies

$$e/kT_e = (i_{+1})_0^{-1} \left[(di_{+1}/dV_{p1})_0 - 2(di/dV)_0\right] \ . \tag{6.19}$$

This formula is used to measure electron temperature. The derivative $(di/dV)_0$ is found from the slope of the measured $V - i$ curve, at a point where $i = 0$. The ionic current and its derivative (note that the latter is much lower than the derivative of the total current) can be found by extrapolating the low-slope part of the $V - i$ curve linearly to the symmetry point (Fig. 6.11). We assume here that $V \approx V_{p1}$ in the range of high negative voltages, that is, the function $i_{+1}(V)$ measured in this range can be treated as $i_{+1}(V_{p1})$, which justifies the extrapolation.

Another method of measuring T_e resembles the technique employed in the single-probe method. Let us divide the second equation of (6.16) by i_{e1}, use Langmuir's formula (6.2) for electronic currents, and take the logarithm of the result:

$$\ln\left(\frac{i_{+1} - i_{+2}}{i - i_{+1}} - 1\right) = \frac{eV}{kT_e} \ . \tag{6.20}$$

Now T_e can be found from the slope of the straight line in the neighbourhood of the symmetry point after ionic currents have been determined by extrapolation and the semilogarithmic curve (6.20) has been plotted as a function of V.

The electron density in the plasma is found as in the single-probe technique, using (6.10) for the ionic saturation current, after T_e has been found and the current $i \approx i_{+sat}$ at the low-slope part of the $V - i$ curve measured.

6.7.3 Measurement of Electric Field

In the case of a potential gradient in a plasma, the space potentials at the pints where the probes are placed, V_{S1} and V_{S2}, are different. For both probes to float and probe currents to vanish, they must be placed at a potential difference $\Delta V = V_{p1} - V_{p2} = V_{S1} - V_{S2}$. By varying the voltage to bring the probe current to zero, and knowing the distance Δx between probes, we find the field $E_x = \Delta V/\Delta x$. However, the plasma potential cannot be found by the double-probe technique in prinicple.

If $\Delta V \neq 0$, the methods of determining T_e and n_0 remain valid, but the symmetry point on the $V - i$ curve at which $i = 0$ shifts along the V axis by ΔV. Formulas (6.19) and (6.20) must operate with this new point. The current in a double probe being much lower than the electronic current of a single probe (which can be used for positive ion currents only), the former produces a much smaller disturbance in the plasma. This is why it is used also for studying nonstationary processes that are especially sensitive to perturbation, since the entire picture of plasma evolution may be disrupted otherwise.

6.8 Probe in a High-Pressure Plasma

When we speak of high pressure, we mean the situation in which the free path lengths of electrons and ions, l_e and l_+, are very small compared with the probe size. The probe is assumed to be spherical, of radius a. For instance, for $p = 30\,\text{Torr}$ we find $l_e \sim 10^{-3}\,\text{cm}$, $l_+ \sim 10^{-4}\,\text{cm}$, while $a \sim 10^{-1} - 1\,\text{cm}$. Under typical discharge conditions ($T_e \approx 10^4\,\text{K}$, $n_0 \sim 10^9 - 10^{10}\,\text{cm}^{-3}$), the Debye radius is $d = (kT_e/4\pi e^2 n_0)^{1/2} \sim 10^{-2}\,\text{cm}$, so that $l \ll d \ll a$. In a dense gas, fluxes of charged particles to a probe are formed as a result of *diffusion* and *drift*. In this case the theory seems to be even more complicated than for rarefied plasma, and has not been fully developed. Furthermore, quantitative results can be obtained only using the data on free-path lengths or mobilities; this introduces additional errors into the final results. Without going into the details of the theory, let us dwell on several general features that will facilitate our understanding of the physical processes.

6.8.1 Approximate Equilibrium in Electron Gas

Fluxes of charged particles can be treated as sums of the diffusion and drift components [see (2.20)]. The electric field $\boldsymbol{E}$ is produced by the voltage applied to the probe and by plasma polarization. Let a negative potential, decelerating the electrons, be applied to the probe. If the potential equals the floating value, the electron and the ion fluxes to the probe are exactly equal. If the potential is more negative, the electron flux is less than the ionic flux. If it is more positive, but only slightly, than the floating value, the electron flux exceeds the ionic flux but has a comparable magnitude. In such cases (when the probe potential is neither positive nor weakly negative), the ionic layer of positive space charge around the probe transforms into a layer of perturbed but now quasineutral palsma that gradually changes into nonperturbed plasma of charge density n_0. The perturbation due to the probe manifests itself in the quasineutral layer as a gradient of the densities $n_e \approx n_+ \approx n$. The densities decrease towards the probe, which ensures the diffusion flux of charges from a remote region to the probe surface absorbing them. The quasineutrality as such follows from the smallness of the Debye radius in comparison with the characteristic length of density variation, which is of the order of the probe size.

As we have mentioned, if the probe potential is sufficiently negative, the electronic current is comparable to the ionic one or is smaller. But the diffusion coefficient D_e and mobility μ_e of electrons are much higher than D_+ and μ_+ of ions. Therefore, oppositely directed high diffusion and drift electronic fluxes balance each other out to yield a relatively small resultant electron flux Γ_e comparable with (or less than) the ionic flux Γ_+. In view of the Einstein relation (2.24) between D_e and μ_e, and assuming in (2.20) that $\Gamma_e \approx 0$, we find that

$$\frac{\nabla n_e}{n_e} \approx -\frac{\mu_e}{D_e}\boldsymbol{E} = \frac{e}{kT_e}\nabla V\ , \quad n_e \approx n_0 \exp\frac{eV}{kT_e}\ , \tag{6.21}$$

where $V(r) < 0$ is the potential measured with respect to the unperturbed plasma. The electron density distribution in a remote neighbourhood of a negative probe is thus approximately described by the Boltzmann law.

6.8.2 Spatial Distributions of Charge Density and Potential in the Quasineutral Region Around a Negative Probe

The electric field in the quasineutral region (quasi-equilibrium for electrons) is related to the gradient of n_e by the first formula of (6.21). Since $n_+ \approx n_e \approx n$, we introduce this value of E into equation (2.20) for the ionic flux. The total ionic current across any spherical surface is

$$i_+ \approx 4\pi r^2 e \left[D_+ + \mu_+ \frac{kT_e}{e} \right] \frac{dn}{dr} . \tag{6.22}$$

The expression in brackets is the familiar *coefficient of ambipolar diffusion* (2.25) in which $\mu_e \gg \mu_+$. If the probe is at floating potential and the electronic and ionic fluxes to the probe are equal, the flux of ions to the absorbing body is in fact the result of ambipolar diffusion (Sect. 2.6). At a different potential, the electron and ion fluxes differ by a quantity comparable with the ambipolar flux. In any case, the ionic flux in the quasineutral zone coincides in magnitude and direction with the ambipolar diffusion flux. In a nonequilibrium flux with $T_e \gg T$, the drift component of the ionic flux, which is proportional to the second term of (6.22), is greater than the diffusion component by a factor of $T_e/T \gg 1$; one is justified then to speak of the pure drift of ions in the total field E of the probe and polarization fields. We neglect the small term depending on D_+ in (6.22).

Under stationary conditions and neglecting relatively slow processes of creation and removal of charges in the plasma region perturbed by the probe (assumed to be small), we have $i_+(r) = \text{const}$. Integration of (6.22) yields the charge distribution in th quasineutral zone which transforms asymptotically into the nonperturbed plasma as $r \to \infty$:

$$n = n_0 \left(1 - \frac{R}{r} \right) , \quad R = \frac{i_+}{4\pi e n_0 \mu_+ (kT_e/e)} . \tag{6.23}$$

The physical meaning of R will now be clarified. According to (6.21) and (6.23), and since $n_e \approx n$, the potential and field distributions in the quasineutral region are

$$V = -\frac{kT_e}{e} \ln \frac{1}{1 - R/r} , \quad E = -\frac{kT_e}{eR} \frac{R^2}{r^2} \frac{1}{1 - R/r} . \tag{6.24}$$

As we move from infinity to the probe, V and E grow from zero, with scales kT_e/e and kT_e/eR, and tend formally to $-\infty$ as $r \to R$, when formally $n \to 0$.

The radius R corresponds to the boundary of the space charge that separates the probe from the quasineutral region: as $r \to R$, (6.23) and (6.24) cease to be valid. Indeed, quasineutrality is violated where the potential $|V(r)|$, decelerating

electrons, reaches several times the electron temperature kT_e/e. At this distance, however, $1 - R/r \ll 1$, so that $r \approx R$. Therefore, R can be interpreted as the effective layer radius; the second relation of (6.23) gives the ionic probe current as a function of R.

6.8.3 Ionic Saturation Current and Evaluation of Charge Density in Plasma

The higher the negative probe potential $|V_p|$, the greater the positive space-charge layer thickness $h = R - a$ and the greater R. According to (6.23), the ionic current grows with increasing R. However, if the layer is thin, R is approximately equal to the probe radius a and the ionic current is independent of potential. The corresponding quantity i_+ is the ionic saturation current. This occurs either when the probe is large and the layer thickness h (in general, it is characterized by the Debye radius d) is small in comparison with a, or if the Debye radius is small, that is, the electron density in the plasma is sufficiently high.

Expressing the ion mobility in (6.23) in terms of free path length, $\mu_+ = el_+/M\bar{v}_+$, where $\bar{v}_+ = (8kT/\pi M)^{1/2}$, and introducing the probe surface area $S = 4\pi a^2$, we can rewrite the ionic saturation current in the form

$$i_{+,\mathrm{sat}} = S\left(\frac{\pi}{8}\right)^{1/2} en_0 \left(\frac{kT_e}{M}\right)^{1/2} \left(\frac{T_e}{T}\right)^{1/2} \frac{l_+}{a} . \tag{6.25}$$

This differs from (6.10) for rarefied plasmas in the last two factors. The first one, $(T_e/T)^{1/2}$, does not exceed 10; the second one is, according to the initial assumption, a very small quantity, much less than 10^{-1}. The ionic saturation current is, therefore, much lower in dense ionized gas than in rarefied gas, and the higher the pressure the lower it is.

The probe characteristic at high pressures is qualitatively similar to the $V - i$ curve in a rarefied plasma; its lower low-slope part corresponds to the ionic current. The charge density n_0 can be estimated on the basis of the measured ionic current via (6.25). Even if the electron temperature in (6.25) cannot be reliably measured, we know that it lies in a much narrower range of values ($T_e \approx 1\,\mathrm{eV}$) than the electron density, which may vary by orders of magnitude in different discharge conditions.

6.8.4 On the Use of Electronic Probe Current for Evaluating Electron Temperature

If the negative probe potential is higher than the floating value, the electronic current is greater than the ionic and increases rapidly as the decelerating potential $|V_p|$ decreases. As in the case of rarefied plasmas, $i = i_e - i_+ \approx i_e$. This situation corresponds to the steep part of the $V - i$ curve, present at high pressure as well. Electrons reach the probe immediately after the last collision, that is, from the sphere of radius $r_1 \approx a + l_e$ that lies at a small distance of order $l_e \ll a$ from the probe surface. Let us denote the density and potential at the radius r_1 by n_{e1}

and V_1, repsectively. The electron probe current can be expressed by a formula similar to (6.2),

$$i_e \approx S(n_{e1}\bar{v}_e/4)\exp\left[e(V_p - V_1)/kT_e\right] , \tag{6.26}$$

because electrons from the sphere r_1 reach the probe without colisions. The electron temperature and $\bar{v}_e(T_e)$ are much less perturbed than the density.

If (6.21) for equilibrium electron density $n_e(V)$ is extrapolated up to the sphere of radius r_1, where $V = V_1$, we define n_{e1} and obtain from (6.26) exactly the expression (6.2) for the probe current, $i \propto \exp(eV_p/kT_e)$. There is some hope, therefore, that the steep part of the $V - i$ characteristic can be used to evaluate the electron temperature (using the semilogarithmic plot ln i vs. V_p). A more detailed analysis [6.8] taking into account that the electron flux in (2.20) is nonzero demonstrated that the electronic current is reduced in comparison with (6.2) by a factor of $\gamma \approx 1 + \alpha(h/l_e)(kT_e/eV_p)$, where α is a numerical coefficient $\approx 1/2$. The reduction may be substantial, of the order of 10, but it depends on V_p much less than the Boltzmann exponential in (6.2). That is why T_e can be estimated on the basis of the slope of the electronic part of the probe characteristic.

6.8.5 Layer of Positive Space Charge

In order to evaluate the thickness or radius of the layer separating the probe from the quasineutral plasma, we have to integrate Poisson's equation. Neglecting the small electron density in the ionic layer, we can write

$$\frac{1}{r^2}\frac{d}{dr}r^2E = 4\pi e n_+ , \quad E = -\frac{dV}{dr} < 0 . \tag{6.27}$$

As in Sect. 6.6, we give the ion density in terms of the ionic flux (drift flux in this case): $n_+ = \Gamma_+/\mu_+|E|$.[5] Introducing the total ionic current (which is independent of r), according to (6.23), we obtain

$$n_+ = \frac{i_+}{4\pi r^2 e\mu_+(-E)} = -n_0\frac{kT_e}{eE}\frac{R}{r^2} . \tag{6.28}$$

For boundary conditions to (6.27) and (6.28), we can set that the field and potential are zero at the boundary between the layer and the quasineutral region at $r = R$. This approximation reflects the fact that the field is small compared with the average field in the layer.

Even after these simplifications, a compact formula for layer thickness, $h = R - a$, is obtained only if the layer is thin, that is, "plane"; correspondingly, $r^2 \approx \text{const} \approx a^2$. In this case,

[5] At very high negative potentials V_p, the field in the layer may be so high that the drift of ions is of the *anomalous* type: $v_{+d} \propto \sqrt{|E|}$ (Sect. 2.5.4).

$$h/a = \left[(3/2\sqrt{2})(d/a)(e|V_p|/kT_e)\right]^{2/3} . \tag{6.29}$$

For a collisionless layer, formula (6.15) gives $h \propto |V_p|^{3/4}$. The plane layer approximation is valid as long as $h < a$. For exmaple: if $d \sim 10^{-2}$ cm, $a \sim 10^{-1}$ cm, and $a/d = 10$, the layer thickness increasing with potential becomes comparable with probe radius, $h/a \approx 1$ for $e|V_p| \approx 10kT_e$. With sphericity taken into account the formulae are very unwieldy, even though the integration does not involve any fundamental problems. If the layer is thick, its radius R and the probe potential obey the crude approximate relation:

$$eV_p/kT_e \approx -(2/3)^{1/2}(a/d)(R/a)(R/a - 1) . \tag{6.30}$$

For example, if $a/d = 12.3$, $R/a = 1.5$ for $e|V_p|/kT_e = 7.5$ and $R/a = 2$ for 20. In the limit of large $|V_p|$, $R/a \sim \sqrt{|V_p|}$, and hence (6.23) implies the probe current $i \approx i_+ \sim \sqrt{|V_p|}$.

6.8.6 Floating Potential and Determination of Potential Distribution

Equating the expressions for the ionic (6.25), and the electronic current (6.2), and taking into account the decreasing factor γ mentioned in Sect. 6.8.4, we arrive at a relation similar to (6.11),

$$\frac{e|V_f|}{kT_e} \approx \ln\left[\frac{2}{\pi}\left(\frac{M}{m}\right)^{1/2}\left(\frac{T}{T_e}\right)^{1/2}\frac{a}{l_+}\gamma^{-1}\right] , \tag{6.31}$$

that defines the floating potential. It is of the order of $10(kT_e/e)$. Measuring the absolute value of potential in a dense plasma is not a simple problem, but the spatial potential distribution is readily obtainable. This can be accomplished, for example, by connecting the probe without any dc supply to the reference electrode in series with a very high resistor Ω. The almost insulated probe is then at the floating potential. The potential difference between the probe and the reference electrode is found by measuring on the weak probe current: $i\Omega = V_S + V_f$. If the floating potential is the same everywhere, we move the probe and find the plasma potential distribution with respect to the reference electrode potential V_S up to the constant V_f. The field distribution is found from potential differences between nearby points.

7. Breakdown of Gases in Fields of Various Frequency Ranges

7.1 Essential Characteristics of the Phenomenon

In the most general sense, *electric breakdown* is the process of transformation of a nonconducting material into a conductor as a result of applying to it a sufficiently strong field. The ionized state produced in the gas by breakdown builds up in a time which varies from 10^{-9} to several seconds, although usually it is between 10^{-8} to 10^{-4} s. Ionization reaches appreciable values, so much so that, as a rule, breakdown is accompanied with a light flash visible to the naked eye. Some modes of flash are commonly known as "sparks". If the external field is applied for a sufficiently long time, the breakdown may start a discharge, sustained as long as the field is there. This occurs in any electric field: constant, pulsed, periodic, or produced by electromagnetic waves, including light waves. Concrete conditions dictate to what limit the degree of ionization will grow. It may reach 10^{-8}, as in the glow discharge where the current is limited by a high resistance in the external circuit, or it may be the total single ionization of all atoms, as occurs in the breakdown by high-intensity laser pulse.

The primary element of the often very complicated breakdown process is the *electron avalanche,* which develops in the gas when a strong enough electric field is applied to it. An avalanche begins with a small number of "seed" electrons that appear accidentally, say, due to cosmic rays. It can even be triggered by a single electron. An artificial source of primary electrons is employed to facilitate breakdown build up in experimental studies, in order to start up the avalanche reliably. For example, the cathode or the gas may be irradiated with UV light to produce photoelectrons. An electron picks up energy in the electric field. Having reached energy somewhat greater than the ionization potential, the electron ionizes a molecule, therebgy losing its energy. The result is the production of two slow electrons. They are again accelerated in the field, ionize molecules, thereby producing four electrons, and so forth. In principle, it is unimportant whether this occurs in an avalanche that drifts systematically in a constant field, or by electrons which are "marking time" executing oscillatory motion in a rapidly oscillating field, although the details and the outward manifestations of the process may be very different.

Gas breakdown is essentially a *threshold* process. This means that breakdown sets in only if the field exceeds a value characterizing a specific set of conditions. Thus no changes in the state of the medium are noticeable for some time while the voltage across a discharge gap or the intensity of electromagnetic radiation

is gradually increased. Suddenly, ionization rises dramatically at a certain value of voltage or intensity, instruments detect a current, and a flash is observed. The threshold is a consequence of the steep dependence of the rate of atomic ionization by electron impact on field strength and by the fact that ionization, producing electron *multiplication,* is accompanied by mechanisms that create obstacles to the development of the avalanche.

The avalanche is *slowed down* by electron energy losses and by the loss of electrons themselves. The former losses slow down the accumulation of energy sufficient for ionization. The latter terminate chains in the multiplication *chain reaction.* Electrons lose energy to excite electron states of atoms and molecules, molecular vibration, and rotation; energy is also lost in elastic collisions. Electron impact chains are also terminated as a result of diffusion leading to the removal of electrons from the field (e.g., precipitation on the walls), and of the attachment in electronegative gases. When gas breakdown occurs between electrodes, the field applied to them removes electrons to the anode. Recombination is not amongst the mechanisms of electron removal that appreciably influence the breakdown threshold. The fate of an avalanche (whether it will grow or die out) is decided at its *early* stage, when the numbers of electrons and ions are so small that their encounters have a very low probability. The recombination rate is proportional to the electron density squared. At low densities, recombination is much less effective than removal mechanisms that are linear in the electron density: transport to the anode, diffusion to the walls, and attachment. However, recombination intensifies after a large number of *generations* of secondary electrons and may set the limit to further ionization, thereby finalizing the level reached by ionization in the breakdown.

Electron energy losses must rather be treated as a factor reducing the ionization frequency. Formally, they do not eliminate the possibility of ionization, only slow it down; practically, though, these losses in insufficiently strong fields suppress the ionization rate. The disappearance of an electron breaks a chain, setting a limit to the possibility of sustaining the chain reaction of mulitplication. The creation and removal of electrons are competing processes. The rate of creation of new electrons is determined by the ionization frequency and is extremely sensitive to field strength. The rate of removal is much less dependent on the field. Even if the field is slightly lower than the *threshold value,* the ionization rate is considerably smaller than the rate of removal, and no multiplication occurs. If the field exceeds the threshold, the ionization process is speeded up catastrophically. The higher the field is above the threshold, the easier and swifter the breakdown develops.

The breakdown threshold is determined by the relation between creation and removal of electrons only if the field is maintained for a sufficiently long time, adequate for producing numerous generations of electrons. If a pulse is very short, the field must be so high that a sufficient, "macroscopic" number of electrons be born during the pulse, even if losses are absent. This is known to happen, for example, in gas breakdown by focussed "giant" laser pulses that last only

$(2-4)\cdot 10^{-8}$ s. A visible flash appears when about 10^{13} electrons are produced in the focal region.

This chapter treats the effects of gas discharges in all frequency ranges, from dc fields to optical frequencies. However, the principal phenomena in discharge-gap breakdown by voltage applied to electrodes are discussed here only with regard to the breakdown of the entire gap volume and the triggering of a self-sustained discharge in moderate-pressure gases. The breakdown in relatively long gaps filled with high (atmospheric) pressure gas, known as the *streamer, leader* or *spark,* discharge in which a thin ionized channel grows from one electrode to the other, will be treated in Chap. 12.

7.2 Breakdown and Triggering of Self-Sustained Discharge in a Constant Homogeneous Field at Moderately Large Product of Pressure and Discharge Gap Width

7.2.1 Non-Self-Sustaining Current in a Discharge Gap

Consider what happens in a plane gap connected to a circuit with a dc power supply if the voltage V on the electrodes is gradually raised. The applied electric field is assumed to be homogeneous, $E = V/d$, where d is the electrode separation. Electrons appear at the cathode occasionally, and the field transports them towards the anode. An electron may not reach the anode: it may stop on the side wall of the discharge chamber, or attach itself to an electronegative molecule. Then ions may recombine. The fraction of electrons lost on the way is smaller, the faster they cross the gap, that is, the stronger the field. As a result, the electric current i in the circuit, determined by the number of charged particles that reach the electrodes in 1 s, increases (at first) with increasing V. Beginning at a certain voltage, practically all the charged particles (electrons and ions) randomly created in the gas reach the electrodes. The current reaches *saturation* and ceases to depend on V. It is determined by the rate of charge generation due to outside sources, cosmic rays, or an artificial ionizer. This discharge is *not self-sustaining.* Its static current-voltage characteristic is shown in Fig. 7.1. It is *static* since it corresponds to a steady state. The voltage is assumed to be raised so slowly that a stationary state is attained at each value of V.

At still higher voltages, the electron impact ionization of gas molecules starts, amplifying the current due to outside sources. Assume, for example, that the cathode is irradiated with the light of a UV lamp producing a photocurrent i_0; attachment is absent (for its effects, see Sect. 7.2.5). The electronic current at the anode and the circuit current i are enhanced in comparison with the current of electrons leaving the cathode by a factor $\exp(\alpha d)$, where α is Townsend's coefficient for ionization (Sect. 4.1.2): $i = i_0 \exp(\alpha d)$. The total cathode current in the steady state also equals i. It consists of the electron current i_0 and the current of ions generated in the course of ionization and pulled by the field to

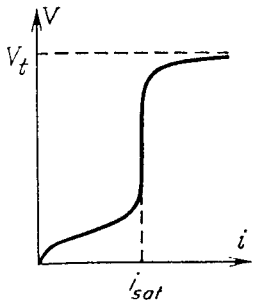

Fig. 7.1. $V - i$ characteristic of non-self-sustaining discharge between plane electrodes

the cathode, $i_0[\exp(\alpha d) - 1]$ (Sect. 4.7.1). The vertically rising curve in Fig. 7.1 becomes less steep. As voltage grows further, *secondary* processes come into play: creation of electrons by particles that appear as a result of the *primary* process of electron impact ionization. Secondary processes affect amplification more strongly if they produce electron *emission* from the cathode. An emitted electron covers the entire path from cathode to anode and therefore produces more ionization than an electron "born" halfway. With secondary emission taken into account, the steady discharge current is given by (4.16):

$$i = i_0 \exp(\alpha d) / \{1 - \gamma[\exp(\alpha d) - 1]\} ,$$

where γ is the effective *secondary emission coefficient for the cathode*; the emission is caused by positive ions, photons, and metastable atoms produced in the gas as a result of ionization and excitation of atoms by electrons. As long as the denominator is positive, the current remains non-self-sustained. As V increases, the current grows even steeper than in the range of simple amplification, owing to a decrease in the denominator which equals unity at small values of the amplification coefficient αd.

7.2.2 Condition for Initiating a Self-Sustaining Discharge

If the voltage between the electrodes $V > V_t$ is such that $\mu = \gamma[\exp(\alpha d) - 1] > 1$, the denominator in the last formula is negative and the expression becomes meaningless. This signifies that the current cannot be steady at this voltage. On the other hand, the current at $V < V_t$, with $\mu < 1$, is steady and non-self-sustained. The transition condition is $\mu = 1$, or

$$\gamma \left[\exp(\alpha d) - 1\right] = 1 , \quad \alpha d = \ln(1/\gamma + 1) ; \tag{7.1}$$

this represents a *steady self-sustained current in a homogeneous* field $E_t = V_t/d$, where the threshold voltage V_t is found from equality (7.1).

Indeed, formally at $V = V_t$, $i = 0/0 \neq 0$ for $i_0 = 0$, that is, current flows even in the absence of an outside source of electrons. Processes in the discharge gap ensure the *reproduction* of electrons removed by the field, without outside help. One electron emitted by the cathode produces $\exp(\alpha d) - 1$ ions which, hitting the cathode, knock out γ electrons each (if this is the ion-electron emission). One primary electron is replaced with one secondary electron ($\mu = \gamma(e^{\alpha d} - 1) = 1$),

etc. The *transition* of non-self-sustaining to self-sustaining discharge can also be interpreted as the *onset of breakdown*. The breakdown voltage V_t is defined by condition (7.1) as a function of gap width d, in terms of γ and the known function $\alpha(E)$. If $\gamma \sim 10^{-1} - 10^{-3}$ (Sect. 4.7.3), an electron triggers a self-sustained discharge if it takes part in $\alpha d / \ln 2 \approx \ln \gamma^{-1} / \ln 2$ (3 to 10) ionizing collisions along the path d.

7.2.3 Formative Time of Breakdown

Strictly speaking, breakdown cannot be sustained if the voltage applied to electrodes is exactly V_t, as it ensures only the primitive *reproduction* of electrons, $\mu = 1$. A negligible seed current at the cathode must grow to a macroscopic value, otherwise we cannot speak of a self-sustained discharge. It will happen if there is at least a small *overvoltage* $\Delta V = V - V_t > 0$ ensuring *expanded* reproduction of electrons, $\mu > 1$. In this case, if, say, a single electron has left the cathode at the initial moment, $\mu > 1$ electrons will be emitted in the next cycle, then μ^2, etc. The current and ionization in the gas will increase until the growth is stopped by recombination or the ohmic resistance Ω of the circuit. As the current increases, this resistance accepts a progressively greater part of the power supply voltage, $i\Omega$, and the voltage across the electrodes decreases. When V drops to V_t, i ceases to grow and the self-sustaining current becomes stationary. Thus starts the so-called dark (Townsend) discharge (Sects. 8.2.2 and 8.3.1). For this to happen, the circuit resistance must be very high, limiting the discharge current to a very small value at which the positive space charge accumulating in the gap does not distort the external field. Otherwise the field becomes spatially inhomogeneous and a glow discharge develops (Sects. 8.3, 8.4). The outlined breakdown is also known as *Townsend process* (to distinguish it from the spark breakdown mechanism).

Let us find the law of current growth at the stage when the overvoltage can be regarded as constant. Assume that emission is caused by positive ions. Ions are created mostly close to the anode, where multiplication results in the maximal number of electrons. By τ we denote the time required to pull an ion from the anode to the cathode. Electron emission from the cathode at a moment t is caused by ions produced by electrons emitted at the time $t - \tau$. The electronic current i_1 from the cathode obeys an approximate equation:

$$i_1(t) \approx i_0 + \mu i_1(t - \tau) \approx i_0 + \mu \left[i_1(t) - \tau \frac{di_1}{dt} \right] ,$$

where i_0 is the seed current due to the external ionizer. Integrating this equation with the initial condition $i_1(0) = i_0$ at the moment of switching on the field, we obtain the following expression for the discharge current (Schade, 1937)

$$i(t) = i_1(t) e^{\alpha d} = i_0 e^{\alpha d} \left[\frac{\mu}{\mu - 1} \exp\left(\frac{\mu - 1}{\mu} \frac{t}{\tau} \right) - \frac{1}{\mu - 1} \right] . \qquad (7.2)$$

The current grows with time exponentially, and the faster, the higher the overvoltage and $\mu - 1$. The time scale of current increase is $\mu\tau/(\mu - 1)$. If the emission is caused by photons, τ is of the order of the drift time of electrons (not ions) that is, breakdown develops two orders of magnitude faster. The ionization coefficient α is a steep function of field, while the amplification $\exp(\alpha d)$ and reproduction coefficient μ depend on α exponentially. Therefore, several percent overvoltage is already sufficient for μ to be appreciably greater than unity and for the breakdown to develop rapidly. For this reason, the critical value V_t, found from the condition $\mu = 1$, is a sufficiently definite characteristic of the breakdown threshold. The real time of breakdown buildup after the voltage has been applied consists of two parts: that discussed above, with a scale $\mu\tau/(\mu - 1)$, and the time until the first seed electron appears (unless an artificial source of sufficient intensity is used). The latter time has a *statistical spread.* The *retardation* time of the Townsend breakdown is of the order of 10^{-5}–10^{-3} s.

The evolution of the Townsend breakdown is best thought of as the multiplication of *avalanches.* Each cycle, from the moment an individual electron leaves the cathode until all $\exp(\alpha d)$ electrons that are its descendents reach the anode, can be treated as a single avalanche. If the breakdown has started with a single spurious electron, then the second cycle following the first avalanche involves, on the average, $\mu > 1$ avalanches, the third cycle involves μ^2 avalanches, and so on. Each avalanche spreads transversally somewhat owing to electron diffusion, so that a new avalanche starts at a different spot on the cathode (which may be quite far in the case of photoemission). Furthermore, a process is not necessarily started by a single electron: several may be emitted simultaneously from different points. As a result, the Townsend breakdown most often involves in a diffuse manner the *entire volume* of the gap. This is a clear external difference to the spark discharge.

7.2.4 Ignition Potential

This is an equivalent term for the break-down voltage V_t. This quantity, and the corresponding breakdown field E_t, depend on the gas, the material of the cathode, the pressure, and the discharge gap width. To arrive at explicit expressions, we make use of (4.5) for α. Substituting it into (7.1), we obtain

$$V_t = \frac{B(pd)}{C + \ln pd}, \quad \frac{E_t}{p} = \frac{B}{C + \ln pd}, \quad C = \ln \frac{A}{\ln(1/\gamma + 1)}. \tag{7.3}$$

The *ignition potential* V_t and E_t/p depend only on the product pd. This is a manifestation of a *similarity law.* The calculation of V_t by (7.3), with experimentally determined constants A and B (Table 4.1), gives a satisfactory agreement with experiment. The experimental curves $V_t(pd)$, the so-called *Paschen curves,* are plotted in Figs. 7.2, 7.3. There exists the minimal breakdown voltage for a discharge gap, and according to (7.3), the parameters of this minimum point are ($\bar{e} = 2.72$) :

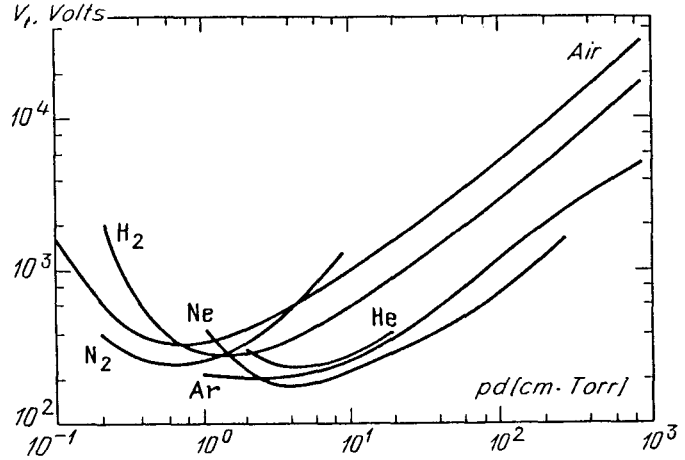

Fig. 7.2. Breakdown potentials in various gases over a wide range of pd values (Paschen curves) on the basis of data given in [7.1,2]

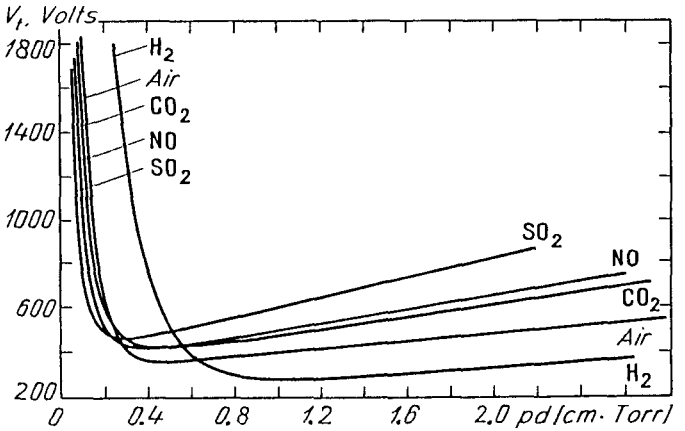

Fig. 7.3. Paschen curves on an enlarged scale [7.3]

$$(pd)_{\min} = \frac{\bar{e}}{A} \ln\left(\frac{1}{\gamma} + 1\right) , \quad \left(\frac{E}{p}\right)_{\min} = B , \quad V_{\min} = \frac{\bar{e}B}{A} \ln\left(\frac{1}{\gamma} + 1\right) . \qquad (7.4)$$

The value of E/p at the minimum corresponds to Stoletov's point (Sect. 4.1.6), where the ionization capability of electrons, $\eta = \alpha/E = A/B\bar{e}$, is at a maximum. The conditions for breakdown are the easiest because the conditions for multiplication are optimal. In contrast to $V_{\min}$ and $(pd)_{\min}$, the product $(E/p)_{\min}$ is independent of the cathode material (of γ), as demonstrated by (7.4) and experimental data [7.1,2]. Let us compare the estimate given by (7.4) with measurements. In air, $A = 15$, $B = 365$. For $\gamma = 10^{-2}$, formulas (7.4) give $C = 1.18$, $(pd)_{\min} = 0.83$ Torr·cm, $(E/p)_{\min} = 365$ V/(cm·Torr), $V_{\min} = 300$ V. Experiments with an iron cathode give: $(pd)_{\min} = 0.57$ Torr·cm, $V_{\min} = 330$ V,

$(E/p)_{min} = 580$ V/(cm·Torr). In inert gases, $(pd)_{min}$ is greater but V_{min} is smaller. Thus in argon with an iron cathode, $(pd)_{min} = 1.5$, $V_{min} = 265$, $(E/p)_{min} = 176$.

In the range of relatively large pd on the *right-hand branch* of the Paschen curve, the threshold value E_t/p decreases rather slowly (logarithmically) as pd increases. Correspondingly, the breakdown voltage increases almost proportionally to pd (slightly slower). This behaviour of threshold values arises because in the case of elevated pressures and large gaps an electron can produce numerous ionizing collisions even at not very high E/p. In this case, however, α depends sharply on E/p, and the condition of the necessary amplification (7.1) fixes the value of E/p rather rigidly.

On the other hand, the possibilities for collisions are very limited on the *left-hand branch* at low pd. A very high value of α/p, that is, a very strong field is required to achieve the necessary amplification. The breakdown voltage grows rapidly as pd decreases. Hence, the voltage has a minimum. The effective ionization cross section being limited, the ionization coefficient is also limited (by Ap). As a result, the necessary amplification cannot be obtained at sufficiently low pd, regardless of the field. In the framework of this approximation, as pd is reduced to its limiting value

$$(pd)_{lim} = A^{-1} \ln(1/\gamma + 1) = (pd)_{min}/\bar{e} , \tag{7.5}$$

$V_t \to \infty$. In fact, the growth of E_t/p and V_t on the left-hand branches of the Paschen curves is not as steep, nor does it tend to infinity. Very different mechanisms come into play "to the left" of the left-hand branches (Sect. 7.2.6).

7.2.5 Breakdown Fields in Moderately Large Gaps in Air and Other Electronegative Gases at Atmospheric Pressure. Limiting Values of *pd* for the Townsend Breakdown Mechanism

This mechanism is characterized by low pressure and not too large $pd(\lesssim$ 1000 Torr cm). If the gap is not too large (and the field is homogeneous), the mechanism of avalanche multiplication is predominant at atmospheric pressure. In room-temperature air in plane gaps, it is realized roughly for $d < 5$ cm ($pd < 4000$ Torr·cm). At such high pd, the breakdown voltage is more or less proportional to pd, that is, it is only slightly dependent on pd; more or less definite values of breakdown voltage or $(E/p)_t$ are characteristic for atmospheric-pressure gases. Figure 7.4 plots the results of measurements in room-temperature air in the range of d where the Townsend mechanism still acts. The typical figure for centimetres-wide gaps is $(E/p)_t \approx 32$ kV/(cm·atm)= 42 V/(cm·Torr). In large gaps (tens of centimetres wide), the breakdown field in room-temperature air reduces to a limit, $E_t \approx 26$ kV/cm. In general, the spark mechanism sets in if $d > 6$ cm (Chap. 12).

The limiting values of threshold fields, $E \approx 32 - 26$ kV/cm, observed at sufficiently high pd, are not accidental. They are clearly related to the possibility of electron multiplication in a gas with *attachment* of electrons. The *attachment coefficient* a, defined by analogy to the ionization coefficient α (Sect. 4.4.2), is

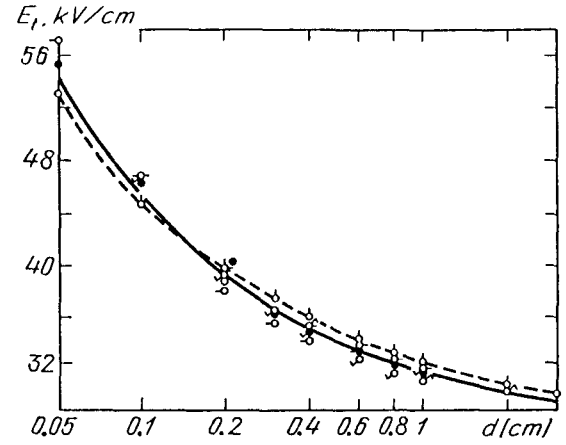

Fig. 7.4. Breakdown fields in a plane gap of length d in air at $p = 1$ atm. From [7.1]

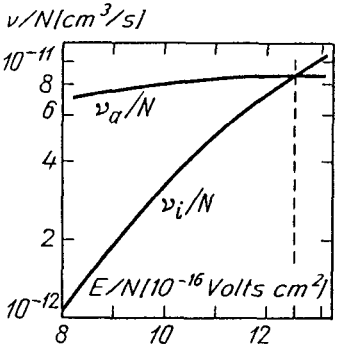

Fig. 7.5. Ionization and attachment frequencies in air, calculated using the solution of the kinetic equation. Intersection at $E/p = 41$ V/cm·Torr

also known to grow appreciably with E/p but much slower than α. The curves of α/p and a/p as functions of E/p intersect at a certain value $(E/p)_1$. Figure 7.5 shows the results of calculation of the coefficients using the kinetic equation; these calculations are similar to that described in Sect. 5.8 (cf. similar plots in Figs. 8.18 and 8.19 in Chap. 8 for laser mixtures with an electronegative component, CO_2). The intersection point lies at $(E/p)_1 \approx 41$ V/(cm·Torr). This figure is close to the limit for the breakdown potential of air; in fact, it is somewhat exagerated, perhaps because of the imperfect data, used in the evaluation, on cross sections of a number of processes. The avalanche equation (4.4) with the effective ionization coefficient $\alpha_{\text{eff}} = \alpha - a$ is

$$dN_e/dx = (\alpha - a)N_e\ ,\quad N_e \propto \exp(\alpha - a)x\ ;$$

the measurements of α_{eff} show that $\alpha_{\text{eff}} \to 0$ at $(E/p)_1 \approx 35$ V/(cm·Torr), in good agreement with $(E/p)_{\text{lim}} \approx 26$ kV/(cm·atm). If $E/p < (E/p)_1$, the multiplication of electrons is obviously impossible; this fact affects the limits of breakdown.

Measurements show that breakdown thresholds in strongly electronegative halogen-containing gases at atmospheric pressure are very high. This is shown in Table 7.1, which also gives the data for gases manifesting no attachment. At low

Table 7.1. Approximate values of breakdown threshold at high pressure

Gas	Constant field, gap width less than several cm, $p \sim 1$ atm		Microwaves, $p \sim 100$–300 Torr
	E/p kV/(cm·atm)	E/p V/(cm·Torr)	E/p V/(cm·Torr)
He	10	13	3
Ne	1.4	1.9	3–5
Ar	2.7	3.6	5–10
H_2	20	26	10–15
N_2	35	46	$\sim$ 25
O_2	30	40	35
Air	32	42	$\sim$ 30
Cl_2	76	100	
$CCl_2F_2^*$	76	100	
CSF_8	150	200	
CCl_4	180	230	
SF_6	89	117	

* Freon

pressure (small pd), the values of $(E/p)_t$ are much greater than $(E/p)_1$ (Fig. 7.4), and α is appreciably greater than a, so that the electronegative properties of gases are not manifested as clearly as at high pd. The high electric strength of electronegative gases has important practical applications.

7.2.6 Breakdown of Vacuum Gaps

If $pd < 10^{-3}$ Torr·cm, an electron crosses the gap practically without collisions, so that there is no multiplication in the volume. This does not mean, however, that a vacuum gap can be an ideal insulator (Figs. 7.6). If high voltage is applied to a narrow gap, a high field is generated, capable of causing field emission from the cathode (Sect. 4.6.3). The field is additionally enhanced in the vicinity of microscopic protrusions. Breakdown occurs in wider gaps at fields insufficient for ejecting an electron from the metal. A spurious electron is accelerated in the field, knocks an ion from the anode, or emits a bremsstrahlung photon. The ion or the photon knock out, in turn, an electron from the cathode, etc. This multiplication proceeds without the residual gas. A process is also possible in which electrodes are sputtered by the particles accelerated in the field, so that the gap gets filled with metal vapor in which gas enhancement then occurs.

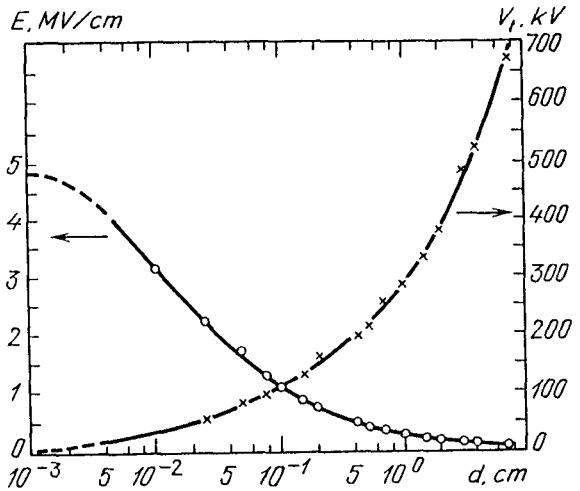

Fig. 7.6. Breakdown voltage and field in the vacuum gap between a steel sphere 2.5 cm in diameter and a steel disk 5 cm in diameter as functions of gap width [7.4]

7.3 Breakdown in Microwave Fields and Interpretation of Experimental Data Using the Elementary Theory

For the time being, let us postpone the case of *radio frequency* fields, since they are more complex and diversified. The *microwave* range is characterized by a small amplitude of electron vibration compared with the size of the discharge volume (which is comparable with the wavelength $\lambda \sim 1$–10 cm, see a numerical example at the end of Sect. 3.1.2). As a result, the evolution of an electron avalanche is localized and almost independent everywhere, the field does not push particles towards the walls, and the emission of the walls is insignificant. The process is of bulk nature and relatively simple. It has been studied quite thoroughly both experimentally and theoretically in [7.2, 5].

7.3.1 Measurements

When the breakdown threshold is measured experimentally, the controlled power of a cw or pulsed magnetron is fed to a *resonator cavity* through a waveguide. The threshold field of a given frequency f depends on the size of discharge volume. This effect is caused by the diffusion leakage of electrons to the walls. On the other hand, the resonator size is related to λ, that is, $f = c/\lambda$. As a result, not just any geometry allows changes of cavity size at unaltered frequency. Actually, such changes are necessary to establish the dependence of the threshold field on size, other conditions being equal. This difficulty can be avoided by using a cylindrical resonator excited at such a *mode* that the resonance frequency is a function of cylinder radius but is independent of its height (Fig. 7.7). The diffusion length Λ (Sect. 4.5) can be varied by changing the cylinder height at unaltered radius and field frequency. Increasing the field by bringing up the power fed into the

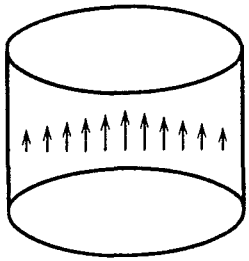

Fig. 7.7. Electric field distribution in the resonator of an experimental device for measuring microwave breakdown thresholds

cavity, one fixes the parameters at which the transmitted power drops abruptly. This is a sign of breakdown followed by the dissipation of electromagnetic energy in the plasma. The breakdown occurs first of all at the central part of the cavity, where the field amplitude is maximal; this field is assumed to be the threshold.

The threshold field (root-mean-square value E_t in Fig. 7.8) as a function of pressure always has a minimum. On the left-hand branch, the threshold decreases with increasing pressure. This threshold is the lower, the greater the discharge volume and the lower the field frequency. The same is true for the minimum value. The minimum at lower frequencies lies at lower pressures. On the right-hand branch, where the threshold increases with increasing pressure, the depen-

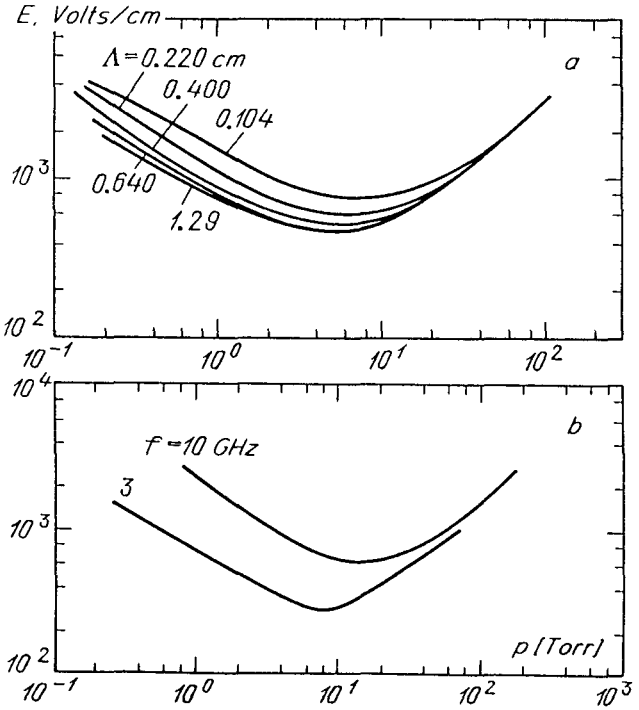

Fig. 7.8. Measured thresholds of microwave breakdown [7.6] (a) air, f = 9.4 GHz, diffusion length Λ is indicated for each curve; (b) Heg gas (He with an admixture of Hg vapor), Λ = 0.6 cm

dence of E_1 on size and frequency becomes less and less pronounced, and almost vanishes in the limit of high pressures: all curves asymptotically merge.

The point of interest is the unusual facility of breakdown in mixtures of helium and neon with a small admixture of argon. The reason is the Penning effect (Sect. 4.2.2); owing to it, electron energy loss to the excitation of He and Ne impedes only slightly, or not at all, the progress of an avalanche. The excited He* and Ne* atoms ionize Ar atoms. The rate of this two-stage process is proportional to the densities of the main and admixture gases, so that the effect is better pronounced at higher pressures. Ionization in the so-called Heg gas (a mixture of He with some mercury) occurs similarly. The cross section of ionization of Hg by metastable He* atoms is anomalously high (Sect. 4.2.2). It can be said that each event of He excitation immediately produces a new electron. The frequency of ionization of a gas mixture by electrons, ν_i, then coincides with the excitation frequency of the main gas atoms (He). Inelastic losses are as if absent. One can thus resort to the *elementary theory* and understand quite a few of the essential features of breakdown without addressing the *kinetic equation*. Qualitatively, they still hold with inelastic losses present.

7.3.2 Ionization Kinetics Equation

When oscillation displacements are small, electron densities obey an equation of type (2.44):

$$\partial n_e/\partial t = D_\nabla^2 n_e + (\nu_i - \nu_a) n_e \ , \quad D \equiv D_e \tag{7.6}$$

(electrons diffuse freely in breakdown). If the condition $\omega \gg \nu_m \delta$ (Sect. 5.5.2) holds (it is satisfied for microwave frequencies), the electron energy distribution is quasisteady and the ionization and attachment frequencies, ν_i and ν_a, are determined by the root-mean-square field E. The dependencies $\nu_i(E)$, $\nu_a(E)$ are much stronger than $D_e(E)$, so that $D_e(E) \approx$ const. For simplification, assume that the field is spatially homogeneous, and hence, ν_i and ν_a are independent of coordinates. Averaging (7.6) over the volume, we obtain, in accord with the results of Sect. 4.5, an equation for the mean density, or (which is equivalent) for the total number of electrons, N_e, in the discharge volume:

$$dN_e/dt = (\nu_i - \nu_a - \nu_d) N_e \ , \quad \nu_d = D/\Lambda^2 \ , \tag{7.7}$$

where ν_d is the frequency of diffusion losses of electrons. This equation describes the ionization kinetics of the gas.

7.3.3 Steady-State Background Criterion

Assume that the external field is switched on in a time small in comparison with the characteristic time of multiplication and remains constant during the avalanche buildup. This constraint covers not only stationary, but also pulsed fields with not too short pulses and sufficiently small rise time. Under this as-

sumption, $\nu_i(t)$, $\nu_a(t)$ = const after the moment $t = 0$ at which the field is switched on, and (7.7) has an exponential solution typical of an avalanche process:

$$N_e = N_{e0} \exp[(\nu_i - \nu_a - \nu_d)] = N_{e0} \exp(t/\Theta) , \tag{7.8}$$

where Θ is the *avalanche time constant,* and N_{e0} is the number of seed electrons that start the avalanche.[1] Breakdown is impeded in experiments with short pulses, since the probability of an electron appearing in the region of the field at the necessary moment is quite low and the avalanche has to be initiated by injecting a small number of electrons. For this purpose, a weak radioactive source is used.

According to (7.8), an avalanche develops if $\nu_i - \nu_a - \nu_d > 0$; this condition is met if the field exceeds a threshold E_t determined by the *steady-state breakdown criterion*:

$$\nu_i(E_t) = \nu_d + \nu_a(E_t) . \tag{7.9}$$

As an example, consider breakdown in helium, for $p = 1$ Torr, $\lambda = 3$ cm, diffusion length $\Lambda = 1$ cm, $D = 2 \cdot 10^6$ cm^2/s, time of diffusion to the walls $\nu_d^{-1} \approx 5 \cdot 10^{-7}$ s, diffusion frequency $\nu_d \approx 2 \cdot 10^6$ s^{-1}, and no attachment. The avalanche develops if $\nu_i > \nu_d \approx 2 \cdot 10^6$ s^{-1}. We will show a little later that the ionization frequency $\nu_i \propto E^2$ under the most favorable conditions for multiplication (zero electron energy losses). If losses, especially inelastic, are nonzero, the ν_i vs. E curve is much steeper. Hence, if the field increases by 10% in comparison with E_t, then $\Theta^{-1} = \nu_i - \nu_d \geq 0.2\nu_d \approx 4 \cdot 10^5$ s^{-1}. The number of electrons is doubled every $\Theta/\ln 2 \leq 1.7\,\mu$s, which is a very high rate. In many cases, it is sufficient for a reliable realization of breakdown. As a result, stationary criterion (7.9) determines with good accuracy [like criterion (7.1)] the breakdown threshold of gases for "not too short" pulses.

7.3.4 Low Pressure

Let us evaluate threshold fields for the Heg gas. At low pressure the diffusion coefficient $D \propto 1/p$ is high and electron diffusion losses are substantial. The losses can be compensated for if the ionization rate is large, that is, if the field is strong. Recall that the role of elastic energy losses in high fields is negligible. Indeed, electron energies ε are not greater than a quantity of the order of the helium excitation energy $E^*_{He} = 19.8$ eV, because at $\varepsilon > E^*_{He}$ an electron enters an inelastic collision with high probability and dissipates energy. The elastic-collision energy transfer to an atom is limited by the quantity $(\Delta\varepsilon_{el})_{max} = (2m/M)E^*_{He}$. Formula (3.10) shows that the energy $\Delta\varepsilon_E$ gained in a collision is proportional to E^2. In sufficiently strong fields necessary to balance out high diffusion losses, an electron gains energy from the field at a rate $d\varepsilon/dt = \Delta\varepsilon_E \nu_m$, where ν_m is defined

[1] The rate of generation of electrons in the atmosphere by cosmic rays at sea level is on the order of 10 cm^{-3}s^{-1}. Usually about 10–10^2 electrons per cm^3 are present in non-electronegative gases. In air, they immediately attach to oxygen, so that charges exist as ions; their density is on the order of 10^3 cm^{-3}.

as in Chap. 2. The energy E^*_{He} is reached over a time $\tau_E = (E^*_{He}/\Delta\varepsilon_E)\nu_m^{-1}$. The ionization frequency is determined simply by τ_E because excitation and Penning ionization follow immediately:

$$\nu_i = \tau_E^{-1} = (\Delta\varepsilon_E/E^*_{He})\nu_m = e^2E^2\nu_m/m\omega^2E^*_{He} . \tag{7.10}$$

We have taken into account here that at low pressure, $\nu_m^2 \ll \omega^2$. As implied by (7.9), the root-mean-square breakdown field is

$$E_i = \left(\frac{Dm\omega^2E^*_{He}}{e^2\nu_m\Lambda^2}\right)^{1/2} = \left(\frac{mE^*_{He}}{3}\right)^{1/2}\frac{\omega}{e\sigma_m N\Lambda} \propto \frac{\omega}{p\Lambda} . \tag{7.11}$$

This calculation operates with the expressions for the diffusion coefficient, $D = lv/3 = l^2\nu_m/3$,and the mean-free-path length, $l = 1/N\sigma_m$, of electrons. The threshold field is proportional to frequency and inversely proportional to gas density (pressure) and to discharge volume size; this is in complete agreement with experiments. Moreover, if the collision cross section $\sigma_m = 4 \cdot 10^{-16}\,cm^{-2}$, corresponding to the midpoint of the electron spectrum, $\varepsilon \approx E^*_{He}/2 \approx 10\,eV$, is substituted into the formula, a satisfactory fit with Fig. 7.8 is obtained. Formula (7.11) gives a correct description of the asymptotic lines on the logarithmic plot which the left-hand branches of the function $E_i(p)$ tends to for different values of ω and Λ.

7.3.5 High Pressure

In this case the diffusion losses of electrons are negligible, and breakdown occurs even at not very high ionization rate. The most important factor now is the energy dissipation, and specifically, purely elastic losses in the Heg gas. These losses limit the ionization frequency. In terms of elementary theory, an electron cannot gain more energy than the limit (3.12) imposed by electronic losses. In the case of high pressures, when $\nu_m^2 \gg \omega^2$, we have

$$\varepsilon_{max} = (M/2m)e^2E^2/m\nu_m^2 \propto (E/p)^2 . \tag{7.12}$$

If this energy is less than E^*_{He}, electrons cannot excite helium atoms and no avalanche can develop. Hence, the possibility of breakdown is determined by the condition $\varepsilon_{max}(E) \geq E^*_{He}$; the breakdown field E_i calculated by this equality is

$$E_i = (m\nu_m/e)(2E^*_{He}/M)^{1/2} \propto p . \tag{7.13}$$

The breakdown field is proportional to p and is independent of both the volume size Λ (in the framework of the approximation chosen here; see Sect. 7.3.8) and the frequency; this is also found to be in qualitative agreement with experiments. The quantitative fit for the Heg gas is also satisfactory. The threshold is frequency-independent because if $\omega^2 \ll \nu_m^2$, the effect of an oscillating field on electrons is indistinguishable from that of a constant field.

7.3.6 The Position of the Minimum

Under a crude approximation, the position of the minimum on the threshold curve $E_t(p)$ can be found using the condition that separates to some extent the limiting cases of low and high pressure, that is, of $\nu_m^2 \ll \omega^2$ and $\nu_m^2 \gg \omega^2$. This condition states that the collision and field frequencies are of the same order of magnitude: $\nu_m \sim \omega$. At this value of ν_m, $d\varepsilon/dt$ as a function of p has a maximum [see (3.11)]. The frequency at the minimum of threshold field is proportional to pressure. This result is qualitatively supported by experimental data. The breakdown of gases by microwave fields is easiest at $p \sim 1$–10 Torr.

7.3.7 Inelastic Losses; Molecular and Electronegative Gases

Inelastic losses are important in most gases; they affect threshold fields in almost the same qualitative manner that elastic losses do. This is demonstrated even by the perfect apparent similarity of $E_t(p)$ curves in Heg and other gases. At low pressure, the threshold field is determined mostly by diffusion. Threshold fields are high, so that electrons gaining energy rush rapidly thruogh the "danger zone" of energies between the excitation and ionization potentials. As a result the probability of energy loss due to atomic excitations is not too high. The threshold field is then given by a formula of type (7.10) in which E_{He}^* must be replaced with the ionization potential.

Diffusion at high pressure being slow, the threshold is mostly determined by energy losses. The rate of both inelastic and elastic energy losses is proportional to pressure. The condition of balancing of energy losses by energy gained from the field implies that if $\omega^2 \ll \nu_m^2$, the mean electron energy as a function of E/p [see (3.12)]. For ionization to proceed, the mean energy cannot be too small compared with the ionization potential; this fact somewhat fixes the ratio E/p. Hence, the threshold field $E_t \propto p$; if $\omega^2 \ll \nu_m^2$, it is independent of ω. In the framework of the approximation chosen here, it is also independent of Λ, as it is in the case of purely elastic loss.

Molecular gases undergo breakdown at higher fields than atomic gases because an electron spends much of its energy on the excitation of vibrational and lower electronic levels of molecules; the rate of energy buildup is thereby slowed down. Thresholds in electronegative gases are also high because of additionial electron losses to attachment.

7.3.8 Similarity of Threshold Values of E/p in Constant and Oscillating Fields at High Pressure and Their Independence of Size

If the effect of oscillating fields on electrons at high pressure is nearly the same as that of constant fields, and if the threshold values of E_t/p in the microwave range are almost independent of p and Λ, there is every reason to expect that the values of E_t/p are close to those for constant field and high pd (where they are also almost independent of pd). On the whole, experiments bear out this conclusion. The right-hand branches of microwave breakdown correspond to the

right-hand branches of Paschen curves far from the minima. The E_i/p values differ by a factor of 1.5–2 (Table 7.1).

It must be emphasized (this is important for understanding the process) that the independence of E_i/p of the diffusion length Λ in (7.13) is a result solely of the elementary theory. The absence of Λ in the formula is equivalent to neglecting electron losses: $\Lambda = \infty$, $\nu_d = 0$. In fact, ionization, even if very weak, takes place in any (no matter how weak) field because the spectrum always contains some energetic electrons. Therefore, the breakdown would have zero threshold if electrons suffered absolutely no losses. The number of electrons with energies $\varepsilon \approx I$ sufficient for ionization is exponentially small: it is mainly proportional to $\exp(-\varepsilon/\varepsilon_0)$ in the case of the Maxwell distribution, and to $\exp(-\varepsilon^2/\varepsilon_0^2)$ in the case of Druyvesteyn's distribution. The scales ε_0 approximately coincide with the mean energies of the spectra or with ε_{max} of the elementary theory, and increase with increasing field. As a result, the real ionization frequency is a characteristic exponential function of E, of type $\exp[-\text{const}/f(E/p)]$.

As an example, take Townsend's law $\nu_i \sim p \exp(-\text{const} \cdot p/E)$. The results of Sect. 7.4.7, where the kinetic equation was solved approximately, imply that this law is not far from the thruth. The breakdown condition $\nu_i = \nu_d$ yields

$$E_i/p = \frac{\text{const}}{\text{const}' + \ln(p\Lambda)} . \tag{7.14}$$

This logarithmic dependence (weak for large $p\Lambda$) is quite similar to the dependence on pd in (7.3); formally, it ensures that the threshold vanishes as $\Lambda, d \to \infty$.

The lengths Λ and d play essentially identical qualitative roles, characterizing the rate of removal of electrons from the discharge volume. The field pulls an electron out over a time from 0 to d/v_d, depending on where the motion started. The inverse, v_d/d, is the scale of the "removal" frequency (loss frequency). The Townsend criterion (7.1), $\alpha d = k$, where k lies between one and ten, and $\alpha = \nu_i/v_d$, can be interpreted, by analogy to (7.9) for $\nu_a = 0$, as the condition of equality of the ionization and loss frequencies: $\nu_i = kv_d/d = \nu_d'$. The mean removal frequency ν_d' is greater than the minimum value v_d/d by a factor of k, because the majority of electrons in an avalanche are created close to the anode.

7.4 Calculation of Ionization Frequencies and Breakdown Thresholds Using the Kinetic Equation

7.4.1 Derivation of the Equation of Ionization Kinetics from the Kinetic Equation

Using (5.24–26), one can recast the kinetic equation for the electron energy distribution function $n(\varepsilon, t)$ in the following convenient form for analysis:

$$\frac{\partial n}{\partial t} = -\frac{\partial J}{\partial \varepsilon} + Q^* + Q_i - \nu_a(\varepsilon)n - \nu_d(\varepsilon)n ,$$

$$J = -A\varepsilon\frac{\partial n}{\partial \varepsilon} + \frac{A}{2}n + nV_{\mathrm{el}} , \tag{7.15}$$

$$A = \frac{2}{3}\frac{e^2E^2\nu_{\mathrm{m}}}{\omega^2+\nu_{\mathrm{m}}^2} , \quad V_{\mathrm{el}} = -\frac{2m}{M}\varepsilon\nu_{\mathrm{m}} .$$

The flux J along the energy axis reflects energy gains from the field and elastic losses. The term Q^* describes the excitation of atoms, Q_{i} represents ionization, attachment is given by $\nu_{\mathrm{a}}(\varepsilon)n$, and diffusion losses by $\nu_{\mathrm{d}}(\varepsilon)n$.

As a result of inevitable excitation and ionization events at energies above the corresponding potentials, electrons cannot reach very high energies. As $\varepsilon \to \infty$, the distribution function falls off very rapidly. The flux also vanishes: $J(\infty) = 0$. Particle sources in equation (7.15) are distributed along the ε axis. There are no electron sources with zero energy, and negative kinetic energy is impossible. Hence, $J(0) = 0$. If we turn to an analogy with one-dimensional diffusion of particles in ordinary space, $x \equiv \varepsilon$, the situation is found to correspond to an impenetrable and nonemitting wall at $x = 0$.

In view of this, we integrate (7.15) over the entire spectrum from 0 to ∞. The integral of Q^* vanishes automatically, since excitation events do not change the number of electrons. Integration in ε of the first term in formula (5.26) for Q_{i} yields $-\nu_{\mathrm{i}}n_{\mathrm{e}}$, where ν_{i} is the ionization frequency averaged over the spectrum. The second term gives $2\nu_{\mathrm{i}}n_{\mathrm{e}}$; this is readily verified if the order of integration in the double integral is reversed. It is as if one electron disappears in each ionization event, while two new ones appear. This gives the equation of kinetics for electron density,

$$dn_{\mathrm{e}}/dt = (\nu_{\mathrm{i}} - \nu_{\mathrm{a}} - \nu_{\mathrm{d}})n_{\mathrm{e}} , \tag{7.16}$$

equivalent to (7.7); ν_{a} and ν_{d} are also frequencies averaged over the spectrum.

7.4.2 Separation of Variables

Strictly speaking, the initial electron distribution function $n(\varepsilon, 0)$ must be specified as the initial condition to (7.15). It is physically clear, however, that the initial spectrum is forgotten after one or two new generations of electrons are generated, and a new spectrum forms, corresponding to the effects of the field and collisions. Indeed, the build-up (relaxation) time of the spectrum is characterized by the mean time during which an electron covers the entire path along the ε axis from $\varepsilon \approx 0$ to the highest realizable energies. In fact, this is the time necessary for ionization and multiplication. If the point of interest is any well-developed stage of the avalanche, there is no sense in going into details of the relaxation process; rather, one should directly search for the stationary spectrum, that is, seek the solution of the nonstationary equation in the form $n(\varepsilon, t) = n(\varepsilon)\Phi(t)$.

The substitution into (7.15) gives

$$n(\varepsilon, t) = n(\varepsilon)\exp(t/\Theta) , \tag{7.17}$$

where the separation constant Θ has the meaning of the time constant of the avalanche, and the spectral function $n(\varepsilon)$ is normalized to the initial density n_e^0. A solution of type (7.17) would always be exact if the spectrum of initial electrons coincided with the one that is established by the end. According to (7.16, 17), the constant Θ is related to spectrum-averaged frequencies by an obvious equality

$$\Theta^{-1} = \nu_i - \nu_a - \nu_d \,. \tag{7.18}$$

7.4.3 Equation for the Spectral Function

We now substitute (7.17) into (7.15) and replace Θ via (7.18). The diffusive removal of electrons to the walls was taken into account in (7.15) in an approximate manner, in order not to add complications to the already complex dependence of the distribution function on spatial coordinates. It would hardly be advisable, therefore, to retain the rather weak and largely unimportant dependence of the spatial diffusion coefficient and ν_d on energy. Let us replace $\nu_d(\varepsilon)$ in (7.15) with the mean value of ν_d. Then, if (7.17, 18) are substituted into (7.15), the diffusive loss term vanishes completely from the equation for the spectral function $n(\varepsilon)$, so that the equation takes the form

$$(\nu_i - \nu_a)n = -dJ/d\varepsilon + Q^* + Q_i - \nu_a(\varepsilon)n \,. \tag{7.19}$$

In this approximation, the spectrum and frequency of ionization are independent of geometry and volume size, and do not differ from those that would be obtained for infinite space and homogeneous field. This is the standard procedure in solving the kinetic equation.

The solution of (7.19) gives the spectrum $n(\varepsilon)$ and ionization frequency ν_i as functions of field and gas characteristics. The rate of multiplication (or removal) of electrons as a function of field and diffusive loss is defined by (7.18). The condition $\Theta^{-1} = 0$ corresponds to the steady state and the steady-state breakdown criterion (7.9). If this condition is imposed on the solution, one can find the threshold field E_t. In fact, the dependence $\nu_i(E)$ obtained in this way has a more general significance. It can be employed for studying some other processes, such as the positive column of a glow discharge (however, one should bear in mind that if ionization is strong, diffusion is *ambipolar* and ν_d is considerably smaller).

7.4.4 Similarity Laws

As we have mentioned in Sect. 5.6.3 and as (7.15) and (7.19) directly demonstrate, the stationary spectrum in the low-frequency limit $\omega^2 \ll \nu_m^2$ (and in constant field) is described by a function $n(\varepsilon, E/p)$, and in the high-frequency limit $\omega^2 \gg \nu_m^2$, by $n(\varepsilon, E/\omega)$. Correspondingly, the ionization frequency is a function of the type $\nu_i = pf_1(E/p)$ in the former case, and $\nu_i = pf_2(E/\omega)$ in the latter case. If the collision frequency is assumed to be constant, $\nu_m(\varepsilon) = \text{const}$, the ionization frequency in an oscillating field, $\nu_{i\omega}$, is expressed in terms of the ionization frequency at constant ν_{i0} by introducing an effective field E_{eff} using (5.33):

$$\nu_{i\omega}(\omega, p, E) = \nu_{i0}(p, E_{eff}) = pf_1(E_{eff}/p) \,. \tag{7.20}$$

In a gas without attachment, we make use of the stationary breakdown criterion (7.9) and of the dependence $\nu_d \propto 1/p\Lambda^2$, and find that the threshold field in the low-pressure (high frequency) limit is $E_t = \omega F_1(p\Lambda)$, and in the high-pressure (low frequency) limit is $E_t = pF_2(p\Lambda)$. The asymptotic form of the functions F_1 and F_2 is given by (7.11), (7.14), or (7.3). Similarity laws for the attachment frequency are the same as for the ionization frequency. Therefore, the breakdown value of E/p in electronegative gases, with attachment dominating diffusion at high pressures, is constant.

7.4.5 Formulation of a Simplified Problem of the Effect of Inelastic Losses on Ionization Frequency

If the complexity of (7.19) is not ignored, only numerical solutions are possible. Cumbersome and time-consuming computations of this type became feasible only with the advent of computers. Numerical solutions do supply information valuable for practical work, but an *analytic* solution, even if crude, is frequently a greater help in understanding the nature and identifying the mechanisms which are important. In view of this, we will construct a simplified solution that clearly demonstrates the effect of inelastic losses on the ionization rate, which is beyond the reach of the elementary theory.

Let us consider heavy inert gases (argon, xenon) which manifest no attachment, have no low energy levels, and where the role of elastic losses is negligible. Assume that the frequency ν_m of elastic collisionss is constant. Assume also that the atomic excitation frequency ν^* is equally energy-independent if the energy exceeds the level E_1^* that is slightly higher than the excitation potential. Next, assume that electrons gaining energy I_1 a little higher than the ionization potential enter in inelastic colision instantaneously, ionizing an atom with a probability β or exciting it with a probability $1-\beta$. The quantities E_1^*, I_1, ν^*, β can be adjusted in a reasonable way after an analysis of cross section curves $\sigma^*(\varepsilon)$ and $\sigma_i(\varepsilon)$. In inert gases, E_1^* and I_1 are 1 to 2 eV higher than the corresponding potentials E and I; $\beta \approx 0.2$.

The assumption of *instantaneous* inelastic collisions at $\varepsilon > I_1$ (which is by no means too crude, because the corresponding frequencies are high) makes it possible to *exclude* the region $\varepsilon > I_1$ from consideration, after replacing the effect of negative sources $Q^* + Q_i$ in this region by an adequate *boundary condition*. Electrons moving along the energy axis then have an infinite capacity sink at the point $\varepsilon = I_1$, so that $n(I_1) = 0$ at this point. In a simple model we "collect" the real positive sources $Q^* + Q_i$ located in the low-energy region and assign them to the point $\varepsilon = 0$. Now the flux $J(0)$ is *nonzero*. It is connected with the flux $J(I_1)$ or ionization frequency, which equals, by definition

$$\nu_i = \beta J(I_1) / \int_0^{I_1} n(\varepsilon) d\varepsilon \,. \tag{7.21}$$

Indeed, $J(I_1)\,\mathrm{cm}^{-3}\mathrm{s}^{-1}$ electrons reach the sink at $\varepsilon = I_1$. They immediately enter into ionizing and exciting inelastic collisions, so that $2\beta J(I_1) + (1-\beta)J(I_1)$

electrons with "zero" energy are created. In addition, electrons that produce excitations in the $E_1^* < \varepsilon < I_1$ zone also emerge with "zero" energy. Therefore,

$$J(0) = (1+\beta)J(I_1) + \nu^* \int_{E_1^*}^{I_1} n(\varepsilon)d\varepsilon \ \mathrm{cm^{-3}s^{-1}} \ . \tag{7.22}$$

This is the second boundary condition. The terms for elastic collisions, attachment, ionization, and distributed sources in the region $0 < \varepsilon < E_1^*$ are dropped from (7.19), which takes the form

$$\begin{aligned} \nu_i n &= -dJ/d\varepsilon \qquad && 0 < \varepsilon < E_1^* \ , \\ \nu_i n &= -dJ/d\varepsilon - \nu^* n \qquad && E_1^* < \varepsilon < I_1 \ , \\ J &= A\varepsilon\, dn/d\varepsilon + An/2 \ , && A = 2e^2E^2\nu_m/3m(\omega^2+\nu_m^2) \ . \end{aligned} \tag{7.23}$$

It is not difficult to verify by integrating (7.23) in ε from 0 to I_1 that only one of relations (7.21), (7.22) is independent. The other is implied by the result of integration.

7.4.6 Results Obtained from the Model

Equations (7.23) may be integrated for functions of type $\exp(\pm\mathrm{const}\sqrt{\varepsilon})$. When the general solution is subject to the boundary conditions $n(I_1) = 0$ and (7.22) and to the continuity of n and J at the boundary between the regions, $\varepsilon = E_1^*$, the outcome is a rather unwieldy transcendental equation for the ionization frequency $\nu_i(E)$ [7.7]. It is successfully solved, however, in two limiting cases; the resulting expressions have a very lucid physical meaning that greatly clarifies the nature of the process.

Let us refer to the quantity

$$\nu_E = \tau_E^{-1} = \frac{1}{I_1}\left(\frac{d\varepsilon}{dt}\right)_E = \frac{e^2E^2\nu_m}{m(\omega^2+\nu_m^2)I_1} = \frac{3}{2}\frac{A}{I_1} \tag{7.24}$$

as the *energy gaining frequency*. A slow electron would need a time $\tau_E = \nu_E^{-1}$ for gaining, in the absence of energy losses, the energy I_1 required for ionizing an atom. The inequality $\nu^* \ll \nu_E$ corresponds to a low probability of inelastic losses in the course of accumulating the ionization energy. In this limiting case, we find $\nu_i \approx \beta\nu_E \propto E^2$. An electron crosses the "dangerous" stretch $E_1^* < \varepsilon < I_1$, where its motion along the ε axis toward the energy I_1 may be impeded, and then produces ionization with a probability β. Multiplication takes a time $\tau_i = \nu_i^{-1} \approx \beta^{-1}\tau_E$, as expected.

In the opposite case of high inelastic loss, $\nu^* \gg \nu_E$,

$$\nu_i \approx a^2\beta\xi\nu_E \ , \quad \xi = \frac{J(I_1)}{J(E_1^*)} \approx 2a\exp\left[-\frac{a-1}{a}\left(\frac{6\nu^*}{\nu_E}\right)^{1/2}\right] \ , \tag{7.25}$$

where $a = (I_1/E_1^*)^{1/2}$ is a number, equal to approximately 1.2 for all inert gases. The factor $\xi \ll 1$ is the ratio of fluxes at the end and beginning of the dangerous

zone; it is the probability for an electron to cross this zone without dissipating energy on the excitation of an atom. On the average, an electron goes through the almost complete cycle of accumulating energy ξ^{-1} times, dissipating it each time "uselessly" on excitation before the barrier of inelastic loss is broken and the electron accomplishes ionization with the specified probability β. The time necessary for multiplication, up to an unimportant factor a^2 of order unity, is $\tau_i = \nu_i^{-1} \approx \tau_E/\beta\xi$. Of course, the result (7.25) is significant not because it states this equally obvious fact, but because it leads to the calculation of the probability ξ. Note that the expression for ξ can be transformed to a form typical for a stochastic process [(7.15) implies that the motion of electrons along the energy axis is indeed stochastic [7.7]].

In the general case, the transcendental equation for ν_i has to be solved numerically. However, this need be done only once, by using similarity laws, because most gases have nearly equal values of a and β (Fig. 7.9). In the figure, $a = 1.2$, $\beta = 0.2$. The situation when $\beta = 1$, useful for some cases of optical breakdown, is also represented (Sect. 7.5).

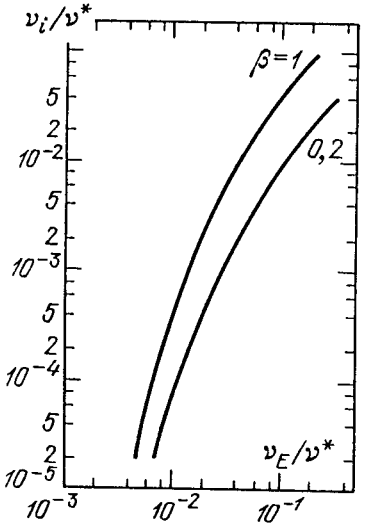

Fig. 7.9. Universal dimensionless function for calculating the ionization frequency as a function of the energy increase frequency which is proportional to E^2 [7.7.]

7.4.7 Comparison of Calculated Ionization Frequencies and Breakdown Thresholds with Experimental Data

Let us compare the theoretical formula (7.25) with the available experimental data on α in view of the relation of Townsend's ionization coefficient α for constant field to ionization frequency and drift velocity, $\alpha = \nu_i/v_d = \nu_i m\nu_m/eE$. Assuming $\omega = 0$ and factoring out pressure via formulae $\nu_m^* = \nu_{m1}p$, $\nu^* = \nu_1^* p$, using (7.25), we find the ionization coefficient:

$$\frac{\alpha}{p} = A_1 \frac{E}{p} \exp(-B_1 p/E) ,$$

$$A_1 = \frac{e}{I_1} 2a^3\beta = \frac{2a^3\beta}{I_1[\mathrm{eV}]} \approx \frac{0.68}{I_1[\mathrm{eV}]} V^{-1}., \tag{7.26}$$

$$B_1 = \frac{a-1}{a} \left(\frac{6 I_1 m \nu_{m1} \nu_1^*}{e^2} \right)^{1/2} \approx 1 \cdot 10^{-8} \sqrt{I_1[\mathrm{eV}] \nu_{m1} \nu_1^*}$$

$$\mathrm{V \cdot cm^{-1} Torr^{-1}} .$$

Formulas (7.25, 26), describing the case of strong inelastic losses, correspond to E/p being only 5–20 $\mathrm{V \cdot cm^{-1} Torr^{-1}}$. Although the exponential factor in (7.26) has the form identical to that in Townsend's formula (4.5), the constant B_1 differs essentially from the data of Table 4.1, which are valid for high values of E/p(> 100). Moreover, the meaning of B_1, connected first of all with the excitation cross section, has nothing in common with the semi-quantitative interpretation given to Townsend's constant B (Sect. 4.1.5).

If the experimental curve of α for argon in the range of $E/p \approx$ 5–20 is approximated by (7.26) (Sects. 4.2.6), we obtain $B_1 = 31$, $A_1 = 0.01$. For argon, $I_1 = I + 1 = 16.8\,\mathrm{eV}$, $\nu_m = 7 \cdot 10^9 \cdot p[\mathrm{Torr}]\,\mathrm{s^{-1}}$, $\nu^* \approx 2.6 \cdot 10^8 p[\mathrm{Torr}]\,\mathrm{s^{-1}}$, which gives $B_1 = 53$ and $A_1 = 0.04$. This agreement between a very simplified theory and experimental data should be regarded as satisfactory, especially in view of the fact that no "adjustment" parameters were used in the calculation. The agreement for xenon is even better. Choosing from the cross section data the values $I_1 = 13.1\,\mathrm{eV}$, $\nu_m = 1.5 \cdot 10^{10} p\,\mathrm{s^{-1}}$, $\nu^* = 4 \cdot 10^8 p\,\mathrm{s^{-1}}$, we find $B_1 = 85$ and $A_1 = 0.05$. The approximation of the experimental α curve gives $B_1 = 85$, $A_1 = 0.1$.

Figure 7.10 compares the calculated and measured microwave breakdown thresholds of argon and xenon. The calculations were based on the theory presented above of ionization frequency and the stationary criterion $\nu_i = \nu_d$. In the high-pressure range, at the ends of the right-hand branches, $\nu_m^2 \gg \omega^2$, $E/p \sim 10\,\mathrm{V \cdot cm^{-1} Torr^{-1}}$. Here, the asymptotic formula (7.25) is valid. The calculation fits the experimental data quite well. The description of the minimum region, where Fig. 7.9 has to be employed, is also good. Discrepancies are greater at low pressures, where inelastic losses are small and another asymptotic formula holds: $\nu_i = \beta \nu_E$. However, at $p < 10^{-1}\,\mathrm{Torr}$ the free path length of electrons reaches the diffusion length (the cavity size), so that the theory of diffusion losses becomes invalid and collisions of electrons with walls become significant when they move in a transverse direction to the applied field; hence, good agreement cannot be expected here.

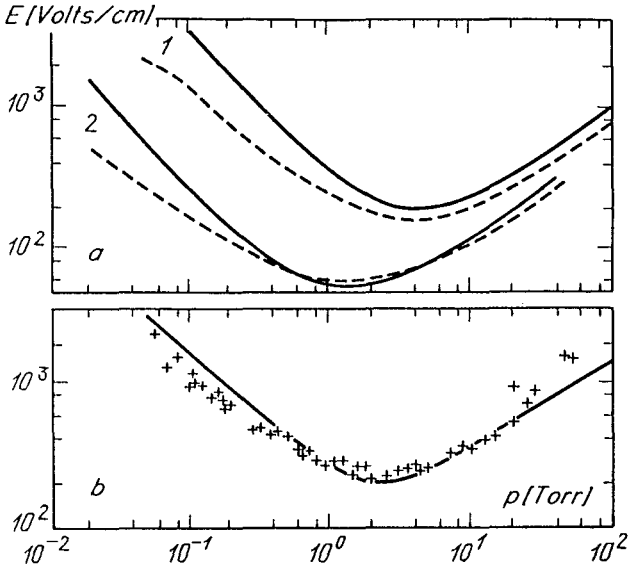

Fig. 7.10. Thresholds of microwave breakdown: (a) Ar, *(1)* f = 2.8 GHz, Λ = 0.15 cm; *(2)* f = 0.99 GHz, Λ = 0.63 cm; (b) Xe, f = 2.8 GHz, Λ = 0.10 cm. *Solid curves*, results of calculations [7.7]; *dashed curves* and *crosses* give experimental data [7.5]

7.5 Optical Breakdown

The discovery of the *optical breakdown* effect, in 1963 [7.8], became possible only after the development of Q-switched lasers that produce light pulses of tremendous power, called "giant pulses". When the light of such a (ruby) laser was passed through a focusing lens, a spark flashed in the air, in the focal region, as in the electrical breakdown of a discharge gap. The discovery was a complete surprise for physicists and produced a sensation at the time, though the element of surprise has worn off by now. Gas breakdown at optical frequencies requires a tremendous field strength, 10^6–10^7 V/cm, in the light wave; this was unthinkable before the advent of the laser. Furthermore, the necessary light intensity, about 10^5 MW/cm^2, could only be reached by focusing the light of not just an ordinary laser, but one operating in th giant pulse regime. The new effect caused unparalleled interest among physicists. In a short time, it was experimentally and theoretically investigated to such a degree [7.7], that by now we know at least as much about it as about its closest analogue, the microwave field breakdown.

7.5.1 Experimental Arrangement

The arrangement of the pioneer experiments on measuring optical breakdown thresholds [7.9] is typical for much later work. Giant pulses of a ruby laser with the following parameters were employed: power output 1 J, pulse length 30 ns= $3 \cdot 10^{-8}$ s, the maximum (peak) power 30 MW= $3 \cdot 10^{14}$ erg/s. These

parameters are typical for modern moderate-power systems.[2] The pulse energy was measured by a calorimeter. The pulse shape was roughly triangular, the rise time being shorter than the decay time.

In order to increase the radiation flux density, the light beam is focused. The diameter of the focal spot d is determined by the divergence angle of the original light beam, θ, and the focal length f of the lens, $d = f\theta$. (Normally, $\theta \sim 10^{-3} - 10^{-2}$ rad, $f \sim 3$–10 cm.) *Meyerand* and *Haught* [7.9] had $d \approx 2 \cdot 10^{-2}$ cm. The spot diameter was measured by the size of the hole burnt in very thin gold foil ($0.05\,\mu$ thick). At the peak power of 30 MW, the radiant power density at the focal spot was $S \approx 10^5\,\mathrm{MW/cm^2} = 10^{18}\,\mathrm{erg/(cm^2 s)}$, the rms electric field in the light wave was

$$E = \sqrt{4\pi S/c} = 19\sqrt{S[\mathrm{W/cm^2}]}\,\mathrm{V/cm} \approx 6 \cdot 10^6\,\mathrm{V/cm}\,,$$

and the photon flux density of the ruby laser, $\hbar\omega = 1.78$ eV, was

$$F = 3.4 \cdot 10^{18} S[\mathrm{W/cm^2}]\,\mathrm{cm^{-2}s^{-1}} \approx 3.4 \cdot 10^{29}\,\mathrm{cm^{-2}s^{-1}}\,.$$

The light beam was focused into a chamber filled with a gas to be investigated, at various pressures. The breakdown was deduced from the appearance of a visible light flash (lasting about $50\,\mu$s). Moreover, the focal spot was placed between a pair of electrodes to which a voltage of ≈ 100 V was applied. About 10^{13} electron charges were extracted by this field from the focal region when breakdown occurred.[3] The radiant powe was varied by an attenuator in order to determine the breakdown threshold, which was found to be very abrupt.

7.5.2 Results of Experiments

The threshold field decreases monotonically as the pressure increases (Fig. 7.11). However, this is observed only in a limited range of pressure. When a wider range from several atm. to two thousand atm. was scanned [7.10] it was found that the threshold has a minimum, as in the case of microwave breakdown. In this case the minima are not at 1–10 Torr, but at hundreds of atmospheres (Fig. 7.12). An interesting fact is that the position of the minimum approximately satisfies the same relation $\nu_m \approx \omega$ (Sect. 7.3.6). For example, for an Ar and ruby laser, $\omega = 2.7 \cdot 10^{15}\,\mathrm{s^{-1}}$, this formula gives $p \approx 225$ atm., while experiments give 190 atm.; for He, $p \approx 1450$ atm., while experiments give 700 atm. The rason for a minimum is the same as in the microwave field: the rate of energy accumulation by an electron in the field of a given frequency is maximal at $\nu_m \approx \omega$ (ν as a function of p).

---

[2] Solid state lasers have been developed recently that produce thousands of megawatts for several nanoseconds.

[3] Breakdown also reduces the power of the radiation that passes through the focal spot because the resulting plasma absorbs some radiation.

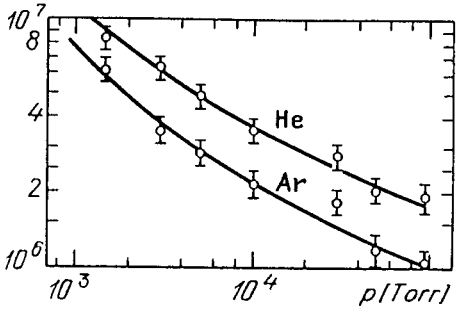

Fig. 7.11. Measured threshold fields for the breakdown of Ar and He by ruby laser radiation; pulse length 30 ns, diameter of focal spot $2 \cdot 10^{-2}$ cm [7.9]

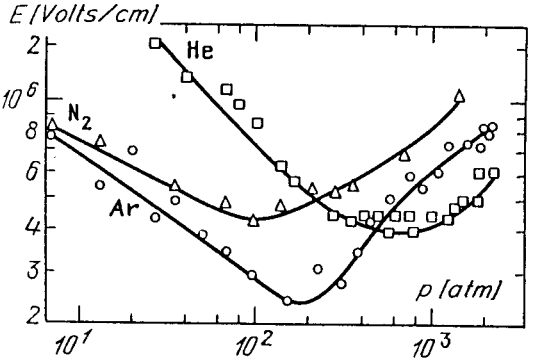

Fig. 7.12. Breakdown thresholds in Ar, He, N_2 for ruby laser radiation over a wide pressure range [7.10]. Pulse length 50 ns, focal spot diameter 10^{-2} cm

When the radiation from a pulsed CO_2 gas laser is focused into a gas, breakdown is also observed. This radiation ($\lambda = 10.6\mu \approx 10^{-3}$ cm) occupies an intermediate position between that emitted by ruby and neodymium lasers ($\lambda \sim 10^{-4}$ cm) and that of microwave radiation ($\lambda \sim 1$ cm), although it is closer to the visible part of the spectrum. As a rule, CO_2 lasers give longer pulses, of about 1 μs. The relation $\nu_m \approx \omega$ for the position of the maximum holds quite well (Fig. 7.13). For example, in Xe $\nu_m \approx 9 \cdot 10^{12} p$ [atm.] s^{-1}; $\omega_{CO_2} = 1.78 \cdot 10^{14}\ s^{-1}$. We find $p \approx 20$ atm., while experiments give about 15 atm.

The breakdown threshold decreases when the focal spot, that is, the size of the region subjected to the field, is increased. Measurements were conducted in the range of diameters from 10^{-2} to 10^{-1} cm, by using lenses with different focal lengths ($d = f \cdot \theta$). This result is qualitatively fairly clear: the greater the region where the field is high, the lower the importance of the loss of electrons due to their diffusive escape from this region. In fact, the situation is more complicated. Estimates show that in some cases the pulse length is too short for an electron to diffuse across the distance d. The effect may be caused by the diffusion, not from the entire focal spot, but from the "hot" points with high local fields that appear in the focal spot as a result of cross-sectional inhomogeneity of the laser beam. The electron avalanche mostly develops at these points.

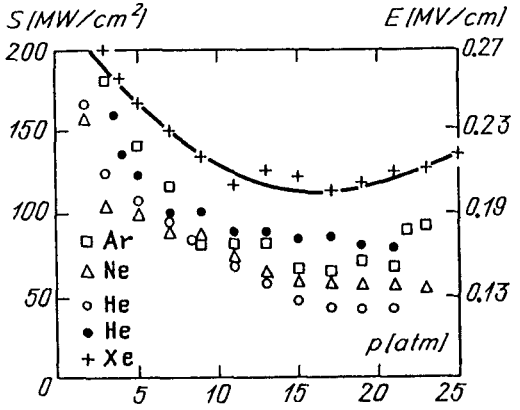

Fig. 7.13. Breakdown thresholds of inert gases in the radiation of a CO_2 laser [7.7]. The *black dots* represent data for helium of a higher purity

7.5.3 Breakdown Thresholds of Atmospheric Air

These data are very important. Quite a few physical experiments employ high-intensity laser beams. Electrical breakdown of air on the beam path to the target is an obstacle for light propagation because of absorption in the plasma. For example, in such experiments with high-power beams as target irradiation for fusion experiments one has to send the beam to the target through vacuum. The threshold intensity for the giant pulse of a ruby laser and an ordinary focal spot diameter of 10^{-2} cm is $S_t \approx 10^{11}$ W/cm^2, and the field is $E_t \approx 6 \cdot 10^6$ V/cm.

The breakdown threshold of nonfiltered air by focused CO_2 laser radiation is roughtly $2 \cdot 10^9$ W/cm^2, and that of dust-free air is not lower than 10^{10} W/cm^2. The tiniest dust particles floating in the air greatly facilitate the breakdown by CO_2 laser radiation, while their effect is negligible for the neodymium and, in particular, ruby lasers. This difference appears because the short-wave radiation of solidstate lasers "supplies itself" with the seed electrons required for starting an avalanche. The long-wave radiation of CO_2 lasers cannot do this in a pure gas.

7.5.4 Multiphoton Photoelectric Effect

Two quite different mechanisms of gas ionization by high-intensity light can be proposed. The first one, the development of an *electron avalanche,* is essentially the same as in fields of other frequencies. The differences are in the detailes the process of energy-gain in the field, which is essentially quantum in nature.

The second mechanism of ionization is characteristic of photons: it has a purely quantum nature. Electrons may be detached from atoms as a result of the *multiphoton photoelectric effect,* that is, in response to the simultaneous absorption of several photons. In the visible light range, the single-photon photoelectric effect is impossible, because atomic ionization potentials are several times greater than the quantum energy. For instance, the ruby laser photon energy is $\hbar\omega = 1.78$ eV, while the argon ionization potential is $I_{Ar} = 15.8$ eV, that is, nine photons are required to detach an electron. Multiphoton processes usually have

a low probability, but the process rate increases sharply when the photon density (the light intensity) increases; at the extremely high intensities that result in optical breakdown, the probability may become substantial.

Both calculations (see below) and experiments show that nanosecond (and longer) laser pulses at pressures above several tenths of one atmosphere always produce *avalanche ionization*. The rate of avalanche ionization is sufficient for breakdown at fields that are insufficient for intensive multi-photon ionization. However, the latter plays an important role as a source of the initial, seed electrons required to ignite the avalanche. The arrival of a spurious electron at a small focal region during a very short pulse is a highly improbable event.

We have mentioned several times that the excitation of atoms by electron impact slows down the avalanche because an electron dissipates its energy and has to accumulate it again and again before it manages to overcome the excitation zone and reach the ionization potential. This process characterizes all fields except that of light. If the photon energy is high, a small number of quanta may be sufficient to eject an electron from an excited atom by the multi-quantum photoelectric effect. In this case excitation even accelerates the growth of the avalanche because it is enough for electrons to reach the excitation, not ionization, potential.

For example, in argon $I_{Ar} = 15.8\,\text{eV}$ and the potential of the first excitation level $E^*_{Ar} = 11.5\,\text{eV}$. The energy necessary to detach an electron from an excited atom is $4.3\,\text{eV}$, that is, what is required is the simultaneous absorption of three photons of a ruby laser or four photons of a neodymium laser ($\hbar\omega = 1.17\,\text{eV}$). A four-photon process has very low probability, but a three-photon process may occur under certain conditions at the ruby laser frequency. There exists both experimental and theoretical evidence supporting the reality of this mechanism.

7.5.5 Nonstationary Breakdown Criterion

If light pulses are very short (as in our case), the field prescribed by the stationary criterion (7.9) may prove insufficient for appreciable ionization of the gas. Indeed, the situation cannot be classified as a breakdown if only two to three generations of electrons are produced during one pulse. Ionization must reach a substantial level. In fact, one typically associates breakdown with a visible light flash. Thus the experments described above recorded that a flash and the breakdown correspond to about 10^{13} avalanche electrons. Assuming an avalanche to be started by a single electron, we find that $\log_2 10^{13} \approx 43$ generations are created by breakdown during one pulse. The field must be so strong that the avalanche time constant Θ be $\ln 10^{13} \approx 30$ times shorter than the pulse duration $t_1 \approx 3 \cdot 10^{-8}\,\text{s} : \Theta \approx 1\,\text{ns}$.

The threshold field E_t is found from the condition that an avalanche initiated by N_0 electrons multiplies during the time t_1 to N_1 electrons:

$$t_1/\Theta(E_t) = (\nu_i - \nu_a - \nu_d)t_1 = \ln(N_1/N_0)\,. \tag{7.27}$$

E_t is insensitive to the rather uncertain quantity N_1/N_0 (due to the logarithmic relationship). For calculations, one can use $t_1/\Theta \approx 30$. The nonstationary criterion (7.27) generalizes the stationary criterion (7.9) and tends to it as $t_1 \to \infty$. If the pulses are very short, the threshold is found to be very high and electron losses become unimportant: $\nu_a, \nu_d \ll \nu_i$. The nonstationary criterion makes the threshold nature of the breakdown even more pronounced. If the ionization frequency ν_i is reduced by half (this requires only a slight field reduction), only 21 generations are produced instead of 43, that is, the number of electrons decreases by 6 to 7 orders of magnitude.

7.5.6 Classical or Quantum Picture?

We all remember from school lessons that light is emitted and absorbed as discrete quanta. Radiation and matter cannot exchange energy if $\Delta\varepsilon < \hbar\omega$: this is forbidden. The classical description of the interaction between electromagnetic waves and electrons is valid if $\Delta\varepsilon \gg \hbar\omega$ in each elementary event. Otherwise quantum theory must be used. It is easy to verify via (3.10) that in microwave fields the mean energy gained by an electron from the field in a collision with an atom $\Delta\varepsilon_E \gg \hbar\omega$. The true amounts of energy, $\Delta\varepsilon_\pm$, exchanged by an electron and the field in individual collisions (Sect. 3.2.5) exceed $\hbar\omega$ by even more. There are no doubts as to the applicability of the classical theory that we have worked with so far. However, for optical frequencies, even at tremendous breakdown fields ($E \sim 10^7$ V/cm), (3.10) gives $\Delta\varepsilon_E \sim 10^{-2}\,\text{eV} \ll \hbar\omega \sim 1\,\text{eV}$. The true increments $\Delta\varepsilon_\pm$ are also smaller than $\hbar\omega$, or at least comparable to $\hbar\omega$. This means that the interaction of light radiation with the electrons of an ionized gas is of a quantum nature.

The interaction proceeds as follows. An electron colliding with an atom may absorb a quantum (photon), $\hbar\omega$, or produce stimulated emission of a photon $\hbar\omega$, provided its energy is sufficiently high.[4] All these events are random, so that the changes in the energy of the electron are of the random walk type (one-dimensional diffusion), by $\hbar\omega$ jumps along the energy axis ε. However, on average the energy of the electron increases with time, just as a particle diffusing away from an impenetrable wall is on the average receding (cf. Sect. 3.2.5). This goes on until the energy reaches the ionization potential and the electron produces a new electron, as in any other field. This is how an avalanche evolves.

It can be shown, in the calculation of $d\varepsilon/dt$ as a difference between the mean rates of quantum absorption and stimulated emission of radiation, that the quantum-mechanical expression reduces to the classical formula (3.11) under the condition $\hbar\omega \ll \varepsilon$, which is much less severe than the classical-physics condition $\hbar\omega \ll \Delta\varepsilon$ [7.7, 11]. The resulting light absorption coefficient, determined by the difference between the rates of absorption and stimulated emission of photons under the same condition $\hbar\omega \ll \varepsilon$, is reduced to the classical coefficient μ_ω

[4] In the field of high-intensity laser radiation, spontaneous emission takes place much less frequently than stimulated emission, so that the former can be ignored.

(3.28). Under the same condition, the quantum kinetic equation scrutinized in [7.7] transforms into the classical (5.24).

These arguments do not mean that our understanding of the relationship between the classical and quantum approaches to the interaction has changed. Actually, when (3.11) is applied to the quantum case, it must be given a statistical meaning. For instance, if this formula gives $\Delta\varepsilon_E = 0.01\hbar\omega$ but $\hbar\omega \ll \varepsilon$, this means that an electron did not interact with radiation at all in, say, 99 collisions but in the 100th collision it suddenly gained $\hbar\omega$ in one portion, 100 times that of the symbolic averaged value $\Delta\varepsilon_E$.

7.5.7 Calculation of Threshold Fields

When evaluating whether the condition $\hbar\omega \ll \varepsilon$ is satisfied, one obviously has to compare $\hbar\omega$ with the mean energy of the electron spectrum; under breakdown conditions, the latter equals about one half of the ionization potential, that is, $\bar{\varepsilon} \sim 8$–13 eV in Ar and He. Hence, the condition is very well satisfied in the case of the CO_2 laser ($\hbar\omega = 0.117$ eV), is only passably met for the radiation of the neodymium laser ($\hbar\omega = 1.17$ eV), and can be considered to be satisfied for the ruby laser radiation, with a number of qualifications. Consequently, one can use the theory presented in Sect. 7.4 and the non-stationary criterion (7.27). In the case of ruby laser radiation, a plausible assumption is that of the fast *three-photon ionization of excited atoms*. The breakdown process is then regardes as similar to that in the Heg gas: inelastic losses are absent and $\beta = 1$. With neodymium and, of course, CO_2 lasers, inelastic losses are important. The CO_2 laser breakdown obeys the stationary criterion (7.9). Experimental data fit the calculated curves quite satisfactorily (Figs. 7.14, 15). We conclude that breakdown processes in the optical and microwave ranges are very similar.

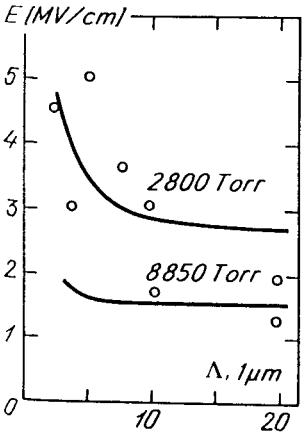

Fig. 7.14. Threshold fields in Ar calculated on the assumption that excited atoms are ionized instantaneously by the incident ruby laser radiation [7.7]. The *circles* are the experimental results obtained using a single-mode laser

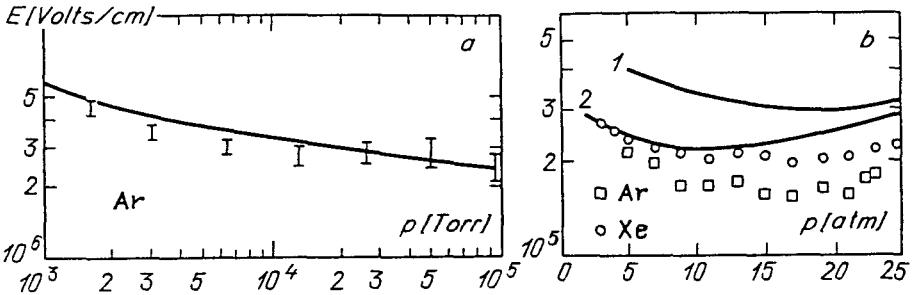

Fig. 7.15. Calculation of breakdown thresholds [7.7]: (a) Ar with neodymium laser, experimental data are shown by *error bars*, $\Lambda = 1.64 \cdot 10^{-3}$ cm; (b) Ar, Xe with CO_2 laser; *circles* and *squares* show experimental data; focal spot radius $4 \cdot 10^{-3}$ cm, pulse length 1 μs

7.5.8 A Bridge Between Microwave and Light Ranges

The experimental observation that the classical similarity law $E_t^2 \sim S_t \propto \omega^2$ holds for threshold values in a wide range of optical frequencies right down to the microwave range is an especially conclusive confirmation of the last statement in the preceding subsection. In the microwave range, the law $S_t \propto \omega^2$ holds only at low pressure ($p < 10$ Torr), corresponding to the left-hand branch of the threshold curves. To generalize, we have to assume that $S_t \propto (\omega^2 + \nu_m^2)$. As for the optical frequency range, here even tens of atmospheres is a low pressure; for example, the entire plot in Fig. 7.11 represents the left-hand curve.

Figure 7.16 shows the curve $S_t \propto (\omega^2 + \nu_m^2)$, which on a logarithmic scale degenerates into a straight line if $\nu_m^2 \ll \omega^2$; experimental pints for air are also shown. In addition to numerous data on the breakdown of atmospheric air by the radiation of ruby, neodymium, and CO_2 lasers [7.7, 11], data for D_2O [7.12] ($\lambda = 385$, $\mu = 0.38$ mm, the last "mastered" range), HF, and DF [7.13] ($\lambda = 2.7\mu$, 3.8μ) lasers were reported recently. Note that the points group well around the theoretical straight line, although the law cannot be expected to hold strictly since different experiments were conducted in nonidentical conditions. Note also that

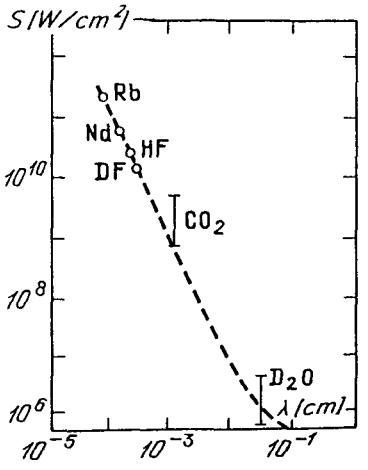

Fig. 7.16. Breakdown thresholds of air for radiation of different lasers. *Dashed curve* shows the classical dependence

the D_2O point lies at the limit of the range where the condition $\omega^2 \gg \nu_m^2$ is satisfied: $\omega = 4.9 \cdot 10^{12}\,s^{-1}$, $\nu_m \approx 3.8 \cdot 10^{12}\,s^{-1}$.

The law $S_t \propto \omega^2$ is obviously violated in the middle of the visible and UV ranges of the spectrum, for secondharmonics of the neodymium ($\hbar\omega = 2.34\,eV$) and especially ruby ($\hbar\omega = 3.56\,eV$) lasers, where quantum effects become important [7.7].

7.5.9 Long Spark

When the suprathreshold power is moderate, optical breakdown is obtained by focusing the laser beam with a short-focus lens. If a laser is very powerful, however, the intensity is sufficient for the breakdown on a long path along the caustic of a long-focus lens. The result is a very impressive optical breakdown: "long spark". A record length of spark – more than 60 meters – was produced in 1976 [7.14] using a neodymium laser pulse of 160 Joules power output, 5 GW mean power and a lens of $f = 40\,m$. The beam was directed out of the laboratory window into the courtyard outside. Long sparks are not continuous: ionized stretches alternate with nonionized gaps (Fig. 7.17). This may be connected with the statistical behavior of seed electrons and also with the space-time and angular inhomogeneity of the beam. A long spark is also obtainable with CO_2 lasers, at intensities of $1–2 \cdot 10^8\,W/cm^2$; the threshold increases to $3 \cdot 10^9\,W/cm^2$ in dust-free air. Long laser sparks are effective in initiating the breakdown in wide gaps between electrodes. The threshold field of breakdown by dc voltage is then reduced to 250 V/cm. In fact, the breakdown is considerably facilitated by the joint action of the laser radiation and microwave or constant field. In this way one can produce a directed or even zigzag breakdown channel between electrodes (some relevant details and references can be found in the review [7.11]).

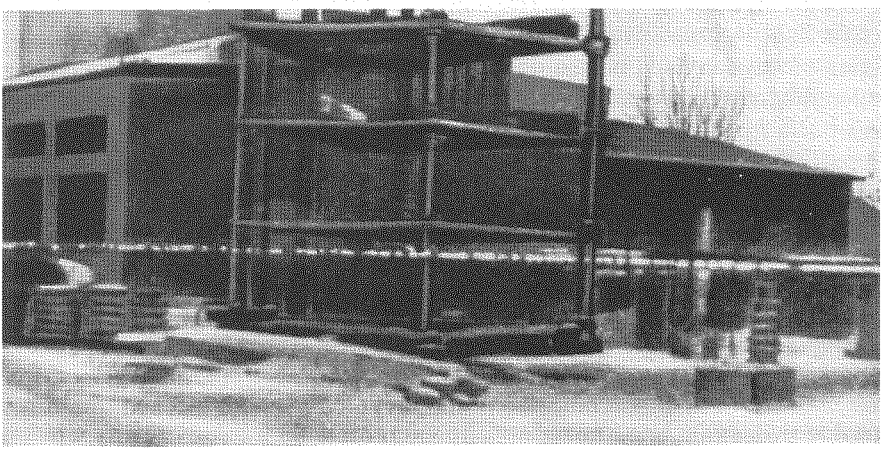

Fig. 7.17. Photograph of a long spark obtained by neodymium laser. Spark length 8 m, focal length of the lens 10 m [7.14]

7.6 Methods of Exciting an RF Field in a Discharge Volume

These methods are classified into two main groups depending on whether the lines of force of the electric field in the discharge plasma reconnect or not, in other words, whether this is a *vortex* (rotational) or a *potential* field. The first group comprises *induction* methods based on using electromagnetic induction.

A typical – and most frequent – approach to implementing this principle is as follows (Fig. 7.18). A high-frequency current is passed through a solenoid "coil" (in fact, the coil may consist of only one or several turns). The oscillating magnetic field of this current within the coil is directed along its axis and induces a vortex electric field, whose lines of force are closed circles concentric with the turns of the coil. This electric field can ignite and sustain a discharge, its currents also being closed and flowing along the closed circular lines of force of the electric field. In actual experiments, a dielectric tube filled with a gas to be studied is inserted into the coil so that breakdown occurs under certain conditions and the discharge can be sustained after breakdown. Pulsed discharges can be produced if a sufficiently strong current pulse is fed into the coil. This type of discharge is known as the inductively coupled, or H-type, rf discharge, with the latter H pointing to the decisive role of the magnetic field. Inductively coupled discharges are apparently *electrodeless*.

In the methods belonging to the second group, the high-frequency (or any other waveform) voltage is applied to the electrodes. In the simplest (and the most widespread) geometry, two parallel plane electrodes are employed. The electrodes may be *bare* and be in direct contact with the discharge plasma, or they may be *insulated* by a dielectric (Fig. 7.18b,c). A system of two electrodes behaves with respect to a variable voltage as a capacitor, so that in contrast to iniduction discharges, those in this category are known as *capacitively coupled*, or E-type, rf discharges (ccrf). The letter E symbolizes the decisive role of the electric field. A capacitively coupled discharge can be ignited in a tube via a pair of ring electrodes fixed on the outside surface at the ends of the tube, creating the longitudinal field. As a result, the discharge can be observed through the end faces.[5]

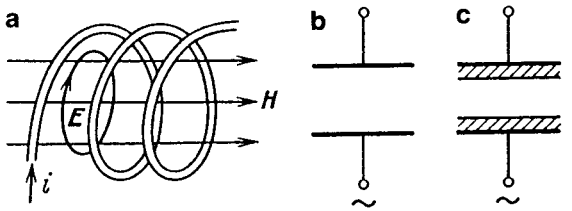

Fig. 7.18. Excitation of rf discharges: **(a)** inductively coupled through a solenoid coil; **(b)** voltage applied to electrodes in contact with plasma; **(c)** electrodes insulated from plasma (electrodeless, capacitively coupled rf discharge)

[5] The ccrf discharge may also arise in the case of inductive coupling, as a result of gas breakdown by voltage between turns.

The induction electric field increases with increasing frequency; it is proportional to frequency in the absence of plasma. Such fields are difficult to create at low frequencies since dangerously high currents have to flow through the inductor. As a result, the induction technique is typically used in the range of $f \sim 10^{-1} - 10^{2}$ MHz. Electrodeless capacitively coupled discharges also present a problem at low frequencies because an insulating dielectric layer has a high impedance, consuming most of the applied voltage. Electrodes used at frequencies $f \leq 10$ kHz are mostly bare. Actually, electrodes can be insulated with a thin layer of high dielectric constant (e.g., barium titanate) but this is not always practicable. As a rule, difficulties arise only if a voltage of many kV is to be applied to a discharge gap, that is, under conditions of wide gaps and high pressures. As for hundreds of volts or a kilovolt, serious problems are not encountered. Practical work in radio-frequency discharge is such that induction techniques are mostly used to sustain plasmas at high pressures about one atmosphere (Sect. 11.3), while capacitor techniques are preferable at medium and low pressures (Chap. 13).

As in the case of discharge analysis in a constant field, the electrode configuration may be arbitrary: two spheres, a sphere and a plane, a wire and a concentric cylinder, etc. In all these geometries, the field non-uniform and additional difficulties appear in the interpretation of results. Plane, parallel electrodes with a relatively narrow gap, that is, planar geometry, are easier and more convenient for experimental data processing, estimates, and theoretical evaluations.

7.7 Breakdown in RF and Low-Frequency Ranges

Many factors may drastically affect the characteristics of the process; these include frequency, pressure, method of introducing the field into the discharge volume, geometry and size of this volume, orientation of the electric vector.

The phenomena can be classified to some extent by comparing their characteristic lengths. Three such lengths are: volume size d, electron free path length l, and the oscillation amplitude of free electrons a, or of drift electrons A (Sect. 3.1.3). The choice between a and A is determined by which of the frequencies is higher: field frequency ω or electron collision frequency ν_m.[6] If pressures are so low that $l \gg d$, an electron suffers no collisions with the atoms of the gas. In typical cases, $d \sim 1$ cm and the upper boundary of such low pressure ($l \sim d$) in most gases is $p \sim 10^{-2}$ Torr. Let us very briefly consider several sets of conditions that produce more or less clearly pronounced effects.

[6] The field oscillation wavelength can be used to characterize frequency but few factors are indeed determined by it. At rf and lower frequencies, $\lambda > 1$ m, $\lambda \gg d \sim 1$ cm, that is, oscillations do not introduce additional spatial inhomogeneity in the field distribution.

7.7.1 Electron Oscillation Amplitude Is Small; Collisions Are Numerous

This is the case of $a, A \ll d, l \ll d$. It is realized at sufficiently high frequencies but not too low pressure, and differs but little from the microwave-field breakdown discussed earlier (Fig. 7.19).

The dependence of V_t on p at a fixed distance, that is, $E_t = V_t/d$ as a function of p, is very similar to Fig. 7.8 for microwaves. The interpretation is straight forward. The amplitude of drift oscillations at the ends of right-hand branches is $A = eE/m\nu_m\omega \approx 2.6 \cdot 10^{-3}$ cm $\ll d$ ($\omega = 10^9\,s^{-1}$; $E/p \approx 3$ V/cm·Torr; $\nu_m \approx 2 \cdot 10^9 p$[Torr] s^{-1} for such E/p). In the region of the minima ($E/p \approx$ 50–100, $\nu_m \approx 4 \cdot 10^9 p$), the amplitude is greater by an order of magnitude, $2.5 \cdot 10^{-2}$, but is nevertheless small in comparison with $d \approx 1$ cm. The positions of the minima fit rather well the earlier-mentioned relation $\nu_m \approx \omega$ that yields $(p)_{min} \approx 2.5$ Torr. At elevated pressures $p \approx 50$ Torr at the ends of right-hand branches, the threshold values are $E_t/p = 2.2$ V/cm for $d = 2$ cm and $E_t/p =$ 4.5 V/cm·Torr for $d = 0.5$ cm, being quite close to those in the microwave range and in constant field (Table 7.1). We are apparently trying to interpret a typical picture of bulk breakdown in which electrons are removed by diffusion.

Figure 7.19 shows plots of the sustaining voltages, measured in the same experiments, of the already ignited discharge. Ionization in the stationary discharge process, determined by the same frequency $\nu_i(E)$, also compensates for the diffusion loss of electrons but charge densities are now considerable and the diffusion, being ambipolar, proceeds much more slowly.[7]

7.7.2 Oscillation Amplitude Is Comparable with Volume Size; Collisions Are Frequent

This situation arises at lower frequencies. It has been known for quite some time that $V_t(p)$ curves similar to those of Fig. 7.19 sometimes display an additional minimum. Measurements plotted in Fig. 7.20 were carried out in a long (30 cm) cylindrical tube with outer electrodes (capacitively coupled rf discharge). With electrodes placed at the end faces (the field along the axis), the pattern was the same as in Fig. 7.19. The second minimum (right) observed on $V_t(p)$ curves at not too high frequencies was found only if the field was applied transversely to the tube. In this case the electron oscillation amplitude is comparable with the distance to the walls in the direction of charge motion, that is, with the tube diameter $d = 2$ cm.

[7] On the weaker field required to sustain a discharge (than to initiate the breakdown), see also Sect. 8.6.3.An example of this is a simple but extremely demonstrative experiment. If ever you have undergone uhf therapy (the field frequency is 40 MHz), you know how the nurse tests the normal functioning of the equipment. A tiny lamp probe (a low-pressure neon-filled bulb) is introduced into the field. If everything is in order, the lamp lights up in bright red. On bringing the probe slowly to an electrode or a lead wire, the lamp flares up. By moving, it slowly out of the field along the same route, the discharge shrinks and then dies out; this occurs quite far from the point of lighting up, in a considerably weaker field.

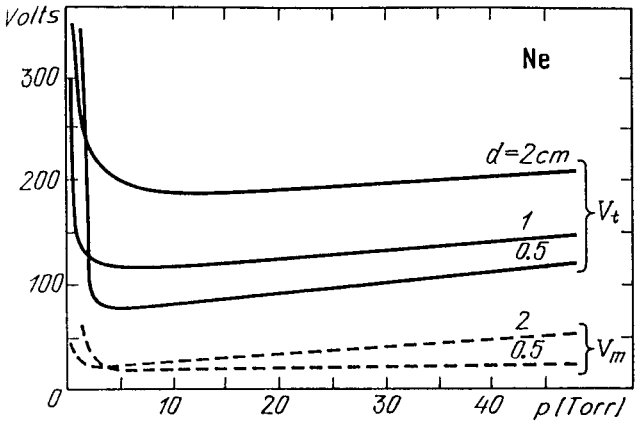

Fig. 7.19. Ignition potential of capacitively coupled rf discharge in neon (V_t), f = 158 MHz; d is the distance between the planar electrodes (which are covered by glass). *Dashed curves* show the burning voltage of a steady discharge, V_m [7.15]

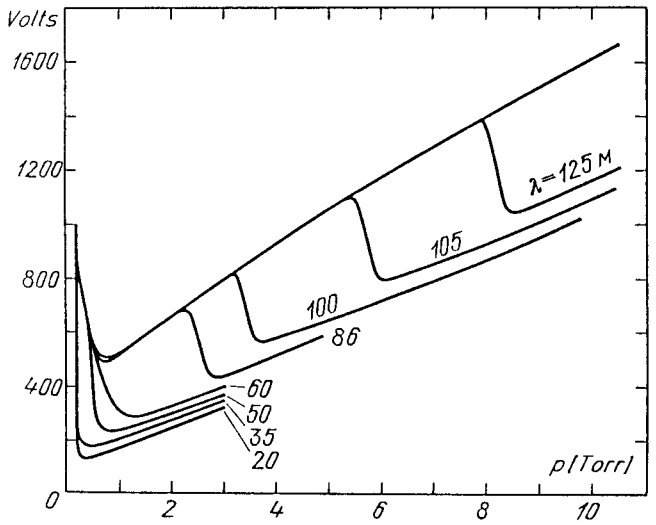

Fig. 7.20. Ignition potentials of ccrf discharge for various oscillation wavelengths [7.15]

Moving along the pressure scale from right to left, we first trace the ordinary right-hand branch, of the type shown in Fig. 7.19, corresponding to diffusion losses. As the pressure is reduced, the amplitude of the electron drift oscillations increases to $d/2$ so that electrons strike the walls on each swing. The loss is sharply increased because diffusion transports electrons to the wall at a slow rate. Discharge initiation requires a higher field; the breakdown potential increases. The positions of the jump and of the minimum are given by the obvious relation $A = eE_0/m\nu_m\omega \approx d/2$, whence $E_0/\omega \approx$ const. According to the data of Fig. 7.20, this relation is indeed valid. The numerical agreement is also satisfactory. For instance, at a frequency f = 3 MHz (λ = 100 m) we have

$\omega = 1.9 \cdot 10^7\ s^{-1}$, $E/p \approx 100$, $\nu_m \approx 4 \cdot 10^9 p$, $A \approx 1$ cm. To the left of the jump, we see the right-hand branch corresponding to enhanced losses. The main minimum (left) corresponds to the ordinary condition $\nu_m \approx \omega$; it is of the same nature as at higher frequencies (Sects. 7.3.6, 7.5.2). At sufficiently high frequencies, $A < d$ for any p, and the second minimum vanishes.

If the field frequency is reduced, with other conditions remaining unchanged, the field required for breakdown abruptly increases at a certain *boundary frequency*. This is observed when drift oscillations bring electrons to the walls. The threshold frequency satisfies the same approximate formula

$$\frac{2eE_0}{m\nu_m\omega d} \approx 0.14 \frac{(E_0/p)[\mathrm{V/cm \cdot Torr}]}{f[\mathrm{MHz}] \cdot d[\mathrm{cm}]} \approx 1\ , \tag{7.28}$$

where d is the distance between the opposite walls normal to the direction of the field, and E_0/p refers to the lower part of the jump. The frequency used in the numerical formula is $\nu_m \approx 4 \times 10^9 p$.

7.7.3 Wide Frequency Range, Including Low Frequencies; Collisions are Frequent

In hydrogen, the threshold field jumps at the boundary frequency are clearly pronounced (Fig. 7.21). This frequency agrees rather well with estimate (7.28). At frequencies below the boundary value, the threshold field is almost constant in a very wide frequency range, from 1 MHz to 50 Hz. This result is puzzling. Indeed, if a frequency is much lower than the boundary value, electrons are "herded" rather rapidly to one wall and kept there for a relatively long time, after which the field rushes them just as rapidly to the opposite wall, and so forth. Most of the time, there are no electrons in the discharge volume. If ionization stopped during these periods, breakdown would be appreciably impeded. It seems, therefore, that some other ionizing agent has not been identified in the volume. In neon, the threshold somewhat increases with λ over a wide range of frequencies (Fig. 7.22). It changes by a factor of 1.5–2 in response to a change in frequency by 3–5 orders of magnitude after a gentle "jump" at the boundary frequency (first rise on the left). Effects due to photons, excited atoms, photoemission from the walls, etc.

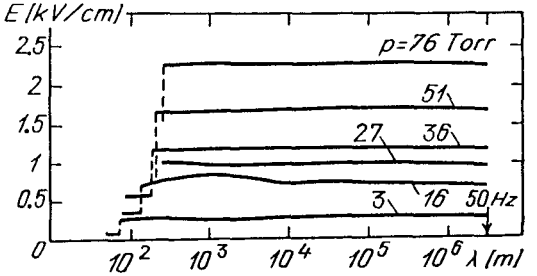

Fig. 7.21. Ignition field of ccrf discharge in hydrogen in a 2 cm long glass cylinder at different pressures over a wide range of frequencies [7.15]

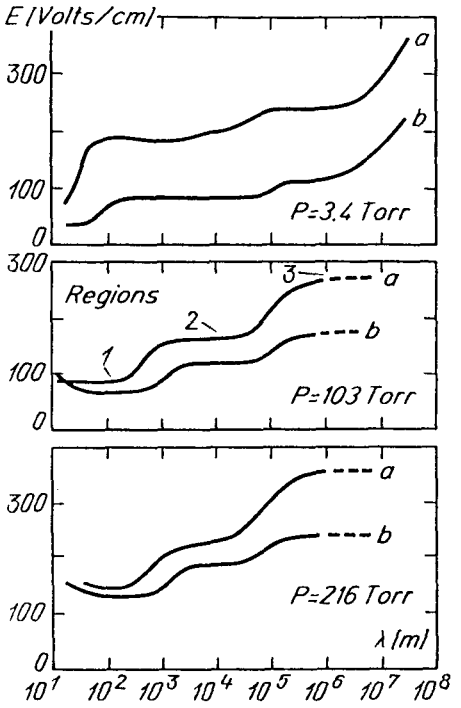

Fig. 7.22. Ignition field of ccrf discharge in neon in glass vessels *(a)* 1 cm in diameter and *(b)* 2.2 cm in diameter over a wide frequency range [7.15]

[7.15] are tentatively employed to explain these and a number of other, complex and tangled circumstances characterizing low-frequency discharges, but much remains to be done before clarity is achieved.

At low frequencies, of the order of 1 kHz and less, especially if electrodes are bare, breakdown develops anew in each half-period and evolves almost as in a constant field. In this respect, it is important that the rms threshold field in hydrogen at elevated pressure $p = 76$ Torr, $E_t/p \approx 20$ V/(cm·Torr), is quite close, according to the data of Fig. 7.21, to the corresponding value for the constant field (Table 7.1). In general, ignition potentials at elevated pressure depend on pd, by analogy to the right-hand branches of the Paschen curves, and assume similar values.

7.7.4 Breakdown of "Vacuum"

In the case of a highly rarefied gas, with electrons undergoing very few collisions ($l \gg d$), multiplication proceeds through secondary electron emission from the walls. Dielectric materials (glasses) produce quite strong emission capable of triggering breakdown in volumes insulated from electrodes. As a result, a discharge takes place in the residual gas in response to breakdown, a light flash appears, and a change in current is measured in the rf voltage generator. Nevertheless, breakdown occurs only at frequencies above the boundary value frequency f_b (Fig. 7.23).

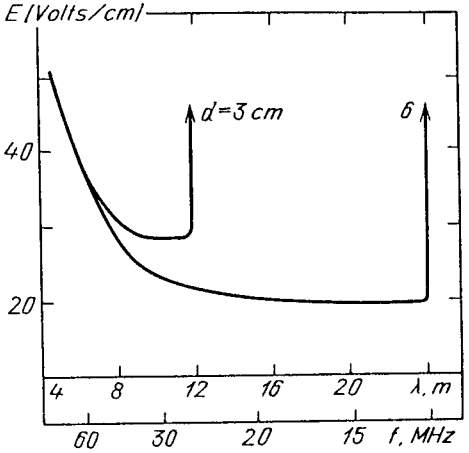

Fig. 7.23. High-frequency vacuum breakdown. Discharge ignition field in glass tubes of length d. The field is parallel to the axis: Hydrogen, $p = 10^{-3}$ Torr [7.15]

This can be explained [7.16]. For multiplication to occur, the energy of the incoming electron, ε, must suffice to detach more than one electron per projectile electron which penetrates the body and stays there (reflection of incident electrons does not lead to multiplication and can be ignored). Efficient emission requires $\varepsilon_m \approx 100\,\text{eV}$ (Sect. 4.5.6). Furthermore, electrons need to cross the gap in synchrony with the field. When an electron leaving one wall is accelerated and reaches the opposite wall, the field must be reversed for the emitted electron to be accelerated to the former.

Let an electron be emitted from the wall at $x = 0$ with velocity $\dot{x} = 0$ at a moment $t_0 = \pi/\omega$ at which the field $E_x = E_0 \sin \omega t$ reverses its direction and begins accelerating the emitted electron. According to (3.1), it reaches the opposite wall $x = d$ with a velocity $v_m = (2\varepsilon_m/m)^{1/2}$ at the moment of the next field reversal, $t_1 = 2\pi/\omega$, if $2eE_0/m\omega = v_m$, $\omega d = \pi(eE_0/m\omega)$ [the second equality corresponds to (7.28), only for free motion]. For $\varepsilon_m = 100\,\text{eV}$, $v_m = 5.8 \cdot 10^8\,\text{cm/s}$, this gives the cut-off frequency $f_b \approx 140/d\,[\text{cm}]\,\text{MHz}$ and the threshold field $E_{0_t} \approx 120/d\,[\text{cm}]\,\text{V/cm}$, in reasonable agreement with Fig. 7.23 and the empirical relation $f_b \approx 80/d\,\text{MHz}$.

If $f < f_b$, the electron reaches the opposite wall at a moment when the accelerating force still points along its line of motion. The emitted electron is hopelessly "trapped" and multiplication possibilities are severely limited. If, however, $f > f_b$, the electron begins decelerating before reaching the wall. Now, something can be done: by transferring more energy to the emitted electron via the increasing field. Therefore, breakdown is possible for $f > f_b$, but the threshold increases as the difference $f - f_b$ grows (see Fig. 7.23). For details concerning radio- and low-frequency fields, see [7.15].

8. Stable Glow Discharge

8.1 General Structure and Observable Features

8.1.1 Distinctive Features

The glow discharge is a *self-stustaining* discharge with a *cold cathode* emitting electrons due to secondary emission mostly due to positive ion bombardment. A distinctive feature of this discharge is a layer of large positive space charge at the cathode, with a strong field at the surface and considerable potential drop of 100–400 V (or more). This drop is known as *cathode fall,* and the thickness of the cathode fall layer is inversely proportional to the density (pressure) of the gas. If the interelectrode separation is sufficiently large, an *electrically neutral* plasma region with fairly weak field is formed between the cathode layer and the anode. Its relatively homogeneous middle part is called the *positive column.* It is separated from the anode by the *anode layer.* The positive column of a dc glow discharge is the best pronounced and most widespread example of a *weakly ionized nonequilibrium plasma* sustained by an electric field. In contrast to the cathode layer, whose existence is vital for the glow discharge, the positive column is not an essential part. No such column is formed if the cathode layer fills the interelectrode gap. If, however, the distance is insufficient for the formation of the required cathode layer, the glow discharge cannot be ignited.

8.1.2 Discharge Devices

The glow discharge is one of the most studied and widely applied types of gas discharge. The *discharge tube* is a device that has been employed for decades for discharge generation and analysis (Fig. 1.1). The glow discharge in tubes of radius $R \sim 1\,\text{cm}$ and length $L \sim 10\text{–}100\,\text{cm}$, at typical pressure $p \sim 10^{-2}\text{–}10^{2}\,\text{Torr}$, is characterized by an electrode voltage $V \sim 10^{2}\text{–}10^{3}\,\text{V}$ and a current $i \sim 10^{-4}\text{–}10^{-1}\,\text{A}$. In a number of modern laser systems, the discharge volume is a plane channel through which a gas is pumped (the flow is not essential for the discharge process as such). Electrodes may be placed along the larger surfaces of the channel or at its narrow ends (Fig. 8.1). The configuration of electrodes is quite different from the parallel disks typical for discharge tubes. An electrode may consist of several segments of various shapes, distributed over a plane, or it may be a long tube. A large discharge channel may allow reaching very high currents and voltages as does elevated pressure, resulting in kilovolts of voltage and amperes of current. Nevertheless, the main attributes of glow

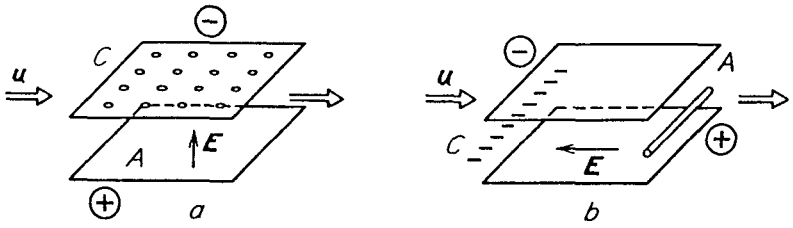

Fig. 8.1. Typical geometry of glow discharge in modern electric discharge CO_2 lasers; u is the direction of gas flow. **(a)** Transverse discharge (current is perpendicular to the gas flow). The upper plate is covered with cathode elements C, the lower plate is the anode A. **(b)** Longitudinal discharge. Cathode elements C are upstream of the gap, the anode A is a tube

discharge are retained, that is, a cathode layer with its inherent structure, and the region of electrically neutral, weakly ionized nonequilibrium plasma filling the space between anode and cathode layers. The familiar term, "positive column", is still applied to the homogeneous electroneutral region. This column forms the *lasing medium* of lasers (see Chap. 14). The main properties of glow discharges being insensitive to specific conditions, our discussion of this discharge will mainly refer to the classical discharge in a tube.

8.1.3 Pattern of Light Emission

The glow discharge normally manifests a stratification into dark and bright luminous layers; a name being ascribed to each (Fig. 8.2). The pattern is easily discernible at low pressure, when laysers are extended along the tube. Indeed, all discharge processes are connected with electrons. The distances from the cathode to characteristic points are dictated by the number of electron free paths, $l \propto p^{-1}$, within these distances. Hence, the coordinate at the boundary of a layer, x_1, corresponds to a specific value px_1. A layered pattern extends to centimetres if $p \sim 10^{-1}$ Torr. Sometimes a positive column has a *periodic* layered structure composed of *striations*. The formation of striations is not inevitable, or they may be not resolvable; in such cases the positive column emits light homogeneously up to the anode region.

If the pressure is low, $p \sim 10^{-2}$ Torr, and the separation between electrodes is moderate, the positive column has no space in which to form and what is seen is mostly the region of *negative (glow)* emission that gave the name to the discharge mode as a whole.

The quiet, sometimes slightly trembling light of a glow discharge has an enchanting beauty. As a rule, the positive column is less bright than the negative glow and is differently coloured. Helium manifests a red cathode layer, a gree negative glow, and a reddish-purple positive column; the respective combination in neon is yellow, orange and red, and in nitrogen, pink, blue and red. Each gas has a characteristic set of colours reflecting its spectrum; this is employed in coloured advertisement tubes. If the pressure in a long tube is not too low, we mostly observe the positive column. In very wide tubes and spherical vessels, the glow of the positive column is weak and often invisible.

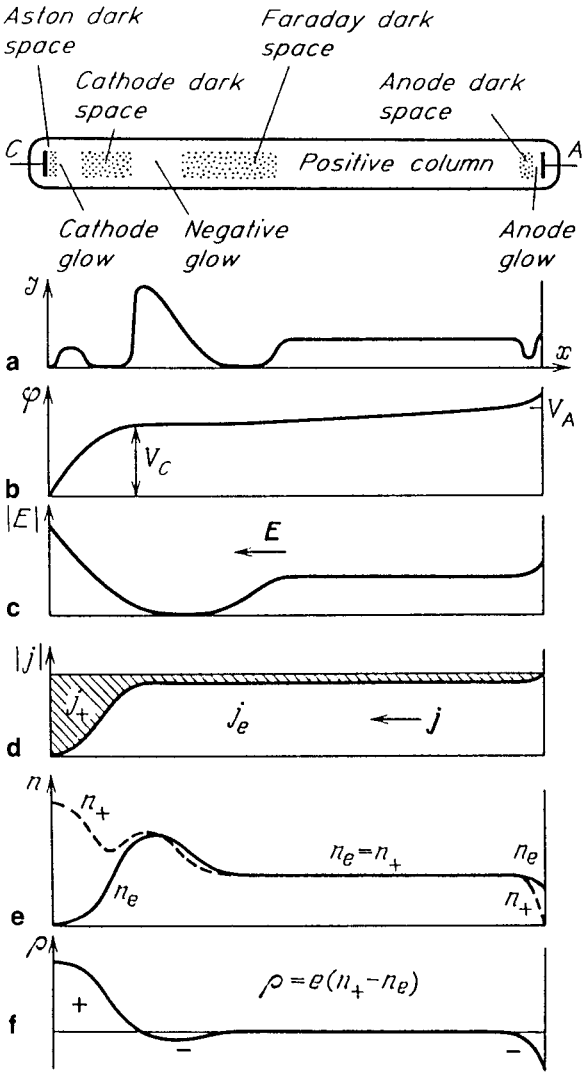

Fig. 8.2. Glow discharge in a tube and the distribution of: **(a)** glow intensity, **(b)** potential φ, **(c)** longitudinal field E, **(d)** electronic and ionic current densities j_e and j_+, **(e)** charge densities n_e and n_+, and **(f)** space charge $\varrho = e(n_+ - n_e)$

8.1.4 Variation of Conditions

As the pressure increases, all the layers become thinner and shift closer to the cathode. At $p \sim 100$ Torr, it looks as if the cathode is burning, although we are merely observing the luminous gas. A more extended Faraday dark space (as in Fig. 8.2) can be distinguished; the rest of the tube or channel is occupied by the positive column. An elevated pressure *causes* the column to *contract* to the axis, while at low pressures the cross section of the tube is filled with

the column in a *diffuse* manner. If the electrodes are moved closer at constant pressure, the positive column is shortened. Intermediate regions between the column and cathode (known as *negative* regions) remain unaltered for some time. If the cathode is shifted, these regions move together with it. Furthermore, if the cathode disk is rotated in a wide vessel with a fixed anode, all negative layers rotate together as if glued to the cathode surface, while the positive column bends so as to reach the anode. This situation is also realized in vessles of complex shape. *Negative layers* are "glued" to the cathode surface and the positive column finds a path connecting the end of the Faraday space with the anode. As the electrodes get closer, the column disappears, then the Faraday space is "eaten up", and finally the negative glow vanishes. When there is no space even for the cathode edge of this glow, the discharge goes out unless the voltage is increased. This discharge is sometimes said to be *obstructed.*

8.1.5 Distribution of Parameters over Length

The sequence of layers and the distribution of brightness along the discharge tube are compared in Fig. 8.2 with the distributions of the main discharge parameters. This is a qualitative picture but a fairly reliable one. It is supported by probe measurements and theoretical arguments. Among the principal features of this picture are a *large space charge* and high field at the cathode, which decreases almost linearly to a very low level at the cathode boundary of the negative glow. This region is known as the *cathode layer;* it is defined not by a visually apparent attribute (light emission), but by an "objective" characteristic, namely, electric field distribution.

This region is followed by a zone of very weak field which sometimes may even be slightly negative, that is, directed to the anode. The longitudinal field in the Faraday space increases and then stays constant over the entire length of the positive column. This column can be arbitrarily long provided the power supply circuit is adequate for maintaining the necessary potential difference across the column. The constancy of the axial potential gradient in the column has been confirmed by probe measurements; it proves the *electric neutrality* of plasma. There is a small region of slight *anode fall of potential* by the anode.

8.1.6 Qualitative Interpretation of the Light Emission Pattern

Electrons are ejected from the cathode at energies less than 1 eV. This is not enough for exciting an atom. The result is the formation of the *Aston dark space*. The field accelerates these electrons to an energy sufficient for excitation, and the *cathode glow* appears. Two, even three layers of cathode glow may be formed. They correspond to the excitation of different atomic levels, lower ones closer to the cathode and higher ones further out. These layers have different colours. The energy of accelerated eelectrons then grows above the *excitation function* maxima, where cross sections fall off (Fig. 5.8). Electrons cease to excite atoms and the *cathode dark space* is formed. This is the region where ionization of atoms predominantly takes place, where most electrons are multiplied. The

newborn ions move much slowly and a large *positive space charge* builds up. The current is transferred mostly by *ions*.

By the end of the cathode layer, the electron flux gets fairly large; as a result of the avalanche process of multiplication, most electrons are generated at the very end of the layer, where the field is not strong any more and continues to fall off. These electrons have moderately high energies, in the region of the maxima of the excitation function. The *negative glow* appears. Close to the cathode, the electron energy increases with the distance from the cathode and more easily excited spectral lines appear (first and second cathode glows), but after the cathode layer, the electron energies decrease with increasing distance from the cathode. Correspondingly, the negative glow first reveals the lines that are emitted from higher atomic levels and then the lines from lower levels, in an order reversed with respect to the cathode glow (*Seeliger's rule*). As electrons dissipate their energy, acts of excitation become less and less frequent because electrons do not gain new energy in the weak field. The negative glow gives way to the *Faraday dark space.*

Most but not all of the electrons in the negative glow region have moderate energies. Some electrons here are energetic ones liberated deep inside the cathode layer or at the cathode, having traversed the cathode layer with only a few inelastic collisions. They ionize atoms; as a result, the electron density immediately after the cathode layer is higher than in the positive column.

In the Faraday space, the longitudinal field gradually increases to the value characterizing the positive column. The column has a random velocity distribution typical of nonequilibrium weakly ionized plasma, with slight asymmetry introduced by the drift towards the anode. The electron energy averaged over the spectrum in the positive column is 1–2 eV. However, the spectrum contains some energetic electrons as well. They excite atoms and generate the luminescence of the column. The anode repels ions but pulls out electrons from the column. Thus a region of *negative space charge* is formed; its higher field accelerates electrons. The result is the *anode glow.*

8.1.7 Guiding Effect of Charges Precipitated on the Walls

Observations show that a discharge can be maintained in tubes of very complicated shapes. Electrons (and ions) that transfer electric current are bound to move along the gas channel but have to follow the lines of force of the electric field. In fact, the lines of force of the applied external field trace their own paths from the anode to the cathode, intersecting quite often the walls of the discharge tube (Fig. 8.3a). How then can current flow?

Actually, charges (mostly electrons) are first transported along a line of force of the external field to a dielectric wall; there they stick and accumulate until they start repelling subsequently arriving charges of like sign away from the wall. The electrostatic field of the precipitated charges adds up vectorially with the external field and redirects a part of the lines of force of the resultant field along a path through the tube that is accessible for charges (Fig. 8.3b, c). Owing to this effect,

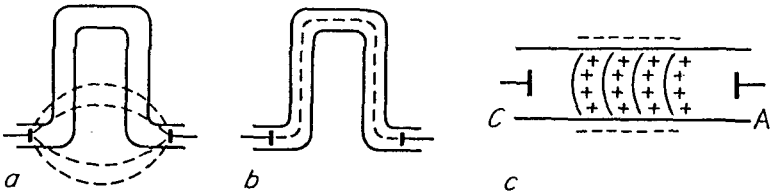

Fig. 8.3. Glow discharge in tubes of complicated shape: (a) Lines of force of the applied field, (b) lines of force of the resulting field (applied field plus that of charged deposited on the walls), (c) equipotential surfaces in a straight tube curved by the field of negative charge deposited on the walls

the longitudinal field in a straight tube or plane channel becomes more uniform in cross section. Nevertheless, a transverse (radial) field component is present in the discharge. Thus in a long positive column, it is uniform along the length and is directed from the axis to the negatively charged wall. Equipotential surfaces in the tube are convex, the convexity pointing to the cathode. Sometimes it is possible to see that the boundary between the positive column and the Faraday dark space, and the striations, are indeed convex. At a flat cathode, the boundaries of negative layers are usually plane; presumably, this indicates the absence of a transverse field component.

8.2 Current-Voltage Characteristic of Discharge Between Electrodes

Let us continue an analysis of the dc current-voltage characteristic ($V - i$ curve) begun in Sect. 7.2, and move to higher currents. As the breakdown voltage is reached across the electrodes, $V = V_t$, a *self-sustaining* discharge begins to burn in the gas. In the framework of the idealized scheme we used in Sect. 7.2.2, the current at $V = V_t$ tends to infinity. Any real circuit with a discharge gap always has an ohmic resistance Ω (a specially introduced resistance or the resistance of the lead wires, and power supply) which sets an *absolute limit* to the current achievable for a given electromotive force $\mathcal{E}$ of the power supply unit. As the discharge current scale largely determines the discharge type (the value of current dictates the degree of gas ionization), the resistance Ω imposes the type of discharge that is produced after breakdown.

8.2.1 Load Line

The equation for the voltage of a closed circuit with a discharge gap is

$$\mathcal{E} = V + i\Omega \,. \tag{8.1}$$

This equation is plotted as a straight line in V vs. i coordinates (Fig. 8.4); it is known as the *load line*. The line is the steeper, the larger the external resistance; the intercept on the abscissa axis is the limiting current $\mathcal{E}/\Omega$. The circuit realizes

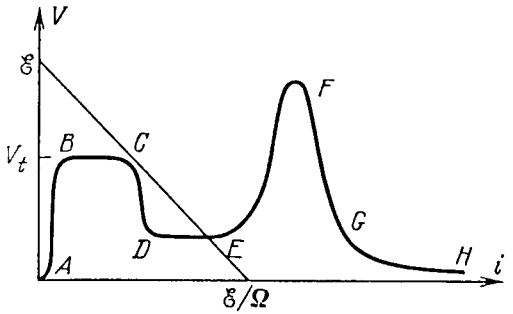

Fig. 8.4. $V - i$ characteristic of discharge between electrodes for a wide range of currents, and the loading line: *(A)* region of non-self-stustaining discharge, *(BC)* Townsend dark discharge, *(DE)* normal glow discharge, *(EF)* abnormal glow discharge, *(FG)* transition to arcing, *(GH)* arc

those values of i and V that correspond to the intersection of load line and the $V - i$ curve, $V(i)$.

8.2.2 Townsend Dark Discharge

Assume the resistance Ω to be so high that the circuit can supply only an extremely weak current. The densities n_e and n_+ are then negligible and the space charge is so small that the external field is not distorted. Thus if the distance L between plane electrodes is small in comparison with the transverse size of electrodes, the field is the same as in the absence of ionization: $E(x) \approx \text{const} = V/L$. This discharge is made self-sustained by applying to the electrodes the voltage equal to the *ignition potential* V_i. This voltage ensures the stationary reproduction of electrons ejected from the cathode and pulled to the anode (Sect. 7.2.2). As long as the field $E(x)$ is independent of charge (and current) densities, the $V - i$ curve of discharge is $V(i) = \text{const} = V_i$. This situation corresponds to the segment BC in Fig. 8.4.[1]

This *self-sustaining* discharge mode is indeed observed experimentally in ordinary tubes at currents of $i \sim 10^{-10}$–10^5 A. This mode is called the *Townsend dark* discharge. Ionization is so small that the gas emits no appreciable light. The current is measured by high-sensitivity instruments.

8.2.3 Glow Discharge

Let us gradually increase the current. This can be realized by reducing the load resistance Ω or by increasing the e.m.f. $\mathcal{E}$. The voltage across the electrodes begins to decrease after a certain current is reached. The fall then stops and the current remains almost constant over a fairly wide range of values (sometimes of

[1] Note that we are now discussing the $V - i$ curve of a steady-state, stationary process. There must be no overvoltage (see Sect. 7.2.3) in comparison with the ignition potential. Overvoltage is needed for the development of the breakdown, that is, for the implementation of the nonstationary process of current buildup. The current increases in the course of breakdown (when $V > V_i$) to a value necessary to eliminate overvoltage.

several orders of magnitude). This segment of the $V - i$ curve, DE, corresponds to the so-called *normal glow discharge*. The lower part of the transition region CD corresponds to a below normal glow discharge.

The normal discharge has one remarkable property. As the discharge current is varied, its density at the cathode remains unchanged. What changes is the area through which the current flows. When Ω or $\mathcal{E}$ is varied, the luminous current spot on the cathode surface expands or contracts.

When no more free surface is left on the cathode, the current is increased by increasing the voltage, hence extracting more electrons from unit surface area. Indeed, the cathode current density must grow. This discharge is said to be *abnormal*. It corresponds to the climbing section EF of the $V - i$ curve. The transition to the abnormal mode is interesting to observe. The glow first covers the entire cathode surface facing the anode, then reaches every spot unprotected by dielectric on the lateral and inner surfaces and on the support pin, and only having exhausted these possibilities does it become more extended and intense to a degree typical of the abnormal discharge. When $i \sim 1$ A, the glow discharge cascades down to an *arc*. The segment FG describes the transition, and GH represents the *arc discharge*.

We have followed the $V - i$ curve as if "turning the handle" that varies Ω or $\mathcal{E}$. In experiments, a certain resistance is in the circuit at the moment of switching on an e.m.f.; if $\mathcal{E}$ is greater than the ignition potential, the discharge mode that sets in immediately after the breakdown corresponds to the point of intersection of the $V - i$ curve and the loading curve. In contrast to the schematic Fig. 8.4, Fig. 8.5 gives the actual $V - i$ curves [8.1]. The curves cover the dark, normal, and partially abnormal modes. The higher the pressure, the wider the current range in which the normal mode is realized (the reason for this will be clear in Sect. 8.4.4). The picture observed in H_2, N_2, and Ar is almost the same as in Ne.

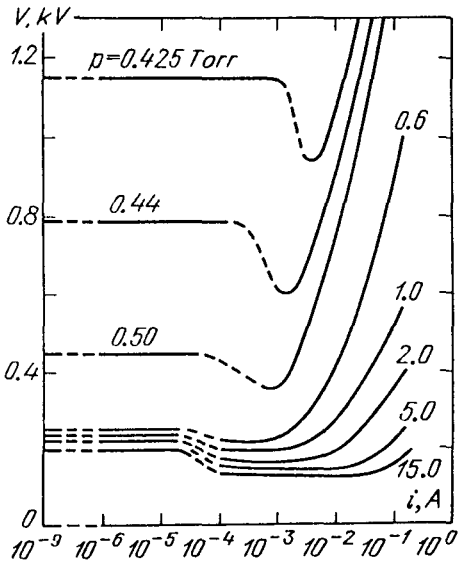

Fig. 8.5. Measured $V - i$ characteristics of discharge in neon bewteen copper disks 9.3 cm in diameter, gap width 1.6 cm. Plateau on the *left*: dark discharge; *lower* plateau or region of minimum: normal glow discharge; rising curve on the *right*: abnormal discharge [8.1]

8.3 Dark Discharge and the Role Played by Space Charge in the Formation of the Cathode Layer

The main distinction of the glow discharge from the dark discharge (with its extremely weak current) lies in a sharply *nonuniform* distribution of the potential difference applied across the gap to the electrodes. In order to find out why and by what mechanism the field is redistributed in the interelectrode gap, let us begin with the dark discharge that does not disturb the external field.

8.3.1 Charge Distribution in Weak-Current Dark Discharges

Assume the gap width to be small in comparison with the transverse electrode size. We choose the x axis to point from the cathode to the anode. The analysis is based on continuity equations (2.22), (2.20) for charge densities. Diffusion fluxes are small in comparison with drift fluxes, the diffusion in the lateral directions also being insignificant; even more so is the recombination. Bulk charge sources are related only to gas ionization: $q = \nu_i n_e = \alpha v_{ed} n_e$; fluxes are due to drift only. Let us work in terms of current densities $j_e = -en_e v_{ed}$, $j_+ = en_+ \cdot v_{+d}$. In the steady-state case,

$$\frac{dj_e}{dx} = \alpha j_e \ , \quad \frac{dj_+}{dx} = -\alpha j_e \ , \quad j_e + j_+ = j = \text{const} \ . \tag{8.2}$$

The third equality stating the constancy of the total current is implied by the first two. The boundary condition at the cathode ($x = 0$) describes the secondary emission, and that at the anode ($x = L$) describes the absence of ionic emission:

$$j_{eC} = \gamma j_{+C} = \frac{\gamma}{1+\gamma} j \ , \quad j_{+A} = 0 \ , \quad j_{eA} = j \ . \tag{8.3}$$

If equation (8.2) for j_e is integrated, starting at the cathode, for the first condition of (8.3) and $\alpha[E(x)] = \text{const}$, we obtain

$$j_e = \frac{\gamma}{1+\gamma} j e^{\alpha x} \ , \quad j_+ = j\left(1 - \frac{\gamma}{1+\gamma} e^{\alpha x}\right) \ . \tag{8.4}$$

Condition (8.3) can be satisfied at the anode only if the *criterion of ignition (self-sustainment)* is met (see Sect. 7.2.2):

$$e^{\alpha L} - 1 = 1/\gamma \ , \quad \alpha L = \ln(1 + 1/\gamma) \ . \tag{8.5}$$

We recast (8.4) using (8.5):

$$j_e/j = \exp[-\alpha(L - x)] \ , \quad j_+/j = 1 - \exp[-\alpha(L - x)] \ ;$$

$$j_+/j_e = \exp[\alpha(L - x)] - 1 \ .$$

The ionic current much exceeds the electronic current over a large part of the gap, beginning with the cathode (Fig. 8.6). For example, for $\gamma = 10^{-2}$ and

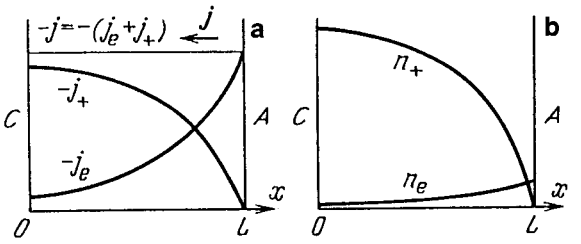

Fig. 8.6. Distributions of electronic and ionic currents (**a**), and charge density distribution (**b**) when the field in the gap is not distorted by space charge

$\alpha L = 4.6$, j_e reaches j_+ only at $x = 0.85L$. The difference in charge densities is even greater. Thus if $\mu_e/\mu_+ = 100$, we find that $n_+/n_e = (\mu_e/\mu_+)(j_+/j_e) = 1$ only if $x = 0.998L$. In most of the gap, $n_+ \gg n_e$ (Fig. 8.6). Practically the entire space is positively charged in dark discharges, but the space charge is small because j and n_+ are low. These quantities are arbitrary, being determined by the current allowed by the circuit and the area of electrodes (see Sect. 8.2).

8.3.2 Distortion of an External Field

This is produced by space charge. Let us evaluate the effect, taking for the zeroth approximation the charge density distributions obtained in the assumption $E(x) = \text{const}$. The spatial field distribution is determined by the equation

$$dE/dx = 4\pi e(n_+ - n_e)\,, \quad E \equiv E_x\,. \tag{8.6}$$

Assuming approximate equalities $n_+ \gg n_e$, $|j_+| \gg |j_e|$, $n_+ \approx j/ev_{+d} \approx j/e\mu_+E$ and denoting by E_C the field at the cathode, we find

$$E = E_C\sqrt{1 - x/d}\,, \quad d = \mu_+E_C^2/8\pi j\,. \tag{8.7}$$

The field decreases in the vicinity of the anode and increases in the vicinity of the cathode, the more the higher the current density (Fig. 8.7). The plane $x = d$ where the extrapolated quantity $E(d)$ vanishes lies far beyond the discharge gap (if the current is low). As j increases, it moves closer to the anode and coincides with the anode surface for $j_L = \mu_+E_C^2/8\pi L$ ($d = L$). As j further increases, at $d < L$, the field implied by (8.7) tends formally to zero inside the gap, and the closer to the cathode the higher the current (Fig. 8.7). However, in this case distribution (8.7) becomes meaningless in the interval $d < x < L$ because the original assumptions become invalidated. Actually, the distributions n_{ge}, n_+, and E take the form given in Fig. 8.2.

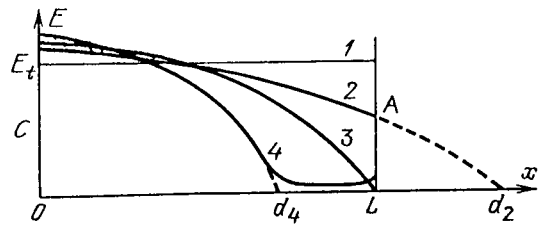

Fig. 8.7. Field evolution due to space charge: *(1)* undisturbed fields as $j \to 0$; *(2)* weak current, $j < j_L$; *(3)* $j = j_L$; *(4)* $j > j_L$, transition to glow discharge

8.3.3 Limiting Current for the Existence of Dark Discharge

When the currents are so small that the field is very little distorted, the field at the cathode, E_C, is quite close to the nonperturbed breakdown field E_t of this gap. As the current increases, the field E_C deviates from E_t more and more; but as long as $d > L$, E_C retains the same order of magnitude (see footnote in Sect. 8.3.5). Hence, E_C in the expression for j_L at $d = L$ can be replaced with E_t. The current density at which the field and discharge structure are considerably modified and which manifests the beginning of dark-to-glow transition of discharge, is given within an order of magnitude, by the formula

$$\frac{j_L}{p^2} \approx \frac{(\mu_+ \cdot p)(E_t/p)^2}{8\pi(pL)} = \frac{(\mu_+ \cdot p)V_t^2}{8\pi(pL)^3} \,. \tag{8.8}$$

It is given a form corresponding to similarity laws. For instance, (8.3) gives the values $E_t/p = 62\,(\mathrm{V/(cm{\cdot}Torr)})$, $V_t = 6200\,\mathrm{V}$ for nitrogen, with α defined by (4.5); $A = 12\,\mathrm{cm^{-1}Torr^{-1}}$ and $B = 342\,\mathrm{V/(cm{\cdot}Torr)}$ taken from Table 4.1; and $\gamma = 10^{-2}$ at $pL = 100\,\mathrm{cm\,Torr}$. For $(\mu_+ p) = 1.5 \cdot 10^3\,\mathrm{cm^2Torr/(V{\cdot}s)}$, we find $j_L/p^2 = 2.5 \cdot 10^{-9}\,\mathrm{A/(cm{\cdot}Torr)^2}$. If, say, $p = 10\,\mathrm{Torr}$ and $L = 10\,\mathrm{cm}$, then $j_L = 2.5 \cdot 10^{-7}\,\mathrm{A/cm^2}$. If the electrode surface area is $100\,\mathrm{cm^2}$, the limiting dark discharge current is $i = 2.5 \cdot 10^{-5}\,\mathrm{A}$.

8.3.4 The Condition of Self-Sustainment of Discharge in a Plane Gap in the Case of Inhomogeneous Fields

It is immediately implied by (8.2, 3) that

$$\int_0^L \alpha\,[E(x)]\,dx = \ln(1 + 1/\gamma) \,. \tag{8.9}$$

Equality (8.9) generalizes (8.5) and expresses the same fact. A specific number of generations have to be produced in the electron avalanche propagating from the cathode to the anode. This number is determined only by the secondary emission coefficient and is independent of whether the field is homogeneous or not. The integral in (8.9) is exactly equal to the value of $\alpha(E_t)L$ corresponding to the breakdown of a given gap in a homogeneous field. Note that $|E_C| > E_t$ at the cathode and $|E_A| < E_t$ at the anode, because $\alpha(E)$ is an increasing function of E, but that $|E(x)|$ is a decreasing function of x if E is distorted by the space charge.

8.3.5 What Happens to Voltage When Space Charge Builds Up

A qualitative tendency is clear from an analysis of the integral in (8.9), of the voltage integral $V = |\int_0^L E\,dx|$, and of the dependence of α on E according to (4.5). If the field is not too strong, the function $\alpha \propto \exp(-Bp/E)$ increases with increasing E at an increasing slope $d^2\alpha/dE^2 > 0$; if the field is very high, the slope decreases: $\alpha \to \mathrm{const}$. The point of inflection of $\alpha(E)$ lies at $E = Bp/2$. For a nonperturbed breakdown field $E_t < Bp/2$, the conditions for multiplication

are facilitated by a redistribution of potential: the enhanced field contributes to integral (8.9) more than the weakened field takes out. Conversely, integral (8.9) is conserved if $E_t - |E_A|$ of the decreasing field is greater than the increment $|E_C| - E_t$. However, if at one place the field is enhanced less than it is weakened at another place, the potential difference $|\int E\,dx|$ decreases. If $E_t > Bp/2$, the situation is reversed: redistribution either impedes multiplication or increases voltage.

The correctness of these qualitative arguments can be verified by considering a weak inhomogeneity, using formulas (8.9,7) and (4.5) and expanding in a small parameter $j/j_L = L/d \ll 1$ (the integral cannot be calculated in the general case).[2] A small increment to the gap voltage in comparison with the breakdown potential $V_t = E_t L$ for a homogeneous field is found to be

$$V - V_t = -(1/48)(Bp/2E_t - 1)(j/j_L)^2 . \tag{8.10}$$

According to (7.3), the condition $E_t < Bp/2$ at which the voltage of sustained discharge falls below the ignition potential is satisfied for gaps with $(pL) > e(pd)_{min}$, where $(pd)_{min}$ corresponds to the minimum breakdown voltage. If $(pL) < e(pd)_{min}$, then $V > V_t$. In actual experiments, one usually has to deal with gaps that are long in the sense defined here; therefore the voltage decreases in the transition from the dark to the glow discharge (Figs. 8.4, 5).

8.4 Cathode Layer

8.4.1 What Is Its Purpose

In a plane gap undergoing breakdown, and in weak-current dark discharges, the loss of charged particles due to field-pulling onto electrodes is made up for by avalanche ionization over the entire length up to the anode. However, if a gap is wide in the sense $pL \gg (pd)_{min}$, this situation (implied by the homogeneity of the field) is obviously not optimal. Unjustifiably high voltage is required to meet the self-sustainment condition (8.9). A lower voltage would be sufficient if the potential drop were concentrated. Indeed, the multiplication efficiency is higher in strong fields.

The potential distribution would be ideal if the potential difference equal to the minimal breakdown voltage, V_{min}, were concentrated over the corresponding length $(pd)_{min}$ at the cathode. This would ensure reproduction at minimum applied voltage. To sustain further flow of electronic current generated in this cathode layer through the remaining (even if long) part of the gap, the additional voltage need only compensate, via weak ionization, for the losses of electrons caused by ambipolar diffusion to the walls, recombination, and attachment. Na-

[2] The field at the cathode is found by setting integral (8.9) equal to $\alpha(E_t)L$; $|E_C| = E_t[1 + L/4d + O(L/d)]$. Second-order terms must be retained. The problem was originally analyzed in [8.2, 3].

ture reveals unparalleled wisdom in its organization. The normal glow discharge comes quite close to the optimum. One of the main mechanisms of optimizing the potential distribution across the gap is the effect of space charge that is generated automatically at the cathode, creating there an enhanced field and a potential drop; this was described in Sect. 8.3.

8.4.2 Current-Voltage Characteristic

The theory of the cathode potential drop (or cathode fall) was developed by *von Engel* and *Steenbeck* in 1934 [8.2]; it has considerable significance for the physics of the glow discharge. Subsequent elaboration and more profound understanding of the process do not nullify the essential aspects of the theory. We will present it here in the simplest and most lucid form that brings forth the fundamental features of the phenomena. Let us take a stationary cathode-fall layer. Assume that pressures and currents are not too low, so that the current spot in the cathode is large and the layer is thin. It can then be assumed plane and one-dimensional. The field at the anode end of the layer, at $x = d$, is substantially less than that at the cathode: $E(d) \ll E(0) \equiv E_C$. Assume $E(d) \approx 0$. Assume also that even if some ionic current enters the cathode layer on the side of the anode, it is very weak (in the electrically neutral part of the gap, $j_+/j_e = v_{+d}/v_{ed} = \mu_+/\mu_e \sim 10^{-2}$). The layer is then an autonomous system satisfying the condition of self-sustainment of current, (8.9). We only have to replace the distance between electrodes L in (8.9) with the layer thickness d. The electronic current generated in this system reaches the anode. It coincides with the total discharge current up to a small quantity of order μ_+/μ_e.[3] The cathode fall is

$$V_C = \int_0^d E\,dx\,, \quad E \equiv |E|\,. \tag{8.11}$$

Von Engel and Steenbeck solved the system of equations (8.9, 11, 6) assuming (4.5) for $\alpha(E)$ and prescribing, in view of the results of probe measurements, a linear field distribution:

$$E(x) = E_C(1 - x/d)\,, \quad 0 \le x \le d\,. \tag{8.12}$$

The integral (8.9) with the field (8.12) is not expressible in terms of elementary functions. Essentially the same results that differ only by numerical factors of order unity but manifest a clear analytic form can be obtained assuming $E(x) = \text{const} \approx E_C$ in (8.9) for $x < d$. Then (8.9) transforms into (8.5), with d for L. However, since we assumed the field in the layer to be homogeneous, (4.5) and a trivial relation $V_C = E_C d$ implied by (8.11) yield (7.3) for the breakdown of the gap d in the homogeneous field:

[3] According to (2.39), a stationary process has $\operatorname{div} \boldsymbol{j} = 0$, whence $i = \text{const}$. In the one-dimensinal case, $j(x) = \text{const}$ as well.

$$\frac{E_C}{p} = \frac{B}{C + \ln pd}, \quad V_C = \frac{Bpd}{C + \ln pd}, \quad C = \ln \frac{A}{\ln(1 + 1/\gamma)}. \tag{8.13}$$

These formulas relate the cathode fall V_C to the cathode layer thickness pd.

Let us now find the relation of these quantities to the current density at the cathode, j. As shown in Sect. 8.3.1, the region of self-sustainment through multiplication is characterized by $n_+ \gg n_e$, $j_+ \gg j_e$. By virtue of (8.6), the ion density in the layer is approximately equal to

$$n_+ \approx (4\pi e)^{-1} |dE/dx| \sim E_C/4\pi ed,$$

where we have already taken into account that the actual field is not constant but decreases from E_C to zero. Hence,

$$j = (1 + \gamma) e n_+ \mu_+ E \approx (1 + \gamma) \mu_+ E_C^2/4\pi d \approx (1 + \gamma) \mu_+ V_C^2/4\pi d^3. \tag{8.13'}$$

Together with (8.13), this formula defines a parametric dependence of the cathode fall V_C and the field at the cathode, E_C, on the current density j. The parameter is the layer thickness d. The function $V_C(pd)$ has a minimum [see (8.13)]. In this approximation, it describes a Paschen curve (Sect. 7.2.3) with V_{min} equal to the minimum gap breakdown voltage.

By virtue of (8.13, 13'), V_C as a function of j has a minimum, reaching the same value V_{min}. It will be convenient to rewrite these formulas in dimensionless form, using the quantities corresponding to the minimum potential difference as dimensional scales. We mark them with subscript "n" for "normal" instead of "min" (they are indeed realized in normal discharge) and denote dimensionless quantities by a tilde:

$$\tilde{V} = \frac{V_C}{V_n}, \quad \tilde{E} = \frac{E_C/p}{E_n/p}, \quad \tilde{d} = \frac{pd}{(pd)_n}, \quad \tilde{j} = \frac{j}{j_n}.$$

The scales V_n, E_n/p, $(pd)_n$ are defined by formulae (7.4); the current density scale, taking into account similarity laws, is

$$\frac{j_n}{p^2} = \frac{(1 + \gamma)(\mu_+ p) V_n^2}{4\pi (pd)_n^3} = \frac{(1 + \gamma)}{9 \cdot 10^{11}} \frac{(\mu_+ p) V_n^2}{4\pi (pd)_n^3} \text{ A/(cm} \cdot \text{Torr)}^2. \tag{8.14}$$

The parametric relations of dimensionless quantities via $\tilde{d}$ are

$$\tilde{V} = \frac{\tilde{d}}{1 + \ln \tilde{d}}, \quad \tilde{E} = \frac{1}{1 + \ln \tilde{d}}, \quad \tilde{j} = \frac{1}{\tilde{d}(1 + \ln \tilde{d})^2}. \tag{8.15}$$

Figure 8.8 plots $\tilde{V}$, $\tilde{E}$, and $\tilde{d}$ as functions of $\tilde{j}$ according to (8.15). The curve $\tilde{V}(\tilde{j})$ gives the "current-voltage" characteristic of the cathode layer, the inverted commas signifying that the argument is current density, not current.

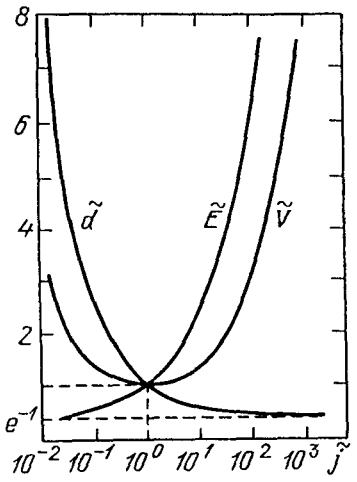

Fig. 8.8. Cathode potential fall ($\tilde{V}$), field at the cathode ($\tilde{E}$) and cathode layer thickness ($\tilde{V}$) as functions of current density (in dimensionless coordinates)

8.4.3 Normal Cathode Fall and Current Density

Formally, (8.15) and Fig. 8.8 imply that as j decreases from j_n, V_C and d increase and E_C decreases. When d grows to the gap width L, solution (8.15) becomes equal to that of Sect. 8.3, and j given by (8.13′) is nearly equal to j_L of (8.8). It may seem that the evolution of dark to glow discharge has been traced.

Experiments definitely show that nothing of the sort takes place. The falling branch of the curve $V(j)$ to the left of $\tilde{j} = 1$, $j = j_n$ is not realized. The mode that sets in at currents i less than $S_C j_n$, where S_C is the cathode surface area, corresponds to the minimum point of the "$V - i$ curve" of the cathode layer. The same mode is realized when current is varied and when $\mathcal{E}$ and Ω are such that, after ignition, the state falls into the region DE of Fig. 8.4. A current spot lights up automatically on the cathode, with area S such that the current density is $j_n \approx i/S$ and the cathode fall is V_n. A $V - i$ curve of a real discharge has nothing in common with the left-hand branch of Fig. 8.8 (this would be the case if the current i passed through the entire cathode, $i = S_C j$). The discharge voltage when the cathode is not totally covered is current-independent, exceeding V_n by the potential drop on the positive column. If this fall is negligible (low pressure, short tube), the voltage on the electrodes is almost equal to V_n. This glow discharge is known as *normal*, and the corresponding values of cathode fall and current density are also said to be *normal*.

The theoretical values V_n, j_n, and $(pd)_n$ somewhat depend on the assumptions about the $E(x)$ profile that were used in the calculation. In the simplest approximation, introduced in Sect. 8.4.2, V_n and $(pd)_n$ coincide exactly with the parameters of the minimum on the Paschen curve, V_{min} and $(pd)_{min}$, and j_n is given by (8.14). If approximation (8.12) is used, we find $V_n = 1.1V_{min}$, $(pd)_n = 1.4(pd)_{min}$,[4] and j_n is 1.8 times the value given by (8.14). Any reasonable theory, as well as

[4] Formula (137) for $(pd)_n$ given in the monograph [8.2], and later in [8.4], contains a wrong numerical coefficient: 0.82 instead of 3.78. The correct coefficient in the above formula is 1.4.

experiment, give for the normal cathode fall and layer thickness values that are close to V_{min} and $(pd)_{min}$ for the breakdown of a plane discharge gap in the same gas and for the same cathode material. Calculations with the mentioned numerical coefficients derived by von Engel and Steenbeck on the basis of approximation (8.12), give satisfactory agreement with the experimental parameters of normal discharges (see Tables 8.1, 2, 3) if the coefficients A and B are taken from Table 4.1 and $\gamma \sim 10^{-2}$–10^{-1} (the dependence on γ is logarithmic).

Table 8.1. Normal cathode fall V_n [V] [8.2, 4]

gas / cathode	air	Ar	He	H_2	Hg	Ne	N_2	O_2	CO	CO_2
Al	229	100	140	170	245	120	180	311	–	–
Ag	280	130	162	216	318	150	233	–	–	–
Au	285	130	165	247	–	158	233	–	–	–
Bi	272	136	137	140	–	–	210	–	–	–
C	–	–	–	240	475	–	–	–	526	–
Cu	370	130	177	214	447	220	208	–	484	460
Fe	269	165	150	250	298	150	215	290	–	–
Hg	–	–	142	–	340	–	226	–	–	–
K	180	64	59	94	–	68	170	–	484	460
Mg	224	119	125	153	–	94	188	310	–	–
Na	200	–	80	185	–	75	178	–	–	–
Ni	226	131	158	211	275	140	197	–	–	–
Pb	207	124	177	223	–	172	210	–	–	–
Pt	277	131	165	276	340	152	216	364	490	475
W	–	–	–	–	305	125	–	–	–	–
Zn	277	119	143	184	–	–	216	354	480	410
glass[a]	310	–	–	260	–	–	–	–	–	–

[a] Thin soft glass disk heated to 300° C. The same holds for Tables 8.2 and 8.3

Table 8.2. Normal cathode layer thickness $(pd)_n$ [cm·Torr] at room temperature [8.2, 4]

gas / cathode	air	Ar	H_2	He	Hg	N_2	Ne	O_2
Al	0.25	0.29	0.72	1.32	0.33	0.31	0.64	0.24
C	–	–	0.90	–	0.69	–	–	–
Cu	0.23	–	0.80	–	0.60	–	–	–
Fe	0.52	0.33	0.90	1.30	0.34	0.42	0.72	0.31
Mg	–	–	0.61	1.45	–	0.35	–	0.25
Hg	–	–	0.90	–	–	–	–	–
Ni	–	–	0.90	–	–	–	–	–
Pb	–	–	0.84	–	–	–	–	–
Pt	–	–	1.00	–	–	–	–	–
Zn	–	–	0.80	–	–	–	–	–
glass[a]	0.30	–	0.80	–	–	–	–	–

[a] see Table 8.1

Table 8.3. Normal current density j_n/p^2 [μA/(cm^{2}Torr^2)] at room temperature [8.2, 4]

gas / cathode	air	Ar	H_2	He	Hg	N_2	O_2	Ne
Al	330	–	90	–	4	–	–	–
Au	570	–	110	–	–	–	–	–
Cu	240	–	64	–	15	–	–	–
Fe, Ni	–	160	72	2.2	8	400	–	6
Mg	–	20	–	3	–	–	–	5
Pt	–	150	90	5	–	380	550	18
glass[a]	40	–	80	–	–	–	–	–

[a] see Table 8.1

8.4.4 Abnormal Discharge

After the entire cathode has been covered with discharge, any further increase of current inevitably increases the density at the cathode in comparison with the normal value. This *abnormal* discharge corresponds to the right-hand branch of the $\tilde{V}(\tilde{j})$ curve of Fig. 8.8; now it actually describes the $V-i$ characteristic of the cathode layer and a discharge without a positive column, sine $i = \text{const} \cdot j = S_C j$. The theoretical curve fits the experimental data (region EF in Fig. 8.4). As $\tilde{j} \to \infty$, equation (8.15) implies that the cathode layer thickness decreases asymptotically to a finite value $\tilde{d} = e^{-1} = 0.37$; $\tilde{V}$ and $\tilde{E}$ grow as $\tilde{j}^{1/2}$. In actual situations, a cathode fall of more than several kV and current densities of order 10–10^2 A/cm^2 result in intense heating of the cathode and transition to an *arc* discharge. Experimental $V-i$ curves of abnormal discharges can be seen in Fig. 8.5.

8.4.5 The Current Range in Which Normal Discharge Is Possible

A dark discharge occupies the entire cathode. The same is true for the normal discharge at the upper limit of its existence. Correspondingly, the current increases from the transition of dark current to normal to the transition of normal current to abnormal by a factor of about j_n/j_L. By virtue of (8.8, 14), $j_n/j_L \approx \tilde{L}(1+\ln \tilde{L})^2$, where $\tilde{L} = (pL)/(pd)_n$. Therefore, the current range in the normal mode (in the region DE of Fig. 8.4) is the greater, the higher the pressure and the longer the tube (Fig. 8.5). For example, one of the experimental versions shown in Fig. 8.5 is characterized by $p = 15$ Torr, $L = 1.6$ cm, $(pd)_n \approx 0.7$ cm·Torr, $\tilde{L} = 34$, and the ratio of currents equals 700, in agreement with experimental data.

8.4.6 Subnormal Discharge

This is a transition region between the glow and dark discharge regions (rather nearer to the normal region) that corresponds to currents so weak that the size of the "quasinormal" cathode spot is found to be comparable to the cathode layer thickness. The loss of charges in the lateral direction is harmful for multiplication, so that the voltage across the layer required for self-sustainment of the discharge is found to be higher than for the normal regime.

8.4.7 Obstructed Discharge

This mode arises at very low pressure in narrow gaps of widths L, such that the product pL is less than the normal layer thickness $(pd)_n$. Roughly speaking, these conditions correspond to the left-hand branch of the Paschen curve, where $V > V_{min}$. The interelectrode separation is insufficient for "normal" multiplication, so that voltage has to be raised in comparison with the normal value. If this is not possible the discharge is extinguished.

8.4.8 Normal Discharge and Minimum Power Principle

Why is it that the discharge current to a partially covered cathode occupies precisely the area preserving the current density? The problem is equivalent to the task of justifying the postulate of the von Engel–Steenbeck theory on the realization of the minimum possible cathode fall by the normal discharge. It is this assumption that provides a good explanation of the experimental facts. The creators of the theory were already able to explain why states with cathode current density below the normal are not observed [8.2]. These states are unstable because they refer to the falling branch of the $V_C(j)$ curve of Fig. 8.8 (in general, discharges with falling $V - i$ characteristics typically produce unstable states; see Sect. 8.7.5). Indeed, if a fluctuation $\delta j > 0$ appears at some point on the cathode layer surface, a lower voltage is required to sustain the current $j + \delta j$ than is actually there, so that j increases. If $\delta j < 0$, the actual voltage is lower than the necessary level and j has to drop still lower. In this sense, the states with $j > j_n$ on the rising branch of the $V - i$ curve, $V_C(j)$, are quite stable. Nevertheless, "abnormal" cathode spots never appear on a partially covered cathode. Obviously, the neighbouring zero-current region proves to be unstable. How does it happen and what does stabilize the boundary of a normal cathode spot?

Twenty years later *von Engel* [8.3] discussed the incomprehensibility of the phenomenon, without resorting to the stability arguments, and appealed to the "minimum power principle". This principle left an important trace in discharge physics; sometimes it is resorted to even now and thus deserves being mentioned. The power released in the cathode layer volume is

$$P_C = S \int_0^d jE\,dx = SjV_C(j) = iV_C(j)\,.$$

If the area S is varied at constant total current i, the power is found to be minimal precisely at the normal current density, such that $V_C(j) = \min$. Gaseous discharges also manifest some other phenomena that realize just those states that require minimal voltages and (or) power, for example, *striations* (Sect. 9.7). Steenbeck proposed in 1932 the above minimum principle on the basis of such facts, demonstrating the spectacular expediency in the organization of nature. It may have been due to the great prestige of Steenbeck, however, that this principle was later employed not only for a better illustration of the observations, but also as a missing condition for completing a theoretical model. This proved to be fraught with errors (masked by an apparent agreement with experimental data),

because the principle is not implied by the fundamental laws of physics. In fact, it is not necessary if the mechanism of the phenomenon has been understood and its theory has been constructed in the usual manner. Such was the case with striations, and with the channels of the arc (Sect. 10.10), induction (Sect. 11.3), and microwave (Sect. 11.4) discharges. The approach to *normal current density* must also follow these lines.

8.4.9 Mechanism by Which Normal Current Density Is Reached

This has only been clarified rather recently [8.5–8].[5] The effect of interest, $i/S \approx$ const, is also revealed by numerical modeling of glow discharge using equations (2.22, 20, 33) for n_e, n_+, $\boldsymbol{E} = -\nabla\varphi$ with boundary conditions of type (8.3) and with α given by (4.5) [8.6, 8]. When the current and cathode layer surface area are sufficiently great, as in Fig. 8.9, the middle part of the layer behaves as a quasi-one-dimensional system whose parameters are described rather well by the formulae of the one-dimensional theory [8.2].[6]

Let us turn to the map of equipotentials in Fig. 8.9 and to the schematic dependence of the voltage V_C across the cathode layer on its thickness d (Fig. 8.10). This dependence follows from an equality of type (8.9) that we write in the form

$$\mu \equiv \gamma \left\{ \exp\left(\int_0^{d(r)} \alpha\,[E(l)]\,dl \right) - 1 \right\} = 1 \,, \tag{8.16}$$

where μ is the charge reproduction coefficient (Sect. 7.2.2). We integrate here along a line of current that sinks into some point r of the cathode surface. If we choose to ignore the diffusion of charges, the lines of current coincide with the lines of force of the field. If $E(l)$ = const, the dependence $V_C(d)$ coincides with the Paschen function (8.13). Note that the linear law (8.12) is fairly well supported by both one-dimensional [8.10] and two-dimensional [8.6, 8] calculations; this law gives the curve [8.2], which is not very different from (8.13). The stationary current mode corresponds to the curve of Fig. 8.10 for $\mu = 1$. Above this curve $\mu > 1$, and below it $\mu < 1$. This is a corollary of the boundedness of the ionization coefficient $\alpha(E)$ as $E \to \infty$, so that the function $\mu(d)$ at V = const has a maximum. This is the root of the effect.

For a qualitative analysis, the curve $V_C(d)$ can be treated as the current-voltage characteristic $V_C(j)$, provided the axis j is directed counter to d. If $j < j_n$, that is, $d > d_n$, the stationary states on the curve are unstable (Sect. 8.4.8). Fluctuations may destroy the cathode layer in its middle part as well, but at the edges the layer decays even without fluctuations. At these edges, where the space charge decreases, the equipotentials shift away from the cathode (Fig. 8.9). When moving away from the midpoint of the spot, we shift to the right of point 1 in Fig. 8.10, where $\mu < 1$. Hence, the current at the edge vanishes with time. According to

[5] The problem was discussed in [8.9], but clarity had not yet been achieved at that time; see [8.8].
[6] Taking into account the correction mentioned in footnote 4 to Sect. 8.4.3.

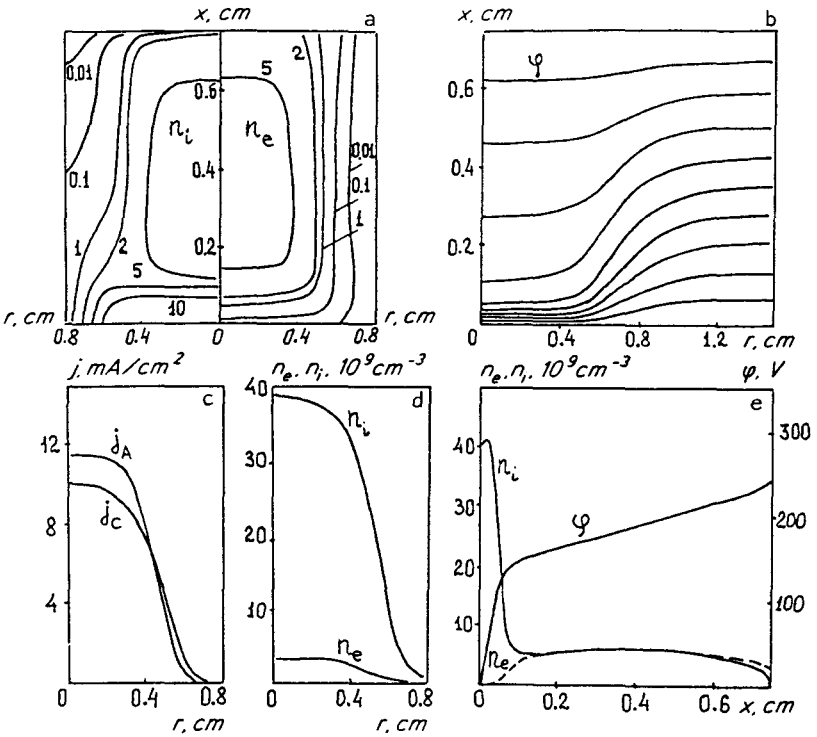

Fig. 8.9. Calculated two-dimensional structure of steady-state axisymmetric glow-discharge column between plane electrodes (nitrogen, p = 15 Torr, interelectrode spacing 0.75 cm, e.m.f. 2500 V, external resistance 300 kOhm). The cathode is placed below, the anode on top and on the electrodes V = 250 V, i = 7.5 mA. **(a)** Lines of equal densities of electrons and ions are plotted (n_e and n_i in 10^9 cm^{-3}, **(b)** equipotentials for each $V/10$ = 25 V, **(c)** radial current density distributions j_C on the cathode and j_A on the anode, **(d)** radial distributions n_i on the cathode and n_e on the anode, and **(e)** the distributions n_e, n_i, φ along the discharge axis [8.8]

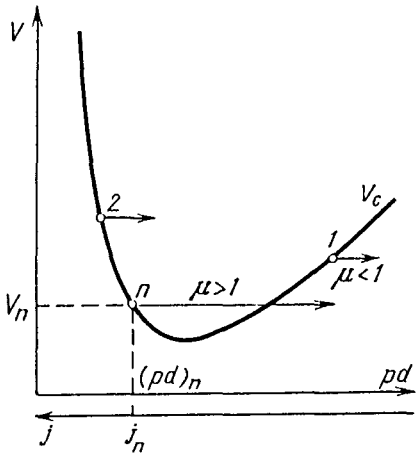

Fig. 8.10. Dependence of cathode fall V_C on layer thickness d and current density j

(8.1), the discharge voltage then increases due to the external resistance Ω, so that j in the homogeneous part of the layer increases until it reaches j_n.

Assume that a strongly supernormal layer has developed (point 2 in Fig. 8.10). The state in its central, quasihomogeneous part is stable. However, when we move to the right of point 2 (edgeward), where equipotential surfaces deviate from the cathode, we enter a region of increasing reproduction of charges, $\mu > 1$. Breakdown occurs at the edge of the cathode spot. A growth in the spot size increases the total current. The voltage across the electrodes decreases and j in the homogeneouss part of the layer drops. Point 2 slides downward until the state stabilizes at the edge, as well as in the middle of the layer.

The normal, that is, completely stable, state corresponds to point n, slightly above the minimum of the supernormal branch [8.5]. This is connected with the diffusion transport of charges to the edge zone, where $\mu < 1$; this transport sustains there a nondecaying non-self-sustaining current. This sustainment requires, however, that charge generation be enhanced ($\mu > 1$) in the region that lies closer to the midpoint. In the absence of diffusion, point 2 would move downward to the bottom, the normal state would coincide with the minimum V_C, and the edge of the cathode spot would become sharply defined. However, this state is incompatible with electrostatics. Equipotentials cannot be parallel up to the edge of the space charge zone and start deviating only beyond this zone.

8.4.10 Nonlocal Nature of Electron Spectrum and of the Ionization Coefficient in the Cathode Layer

So far, when establishing the conditions of self-sustainment of the discharge and the integral characteristics of the layer (V_C, d, j), we regarded the ionization coefficient α as a function of the local field $E(x)$. The (Townsend) dependence $\alpha(E)$ was taken from experimental data on ionization in homogeneous fields. This approximation is sufficient for obtaining integral characteristics, but it gives a severe distortion to the pattern of ionization produced by electrons at the end of the cathode layer and in the adjacent region; the understanding of the processes in this region is therefore seriously thwarted (Sect. 8.5). The point is that within the cathode layer, the field varies by a factor of 10^2–10^3; the thickness of this layer does not exceed 10 free path lengths for inelastic collisions, or $\ln(1 + 1/\gamma) \approx 3$ ionization length (α^{-1}). This inhomogeneity of E is too sharp for the equilibrium energy spectrum [corresponding to the local field $E(x)$] to set up, as it would in the case of a weak inhomogeneity. The actual ionization coefficient $\alpha(x)$ is also different from the Townsend one, $\alpha[E(x)]$.

Electrons move in the direction of weaker field; their spectrum is *harder* (i.e. of higher energy) than the equilibrium spectrum, and the ionization coefficient is greater because before arriving at a given point, electrons had gained energy in a stronger field and did not "forget" this fact. In the limiting case of a very small number of inelastic collisions, the energy of electrons is determined not by the field as such, but by the *potential difference* traversed. As a result of *nonlocal effects*, electrons with substantial energies are present among those emerging

from the cathode layer; some of them have been created at the cathode and crossed the entire layer without a single inelastic collision. Their energies are eV_C, that is, hundreds of electron volts. These electrons, discovered a long time ago, are known as the "beam".

Current efforts in the cathode-layer theory are aimed at taking into account the nonlocal effects.[7] The rigorous approach is possible only on the basis of the solution of the kinetic equation for electrons in an inhomogeneous field. One of the approximations is to replace the local field $E(x)$ in the Townsend coefficient α with the mean field over the preceding path Δx on which the electron gains the energy $\int_{x-\Delta x}^{x} eE\,dx$ equal to th ionization potential [8.11]. The most complete and reliable information is obtained by *Monte Carlo simulation* of the stochastic process in the cathode layer; this has so much advanced in recent years [8.12] that it has become essentially a method of numerical solution of the kinetic equation. The solution is obtained by extensive, time-consuming computations that are only feasible if powerful computers are employed.

The results of computations, even though involvinig a number of simplifications, are impressive (Figs. 8.11, 8.12) and enable us to look at a sequence of stages of the process. Electrons with energies from small values up to 10–

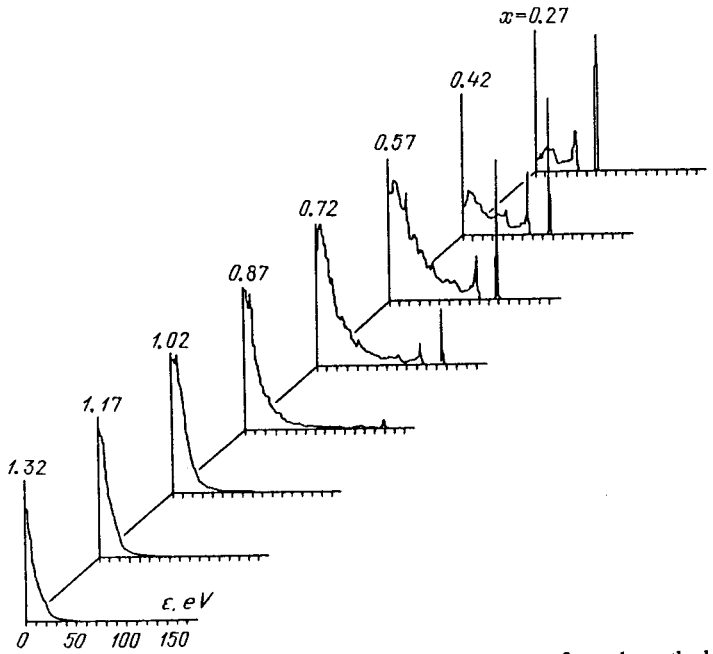

Fig. 8.11. Electron energy spectra at various distances x from the cathode in the cathode layer of normal glow discharge in He at p = 1 Torr. Calculations assume V_0 = 150 V, the field E = $230(1-x/1.3)+1$ V/cm in the cathode layer if $0 < x < 1.3$ cm, and E = 1 V/cm if $1.3 < x < 1.5$ cm [8.12]

[7] This aspect is unrelated to the problem of normal current density.

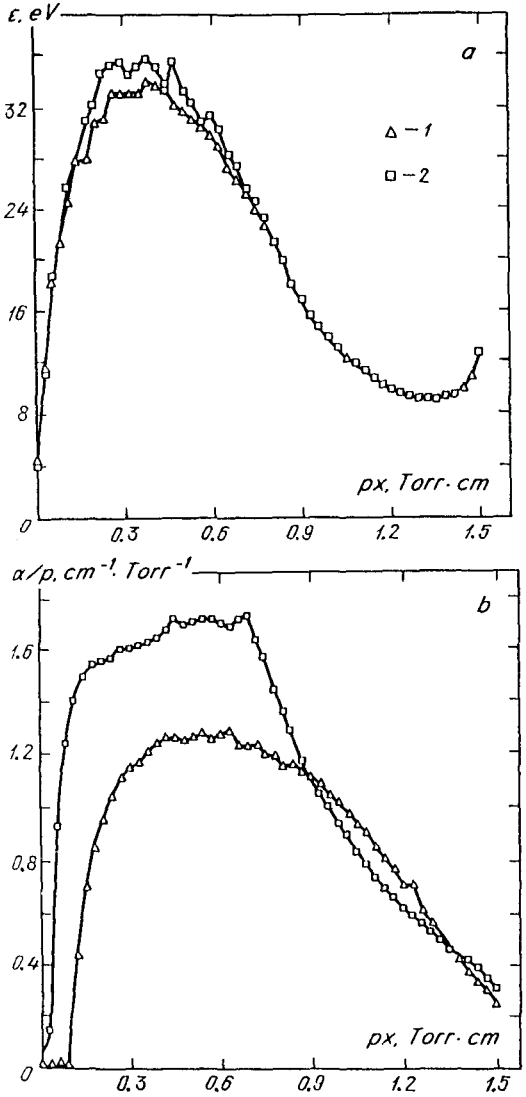

Fig. 8.12. The distributions of (a) mean electric energy $\bar{\varepsilon}$ and (b) the ionization coefficient α as a function of the coordinate x of the cathode ($p = 1$ Torr); calculations used the spectrum of Fig. 8.11 [8.12]:
Δ – isotropic elastic scattering
□ – anisotropic elastic scattering, with forward scattering dominating

20 eV are detected on emergence from the layer, and a low-intensity beam is also found. Away from the cathode, the peak of the "beam" rapidly diminishes and disappears on the scale of Fig. 8.11. On the emergence from the cathode layer, it constitutes 10^{-3} of the distribution function for $\varepsilon = 0$; the mean energy on the emergence from the layer at $x = 1.3$ cm is $\bar{\varepsilon} \approx 10$ eV. If nonlocal effects are neglected, one gets $\bar{\varepsilon} \approx 2.9$ eV ($E/p = 1$ V/(cm·Torr); Sect. 2.3.5) and $\alpha \approx 0$.

The real ionization coefficient at the farther layer boundary is half the maximum value at the middle; on the other hand, the equilibrium coefficient $\alpha[E(x)]$ has its maximum at the cathode ($1.7\,\mathrm{cm}^{-1}$), and is many orders of magnitude smaller (practically zero) at the boundary. However, the details of the output spectrum do not agree with experimental data. Three groups of electrons were detected at the emergence from the cathode layer in helium: electrons with the mean energy of 2 eV (they are predominant), those with 22.5 eV (their number is two orders of magnitude less), and a weak beam with $\varepsilon = 150\,\mathrm{eV} \approx eV_\mathrm{n}$ [8.13].

Section 5.9 outlined the "forward-backward" approximation for solving the kinetic equation in strong nonuniform fields. The approximation was tested under conditions assumed in the calculations of [8.12]. Satisfactory agreement with Figs. 8.11 and 8.12 was obtained. The method was used to take into account nonlocal effects in the von Engel–Steenbeck self-consistent calculation of the current-voltage characteristics of the cathode layer in helium (Sect. 8.4.2). The normal-discharge parameters found in [8.14], $V_\mathrm{n} = 142\,\mathrm{V}$, $j_\mathrm{n} = 3 \cdot 10^{-6}\,\mathrm{A/cm^2}$, $d_\mathrm{n} = 2.2\,\mathrm{cm}$ for $p = 1\,\mathrm{Torr}$, and also the abnormal branch, are in much better agreement with the experiments than those using the Townsend coefficient $\alpha[E(x)]$ and A and B of Table 4.1. The rate of electron production increases away from the cathode, reaches a maximum (in normal discharge) of $q \approx 8 \cdot 10^{12}\,\mathrm{cm^{-3}s^{-1}}$ at the end of the cathode layer, for $x \approx 2\,\mathrm{cm}$, and vanishes only at a distance of $x \approx 4$ to 5 cm. Roughly a half of the electrons are produced byond the cathode layer, in the weak field assumed to be 0.1 V/cm. A self-consistent (in contrast to [8.12]) cathode layer calculation using Monte Carlo techniques has recently appeared in [8.15]. Like the calculation of [8.10] with $\alpha(E)$, it mostly confirmed the linear law (8.12) of field decrease with distance from the cathode.

8.5 Transition Region Between the Cathode Layer and the Homogeneous Positive Column

The section heading refers to the regions of negative glow and Faraday dark space, terms that reflect the visual attributes. We are interested in the processes responsible for the longitudinal structure of glow discharges: the field and charge density distributions along the x axis and the current transport. In this respect, the two regions are a coherent whole (Fig. 8.2).

8.5.1 The Decisive Role of Energetic Electrons Supplied by the Cathode Layer

These electrons dissipate energy in the excitation and ionization of the gas, thereby causing intensive light emission (and sharply increased ionization in the region where the field is insufficient for such processes). On the other hand, intense ionization is a factor causing a drop in field strength, because the current density along the direction of current remains constant in one-dimensional

stationary discharges (this is also valid for discharge in a tube). Therefore, in the framework of the frequently justified assumption of constant mobility μ_e, we have $n_e E$ = const; hence, the field E at the point $n_{e,max}$ is weaker than in the positive column, where n_e is lower; this is indeed supported by Fig. 8.2, which schematically represents the results of experiments.

The rôle of nonlocal effects that produce a powerful electron source not attributable to the effect of the local field is especially well pronounced if we ask what would happen if the ionization decreased everywhere monotonously as the field decreased (as in the case of ionization with equilibrium Townsend coefficient). The distributions of n_e, n_+, and E along the x axis within the gap are then described by (8.2, 6, 3). Actually, (8.2) must be complemented with terms for charge loss in order to allow for the formation of a homogeneous lpositive column, with ionization compensating for losses (Sect. 8.6). Both a qualitative analysis and a numerical integration of the system show that the field monotonically decreases from the cathode value to that corresponding to the positive column, and n_e also increases in a monotonic manner. We thus come to a natural transition from the cathode layer to the positive column, without a region of field drop [8.9]. We can say that the Faraday space would not form without a flux of energetic electrons outside the layer in which current is self-sustained, that is, without nonlocal effects.

8.5.2 Probe Measurements

The relevant data are plotted in Fig. 8.13. The measured electron temperature $T_e \approx 0.12\,\text{eV}$ is practically constant across the region and does not depend on the current. The potential is almost unchanged within the investigated length, and E/p does not exceed 0.01 V/(cm·Torr). The latter result is likely to be beyond the accuracy of the measurements. It is easy to evaluate that this E/p is too small for supporting the drift transport of the current at $n_{e,max}$, when both the gradient of n_e and diffusion current vanish. Slow electrons are maxwellian because the frequency of electron-electron collisions at such low temperatures substantially exceeds the energy loss frequency (2.17) in collisions with atoms. These are the electrons that were created at the very end of the cathode layer, where the field that could accelerate them is almost zero, and also electrons, created by high-energy electrons, that have dissipated their energy. They are known as "final" electrons. Probe measurements of the distribution function pointed to the exis-

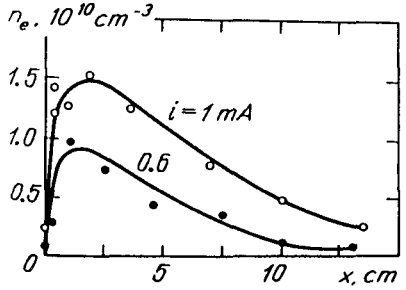

Fig. 8.13. Measured density distributions of slow electrons in the negative glow and Faraday space on the tube axis. Discharge in helium, p = 1.5 Torr. Coordinate x is measured from the beginning of the negative glow, towards the anode [8.1, 16]

tence of a second group of electrons with $T_e \approx 3$–4 eV. Their density is smaller by a factor of 100–200. These electrons are sometimes called "secondary". They are produced somewhat deeper in the cathode layer and are slightly accelerated in the field. Not too energetic electrons having undergone an inelastic collision and retaining this energy are likely to belong to this group too. The third group comprises a small number of electrons; this is the beam (the three groups were also mentined in Sect. 8.4.10).

Recent measurements in helium under similar conditions [8.17] (p = 1 Torr, R = 1.5 cm) but at a higher current (i = 15 mA) yielded greater values of E/p and $T \sim 1$ eV and a shorter Faraday space (about 3 cm). It is of interest that the diffusional current is almost balanced out by the oppositely directed thermodiffusional current, so that only the drift component is present.

8.5.3 Role Played by Electron Diffusion

As a result of a sharp maximum of electron density that falls off steeply towards the anode, the current in the region of density drop may be sustained by electron diffusion, as described in Sect. 2.7.2.[8] The field is thereby cancelled. Owing to the drop in electron density, the diffusion flux gradually decreases, the field gets restored [see (2.42)], the diffusion is gradually replaced with drift, and the Faraday space is transformed into the positive column (provided the anode is still far removed; see Fig. 8.2). This situation also arises in a low-voltage arc. It has been approximately modelled in [8.18, 19, 1].

The drop in n_e from the maximum towards the anode is caused by electron losses not replenished by ionization (which is absent). Under the conditions of Fig. 8.13, electrons are removed by ambipolar diffusion to the walls, where subsequent neutralization takes place. *Bulk recombination* (and attachment in electronegative gases) becomes predominant at high pressures when diffusion is impeded.

8.5.4 Main Factors Determining the Longitudinal Structure of Discharge in a Gap

Three factors are thus important for the formation of the transition from the cathode layer to the homogeneous positive column via the negative glow and Faraday space. (1) The presence of a powerful ionization source at the end of the cathode layer; the source is not dependent on the local field strength. (2) Local charge loss (bulk recombination, ambipolar diffusion to the wall) not related to its current to the electrodes. (3) Diffusion of electrons along the current direction. No adequate theory of the transition region is possible if anyone of these factors

[8] It is sometimes mentioned (see, e.g. [8.1]) that the beam participates in charge transfer. In fact, only a small fraction of the electrons emitted from the cathode is transformed into the beam; besides, the electronic current from the cathode is a small fraction, $\gamma/(1+\gamma)$, of the total. The current is not increased by accelerating the beam to a high velocity, but the electron density is reduced.

is ignored (advances in this theory are very moderate). Early work in this field is described in [8.1], and the problem is discussed in [8.9].[9]

8.5.5 Hollow Cathode Discharge

If the cathode is arranged as two parallel plates (the anode being shifted to the side) and the cathode plates are brought closer and closer, the current increases hundreds and thousands of times after a certain distance is reached. This takes place when two formerly nonoverlapping regions of negative glow merge: the glow becomes considerably more intensive, and the voltage changes slightly. A similar effect can be obtained if the cathode is a hollow cylinder and the anode lies far along the axis. The pressure must be such that the cathode layer thickness is comparable with the cylinder diameter. In a hollow cathode, electron streams converge to the axis and produce intensive ionization and excitation of the gas. Photoemission excited on the cathode by UV radiation produced in this region also plays a role here.

8.6 Positive Column

8.6.1 The Function It Serves; Causal Relationships

The positive column closes the electric circuit in the space between the cathode layer and the anode; this is its only function. The state of the plasma in a sufficiently long column is completely independent of the situation in the *regions adjacent to the electrodes*. It is determined by *local* processes and by the electric current. The inevitable loss of charge carriers (electrons) in the column must be

[9] *Note added in proof.* The author and M.N. Shneider have recently computed the glow discharge longitudinal structure. Distributions of n_e, n_+, E, $\bar{\varepsilon}$ (or T_e) are obtained along the x-axis from the cathode to the uniform positive column (PC) inclusively. The patterns look like those in Fig. 8.2. Non-local effects in the cathode layer (CL) and the negative glow region (NG) are described by the method discussed at the end of Sects. 8.4.10 and 5.9. Besides the three necessary factors mentioned in Sect. 8.5.4, electron heat conductivity and thermodiffusion are also taken into account. In helium for $p = 1$ Torr and $j = 2.7\ 10^{-5}$ A/cm^2 (this is an order of magnitude higher than normal j_n) the CL stops at $x = 1.3$ cm, and NG at $x = 2$ cm. The Faraday space (FS) stops at $x \approx 4$–6 cm for a tube radius of $R = 1.35$ cm and $x \approx 8$–10 cm for $R = 5$ cm (the length of the FS for low pressure is about a few R). At the beginning of the FS the field falls to a very small magnitude and changes direction, remaining very weak. The temperature T_e falls to a few tenths of an eV in the middle of the FS. The maximum of n_e at the end of the NG is $n_{e\,\max} \approx 3 \cdot 10^9$ cm^{-3} while in the PC $n_e \approx 10^8$ cm^{-3} (for $R = 1.35$ cm). From a physical point of view the magnitude of $n_{e\,\max}$ is determined by the condition that the current in the region of falling n_e, after the maximum is carried by diffusion $j \approx eD_e dn_e/dx \approx eD_e n_{e\,\max}/X$, where the scale X of n_e decrease is determined by ambipolar diffusion of electrons to the wall, with the longitudinal drift as a background $X \approx v_d(R/2.4)^2/D_a$. Such an estimation of $n_{e\,\max}$ agrees well with calculations. The transition from the FS to the PC is found to be non-monotonic (n_e passes through a minimum, E and $\bar{\varepsilon}$ through a maximum). This is connected with the time lag of $\bar{\varepsilon}$ and ionization growth, while the restoring E (as in the case of striations; Sect. 9.7). These results are published in [8.14].

compensated for by ionization. The field strength E necessary for sustaining a stationary plasma is fixed because the ionization rate depends, and quite sharply, on the field, through the dependence of the electron energy distribution. This determines the longitudinal potential gradient and the voltage difference across a column of a given length. If the spectrum is maxwellian, the relationship can be separated into two causally linked parts: (1) The requirement of loss compensation by ionization shows what the electron *temperature* T_e must be; (2) The *field* must supply the necessary energy to electrons. The relation between E and T_e follows from the balancing of the electron energy (Sect. 2.3). The *gas temperature* T is determined by the balance of the gas energy as a whole. In the positive column of glow discharge, we have $T_e \gg T$.

The creation and removal of electrons in the column proceed against a steady background of unceasing electron replacement due to the drift motion from the cathode to the anode. It cannot be said that a considerable fraction of charge carriers are generated in the glow discharge column. Rather, the majority of electrons reaching the anode enter the column from the outside (from the cathode region). The probability for them to be lost on the way is not high, except for cases of exceptionally long interelectrode separations.

8.6.2 Balance of Charge Numbers in Cases Without Attachment

Consider a long positive column in a tube (or plane chanel) so long that it can be treated as homogeneous along the current direction x. According to (3.14), curl $\boldsymbol{E} = 0$ in stationary conditions; hence, a longitudinal field homogeneous in x is independent of transversal coordinates (the transverse polarization field is neglectigible in comparison with the longitudinal one). The charge density in the quasineutral plasma of the column is described by (2.44), where q includes ionization and bulk recombination. Denoting the transverse part of the Laplacian by the subscript $\perp$, we arrive at the equation

$$D_a \nabla_\perp^2 n + \nu_i(E) n - \beta n^2 = 0 \,. \tag{8.17}$$

Assume that the precipitation of charges on the walls is more intensive than bulk losses. It is said in such cases that the discharge is *controlled by diffusion or by recombination at the walls*. Without the term βn^2 and with the boundary condition $n = 0$ at $r = R$, (8.17) results in the Bessel radial profile $n \propto J_0(2.4r/R)$, (see Sect. 4.8) and in the condition of equality of ionization frequency and the effective frequency of diffusional loss:

$$\nu_i(E) = D_a/\Lambda^2 \equiv \nu_{da} \,, \quad \Lambda = R/2.4 \tag{8.18}$$

[*Schottky*, (1924)].[10] The case $\beta n \ll \nu_{da}$ is realized at low pressure and small transverse dimensions ($\nu_{da} \propto 1/p\Lambda^2$), at not too high currents, so that n is moderate; it is facilitated in monatomic gases where the bulk recombination proceeds slower than in molecular gases.

[10] In plane geometry, the profile is cosine-shaped and Λ is given by (4.12).

Let us look at an example. In nitrogen, $\mu_+ p \approx 1.5 \cdot 10^3\,\mathrm{cm^2 \cdot Torr/(V \cdot s)}$, $T_e \approx 1\,\mathrm{eV}$, $D_a p = (\mu_+ p) T_e \approx 1.5 \cdot 10^3\,\mathrm{cm^2 Torr/s}$. If $p = 10\,\mathrm{Torr}$, $R = 1\,\mathrm{cm}$, and $D_a \approx 150\,\mathrm{cm^2/s}$, we find $\nu_{da} \approx 900\,\mathrm{s^{-1}}$. If the recombination coefficient (dissociative: see Sect. 4.3.2) $\beta = 1.6 \cdot 10^{-7}\,\mathrm{cm^3/s}$, the condition $\beta n < \nu_{da}$ holds up to $n \approx 6 \cdot 10^9\,\mathrm{cm^{-3}}$, which corresponds to current density $j = e(\mu_e p) n_e (E/p) \approx 1.2\,\mathrm{mA/cm^2}$ [by Table 2.1, $\mu_e p \approx 4.2 \cdot 10^5\,\mathrm{cm^2 Torr/(V \cdot s)}$; $E/p \approx 3\,\mathrm{V/(cm \cdot Torr)}$]. The total current $i \approx j\pi R^2 \approx 3.5\,\mathrm{mA}$. if the current is smaller than this value, the discharge is controlled by diffusion, otherwise it is controlled by *bulk recombination.*

The probability for an electron drifting along the column of length L to attach to the wall is $\nu_{da} t$, where $t = L/v_d$ is the drift time. The probability can be expressed in terms of gas characteristics and size using (2.36, 24, 21, 16):

$$\frac{\nu_{da} L}{v_d} = \frac{D_e L}{\Lambda^2 v_d} \frac{\mu_+}{\mu_e} = \frac{1}{3} \frac{lL}{\Lambda^2} \frac{\bar{v}}{v_d} \frac{\mu_+}{\mu_e} \approx \frac{0.4 lL}{\Lambda^2 \sqrt{\delta}} \frac{\mu_+}{\mu_e} . \tag{8.19}$$

In our case the probability is $7 \cdot 10^{-4}$ per 1 cm of length. Even a metre-long column transmits 93 % of electrons (provided the bulk recombination is low). The estimate assumes $lp = 0.03\,\mathrm{cm \cdot Torr}$, $\delta = 1.2 \cdot 10^{-3}$.

If $\beta n \gg \nu_{da}$, the recombination of charges in the bulk dominates over their diffusion to the walls. If the diffusion term in (8.17) is dropped, we find $\nu_i(E) = \beta n$, that is, the density is constant over the cross section. In fact, a large gradient of n appears at the absorbing walls, and diffusion there cannot be neglected. Density changes only slightly in the main part of the section but drops sharply near the walls. Using (8.17), one can write an interpolated balance equation covering both limiting cases and ensuring a smooth transition between the two:

$$\nu_i(E) - \nu_{da} - \beta n = 0 . \tag{8.20}$$

8.6.3 Field Strength and Current-Voltage Characteristic

If the column is diffusion controlled, E is found from (8.18) and is independent of electron density, and hence, of current. This occurs because the rates of creation and removal of electrons are proportional to n. In this approximation, the $V - i$ curve is represented by a horizontal line both for the column and for the discharge as a whole, provided it is normal: $V(i) = V_n + EL = \mathrm{const}$. The field in the column (Fig. 8.14) obeys the similarity law $E/p = f(p\Lambda)$, which follows from the dependences $\nu_i = p f_1(E/p)$, $\nu_{da} \propto 1/p\Lambda^2$. As we see from Fig. 8.14, some decrease in E/p as the current increases by an order of magnitude is caused by a rise in gas temperature (Sect. 8.7.4). It is worthy of note that the discharge is sustained in air, in which ionization dominates attachment only if $E/p \gtrsim 35$ (Sect. 7.2.5), at substantially lower values of E/p. The reason is that many molecules that are active with respect to detachment accumulated under stationary conditions to high concentration. Attachment is then partially balanced out by detachment, with electron losses being lower than in breakdown or in short transient discharges (Sect. 8.8). The effect of two-stage ionization (ionization of excited molecules) may also be involved.

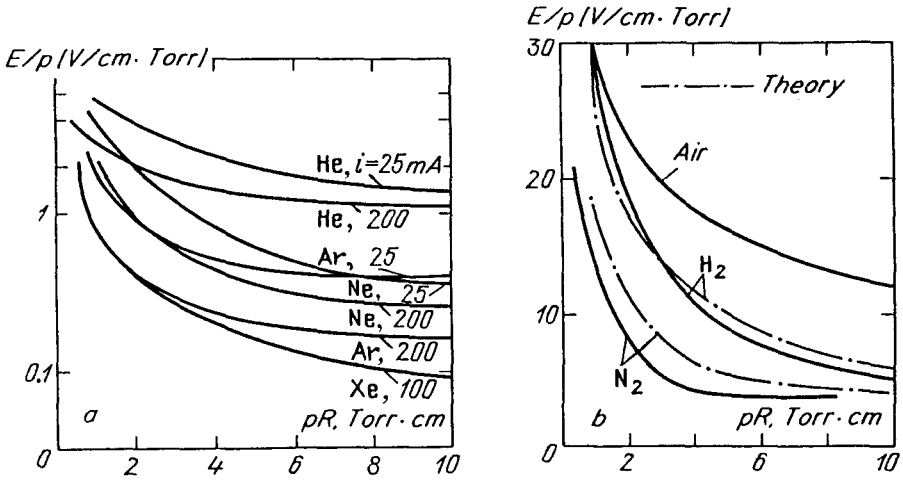

Fig. 8.14. Measured values of E/p for the positive column in tubes: (a) inert gases, (b) molecular gases [8.3]

It must be emphasized that the field required for plasma sustainment in the column is always lower than that required for gaseous breakdown under the same conditions. In breakdown, electrons are freely diffusing towards the walls. The diffusion in a well-developed discharge is ambipolar and substantially slower.

If discharge currents are considerable, the degree of ionization increases and bulk recombination becomes important. The current-voltage characteristic of the column is then given by the expression

$$n_e = \frac{\nu_i(E) - \nu_{da}}{\beta}\,, \quad j = \frac{e(\mu_e p)}{\beta}\,\frac{E}{p}\,[\nu_i(E) - \nu_{da}] \tag{8.21}$$

that follows from (8.20). If the discharge is controlled by bulk recombination ($\nu_i \gg \nu_{da}$), E increases with j, albeit slowly. This mode is more likely to manifest itself in molecular gases, where recombination is strong. In inert gases the *contraction* of the positive column into the *current filament* occurs earlier (Sect. 9.8).

8.6.4 Electron Temperature and Its Relation to Field Strength

Consider a diffusion-controlled discharge. Substituting (4.2) for ν_i in (8.18) if the spectrum is maxwellian, and (2.36) for D_a, gives an equation for T_e:

$$\left(\frac{kT_e}{I}\right)^{1/2} \exp\frac{I}{kT_e} = \frac{C_i}{\mu_+ p}\left(\frac{8I}{\pi m}\right)^{1/2}\frac{N}{p}(p\Lambda)^2 = \text{const}\,(pR)^2\,. \tag{8.22}$$

In this way von Engel and Steenbeck [8.2] determined the dependence, universal for all gases, of kT_e/I on cpR (Fig. 8.15); here c is a constant, specific for each

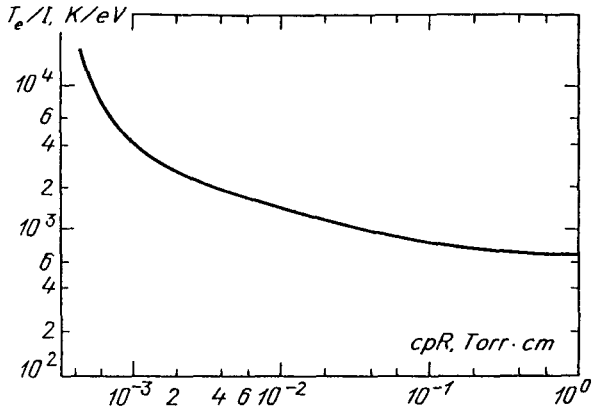

Fig. 8.15. Universal curve for calculating T_e in a positive column as a function of cpR. The constants c for several gases are given in the text [8.3]

gas, and is calculated using the data on μ_+, C_i, and I. The constant c in different gases is:[11]

$$\text{He} - 4 \cdot 10^{-3}\,, \quad \text{Ne} - 6 \cdot 10^{-3}\,, \quad \text{Ar} - 4 \cdot 10^{-2}\,,$$
$$\text{H}_2 - 1 \cdot 10^{-2}\,, \quad \text{N}_2 - 4 \cdot 10^{-2}\,.$$

For instance, for nitrogen and $R = 1\,\text{cm}$, $p = 10\,\text{Torr}$, we find $T_e \approx 0.9\,\text{eV} = 10,400\,\text{K}$. The electron temperature decreases with increasing tube radius and pressure: diffusion losses are reduced and a lower ionization rate is sufficient. It is clear why the positive column is dark in wide vessels: the electron temperature is too low.

The relation between the mean electron energy $\bar{\varepsilon} = 3kT_e/2$ and the field was discussed in Sect. 2.3.5. Assuming the electron path length to be independent of energy, we have $T_e \propto E/N$; if the collision frequency is assumed constant, $T_e \propto (E/N)^2$. The former assumption is preferable. It was shown in Sect. 2.3.6 that except at very low pressures, the electron drift velocity under the conditions exactly corresponding to the glow discharge positive column is much lower than the random one. Roughly speaking, the electron spectrum is said to be maxwellian if the frequency of electron-electron collisions ν_{ee} is appreciably higher than the energy loss frequency $\nu_u = \delta\nu_m$ (Sect. 2.3.7).

8.6.5 Why Is the Degree of Ionization in Weakly Ionized Gas Discharge Plasma Strongly Nonequilibrium?

The electron density in a *diffuse* positive column of a glow discharge (a *noncontracted* column filling the entire cross section of a tube is said to be diffuse) is of order $n_e \sim 10^8$–10^{11}, or 10^{12} at the most. If $p \sim 1$–$10\,\text{Torr}$, $N \sim 3 \cdot 10^{16}$–$3 \cdot 10^{17}\,\text{cm}^{-3}$, the degree of ionization of the gas is 10^{-8}–10^{-7}. At the same

[11] The proportionality factor in (8.22) is equal to $1.2 \cdot 10^7 c^2$.

time, the actual electron temperatures $T_e \approx 1$–$3\,\mathrm{eV}$ correspond to thermodynamical equilibrium ionizations of 10^{-2} to 1. This discrepancy results from the violation of the foremost requirement that ensures the attainment of thermodynamic equilibrium: the direct and reversed processes in the main reactions must be balanced.

In a glow discharge, atoms are ionized by electron impact, often from the ground state. Charge losses in cold rarefied gases occur at the walls and via dissociative recombination. The charge loss frequency in the example considered in Sect. 8.6.2 was $\nu_{da} \sim 10^3\,\mathrm{s}^{-1}$ for $n_e \lesssim 10^{10}\,\mathrm{cm}^{-3}$. The field and the electron temperature accomodated to these losses and produced the required ionization rate. However, three-body recombination with an electron trapped in the ground state of the atom [this process is reversed with respect to ionization described by (4.2)] gives a loss frequency of $10^{-10}\,\mathrm{s}^{-1}$. This is less by 13 orders of mangitude! There are no reverse processes of ionization that oppose the fast diffusional and dissociative losses.

The situation with strongly ionized equilibrium plasma is different. Diffusion and dissociative recombination are not important there because the gas is hot and dense, and molecular ions are rare. The charge density is high, and collision-radiative recombination is predominant, with electrons captured to upper levels (Sect. 4.3.4). Atoms are ionized as a result of a reverse process to this recombination: stepwise ionization from excited states. This is how the thermodynamically equilibrium ionization is achieved.

8.6.6 Inhomogeneous Plasma Column

When the geometry of the discharge volume and the electrode configuration are complicated, and there is a rapid transverse gas flow that offsets and bends the current channel, the plasma column between electrodes may be quite inhomogeneous and at the same time approximately electrically neutral; such conditions are encountered in high-power lasers (Sect. 14.4.2). In such cases, it is not expedient to employ the general system of equations (2.22, 20, 43) for finding the spatial distributions of plasma density and field $\boldsymbol{E} = -\nabla\varphi$, because Poisson's equation (2.43) then involves a small difference $n_+ - n_e$ of relatively large quantities. Two slightly different quantities n_e and n_+ must be replaced with a single one, $n \approx n_e \approx n_+$; this operation reduces the system of three quations to a system of two, (2.46) and (2.40).[12] If we assume $\mu_e = \mathrm{const}$, (2.40) reduces to $\mathrm{div}\,(n\boldsymbol{E}) = 0$. If the discharge is burning in a gas flux moving at a velocity $\boldsymbol{u}$, the convective term $n\boldsymbol{u}$ must be added to the plasma flux under the div sign in (2.46).

The elimination of $n_+ - n_e$ from the system is in accord with the actual causal relationship of the phenomena. When the space charge is small, the field in a nonhomogeneous conducting medium is determined by current distribution and

[12] The current distribution is quasistationary even in nonstationary plasma processes, owing to high relaxation rate of the bulk charge (Sect. 9.2.2). Consequently, the replacement of (2.39) with (2.40) is justified.

time, the actual electron temperatures $T_e \approx 1$–$3\,\mathrm{eV}$ correspond to thermodynamical equilibrium ionizations of 10^{-2} to 1. This discrepancy results from the violation of the foremost requirement that ensures the attainment of thermodynamic equilibrium: the direct and reversed processes in the main reactions must be balanced.

In a glow discharge, atoms are ionized by electron impact, often from the ground state. Charge losses in cold rarefied gases occur at the walls and via dissociative recombination. The charge loss frequency in the example considered in Sect. 8.6.2 was $\nu_{da} \sim 10^3\,\mathrm{s}^{-1}$ for $n_e \lesssim 10^{10}\,\mathrm{cm}^{-3}$. The field and the electron temperature accomodated to these losses and produced the required ionization rate. However, three-body recombination with an electron trapped in the ground state of the atom [this process is reversed with respect to ionization described by (4.2)] gives a loss frequency of $10^{-10}\,\mathrm{s}^{-1}$. This is less by 13 orders of mangitude! There are no reverse processes of ionization that oppose the fast diffusional and dissociative losses.

The situation with strongly ionized equilibrium plasma is different. Diffusion and dissociative recombination are not important there because the gas is hot and dense, and molecular ions are rare. The charge density is high, and collision-radiative recombination is predominant, with electrons captured to upper levels (Sect. 4.3.4). Atoms are ionized as a result of a reverse process to this recombination: stepwise ionization from excited states. This is how the thermodynamically equilibrium ionization is achieved.

8.6.6 Inhomogeneous Plasma Column

When the geometry of the discharge volume and the electrode configuration are complicated, and there is a rapid transverse gas flow that offsets and bends the current channel, the plasma column between electrodes may be quite inhomogeneous and at the same time approximately electrically neutral; such conditions are encountered in high-power lasers (Sect. 14.4.2). In such cases, it is not expedient to employ the general system of equations (2.22, 20, 43) for finding the spatial distributions of plasma density and field $\boldsymbol{E} = -\nabla\varphi$, because Poisson's equation (2.43) then involves a small difference $n_+ - n_e$ of relatively large quantities. Two slightly different quantities n_e and n_+ must be replaced with a single one, $n \approx n_e \approx n_+$; this operation reduces the system of three quations to a system of two, (2.46) and (2.40).[12] If we assume $\mu_e = \mathrm{const}$, (2.40) reduces to $\mathrm{div}\,(n\boldsymbol{E}) = 0$. If the discharge is burning in a gas flux moving at a velocity $\boldsymbol{u}$, the convective term $n\boldsymbol{u}$ must be added to the plasma flux under the div sign in (2.46).

The elimination of $n_+ - n_e$ from the system is in accord with the actual causal relationship of the phenomena. When the space charge is small, the field in a nonhomogeneous conducting medium is determined by current distribution and

[12] The current distribution is quasistationary even in nonstationary plasma processes, owing to high relaxation rate of the bulk charge (Sect. 9.2.2). Consequently, the replacement of (2.39) with (2.40) is justified.

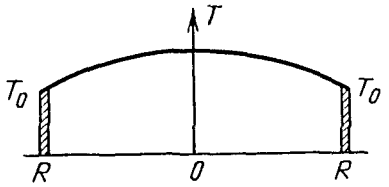

Fig. 8.16. Variation of gas temperature in a tube heated to a moderately high temperature

8.7.2 Convective Heat Transport

Another mechanism is possible for transporting heat out of a discharge: pumping of gas through the discharge volume, used in modern high-power laser systems (Sect. 8.1.2). This mechanism is *convective cooling*. Actually, a given mass of gas undergoes no cooling at all. Quite the opposite, a macroscopic portion of the gas is heated when it moves through the discharge; its temperature is gradually increasing in time and along the path. What is meant is the removal of heat from the discharge volume. If we again talk in terms of temperature T averaged over the flow length L_1, the rate of heat removal from the discharge volume can be written in the familiar form: $Nc_{p1}(T - T_0)\nu_F$. Now T_0 is the temperature of the gas entering the discharge, and $\nu_F \approx 2u/L_1$, where u is the flow velocity. The factor "2" takes into account that, on average, the heat is transported "half the distance". In a longitudinal discharge (Fig. 8.18), L_1 coincides with the interelectrode spacing L.

8.7.3 Energy Balance in the Gas

For greater clarity, let us start with the nonstationary balance equation. We take into account that the energy transfer from electrons to molecules is much faster than the outward transport from the gas. Hence, we consider the balance of electron energy to be stationary even if the gas temperature varies with time. The simplified equation for gas temperature is

$$Nc_{p1}\frac{dT}{dt} = jE - Nc_{p1}(T - T_0)\nu_{T,F} \,. \tag{8.23}$$

Under stationary conditions, the mean temperature is found from the equality

$$Nc_{p1}(T - T_0)\nu_{T,F} = jE \equiv w \,. \tag{8.24}$$

8.7.4 Dropping $V - i$ Characteristic

Experiments show that the $V - i$ curve of a diffusion-controlled discharge is not a horizontal but a slightly declining curve: as the current increases, the voltage slowly decreases. This effect results from gas heating. The current density is greater at the axis than at the walls, because the electron density there is greater (the field being constant over the cross section). The energy release and gas temperature at the axis are also higher than at the walls. However, pressure levels off in space (velocities are usually strongly subsonic even in discharges with flowing gas). Hence, the density of the gas is lower in regions of higher

temperature. The ionization frequency being actually a function of E/N, not of E/p, a lower field is required to sustain ionization in the main part of current cross section; the voltage is also reduced. The law of fall-off can be evaluated using (8.24), $p = NkT = \text{const}$, and an approximate condition $E/N \sim ET \approx$ const that follows from (8.18). We find

$$j/j_0 = (E_0/E)^{3/2}(E_0/E - 1)\,. \tag{8.25}$$

Here E_0 is the field required to maintain a very weak current $j \to 0$ when the gas heats up negligibly and its temperature does not deviate from the room value T_0;

$$j_0 = N_0 c_{p1} T_0 \nu_{T,F}/E_0\,,\quad w_0 = j_0 E_0\,. \tag{8.26}$$

These are characteristic scales of the current density and the rate of Joule heat release. With this energy release, the gas becomes heated to a temperature T twice as high as that of the walls.

8.7.5 Stable and Unstable States

When the $V - i$ characteristic is a dropping one, the load line often intersects it not at one but at two points (Fig. 8.17). One of the states, namely, the upper one, is unstable; hence, it cannot be realized. Indeed, if current fluctuates upward, a lower voltage is required to sustain it than the one that is prescribed by the load line for the new current value. The result is a disbalance between ionization and removal of electrons; ionization begins to rise, the discharge resistance decreases, so that the current starts to grow until the state reaches the lower intersection point. If the current fluctuation is negative, $\delta i < 0$, electrons begin to disappear until the discharge burns out. The lower state is stable. If $\delta i > 0$, $\delta n_e > 0$, voltage drops below the necessary value, and enhanced decay brings ionization back to the original state.

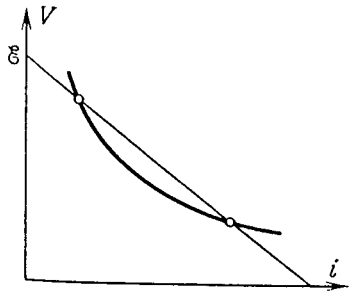

Fig. 8.17. $V - i$ characteristic, including gas heating effects. The loading curve is also shown

8.7.6 Gas Temperature and the Scales of Electric Parameters in Diffuse Glow Discharge

One of the most typical properties of this discharge is a sharp difference between the electron and gas temperatures. We have already discussed why the electron temperature is necessarily high: electrons are to ionize atoms. The same factors determine the order of magnitude of E/p in the column: $E/p \approx 0.2$–$20\,\mathrm{V/(cm{\cdot}Torr)}$. The gas temperature T is determined by the balance of energy release and heat removal, (8.24). The relative increase over the wall temperature (room temperature) is

$$(T - T_0)/T_0 = w/w_0 = jE/j_0E_0 \,.$$

The scales of energy release w_0 and current density j_0 are given by (8.26). They correspond to doubling the temperature. The thermal conductivity of most gases at $T \approx 300$–$600\,\mathrm{K}$ is $\lambda \approx (2\text{–}5) \cdot 10^{-4}\,\mathrm{W/(cm{\cdot}K)}$. In monatomic gases, $c_{p1} = (5/2)k$, and in two-atom gases, $(7/2)k$. With intermediate values $\lambda = 3 \cdot 10^{-4}$, $c_{p1} = 3k$, the thermometric conductivity is $\chi = 220/p\,\mathrm{cm^2/s}$ [p in Torr]. In tubes (or channels) of $R = 1\,\mathrm{cm}$, the heat transport to the walls is characterized by a frequency $\nu_T \approx 1.3 \cdot 10^3/p\,\mathrm{s^{-1}}$. For a typical value $E/p = 3\,\mathrm{V/(cm{\cdot}Torr)}$, the energy release and current density scales are $w_0 = 0.5\,\mathrm{W/cm^3}$ and $j_0 = 170/p\,\mathrm{mA/cm^2}$. According to (2.6,7), the electron density scale for $\nu_m = 3 \cdot 10^9 p\,\mathrm{s^{-1}}$ is $n_e^0 \approx 6 \cdot 10^{11}/p\,\mathrm{cm^{-3}}$.

Experience shows that discharge rarely preserves a diffuse form if the gas in it is heated appreciably, say, to twice the original temperature. *Contraction* transforms the column into a *filament* with sharply increased current density and gas temperature; this stage is intermediate to the transition of a glow discharge into an arc at still greater current. The scales given above characterize the upper bounds on the realization of the weakly ionized cold plasma of the diffuse glow discharge. The higher the pressure, the lower this upper bound in current and electron density, the more intensive the heating of the gas at a given current. Therefore, low pressure is favourable for sustaining nonequilibrium weakly ionized plasma, and high pressure (of the order of atmospheric) is favourable for equilibrium plasma; this is indeed supported by discharge experience.

In convective heat transport, the scales depend on pressure differently: ν_F, j_0, and n_e^0 are independent of pressure, and $w_0 \propto p$. For example, for $L_1 = 10\,\mathrm{cm}$, $u = 50\,\mathrm{m/s}$, $\nu_F \approx 10^3\,\mathrm{s^{-1}}$, we find $w_0 \approx 0.4p\,\mathrm{W/cm^3}$. Taking a more realistic value, $E/p \approx 10$, we have $j_0 \approx 40\,\mathrm{mA/cm^2}$ and $n_e^0 \approx 1.5 \cdot 10^{11}\,\mathrm{cm^{-3}}$.

8.7.7 Positive Column in Nitrogen

For a number of reasons, among which we find applications to gas lasers and plasma chemistry, nitrogen attracts the attention of researchers in electronic, vibrational, and ion-molecular processes in weakly ionized non-equilibrium discharge plasmas. Experiments and efforts toward their theortical interpretation [8.21–26] indicate both the diversity and the complexity of ionization mecha-

nisms in the positive column plasma. These mechanisms not always satisfy the simplest scheme of electron impact ionization of atoms and molecules in the ground state, as the general description of discharge columns often assumes. Any attempt to interpret the observed values of E/N in the column immediately reveal the inadequacy of this mechanism.

Table 8.4 gives an idea of the state of discharge on the axis of the column in extra-pure nitrogen within a long tube of 1.6 cm radius [8.21]. The last column of the table gives the effective ionization rate constant, $k_{i,eff}$ found from the relation $q_{loss} = k_{i,eff} N n_e$ which is equivalent to (8.20). Even if we take into account high vibrational temperature $T_v \approx 5000$ K, formulas (5.40, 41) give k_i several orders of magnitude lower. Stepwise ionization does not give anything significantly greater. In order to explain the observed ionization rates by electron impacts, we need $E/N \approx (7\text{–}8) \times 10^{-16}$ Vcm^2 ($E/p_{20} \approx 25$ V/cm Torr). In fact, even lower values of E/N were observed at pressures of tens of Torr, down to $(1.5\text{–}2)\times 10^{-16}$ Vcm^2 [8.22, 23].

According to current understanding, associative ionization of the type $N_2 + N_2 \rightarrow N_4^+ + e$ takes place in such weak fields, involving all molecules in the upper vibrational ($v \geq 32$) and/or upper electronic states. The latter are produced not ordinarily, through electron impact, but in collisions of two vibrationally excited molecules with $v \geq 16$. The population at the upper vibrational levels rapidly increases owing to the intense exchange of vibrational quanta in molecular collisions.

8.8 Electronegative Gas Plasma

8.8.1 Attachment-Controlled Discharge

In some cases the main mechanism of removing electrons is via attachment that is not accompanied by detachment, so that attachment acts in a straightforward manner. This situation takes place in short-pulse discharges, and at an early stage ($t < 10^{-5}$–10^{-3} s) of longer discharges while a sufficient number of molecules active with respect to detachment has not yet built up. Pressure must not be too low ($p \gtrsim 10$ Torr), in order to avoid diffusional losses. For recombination to be dominated by attachment, the current and density of electrons must not be too high, $n_e < 10^{12}$–10^{13} cm^{-3}.

Most often, attachment proceeds via the dissociative mechanism, with energy consumption (Sect. 4.4). The reaction $e + CO_2 \rightarrow CO + O^-$, which is the main one in laser mixtures of $CO_2 + N_2 + Ne$, requires 3.85 eV.[13] For this reason, the frequency ν_a and the coefficient of attachment $a = \nu_a/v_d$ increase quite considerably with E/p, but not as sharply as the ionization frequency and ionization coefficient ν_i and α : the ionization potential is several times greater (Figs. 8.18, 19) [8.27–29]. The molecules ionized in the laser mixture are CO_2, having the lowest

[13] O^- ions then join CO_2 molecules and form stable CO_3^- complexes.

Table 8.4. The state of nitrogen plasma in the positive column in a tube at $p = 3.9$ Torr [8.21] [a]

i [mA]	j [mA/cm^2]	E [V/cm]	T [K]	N [10^{16}cm^{-3}]	E/N [10^{-16}V/cm^2]	E/p_{20} [V/(cm Torr)]	n_e [10^{10}cm^{-3}]	N_A [10^{12}cm^{-3}]	N_{35} [10^{13}cm^{-3}]	ε_v [eV]	$k_{i,eff}$ [10^{14}cm^{-3}]
10	1.3	41	420	9.0	4.5	15	0.36	1.2	1.6	0.23	2
75	9.5	23	650	5.8	4.0	13	2.9	1.2	3.6	0.60	5

[a] p_{20} corresponds to N and $t = 20°$ C ;
N_A is the density of metastables $A^3 \sum_u^+$;
N_{35} is the calculated density at the vibrational level with $v = 35$;
ε_v is the mean vibrational energy of molecules

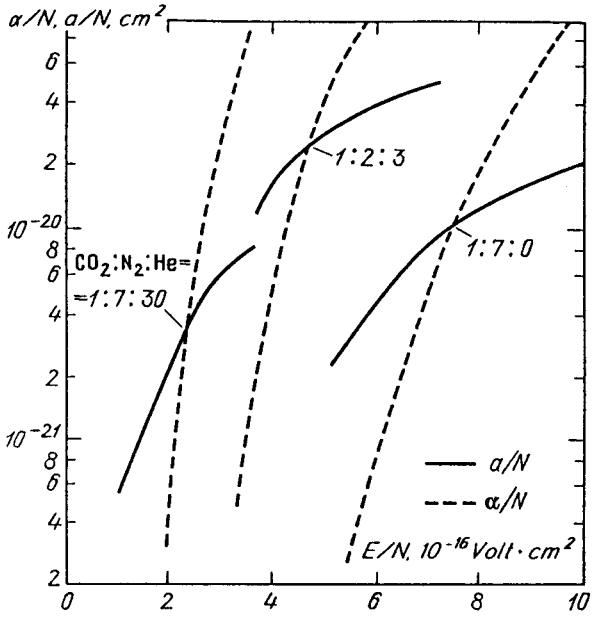

Fig. 8.18. Coefficients of ionization and attachment for several ratios of laser mixtures (CO_2 :N_2 :He); calculated on the basis of the kinetic equation [8.27, 28]

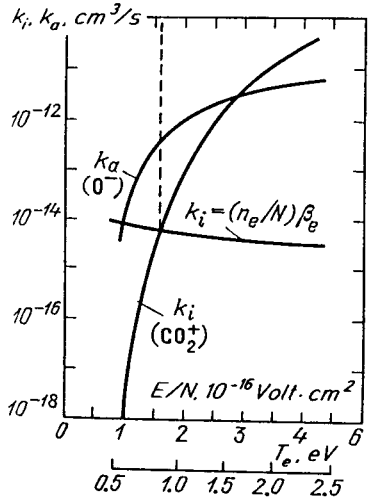

Fig. 8.19. Ionization and attachment rate constant and T_e calculated using the kinetic equation for the mixture CO_2 :N_2 :He= 1 : 7 : 12 [8.29]

ionization potential, $I_{CO_2} = 13.8\,\text{eV}$. The steady state corresponds to the equality of production and removal rates for electrons:

$$\nu_i(E/p) = \nu_a(E/p)\,, \quad \alpha(E/p) = a(E/p)\,. \tag{8.27}$$

The point of intersection of the ionization and attachment curves determines the value of E/p necessary for sustaining the *attachment-controlled discharge*. Sim-

ilar results for another important electronegative gas, namely air, were given in Sect. 7.2.5. The values of E/p and the corresponding ionization and attachment frequencies are summarized in Table 8.5. These data are of special interest: they indicate upper bounds, since detachment reduces losses and facilitates plasma sustainment. Thus for the 1 : 7 : 12 mixture the curves k_i and k_a in Fig. 8.19 intersect at $E/N = 2.8 \cdot 10^{-16}$ V·cm^2, $T_e = 1.6$ eV, which corresponds to an attachment-controlled discharge. If detachment is intensive, that is, if the discharge is recombination-controlled, then $k_i = (n_e/N)\beta_e$. If $n_e/N = 10^{-7}$, we obtain $E/N = 1.65 \cdot 10^{-16}$, $T_e = 0.9$ (for this point, $\beta_e = 6 \cdot 10^{-8}$ cm^3/s).

For Table 8.5 also gives experimental data [8.27] that agree quite satisfactorily with calculations. Measurements were conducted in pulsed discharge between plane copper electrodes 29 cm^2 in area, separated by gaps from 1.2 to 4.2 cm, at pressures from 100 to 1200 Torr. The discharge voltage at such high pressure is high, up to 10 kV. The cathode fall is 200 V, so that almost the entire potential drop is across the positive column. The quasistationary voltage was built up at the electrodes in less than 0.1 μs from the moment of ignition, and was sustained for 10 μs. In a given mixture, the voltage and E/p were independent of current when the latter varied over several orders of magnitude: $j/p \sim 10^{-1}$–10^2 mA/(cm^{2}Torr). (The $V-i$ curve was strictly horizontal.) Water vapour added at a concentration of a fraction of 1 % resulted in an increase of the voltage due to enhanced attachment.

8.8.2 Charge Kinetics Affected by Detachment

If the pressure is not too low ($p > 10$ Torr), which is typical of laser discharge, diffusional charge loss is of secondary importance. The bulk processes involving negative ions, which on the whole determine the density of electrons and the

Table 8.5. Field and frequencies of ionization in attachment-controlled discharges

$CO_2 : N_2 : He$ [a]	E/p, V/(cm·Torr) calculated	ν_i/p, 10^4 s^{-1}Torr^{-1}, calculated	E/p, V/(cm·Torr), experimental
1 : 7 : 30	7.9	0.052	9.1
1 : 1 : 8	8.6	0.35	9.5
1 : 7 : 12	9.2	8.2	
1 : 2 : 3	16.5	1.1	17
1 : 2 : 1			23.5
1 : 7 : 0	25		28
1 : 0 : 9			6
nitrogen [b]			22.3
nitrogen + 1 % H_2O			27
air	41	30	

Calculation results were taken from [8.28], with two exceptions: the 1 : 7 : 12 mixture [8.29], and air (Sect. 7.2.5). Experimental data were taken from [8.27].

[a] – the ratio of the numbers of molecules

[b] – technical-grade nitrogen (not too pure: contaminated with O_2, etc.)

conductivity of the mixture, are described by a system of kinetics equations for charge densities n_e, n_+, n_-:

$$dn_e/dt = k_i N n_e - k_a N n_e + k_d N n_- - \beta_e n_e n_+ ,$$

$$dn_-/dt = k_a N n_e - k_d N n_- - \beta_- n_- n_+ , \tag{8.28}$$

$$dn_+/dt = k_i N n_e - (\beta_e n_e + \beta_- n_-) n_+ .$$

Here $k_i N = \nu_i$, $k_a N = \nu_a$, k_d is the detachment rate constant for any molecule (we assume that the concentration of active molecules has stabilized), and β_e and β_- are the electron-ion and ion-ion recombination coefficients, respectively. Only two of the differential equations are independent; the third one is equivalent to the electroneutrality condition $n_e + n_- = n_+$. Nonstationary processes, say plasma decay, can also be analyzed using these equations.

8.8.3 Effective Recombination Coefficient

If detachment processes are fast, thus greatly compensating for attachment, system (8.28) can be approximately reduced to a single equation of kinetics for electron density [8.30]. Assume that negative ions decay much faster than they recombine: $k_d N \gg \beta_- n_+$. The result is an approximate *dynamic equilibrium* of attachment and detachment: $k_a n_e \approx k_d n_-$. The ratio of the numbers of electrons and negative ions stays constant, $n_-/n_e \approx k_a/k_d \approx \eta$, even though the numbers n_e and n_- may slowly change. Under such conditions, $n_+ \approx n_e(1+\eta)$, and the third equation of (8.28) gives

$$\frac{dn_e}{dt} = \frac{k_i N n_e}{1+\eta} - (\beta_e + \beta_- \eta) n_e^2 . \tag{8.29}$$

The first term on the right can be interpreted to indicate that less than one electron is produced in an ionization act. The rate of recombination of electrons appears to increase because an electron merging with a molecule disappears in the course of ion-ion recombination. If we consider plasma decay without the first production term, the quantity

$$\beta_{eff} = \beta_e + \beta_- \eta , \quad \eta = k_a/k_d \tag{8.30}$$

plays the role of the *effective recombination coefficient*. But if the steady state is considered, the equation for the balance of electron numbers can be written in the form

$$k_i N n_e = (1+\eta)(\beta_e + \beta_- \eta) n_e^2 = \beta'_{eff} n_e^2 . \tag{8.31}$$

This equation looks as if ionization proceeds in a normal way at the true frequency $\nu_i = k_i N$: negative ions are completely absent, but electrons recombine with a still higher effective coefficient

$$\beta'_{eff} = (1+\eta)(\beta_e + \beta_- \eta) , \quad \eta = k_a/k_d . \tag{8.32}$$

8.8.4 $V - i$ Characteristic, Charge Composition of Plasma, and Detachment Rate

We can only hypothesize on which particles in the discharge actively destroy negative ions (Sect. 4.4.3). At present the data on detachment rate is obtained indirectly, by comparing the experimentally obtained $V - i$ curve of a stationary discharge in an electronegative gas with calculations made under specific assumptions on k_d. An example of such analysis [8.31] which gave also the charge composition of the plasma is shown in Fig. 8.20. Triangles and circles illustrate experimentally measured current-voltage characteristics [8.32].

The discharge (longitudinal) was maintained in a plane channel of $5 \times 15\,\text{cm}^2$ cross section, 46 cm long in the field direction (Fig. 8.18). In order to remove heat from the discharge volume, the gas was pumped in the same direction at a velocity 100 m/s. The flow does not greatly affect the discharge but prevents overheating of the gas. According to experimental $V - i$ curve, the value of E/p depends on current and pressure only slightly, being equal on the average to $E/p \approx 7\,\text{V/(cm·Torr)}$ ($E/N \approx 2.1 \cdot 10^{-16}\,\text{V·cm}^2$).

The same figure shows the results of $V - i$ curve calculations on the basis of stationary equalities (8.28). The rate constants k_i and k_a are taken from Fig. 8.19, assuming $\beta_e = \beta_- = 10^{-7}\,\text{cm}^3/\text{s}$ and taking into account such details as the potential drop at the electrode and gas heating, and choosing a sequence of values of k_d from 0 to ∞. Obviously, experimental data are in contradiction with both extreme assumptions: no detachment ($k_d = 0$), and detachment completely compensating for attachment ($k_d = \infty$). The best fit is found for the value $k_d = 0.9 \cdot 10^{-14}\,\text{cm}^3/\text{s}$. If the detachment cross section is assumed to be of the order of the collision cross section of molecules, the resulting number of active molecules is about 10^{-4} of the total number, which seems to be reasonable. The experimental value $E/p \approx 7$ corresponds to rate constants $k_i = 1.5 \cdot 10^{-14}\,\text{cm}^3/\text{s}$, $k_a = 6 \cdot 10^{-14}\,\text{cm}^3/\text{s}$. If $p = 20\,\text{Torr}$, $N = 6.7 \cdot 10^{17}\,\text{cm}^{-3}$, the frequencies are

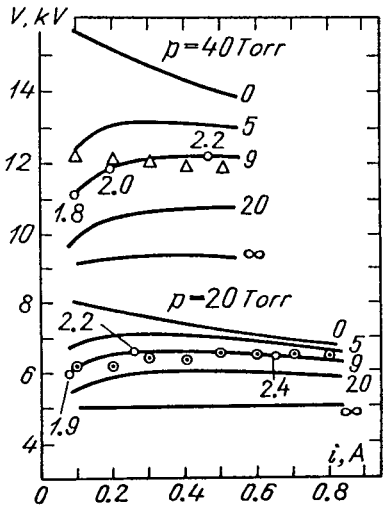

Fig. 8.20. Experimental [8.32] and calculated [8.31] $V - i$ curves of discharges in a 1 : 7 : 12 mixture. *Numbers* to the *right* of the *curves* mark the values of k_d in units of $10^{-15}\,\text{cm}^3/\text{s}$ ($k_d = 0$ denotes pure attachment, $k_d = \infty$ indicates no attachment or no negative ions). Experimental data (*dots* and *triangles*) are best fitted by the curves calculated with $k_d = 9 \times 10^{-15}\,\text{cm}^3/\text{s}$. *Numbers* along these *curves* are the values of E/N in units of $10^{-16}\,\text{V cm}^2$

$\nu_i = 10^4\,s^{-1}$, $\nu_a = 4 \cdot 10^4\,s^{-1}$. The plasma contains a considerable number of negative ions: $\eta = n_-/n_e = k_a/k_d \approx 5.3$. The effective coefficient of electron recombination $\beta'_{eff} \approx 40\beta_e \approx 4 \cdot 10^{-6}\,cm^3/s$ is very high, 40 times the actual value (owing to attachment). Detachment compensates for about 80 % of attachment.

The $V - i$ characteristic of a stationary discharge in an air-filled tube is a clear illustration of the effect of detachment (Fig. 8.14); this was discussed in Sect. 8.6.3.

8.9 Discharge in Fast Gas Flow

Gas is pumped through a discharge volume in order to remove the Joule heat and prevent overheating of the gas itself and of the walls of the discharge chamber. Experiments reveal different degrees of the response of stationary discharges to gas flow but invariably confirm that as the flow velocity increases, the discharge voltage can only increase to a greater or lesser extent. We conclude that charge losses must increase and be compensated for by enhanced ionization. Several mechanisms for the effect of flow can be proposed.

8.9.1 Turbulence Transport of Charges to the Walls

The gas in a sufficiently fast flow becomes turbulent. *Small-scale turbulence* is often deliberately introduced, especially in high-power lasers, because this improves discharge stability and increases the upper limit of energy input. The effect of turbulent stirring of plasma volumes is similar to ambipolar diffusion. It transports more strongly ionized volumes from central regions to the walls while carrying less ionized volumes from the periphery toward the axis. This mechanism may prove to be efficient in a discharge that is diffusion controlled when flow is absent (that is, discharge at reduced pressure, in narrow tubes, and in narrow channels). The effect can be described by adding the turbulence diffusion coefficient to the ambipolar diffusion coefficient D_a.

Gas dynamics offers several empirical formulas for the former coefficient (the effect of weak ionization on turbulence is unlikely to be appreciable). Thus, if u [cm/s] is the mean flow velocity and a [cm] is the tube radius or half the height of a plane channel, then

$$D_T \approx 0.009 a u\,cm^2/s\,. \tag{8.33}$$

For instance, in the experiment described in Sect. 8.8.4, $a = 1.5\,cm$, $u = 10^4\,cm/s$, $D_T = 225\,cm^2/s$. This coefficient is several times greater than $D_a \approx 75\,cm^2/s$ at $p = 40\,Torr$; nevertheless, the frequency of total "diffusional" losses, $\nu_{dT} = (D_a + D_T)/(2a/\pi)^2 \approx 120\,s^{-1}$, is less than that of bulk losses, $10^4\,s^{-1}$, so that turbulence diffusion plays a minor role under these specific conditions.

8.9.2 Convective Charge Transport

The loss of charge from the current channel due to the entrainment by the gas flow may be significant if the discharge length L_1 along the gas flow is small. This situation occurs in transverse discharges when the length of at least one electrode is much shorter than the interelectrode gap. The "convective transport frequency" is $\nu_F \approx 2u/L$. Presumably, this mechanism was dominant in the experiments [8.33] with air whose results plotted in Fig. 8.21. The cathode was a narrow strip $0.4 \times 40\,\text{mm}^2$, transverse to the flow, the anode was a large plate, and the gap width was 3 cm. If the positive column is characterized by $L \sim 1$ cm, then $u \sim 100$ m/s entails $\nu_F \sim 10^4$, which is comparable to the bulk loss frequency. The values of E/p, evaluated using the data of Fig. 8.21, increase from 15 to 25 in the range of u from 50 to 180 m/s. If a transverse discharge is extended along the flow, with geometry close to that in Fig. 8.1a, the discharge voltage is almost independent of the flow velocity. Indeed, the arrival of charges from the left in some middle section of the channel and their removal to the right do not disturb the overall charge balance.

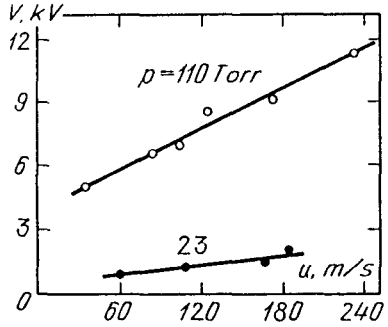

Fig. 8.21. "Burning" voltage of transverse discharge in air as a function of flow velocity. *(1)* $p = 23$ Torr, *(2)* $p = 110$ Torr [8.33]

8.9.3 The Effect of Flow on the Accumulation of Molecules Active with Respect to Detachment

This is similar to the time effect discussed in Sect. 8.8.1. If a macroscopic gas element moving through the discharge zone spends little time there, it cannot accumulate the number of active molecules that corresponds to the established conditions. Hence, the faster the motion of the gas through the discharge zone, the weaker the compensation by detachment of the electron attachment, which is equivalent to enhanced attachment losses. If the characteristic time of buildup of a stationary concentration of active molecules is of order 10^{-5}–10^{-3} s, the flow velocity must affect the discharge in electronegative gases if the time of flight of a gas particle through the discharge zone, L/u, is also of this order of magnitude. Presumably, this effect could accompany the convective transport in the experiment of Fig. 8.21.

No appreciable effect of flow velocity on discharge sustainment voltage has been observed in long, longitudinal self-sustaining discharge systems (Fig. 8.22).

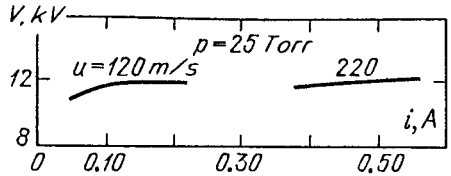

Fig. 8.22. $V - i$ characteristic of longitudinal discharge with gas flow. Laser mixture $CO_2 : N_2 : He = 1 : 2.5 : 15$, $p = 25$ Torr; *(1)* $u = 120$ m/s *(2)* 220 m/s [8.34]

In these experiments [8.34], the discharge was burning in a plane channel (Fig. 8.1b) 5.5 cm in height, 76 cm wide and with its length oriented along the flow (i.e. with an electrode gap spacing) of $L = 65$ cm. Even for $u = 220$ m/s, the time of flight is very large: $\tau_F = L/u = 3 \cdot 10^{-3}$ s. The concentration of active molecules has evidently stabilized. Under these conditions, the diffusion and turbulence loss frequency is not high: $D_{eff} = D_a + D_T \approx 650\,cm^2/s$, $\nu_{dT} \approx 220\,s^{-1}$. If the discharge length is smaller, the voltage is observed to increase as the flow velocity increases (in a self-sustained discharge). The dependence of V on u is always stronger in non-self-sustaining discharges (Sect. 14.4.5, Fig. 14.9). It should be mentioned that the effects of flow velocity on the characteristics of longitudinal discharges are not yet known sufficiently well. Discharges in transverse flow are analyzed in the review [8.35].

8.10 Anode Layer

8.10.1 Production of Ions

There are no positive ions at the metal anode surface because they are not emitted by the anode and are repelled by it. The anode is separated from the electroneutral plasma of the positive column by a layer of negative space charge in which the magnitude of the field decreases towards the column.[14] The electron current density j_e changes in the layer by a negligible amount $(\mu_+/\mu_e)j$, while the ionic current density in the plasma increases from zero to $j_{+c} = (\mu_+/\mu_e)j$. The ionic current j_{+c} flowing into the positive column is formed as a result of charge production in the anode layer, in response to a very small number of ionization acts of one electron, μ_+/μ_e. Indeed,

$$\frac{dj_+}{dx} = \alpha j_e \approx \alpha j\ ;\quad j_{+c} \approx j \int \alpha\, dx\ ;\quad \int \alpha\, dx = \mu_+/\mu_e\ .$$

This number is three orders of magnitude smaller than the number of generations of electrons produced in the cathode layer. Consequently, the anode fall V_A is much lower than the cathode fall.

[14] The sign of anode drop may be reversed at very low pressure.

8.10.2 Potential Drop and Current Density

According to early measurements in tubes [8.3, 36] at $p \lesssim 1$–10 Torr, $V_A \approx 10$–20 V and the anode fall is in each gas comparable with the ionization potential. The anode current density is of order 10^{-4}–10^{-3} A/cm^2; fields $E/p \approx 200$–600 V/(cm·Torr) were measured in nitrogen near the anode, which corresponds to the layer thickness $d_A \sim 0.05/p$ cm (of the order of the electron free path length l). Recent studies demonstrated that at medium pressures, the anode fall increases as the pressure is increased, the increase being greater in electronegative gases (Fig. 8.23). According to [8.37], the current density at the anode is independent of the value of current: $j/p^2 \approx 4.3 \cdot 10^{-4}$ A/(cm·Torr)^2 in nitrogen at $p \approx 5$–30 Torr, and $j/p^2 \approx 2.7 \cdot 10^{-4}$ in air at $p \approx 8$–60 Torr. (The figures refer to discharges between plane steel electrode disks 1.6 cm in diameter.)

The measured values of j/p^2 are quite close to the normal values at the cathode (Table 8.3). It appears that if the current column diameter is not less than the interelectrode distance, the normal cathode layer imposes the value of j on the entire column, including the anode. As follows from the calculations [8.8], even the radial distribution $j(r)$ originating at the cathode is repeated in such cases at the anode (Fig. 8.6). The anode fall calculated for nitrogen (Fig. 8.6) gives a good fit to the measured values (Fig. 8.23). The anode spot is small at low current. Numerical experiment [8.8] indicates that the spot radius r_A is determined by the spreading due to the transverse (radial) diffusion of electrons, and is related to the anode layer thickness ($pd_A \approx 0.25$ Torr·cm) by a formula typical of diffusion: $r_A \approx (D_e d_A/v_d)^{1/2} \approx d_A(T_e/V_A)^{1/2}$.[15]

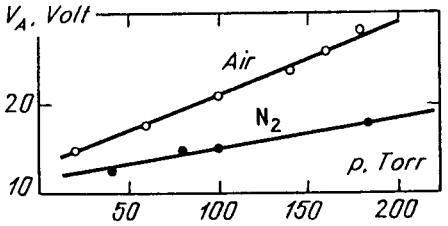

Fig. 8.23. Anode fall for discharges in nitrogen and in air as a function of pressure [8.37]

8.10.3 Do the Ions Produced in the Anode Layer Pierce the Positive Column?

Quite frequently, they do not. The probability that an ion perishes is μ_e/μ_+ times greater than that for an electron, since an ion drifts through the column longer by just this factor. In the example given in Sect. 8.6.2 [see (8.19)], the probability is 0.2 per 1 cm of column length, that is, a 5 cm long column does not let ions through. Here we ignore all possible processes of resonance charge transfer in which one ion is instantaneously replaced with another, indistinguishable from

[15] The results of [8.8] do not support the theoretical model suggested in [8.37].

it – the ion cannot really be said then to have perished in the usual sense of the word.

If a longitudinal discharge is maintained in a flow of gas, the flow is usually directed from the cathode to the anode, in order to immediately blow out of the discharge the perturbations generated in the anode region. The velocities that are employed in actual systems, $u \approx 100$–200 m/s, are comparable with the ion drift velocities v_{+d}. For example, in a self-sustained discharge in the mixture $CO_2 : N_2 : He = 1 : 7 : 12$ at $E/p \approx 7$ V/(cm·Torr), the velocity of the main ions CO_2^+ is $v_{+d} \approx 200$ m/s. Fast flow decelerates ions, and blows them out completely if $u > v_{+d}$. In contrast to their natural behavior, ions are entrained then against the field, towards the anode. This effect cannot, however, stop the current in the discharge, because it is carried mainly by electrons [8.9].